INTERACTIONS OF ADAM15 SPLICE VARIANTS WITH SH3 DOMAIN PROTEINS

Elizabeth Shedden

A thesis submitted to the School of Chemistry, University of East Anglia in fulfilment of the requirement for the degree of Doctor of Philosophy.

March 2015

Declaration

I declare that the work contained in this thesis, submitted by me for the degree of Doctor of Philosophy, is my own original work, except where due reference has been made to the other authors or co-workers and has not been previously submitted by me for a degree at this or any other university.

Elizabeth Shedden

March 2015

Abstract

A Disintegrin And Metalloproteinase 15 (ADAM15) is a membrane-bound metalloproteinase which has been shown to be significantly raised throughout breast cancer progression. The intracellular domain (ICD) of ADAM15 exists in multiple splice variants that contain varied combinations of polyproline regions, which interact preferentially with proteins containing Src Homology 3 (SH3) domains. Patients suffering from node-negative breast cancer exhibited a poorer prognosis when expressing high levels of variant A and B whereas those patients suffering from node-positive cancer exhibited an improved prognosis when expressing high levels of ADAM15 variant C.

Nuclear Magnetic Resonance (NMR) spectroscopy titrations were used to elucidate the interaction interface between the ADAM15 ICD variants and the SH3 domains of Grb2, Src and Brk. Chemical Shift Perturbations (CSPs) indicated that Grb2 interacted with all ADAM15 ICD variants via residues 22Glu, 44Trp and 56Phe. Analysis of the common regions of the ICD variants implicated the polyproline region 4 in this interaction. The Src SH3 domain interacted with ADAM15 B, C and E via residues 17Arg, 21Asp, 40Trp and 56Ser-58Tyr; residues which are present in the hydrophobic pocket of the domain. This interaction likely involves a RPLPXDPV motif apparent in polyproline regions 2 and 3 of the ADAM15 ICD. The Brk SH3 domain also interacted with ADAM15 B via residues 34Arg, 56Trp, 74Val, 77Asn and 79Leu in a manner similar to the internal interaction of the Brk SH3 domain with its own linker region. ADAM15 D does not interact with any of the SH3 domains as it does not include any polyproline regions.

This work has highlighted the manner by which certain SH3 domains preferentially interact with the polyproline regions of the ADAM15 ICD and open a line of investigation into the downstream functions of these interactions particularly with regards to breast cancer expression.

Acknowledgements

Firstly I would like to thank Big C Cancer Research for funding my PhD. They do amazing work in Norfolk and Waveney, both in research funding and patient support. I would also like to thank my supervisors Dr Tharin Blumenschein and Prof Dylan Edwards, for their ongoing support, expertise, guidance and patience. I would not have made it without you both! Special thanks to Dr Christian Roghi for friendship, lab advice and sarcasm. For the long-serving listening ears of Dr Stephen Robinson and Dr Helen James, thank you for letting me moan at you and giving me sympathetic advice; It has been much appreciated!

To the friends who have supported me through my PhD, through coffee breaks, distractions, nights out and entertainment, I love you all very dearly. You keep me sane (ish)! Whether you're a member (past or present) of the Blumenschein group, the Edwards group, the Robinson group, the Khimyak group or the Russell group, you have all helped me to survive my PhD as well as some difficult personal events over the years and I have very much appreciated you all! A special mention has got to go to Sooz, Sophie, Justin and Salma for your consistent support, encouragement, cat sitting and for putting up with me through the craziness of thesis writing and to Hayley who has been there for nearly 10 years and still comes back for more! Whether it has been trips to the seaside, the cinema, the coffee shop, the gin bar or simply enjoying the sunshine on the balcony, you have made my time in Norwich particularly special and I hope to be able to reminisce about these times with you all for many long years to come.

Finally, I would like to thank my wonderful family, my parents Maureen and Keith, my sister Alex and her husband Matt and my grandmother, Winnie. I love you all so much and you have taught me to be the person that I am today. You are the best family a girl could ever ask for and have always been my emotional backbone. I like to think Grandma Do, Jimmydad and Grandad would be proud of us all!

Abbreviations

ADAM	A disintegrin and metalloproteinase
ADAMTS	A disintegrin and metalloproteinase with thrombospondin motifs
ADH	Antidiuretic hormone
ADH	Atypical ductal hyperplasia
ALL	Acute lymphoblastic leukaemia
ApoE	Apolipoprotein E
ATP	Adenosine triphosphate
BCA	Bicinchoninic acid
BRCA1	Breast Cancer genes 1
BRCA2	Breast Cancer genes 2
BRK	Breast tumour kinase
BSA	Bovine serum albumin
CAM	Cell adhesion molecules
cAMP	Cyclic adenosine monophosphate
CD	Cluster of differentiation
CDC45	Cell-division cycle protein 45
CDK2	Cyclin-dependent kinase
cDNA	Complementary DNA
CHK	Checkpoint kinases
CHO	Chinese hamster ovary
CIA	Collagen-induced arthritis
CML	Chromic myeloid leukaemia
CSK	C-terminal Src Kinase
CSP	Chemical shift perturbations
CV	Column volumes
DCIS	Ductal carcinoma in situ
DSS	Disuccinimidyl suberate
DTT	Dithiothreitol

ECL	Enhanced chemiluminescence
ECM	Extracellular matrix
EDTA	Ethylenediaminetetraacetic acid
EET	Epoxyeicosatrienoic acids
EGF	Epidermal growth factor
EGFR	Epidermal growth factor receptor
ELISA	Enzyme-linked immunosorbent assay
EMT	Epithelial-mesenchymal transition
ER	Estrogen Receptor
ERK	Extracellular signal-regulated kinases
FAK	Focal adhesion kinase
FasL	Fas ligand
FCS	Fetal calf serum
FDA	Food and Drug Administration
FGF	Fibroblast growth factor
FGFR	Fibroblast growth factor receptor
FID	Free induction decay
FLSs	Fibroblast-like synoviocytes
GB1	Protein G immunoglobulin binding domain 1
GDP	Guanosine diphosphate
GPCR	G protein-coupled receptor
GRB2	Growth factor receptor-bound protein 2
GST	Glutathione S-transferase
GTP	Guanosine-5'-triphosphate
Hck	hematopoietic cell kinase
HER	Human epidermal growth factor receptor
HGF	Hepatocyte growth factor
HGFR	Hepatocyte growth factor receptor
HIV	Human immunodeficiency virus
HRG	Histidine-rich glycoprotein

HRP	Horse radish peroxidase
HSQC	Heteronuclear Single-Quantum Coherence
ICAM1	Intercellular adhesion molecule 1
ICD	Intracellular domain
IFN	Interferon
Ig	Immunoglobulin
IL	Interleukin
IRS	Insulin receptor substrate
JNK	c-Jun N-terminal kinases
Lck	lymphocyte-specific protein tyrosine kinase
LMTK3	Lemur tyrosine kinase 3
LPA	Ligand lysophosphatidic acid
LPS	Lipopolysaccharide
Mad	Mothers Against Decapentaplegic
MAPK	Mitogen-activated protein kinase
mEFs	Mouse embryonic fibroblasts
MEM	Minimal Essential Medium
MHC	Major histocompatibility complex
MICB	MHC class I polypeptide-related sequence B
MMP	Matrix metalloproteinase
mRNA	Messenger RNA
MTMMPs	Membrane-type MMP
MZF1	Myeloid zinc finger 1
NCK	Non-catalytic region of tyrosine kinase adaptor protein
NMR	Nuclear magnetic resonance
OA	Osteoarthritis
OE	Over expression
PAGE	Polyacrylamide gel electrophoresis
PAK1	p21-activated kinase 1
PANC	Human pancreatic carcinoma, epithelial-like cell line

PBS	Phosphate buffered saline
PC3	Prostate cancer cell line
PCR	Polymerase chain reaction
PDGF	Platelet-derived growth factor
PDGFR	Platelet-derived growth factor receptor
PECAM1	Platelet endothelial cell adhesion molecule
PES	Polyethersulfone
PgR	Progesterone receptor
PI3K	Phosphoinositide 3-kinase
PIC	Pre-integration complex
PKCdelta	Protein kinase C delta type
PMSF	Phenylmethanesulfonylfluoride
PR	Progesterone receptor
PSF	Protein-associated splicing factor
PTD	Protein transduction domains
PTK6	Protein-tyrosine kinase 6
RA	Rheumatoid arthritis
RECK	Reversion-inducing-cysteine-rich protein
RIP	Regulated intramembrane proteolysis
RTKs	Receptor tyrosine kinases
SDS	Sodium dodecyl sulfate
SH1	Src Homology Domain 1
SOS1	Son of Sevenless
SP1	Specificity protein 1
SPB	Sodium phosphate buffer
Src	human protein tyrosine kinase (sarcoma)
STAT	Signal transducer and activator of transcription protein
SVMP	Snake venom metalloproteinases
TBS	Tris buffered saline
TCR	T-cell receptor

TGF	Transforming growth factor β
TIMP	Tissue inhibitor of metalloproteinase
TLR	Toll-like receptor
TNF	Tumour necrosis factor
TNFR	Tumour necrosis factor receptor
TNM	Tumour Node Metastasis
UTR	Untranslated region
VCAM1	Vascular cell adhesion protein 1
VEGF	Vascular endothelial growth factor
VEGFR	Vascular endothelial growth factor receptor
WASp	Wiskott–Aldrich syndrome protein

Contents

List of Figures

List of Tables

Chapter 1: Introduction

1.1 Breast Cancer

Breast cancer was the most common cancer affecting women in the United Kingdom in 2011 with 49,936 women and 349 men diagnosed and approximately 1.68 million cases worldwide. Women have a 1 in 8 lifetime chance of developing the disease in Western Europe. The number of cases of breast cancer in the UK have increased 74% since the mid-1970s but due to increased screening rates (16,500 cases detected by the NHS screening program in 2009-2010 financial year) and more effective treatments, death rates have decreased by 40% since the mid-1980s. Although the 10-year survival rates have increased from half of those diagnosed to 8 in 10 in the last 40 years, only 15% of those diagnosed with the most advanced forms of the disease survive for at least 5 years after diagnosis. Despite progress in the treatment, detection and awareness of breast cancer, the disease remains the second most common cause of death for women in the UK after lung cancer (2011a).

The normal breast comprises fatty tissue, milk ducts, glands and lymph nodes (figure 1.1) and cancer can arise in any of these structures. The most common form of breast cancers are carcinomas which arise from epithelial cells such as those of the lining of the milk ducts or lobes and account for 75% of all breast tumours (Bombonati and Sgroi, 2011).

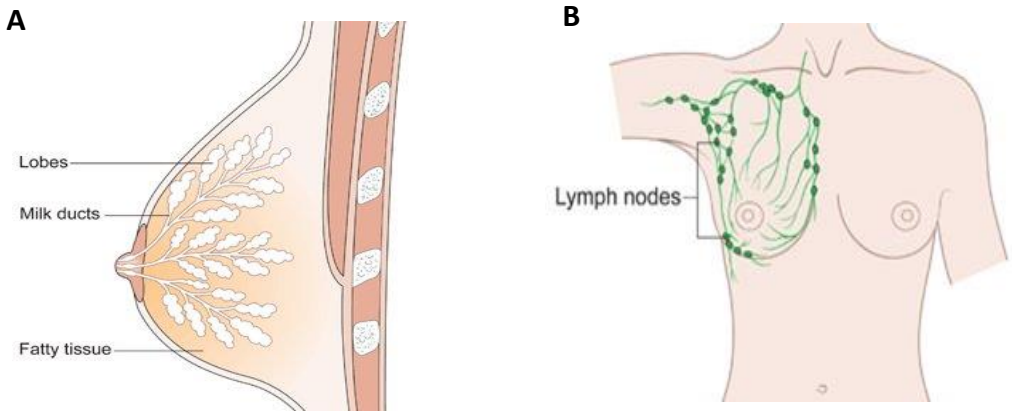

Figure 1.1 A) Structure of the breast. B) Network of lymph nodes in the breast and under-arm. Adapted from Cancer Research UK (2011a).

The lymph nodes are a common biopsy target as the system drains the tissue fluid from around the breast cells and so can contain any cancer cells that have broken away from a tumour. If there are no cancer cells present in the lymph nodes, the likelihood of the cancer having metastasised beyond the breast tissue is low.

Carcinomas emerge due to a loss of functional control of processes such as proliferation and cell cycle which cause a colony of neoplastic pre-cancerous, benign cells to develop (figure 1.2). Under the right micro-environmental conditions, this can further progress to atypical ductal hyperplasia (ADH) and eventually to ductal carcinoma in situ (DCIS) through the accumulation of genetic and epigenetic changes (Burstein et al., 2004). While DCIS is non-invasive and can stay as such for many years without developing further, it has the potential to eventually gain invasive characteristics.

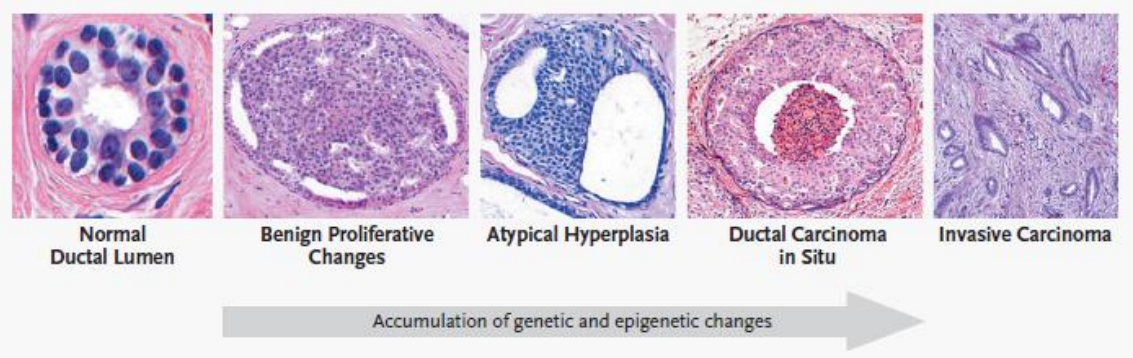

Figure 1.2 Histological images of progression of breast cancer development from normal ductal lumen tissue through Ductal Carcinoma in Situ to invasive carcinoma. Adapted from Burstein et al, N Engl J Med, 2004 (Burstein et al., 2004).

The TNM System (Tumour, Node, Metastasis) is used to assess the severity of a patient's condition upon diagnosis taking into account the size of the tumour, whether it has yet infected the lymph nodes and whether it has metastasised to distant tissues and organs. DCIS is classed as Stage 1 by this system and is shown in figure 1.3 along with stages 2 and 3 which also exhibit cancerous cells in the lymph nodes which DCIS does not. Under the TNM System, Stage 4 is invasive carcinoma that has metastasised to remote tissues and organs (2011d). Other classifications used to distinguish the severity of the disease include the differentiation status of the tumour (grade) and steroid hormone receptor status.

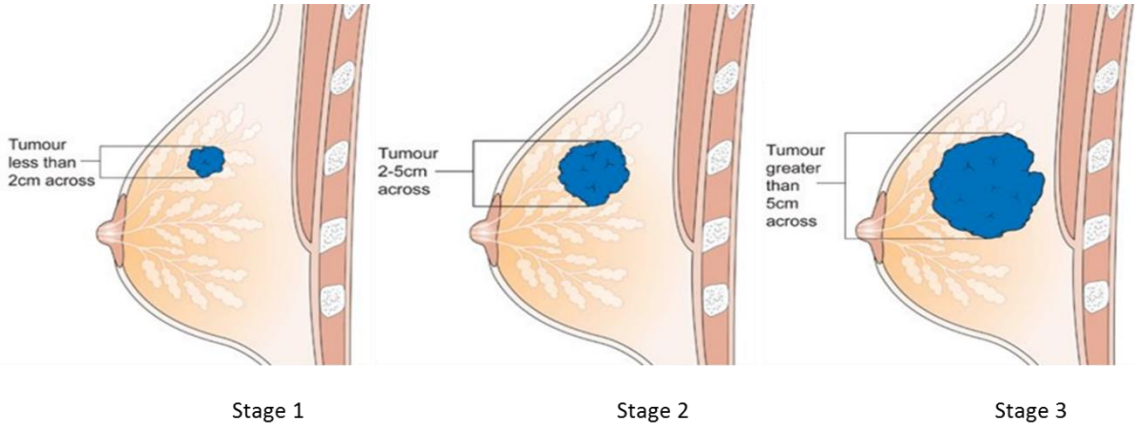

Figure 1.3 TNM System of grading the severity of breast cancers. Stage 1 is also known as DCIS. Stages 2 and 3 display lymph nodes positive for cancerous cells and Stage 4 is metastatic disease (not shown here). Adapted from Cancer Research UK (2011d).

The expression of certain receptors is also used to define different breast cancers, specifically the Progesterone Receptor (PR), the Estrogen Receptor (ER) and the Human Epidermal Growth Factor Receptor 2 (Her2) (Burstein et al., 2004). Hormone based treatments have been effective in treating cancers expressing these receptors. However, those patients whose cancer is "triple-negative" for these receptors do not respond to such treatments and are consequently much more difficult to successfully treat.

Although the hereditary forms of breast cancer (those who have inherited mutations in the BRCA1 and BRCA2 genes for example) have been well publicised, 95% of all breast cancers are sporadic in nature (2001). Risk factors include obesity, age, menopausal status, the use of oral contraceptives and smoking (2011b).

Breast cancer research has increasingly demonstrated the importance of multiple metalloproteases in cancer progression. Some metalloproteases, such as MT1-MMP, have been shown to increase invasion, metastasis, angiogenesis and 3-dimensional tumour growth (Lee et al., 2007). Alternatively, some, such as MMP8 and ADAMTS15, have been shown to possess tumour suppressive abilities (Decock et al., 2011). The family of metalloproteases to be investigated here is that of the ADAMs. As will be explained in more detail later, ADAM15 has been implicated in varying prognoses in women with node-negative tumours compared to node-positive tumours (Zhong et al., 2008).

1.2 A Disintegrin And Metalloproteinase (ADAM) Family

The ADAM family of metzincin endopeptidases, belong to the M12B adamalysin protease subfamily (MEROPS) (Rawlings et al., 2008) and are related to the ADAMTS (A Disintegrin And Metalloproteinase with Thrombospondin motifs) family and the SVMP (Snake Venom Metalloproteinase) family. They are generally approximately 750 residues in length and are mostly transmembrane proteins, with a few secreted exceptions (Edwards et al., 2008). Well-conserved in evolutionary terms, orthologs of ADAMs can be found in vertebrates, with only ADAM22 missing from the *mus musculus* genome compared to humans (Puente et al., 2003).

In humans, 25 ADAM genes have been identified, 4 of which appear to be pseudogenes (Edwards et al., 2008). Of the 21 active genes, only 12 include the reprolysin-type active site sequence (HEXGHXXGXXHD) and the Metzincin specific "Met turn" necessary for proteolytic action (Bode et al., 1993). Those that do not include these sequences would appear not to have catalytic capabilities although several have been shown through gene knock-out mice studies to still have important roles in development (Edwards et al., 2008) .

The ADAM family proteins exhibit tissue specific expression. Within both the catalytically active and inactive subgroups, the human ADAMs are divided into testis-specific and non-testis-specific groups. Those that are testis specific are involved in spermatogenesis and sperm function whereas the non-testis specific proteins are expressed in a widespread manner throughout other tissues. A minority buck this trend and are expressed predominantly in haematopoietic tissues, for example ADAM8 and -28 (Edwards et al., 2008). These variations within the family are highlighted in Figure 1.4.

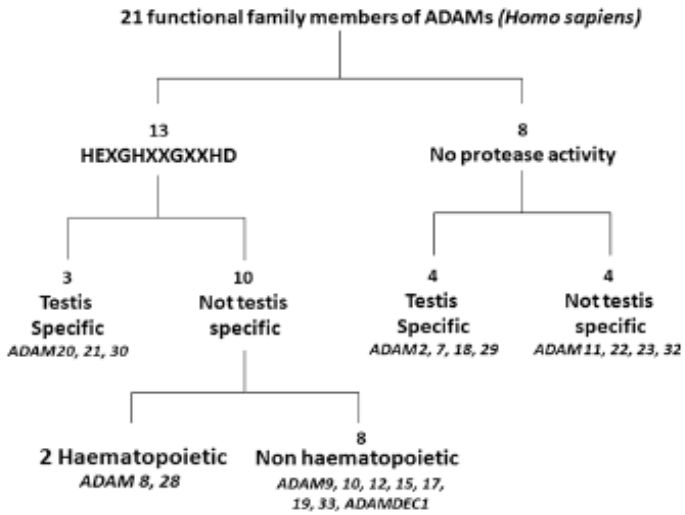

Figure 1.4 Schematic of the subdivisions of the ADAM family of metalloproteinases (Edwards et al., 2008).

1.2.1 Structure of the ADAM family proteins

The general structure for this family is consistent with each ADAM including a pro-domain, a metalloprotease domain, a disintegrin-like, a cysteine-rich domain, an EGF-like domain, a transmembrane region and an intracellular domain (ICD) (Edwards et al., 2008). The organisation of these domains is comparable to other members of the Metzincin superfamily as shown in figure 1.5. ADAMs differ from the rest of the superfamily through having a combination of the disintegrin domain, the cysteine-rich region and the EGF-like domain while lacking any thrombospondin repeats or a hemopexin domain (Seals and Courtneidge, 2003).

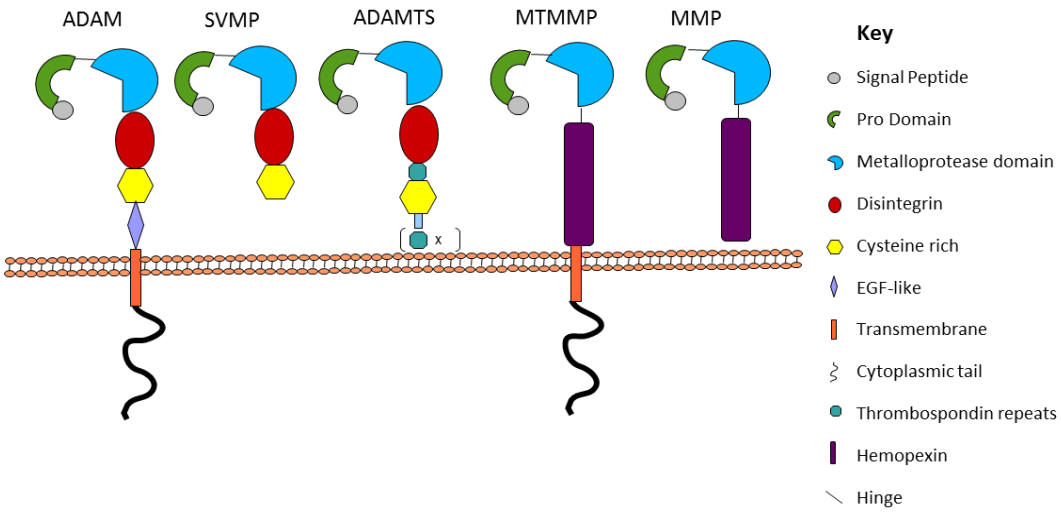

Figure 1.5 Schematic of the general structure of the ADAM family along with other Metzincins including SVMPs, ADAMTS', MTMMPs and MMPs. Adapted from Edwards et al 2008 (Edwards et al., 2008).

The Pro-Domain

The ADAM family proteins are synthesised as inactive enzymes, inhibited by a cysteine switch mechanism generated by the pro-domain (Roghani et al., 1999; Seals and Courtneidge, 2003). The cleavage of this region and thus activation of the enzyme, is catalysed by a pro-protein convertase enzyme, such as furin, which recognises a conserved RX(R/K)R motif (Lum et al., 1998). ADAM -8 and -28 are unusual are they have the ability to auto-catalyse their pro-domain and thus activate themselves (Howard et al., 2000; Schlomann et al., 2002). The pro-domain is also necessary for correct protein folding (Roghani et al., 1999). Once cleaved, the pro-domain can act as a signalling ligand to inhibit mature ADAMs as is the case for ADAM -10 and -17 (Gonzales et al., 2004; Moss et al., 2007).

The Metalloprotease domain

The two globular subdomains of the metalloproteinase domain are orientated to hold the active site in a cleft. The N-terminal upper domain is a 5 stranded β-sheet holds the substrate parallel to itself once in the active site and the C-terminal lower domain is an α-helix and contains the HEXXH zinc-binding catalytic site. These are held in place by the Met turn, which is characteristic of the Metzincin family of endopeptidases and uses a 1,4 β-turn to do so, further stabilised by three disulphide bonds (Bode et al., 1993; Gomis-Ruth, 2003). The main function of this domain is as a sheddase.

The Disintegrin-like domain

Disintegrin domains have the ability to bind to heterodimeric adhesion receptors called integrins through a conserved RGD sequence (Lu et al., 2010). Integrins include an α type chain and a β type chain to which disintegrins bind (specifically the β-1 and β-3 type chains). A normal disintegrin domain includes of two sub domains that form an arc and can include calcium ions for stability (Lu et al., 2010). However, most ADAMs do not actually contain the conserved RGD sequence necessary for integrin interactions hence being termed “disintegrin-like” here. The only exception is that of human ADAM15 which does have the RGD sequence and has been shown to interact with αvβ3 though this (Lu et al., 2010). The functional relevance of this is unclear as this is not the case in mouse ADAM15. ADAM15 can also interact with α9β1 through an alternative integrin

binding sequence, RXXXXXXDLPEF, as can ADAM10 and -17 (Eto et al., 2002). However, as the disintegrin loop, which is responsible for integrin interactions, is buried within the 3D structure of ADAM15, the functional roles of this are less clear. The predicted homology structure for the ADAMs is shown in figure 1.6.

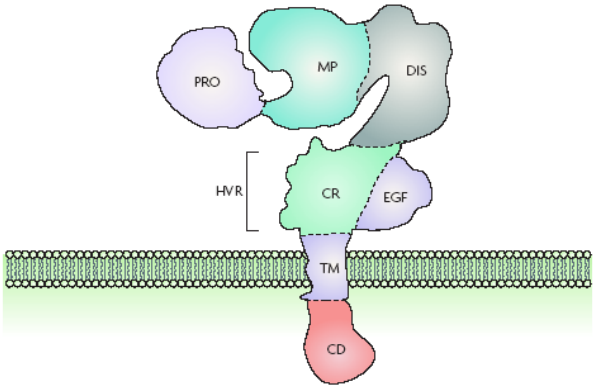

Figure 1.6 Schematic showing the structure of the domains of the ADAM family metalloproteases. Pro indicates the pro-domain, MP: the metalloprotease domain, Dis: the disintegrin domain, CR: the cysteine-rich region, EGF: the EGF-like region, TM: the transmembrane domain and CD: the intracellular domain. HVR indicates the high variability region. Taken from Murphy, Nature Reviews: Cancer, 2008 (Murphy, 2008)

The Cysteine-rich Region and EGF-like Domain

There is significantly less evidence as to the role of the cysteine-rich region in ADAM biology as for other domains. It contains a hypervariable region and appears, in some cases, to allow the ADAM to bind to the extracellular matrix although its role appears varied (Smith et al., 2002). For example, in ADAM12, it has been shown to allow interaction with proteoglycans, specifically syndecans (Iba et al., 2000). In ADAM13, it is involved with interactions with fibronectin (Smith et al., 2002). ADAM17 is incapable of shedding IL-1 Receptor-II without it, although it remains able to shed other substrates (Reddy et al., 2000). The cysteine-rich region also shares a strong homology with viral fusion proteins and so is potentially involved in the membrane fusion process for example myoblast fusion (Edwards et al., 2008). This has yet to be proven through experimentation.

Of all of the domains within the ADAMs, the least is known about the function of the EGF-like domain and currently no function of any ADAM has been linked their the EGF-like domain (Janes et al., 2005).

The Intracellular Domain

This is the most varied of the domains within the ADAMs. Those ADAMs that are secreted do not have an intracellular domain (ICD). For those that do, the length of this domain can vary from as little as 11 residues in ADAM11 to 231 residues in ADAM19 (Seals, 2003). The most common motif found within this domain is the PXXP proline-rich region capable of binding to proteins which contain Src homology domain 3 (SH3) domains. This motif is highly conserved across the family occurring in ADAMs -7, -10, -12, -15, -17, -19, -22, -29 and -33 (Edwards et al., 2008).

One example of the importance of the ICD of the ADAMs is that of ADAM10. If the proline-rich regions of the ICD of ADAM10 are removed, it is not correctly localised to the right basolateral location in polarised epithelial cells, removing its ability to cleave E-cadherin and thus removing ADAM10's effect on the promotion of cell migration (Wild-Bode et al., 2006). ADAM15 is an unusual case, in terms of its ICD, as it has 11 possible splice variants of this domain. These have been shown to preferentially interact with different SH3-containing signalling proteins which will form the basis of this project (Zhong et al., 2008).

An alternative function of the ICD in ADAMs derives from the availability of potential sites for phosphorylation by serine-threonine kinases and/or tyrosine kinases. Speculation would suggest that these give the ADAMs a role in outside/in signalling pathways. These sites could be involved in regulation of the ADAMs but would also create sites with the potential for binding to proteins containing SH2 domains. In the case of ADAM9, phosphorylation of these residues by PKCδ is necessary in order for ADAM9 to be activated by phorbol esters (Izumi et al., 1998).

1.2.2 Biological Functions of the ADAMs

ADAMs have a wide variety of functions. For example, ADAMs 1-3 have a role in fertility displaying functions in cell-cell adhesion between sperm and ovum through integrin-binding ability. By comparison, ADAM12 has a major role in myoblast fusion in skeletal muscle deposition which requires the removal of the pro-domain and the metalloprotease domain.

Shedding

The primary proteolytic function of ADAMs is that of shedding; the proteolytic cleavage of the ectodomain of a membrane-bound protein in order to release a potential ligand for downstream signalling or terminate signalling by removing a ligand from a receptor or removing the ectodomain of the receptor itself. As this requires an active metalloprotease domain, only those ADAMs that contain the HEXGHXXGXXHD sequence required for activity can act as sheddases (Bode et al., 1993). ADAM17, which is also known as tumour necrosis factor-α-converting enzyme (TACE) due to its ability to shed TNFα, is the most well-known sheddase. It has subsequently been shown to shed HB-EGF, TGFα, epiregulin, amphiregulin, IL-6 and β-cellulin amongst many other cell surface proteins (Gooz, 2010). The release of ligands for signalling by shedding has a wide range of roles from cell migration to cell fate determination to osteoclast differentiation and angiogenesis. In the case of ADAM15, an example of its shedding is that of E-cadherin which leads to an increase in β-catenin which initiates a signalling cascade to induce epithelial-mesenchymal transition and cell proliferation mechanisms (Najy et al., 2008b).

RIPping

Regulated intramembrane proteolysis (RIPping) is the cleavage of the intracellular domain of a transmembrane protein by a presenilin-containing γ-secretase complex. This process is regulated by ADAMs as the extracellular cleavage of the substrate by shedding is necessary for the binding of the nicastrin unit of the γ-secretase complex. While this is mainly a role fulfilled by ADAM10, other ADAMs can also be involved instead. Some examples of RIPping targets are Notch, CD44, ERBB4 and amyloid precursor proteins (Murphy et al., 2008).

Cellular Adhesion

Conflicting functions in cellular adhesion displayed by members of the ADAM family have made this topic a source for some debate. The ability of some ADAMs to solubilise adhesion molecules such as L-selectin, L1-CAM, VCAM1, CD44, E-cadherin and N-cadherin implies a role in reducing cellular adhesion. However, this is in contrast with the ability of other ADAMs to bind to syndecans and integrins through their disintegrin and cysteine-rich domains (Edwards et al., 2008; Seals, 2003).

1.2.3 Regulation of the ADAMs

Post-Translational Modifications

A primary form of post-translational modification of the ADAMs is the removal of the pro-domain by proprotein convertases such as furin which target conserved recognition sequences in the ADAM (Lum et al., 1998) thus activating enzymatic activity.

Another form of modification is phosphorylation. Many ADAMs require a change in the phosphorylation state of their ICD by intracellular kinases and phosphatases in order to function. For example, phorbol esters activate protein kinase C to phosphorylate ADAM9, thus increasing activity (Izumi et al., 1998). In the case of ADAM10, an increase in calcium in the cell causes an increase in ADAM10 mediated CD44 shedding although the mechanism and kinases involved are unknown (Stoeck et al., 2006).

Other major forms of post-translational modification involved in ADAM regulation are trafficking and cell membrane compartmentalisation. Most ADAMs are only active once presented on the surface of the cell and so incorrect trafficking would prevent the ADAM from its purpose (Seals, 2003). Additionally, some ADAMs need to be further localised on the cell surface in order to function such as ADAM10 targeting to adherens junctions of polarised epithelial cells where many of its substrates are present (Wild-Bode et al., 2006).

Finally, recycling is an important regulator of ADAM function through post-translational modification. For example, endocytosis of ADAM17 regulates activity. While phorbol esters increase the activity of ADAM17 via the action of protein kinase C, in the long term, the presence of phorbol esters leads to the endocytosis of ADAM17 (Doedens and Black, 2000).

Inhibitors

The main type of inhibitor to the ADAMs is the TIMP family. These co-ordinate with the Zn from the active site and thus prevent any metalloprotease functionality. TIMP-3 has been shown to inhibit ADAMs -10, -12, -17, -28 and -33 (Edwards et al., 2008). A second inhibitor is RECK (reversion inducing cysteine-rich protein with kazal motif), a

membrane-anchored glycoprotein, primarily a MMP-9 inhibitor that has also been shown to regulate Notch signalling via its inhibition of ADAM10 (Muraguchi et al., 2007).

Synthetic Inhibitors

Due to the many roles of the ADAMs in disease, as will be discussed shortly, a number of small molecule inhibitors have been developed. The ADAMs are sufficiently different to the rest of the Metzincin family to allow more specific inhibitors to be designed. For example, a number of ADAM17 inhibitors are in phase I trials but it is important to note that due to mechanism-based liver toxicity, several other inhibitors were halted in phase II trials (Edwards et al., 2008). Other ADAMs currently being targeted include ADAM10 which is being targeted due to its role in Her2 shedding in breast cancer (Moss et al., 2008).

1.2.4 Role of ADAM Family in Disease

Cancer

As the normal functions of the ADAM family proteins include cell proliferation, adhesion and ECM cleavage, it is not unexpected that the ADAMs are often implicated in cancers. Extracellular matrix (ECM) cleavage, such as ADAM9 cleavage of laminin, has a role in increasing metastasis and invasion (Mazzocca et al., 2005). Other repercussions of ADAM-mediated proteolysis include the release of many growth factors and chemokines which can lead to a number of processes in tumour cells such as proliferation or angiogenesis. The shedding and RIPping of N-/ E-/ VE- cadherin, along with that of selectins, ICAM1, VCAM1 and PECAM1, lead to altered tumour cell adhesion and changes to local vasculature (Edwards et al., 2008). Also, the ability of several ADAMs to interact with integrins and proteoglycans has implications for the ability of tumour cells to adhere to each other.

Inflammation

An important process in inflammation is the recruitment of leukocytes. This involves many of the substrates of the ADAMs including selectins, integrins and adhesion partners, PECAM1 and CD99 (Ponnuchamy and Khalil, 2008). An example is that of TNFR-

associated periodic syndrome, a chronic inflammatory disorder which is caused by mutations in TNF-R1 which prevent the shedding of this receptor by ADAM17 (Garton et al., 2006).

Other Diseases

For the purpose of this report, the role of ADAMs in cancer will be the focus, however ADAMs have been linked to many different diseases including asthma and Alzheimer's disease. ADAM33 expression is increased in asthma sufferers, as is ADAM8, although to a lesser extent. It is also usually over-expressed along with several polymorphisms that appear to be specific to asthma (Holgate, 2010). The mechanism underlying these observations is unknown.

ADAMs -9, -10 and -17 have been linked to Alzheimer's disease through their role as α-secretases which are required for altering the balance of amyloid precursor protein towards the non-amyloidogenic pathway. ADAM10 is the only ADAM to be shown to be reduced in the brains of patients (Deuss et al., 2008).

The ability of ADAMs to act as sheddases and as participatants in RIPing is associated with immunity. ADAM10 and ADAM17 are required for cleavage of LAG3, necessary for clonal expansion of lymphocytes. FasL is required to kill T lymphocytes after an antigen has been dispatched and this is also shed by ADAMs -10 and -17. ADAM10 also has links to the allergic response through the shedding of FcεRI and CD23 (FcεRII) which bind to IgE during this response (Murphy et al., 2008).

1.3 Introduction to ADAM15

ADAM15 follows the standard structure of the ADAM family and contains a furin-sensitive pro-domain, an active metalloprotease domain, a disintegrin domain, a cysteine-rich region, an EGF-like domain, a transmembrane region and an intracellular domain (Kratzschmar et al., 1996) as can be seen in figure 1.7. It exists in 11 potential splice variants with all the variation in the intracellular domain and was chosen for study here due to links to breast cancer prognosis as will be discussed further in 1.3.5.

1.3.1 Functions of ADAM15

Integrin Binding Ability

ADAM15 is one of the few ADAMs with the capability to interact with integrins through its disintegrin-like domain due to possession of the canonical RGD sequence required for this function (Zhang et al., 1998), although $\alpha_9\beta_1$ interacts here through an alternative sequence RXXXXXXDLPEF instead. Through this ability ADAM15 has been linked to cell adhesion and cell-cell interactions. For example, it has been shown to mediate cell adhesion to fibrinogen through $\alpha_v\beta_3$ by interfering with its function in such a manner that can also alter cell motility (Lu et al., 2010). In addition, it has been reported that $\alpha_5\beta_1$ was also an ADAM15 ligand (Kratzschmar et al., 1996) but it was later demonstrated that this was dependent on cellular source, with different cell lines responding differently in immunoprecipitation and immunofluorescence experiments. Despite this contradicting evidence for a direct interaction, it has been shown that ADAM15 can upregulate $\alpha_5\beta_1$ in chinese hamster ovary (CHO) cells via down regulation of ERK 1/2 phosphorylation (Ham, 2002).

Shedding

Unlike other highly catalytically active ADAMs such as ADAM17, which has a high number of substrates (Arribas and Esselens, 2009), ADAM15 has relatively few substrates for its metalloprotease function. One such substrate is CD23, otherwise known as FcεRII, which is a low-affinity receptor for IgE (Fourie et al., 2003). When cleaved by ADAM15, the soluble form of CD23 interacts with non-sensitised B-cells (those that have not become specific to an allergen) to increase the production of IgE (Acharya et al., 2010) whereas the membrane-bound version of CD23 binds to IgE, when it is bound to an allergen, to initiate an immune response.

Desmoglein-2 (Dsg-2) is another substrate of ADAM15 (Brooke et al., 2012; Klessner et al., 2009) that forms a transmembrane glycoprotein component of a type of cell-cell junction called a desmosome. Shedding of the extracellular domain of Dsg-2 removes its capability to anchor the junction to the desmocollin 1 component of a desmosome of a neighbouring cell, thus reducing cell adhesion.

Epithelial specific cadherin (E-cadherin) is also a reported substrate of ADAM15 (Acharya et al., 2010) which links ADAM15 catalytic function to cell adhesion changes through E-cadherin's role in adherens junction complexes (Klessner et al., 2009). Proteolytic cleavage of E-cadherin by ADAM15 causes a loss in cell contact integrity resulting in the dissolution of the adherens junction (Najy et al., 2008a). The soluble ectodomain of E-cadherin (sE-cad) can act as a competitive inhibitor of normal E-cadherin, disrupting its role in tissue integrity, wound healing, embryonic development and organ morphogenesis (Brooke et al., 2012). The sE-cad fragment can also stabilise HER2 and HER3 homodimerisation, initiating ERK-dependent signalling which increases cell proliferation, differentiation and survival (Gooz, 2010).

Proteolytic cleavage of neural cadherin (N-cadherin) by ADAM15 (Najy et al., 2008a) interferes with N-cadherin's role in such biological mechanisms as myoblast differentiation, migration and FGFR dimerisation (Derycke and Bracke, 2004). Additionally, the soluble fragment of N-cadherin generated has been implicated in increased angiogenesis and increased migration in wound healing assays.

Fibroblast Growth Factor Recepter 2iiib (FGFR2iiib) is most commonly expressed in epithelial cells and binds to stromal cell derived factor FGF7 with roles including proliferation, morphogenesis and tissue effects. While shedding of this receptor by ADAM15 has been demonstrated (Maretzky et al., 2009a), the full downstream function of this has yet to be elucidated.

1.3.2 Intracellular Domain Splice Variants of ADAM15

Eleven splice variants of the intracellular domain of ADAM15 exist. In this thesis, the nomenclature established by *Poghosyan et al* (2001, (Poghosyan, 2001)) will be used and the alternative nomenclatures used in the literature are listed in Table 1.1, along with the amino acid length of the whole proteins. A schematic of the exon usage in five of the splice variants is shown in figure 1.7.

Poghosyan Style (2001)	**Kleino Style (2009)**	**Uniprot**	**Amino Acids No**
D	1	Q13444-10	772
A	2	Q13444-2	814
	3a	Q13444-9	796
B	4a	Q13444-4	839
E	5	Q13444-5	838
C	6a	Q13444-3	862
	6b	Q13444-1	863
	7a	Q13444-7	821
	7b	Q13444-6	822
	8	Q13444-8	797
	9		809

Table 1.1 Nomenclature of the ADAM15 splice variants used in the literature. The Poghosyan style will be used here (Kleino et al., 2009; Poghosyan, 2001).

ADAM15 expression is widespread across a variety of tissues but the proportion of the potential variants varies by tissue, as can be seen in the heat map shown in figure 1.8. The placenta, for example, expresses high proportions of variants A, D and E but very little, if any, of the other variants. Other tissues, such as the spleen and peripheral leukocytes, have more varied expression profiles. Expression of ADAM15 variant A accounts for 58.6% of all ADAM15 expression across all tissues, followed by variant D at

11% and B/E at 7.6% It was not possible here to detect the differences in mRNA of variants B and E using the size dependent techniques applied (Kleino et al., 2009).

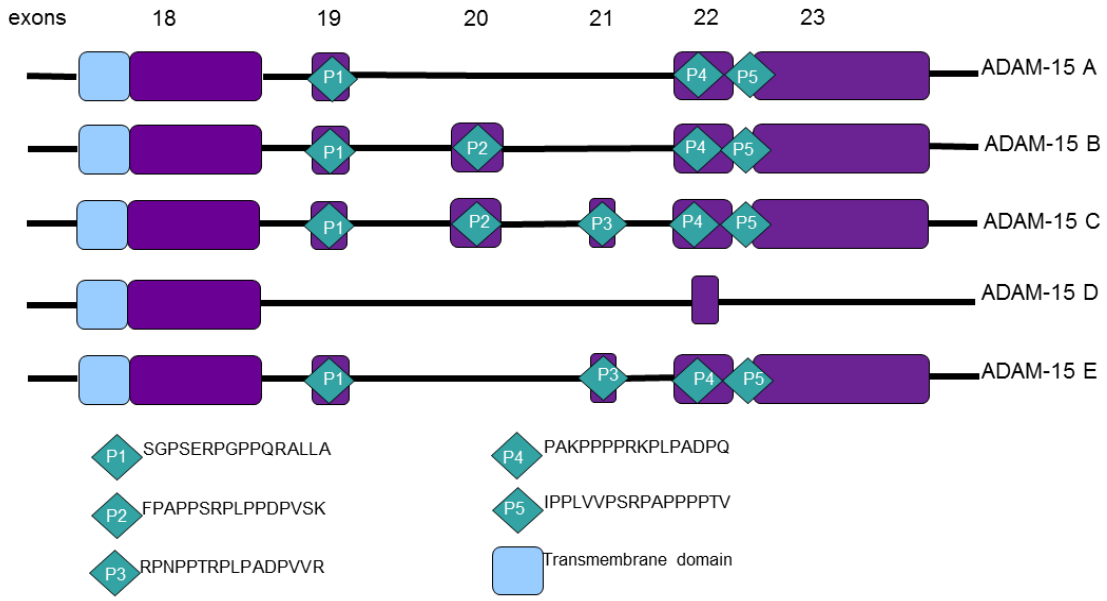

Figure 1.7 Schematic of the proline-rich regions of the ADAM15 ICD splice variants with the exons that encode for them indicated. Adapted from *Zhong et al* (2008, (Zhong et al., 2008)).

All the variants studied in this thesis contain two potential phosphorylation sites at tyrosine 735 and the penultimate residue at the C-terminus. The variants arise due to the variable inclusion of exons 19-22 during splicing, with the exception of D which also includes a frameshift after tyrosine 735 and this does not contain any of the proline-rich regions encoded by the exons of the intracellular domain, nor the terminal C-terminal tyrosine.

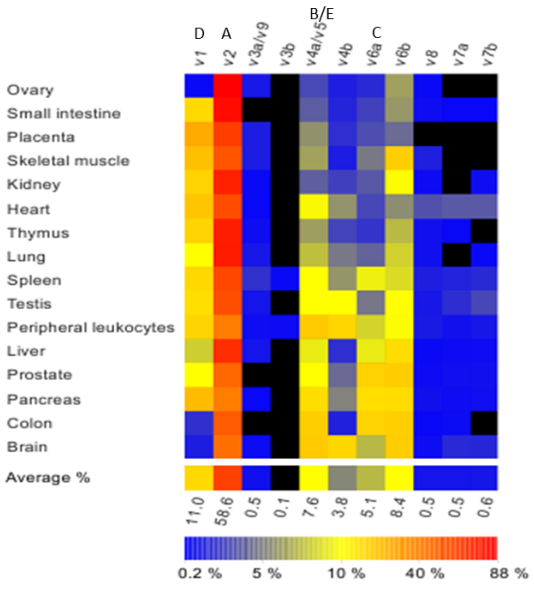

Figure 1.8 Heat map of the expression variability of the ADAM15 splice variants across different tissues. Adapted from (Kleino et al., 2007).

Proline-rich motifs including the sequence ΦPpΦP, where Φ is a hydrophobic residue and p can be another proline, can interact with Src homology 3 (SH3) domains via a left-handed poly-proline helix which aligns along a flat hydrophobic surface on the SH3 domain within which there are hydrophobic clefts. The ΦP sequences then sit within these clefts formed by conserved aromatic residues. Any binding specificity arises from interactions of the residues in the surrounding regions (Kaneko et al., 2008). There are two types of proline-rich motif possible within this general mechanism. Class I poly-proline motifs follow the general sequence +ΨPpΨP where the aliphatic (Ψ) residues is preferably hydrophobic to match the general sequence above and + indicates a basic residue. Class II poly-proline motifs follow the sequence ΨPpΨPp+. However, the thermodynamics for these interactions were unusual for what appears to be a simple interaction based upon hydrophobicity. This was explained by *Martin-Garcia et al* (2012, (Martin-Garcia et al., 2012)), as being due to the presence of highly conserved, tightly bound, structural water molecules found in many SH3 domains which act to add polar interactions across the interface. The proline-rich regions included in the splice variants of the ADAM15 intracellular domains (ICDs) are displayed in figure 1.7.

The interaction capability of the ADAM15 ICDs with SH3 domain-containing proteins has been established in a number of publications. Many of the proteins studied have similar phenotypic functions as ADAM15. In some cases, such as those of endophilin 1 and SH3PX1, the variant required has not been elucidated but it was shown that they only interacted with the pro form of ADAM15, implying a role in ADAM15 localisation (Howard et al., 1999). PACSIN3, which is necessary for ADAM12-mediated shedding of proHB-EGF, also interacts with the ADAM15 ICD (Mori, 2003). As endophilin 1 and SH3PX1 also bind to ADAM12, a crossover of functions between ADAM15 and ADAM12 could be suggested. Another such case is that of the Src family tyrosine kinase Fyn which can interact with the ADAM15 ICD and has overlapping roles in integrin signalling, T/B cell receptor signalling, cell adhesion and platelet activation (Poghosyan, 2001). The SH3 domain-containing protein Mad2 functions as a spindle checkpoint protein essential for transition of the cell from metaphase to anaphase during mitosis and preferentially interacts with the phosphorylated ICD of ADAM15 (Poghosyan, 2001), which also promotes cell proliferation as discussed before.

As with Mad2, the interactions of some SH3 domain-containing proteins with the ADAM15 ICD are phosphorylation dependent. Two such examples are Hck and Lck which show greater binding when the ADAM15 ICD is tyrosine-phosphorylated. In the case of Hck, ADAM15 is a substrate. In the case of Lck, the N-terminal tyrosine of the ADAM15 ICD was required for functional interaction, regardless of phosphorylation status (Poghosyan, 2001).

While some SH3-domain containing proteins preferentially bind to the ADAM15 ICD based upon phosphorylation status, others interact in a splice variant dependent manner. A summary of these can be seen in table 1.2 and include further studies into Hck and Lck.

SH3 Protein	ADAM-15 A	ADAM-15 B	ADAM-15 C
Nephrocystin	✓	N/A	✓
SNX33	✓	N/A	✓
SNX9	✓	N/A	✓
Tsk5/FISH I/V	✓	✓	✓
Src	✗	✓	✓
Lyn	✗	N/A	✓
Hck	✓	N/A	✓
Yes	N/A	N/A	✓
p47phox	✓	N/A	✓
p85α	✗	N/A	✓
Intersectin 1 3/5	✗	N/A	✓
Intersectin 2 3/5	✗	N/A	✓
Lck	✓	N/A	✓
Grb2	✓	✓	✓
Nck	✗	✓	✓
pERK	✓	✓	✓
Brk/PTK6/Sik	✓	✓	✗

Table 1.2 Summary of the preferential interactions studied across the literature. Techniques used to establish these interactions include Binding ELISA using a phage library, binding blot, co-immunoprecipitation assays (Kleino et al., 2009; Yasui et al., 2004) and pull down assays (Zhong et al., 2008). Interactions are indicated by a tick, no interaction a cross and those not investigated are highlighted by N/A.

Further confirmation that these interactions require the proline-rich regions of ADAM15, rather than any non-specific pathways, comes from *Kleino et al* (2009, (Kleino et al., 2009)). By repeating their interaction studies using synthetic peptides corresponding to the proline-rich clusters of the ADAM15 ICD, they confirmed the necessity of the proline-rich regions for many interactions and also indicated some preference for specific clusters by the SH3 domains as can be seen in figure 1.9. In some cases, this correlates with the variants they preferentially bind to and which proline-rich clusters those variants include. None showed significant interaction with the peptide corresponding to proline-rich region 1 as this contains a glycine residue within the PxxP motif, which is unusual and could potentially hinder any interaction through this motif.

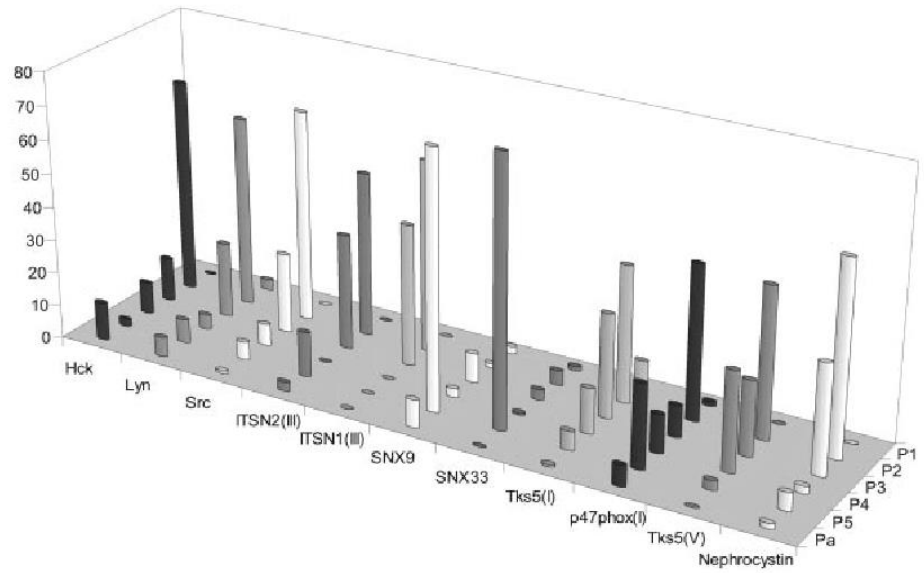

Figure 1.9 Selective binding of SH3 domains to different ADAM15 proline clusters. GST fusion SH3 domains were used to probe synthetic peptides corresponding the proline-rich clusters of the ADAM15 ICD (printed onto solid support). The height of the bar indicates the relative affinity of each SH3 domain within the set of proline cluster peptides and the bars were averaged from three parallel spots (Kleino et al., 2009).

The ADAM15 splice variant expression profile of a cell affects behaviour *in vitro*. In the cell line, MDA-MB-435, which express protein markers for both breast cancer and melanoma, those cells transfected with ADAM15 B, as opposed to ADAM15 A or a vector control, were less well spread, smaller and contained fewer, shorter actin fibres, despite displaying similar levels of vinculin, ERK 1/2, FAK, Src and pSrc (Poghosyan, 2001). In adhesion assays using these cells, those transfected with ADAM15 A demonstrated greater adhesion than those transfected with ADAM15 B. Poor cell adhesion was

exhibited by cells transfected with ADAM15 B even compared to the vector control, irrespective of the adhesion material (tissue culture plastic, fibronectin or laminin). These results were consistent with de-adhesion assays and in the breast cancer cell line, MCF-7. In scratch wound assays, ADAM15 A transfected cells migrated faster than ADAM15 B transfected cells or the vector control, also supported by Matrigel Invasion assays (Zhong et al., 2008).

1.3.3 Regulation and Inhibition of ADAM15

The mechanism of transcriptional regulation for ADAM15 expression has yet to be fully explored. Its promoter lies at -266 to -23 base pairs relative to the start of the *ADAM15* gene (Kleino et al., 2007) and contains potential binding sites for the transcription factors Sp1, p300, MZF1 and c-Ets. This promoter is sensitive to upregulation in response to VEGF and potentially to TNF-α, TGF-β and IL-1β (Murphy, 2009). The promoter for the *ADAM15* gene also contains seven adjacent series of 3 or more consecutive guanines which, when under superhelical stress, can relax from duplex form into intrastrand secondary G-quadruplex structures. These can function as a biological silencer for the gene and provide a potential therapeutic target (Brown et al., 2013).

As the expression of the different ADAM15 splice variants varies by tissue and they can lead to potential changes in cell behaviour (Kleino et al., 2007), along with preferential interaction profiles (Kleino et al., 2009; Zhong et al., 2008), it is highly likely that this is a form of regulation linked to function. Unfortunately, the full scope of this remains unclear.

The removal of the pro-domain of ADAM15 by the proprotein-convertase furin, controls the enzymatic function of the metalloproteinase. Despite furin inhibition preventing catalytic function in ADAM15 (Lum et al., 1998), it also inhibits catalytic function in other ADAMs too so this is a non-specific form of control. This may be controlled to some extent by the interactions of the ICD with certain SH3-containing proteins. Endophilin and SH3PX1 have been shown to only bind to pro forms of ADAM15 rather than mature forms although whether this has an effect on furin cleavage of ADAM15 is as yet unknown (Howard et al., 1999). It is also worth considering that the cleaved pro-domain

could potentially act as an inhibitory ligand to mature ADAM15. This is the case with ADAM10 but has not been investigated for ADAM15.

In terms of inhibition as opposed to regulation, TIMPs 2 and 3 have been shown to be the main inhibitors of ADAM15 although this inhibition is accomplished in a much less efficient manner than the inhibition of MMPs by TIMPs (Maretzky et al., 2009b). It has also been shown that recombinant forms of the ADAM15 disintegrin domain (RDD) can inhibit functions enacted by ADAM15 through its disintegrin domain (Lucas et al., 2009). This includes endothelial cell growth, migration and angiogenesis. This is a potential therapeutic strategy for inhibiting ADAM15 in diseases. ADAM15 makes a good therapeutic target not only due to its links to disease, especially cancer, but also due to the relatively innocuous phenotype of ADAM15 null mice, which are viable through development and fertile as adult animals (Bohm et al., 2005).

1.3.4 ADAM15 in non-cancerous disease

Angiogenesis Related Conditions

Although ADAM15 plays a role in developmental angiogenesis, it is not essential for angiogenesis to occur. However, in response to a synthesised peptide based upon the metalloproteinase domain of ADAM15 and VEGF stimulation, endothelial cells have exhibited increased proliferation, migration and tube formation which increased overall angiogenesis (Raiter et al., 2010).

Atherosclerosis is a condition of the artery wherein the artery becomes hardened due to the development of an atheromatous plaque formed by a build-up of cholesterol and macrophages. In the rabbit model for atherosclerosis, the progression of the conditions can be reduced by the expression of ADAM15 in a catalytically dependent manner (Bultmann et al., 2011). However, endothelial-mediated vasoreactivity is reduced by ADAM15 in a catalytically independent manner. This is contradicted by *in-vitro* studies on human atherosclerotic tissue where ADAM15 mRNA and proteins levels were elevated and increased further in response to PDGF. Increased expression of αvβ3 and α5β1 were linked to increased ADAM15 expression and these have been shown to increase platelet interactions (Al-Fakhri et al., 2003; Pelisek et al., 2012). Increased

ADAM15 in response to PDGF also initiated increased smooth muscle migration and proliferation. Additionally, knockdown of ADAM15 in ApoE-deficient mice led to reduction in aortic atherosclerotic lesion size and smooth muscle deposition. Further study showed that ADAM15 had a role in barrier dysfunction and monocyte transmigration across endothelial cell monolayers in a manner dependent on the intracellular domain of ADAM15, although only variant A was used and requires the presence of Src and Yes (Sun et al., 2012). It is clear that ADAM15 plays some role in atherosclerosis but what that is, and if it varies across species, is yet to be established.

Psoriasis lesions affect 2% of the population and these lesions form in a pro-angiogenic microenvironment. Interaction ability with pro-angiogenic integrins $\alpha_v\beta_3$ and $\alpha_5\beta_1$ potentially link ADAM15 to these conditions. Reduced endothelial cell migration *in vitro* and reduced vascularisation and blood flow in mice designed to exhibit reduced blood flow in response to a recombinant form of the ADAM15 disintegrin domain has been demonstrated and these results were supported by *in vivo* studies using psoriasis positive mice (Zibert et al., 2011).

Inflammatory Conditions

In normal intestinal tissue, ADAM15 is expressed in both the pro- and mature forms, while in colonic tissue, a previously undescribed post-translational modified form with a molecular weight between that of the pro and mature forms is seen, despite normal expression in the mRNA (Charrier-Hisamuddin et al., 2007). ADAM15 expression can be seen in healthy intestinal cell types including endothelial cells, pericryptic myofibroblasts and smooth muscle cells but not the myenteric cells or submuscosae (Mosnier et al., 2006). Protein and mRNA levels of ADAM15 are increased in the tissues of patients suffering from ulcerative colitis or Crohn's disease, although the splice variants involved have not been assessed. Leukocyte-endothelial cell-cell interactions, which are involved in inflammatory pathways, have been demonstrated in endothelial cells expressing ADAM15, in a manner dependent on the presence of the RGD sequence in the ADAM15 disintegrin-like domain (Charrier-Hisamuddin et al., 2007).

Similarly, ADAM15 is up-regulated in inflammation and sepsis and mediates endothelial hyperpermeability. The microRNA, miR-147b, targets the 3' UTR of *ADAM15*, decreasing

total and cell surface expression of ADAM15 in endothelial cells (Chatterjee et al., 2014). This then reduced LPS-induced barrier dysfunction across endothelial monolayers, further underlining an inflammatory role for ADAM15. Further to this, ADAM15 expression was found in association with pulmonary oedema in mice suffering LPS-induced inflammatory lung injury with high levels seen in endothelial cells but not in neutrophils, despite increased neutrophil transmigration across the endothelial barrier. Considered together, this shows that ADAM15 has a role in hyperpermeability and neutrophil transmigration in acute inflammatory lung injury (Sun et al., 2013).

Finally, proteolytic cleavage of TIR-domain-containing adapter-inducing interferon-β (TRIF) by ADAM15 removes the ability of TRIF to facilitate Toll-like receptor (TLR) 3 and 4 signalling and thus reduces activation of the transcription factors NFκB and IFN signalling which initiate production of pro-inflammatory cytokine production. This is the first time a role for ADAM15 has been seen in TLR signalling (Ahmed et al., 2013).

Degenerative Joint Conditions

The link between ADAM15 and osteoarthritis (OA) was first established by the increased severity of OA in older mice and accelerated osteoarthritic lesions in ADAM15 null mice with male mice affected more severely and earlier than female mice (Bohm et al., 2005). This is supported by the increased ADAM15 mRNA and protein in the immortalised chondrocyte cell line, T/C28a4, which also demonstrated increased adhesion to type II and IV collagen but not fibronectin in an integrin-dependent fashion requiring the RGD motif of ADAM15. Additionally, those cells overexpressing ADAM15 showed a decrease in caspases 3 and 7 and an increased in the caspase 3 inhibitor, XIAP (Bohm et al., 2010). The longer survival rates induced by this in chondrocytes can allow a collective build-up of cell damage due to stress which leads to OA and is more damaging for the joint in the long term through articular cartilage loss and subchondral bone damage.

The expression levels of ADAM15 are even more extreme in rheumatoid arthritis (RA) across multiple tissue layers in the joint including endothelial cells and immune cell filtrates suggesting a role in the recruitment of immune cells to the joint (Bohm et al., 2001). The ADAM15 substrate, CD23, which functions to recruit non-specific B-cells and increase the inflammatory response, is also upregulated in RA in both the cleaved and

intact forms (Bonnefoy et al., 1996). Due to the highest levels of expression of ADAM15 being at the border of the cartilage destruction, it has been suggested that ADAM15 could be degrading cartilage directly although this has yet to be proven experimentally (Bohm et al., 2001). Given the raised angiogenesis observed in RA positive joints, the evidence strongly implicates ADAM15 in RA pathology. More recently, RA synovial fibroblasts have been shown to avoid apoptosis upon FasL exposure by phosphorylating FAK and c-Src in an ADAM15 dependent fashion, indicating ADAM15 as a potential target for therapy in rheumatoid arthritis (Bohm et al., 2013). A similar study which silenced ADAM15 in human fibroblast-like synoviocytes (FLSs) indicated suppression of pro-inflammatory cytokines and chemokines preventing cell migration and invasion via inhibition of VEGF-A, MMP1 and MMP3, via LPS stimulation (Gao et al., 2015). Silencing ADAM15 in collagen-induced arthritis (CIA) rats reduced the arthritis score and the extent of joint damage (Gao et al., 2015) thus supporting the potential of ADAM15 as a therapeutic target in rheumatoid arthritis.

Human Immunodeficiency Virus (HIV)

The expression of another member of the ADAM family, ADAM10, in $CD4^+$ T lymphocytes is required for infection by the more common and virulent HIV-1 strain. This is also dependent on the expression of ADAM15 and γ-secretase, which are responsible for ADAM10 proteolytic processing, supporting a model whereby the processing of ADAM10 releases the ICD which then incorporates with HIV-1 Pre-Integration Complex (PIC), facilitating nuclear trafficking (Endsley et al., 2014).

Intrauterine Adhesions

Intrauterine adhesions are uterine blockages which can develop sporadically and as a complication of operative hysteroscopy, caesarean section, normal delivery and infections such as tuberculous endometritis, causing infertility, recurrent miscarriages and irregular periods. The protein and RNA levels for both ADAM15 and ADAM17 are significantly raised in intrauterine tissues, particularly in the most severe forms although the specific relevance of this is as yet unclear (Liu et al., 2013).

1.3.5 ADAM15 in cancer

ADAM15 has been shown to have both tumour promoting and tumour inhibiting functions depending on the location of the primary tumour. For example, ADAM15 is released into the extracellular space within an exosome and those exosomes which are rich in ADAM15 have tumour suppressing capabilities across a number of cancerous cell lines including MCF-7 (human breast adenocarcinoma), NCI-H460 and A549 (human lung carcinoma), MDAH2774 (human ovarian adenocarcinoma) and SK-MEL-28 (human melanoma) (Lee et al., 2012). The ectodomain of ADAM15 can be shed from these exosomes and, in a similar manner to the ADAM15-rich exosomes, reduced vitronectin-induced cell migration and activation of the MEK-ERK pathway in MDAH2774 cells (Lee et al., 2014). Further examples of the role of ADAM15 in various types of cancer will be discussed here although the future focus of this study will be on those interactions involved in breast cancer.

Colon Carcinoma

Colon carcinoma exhibits reduced ADAM15 in 23% of cases with a corresponding loss of differentiation. ADAM15 substrates, E-cadherin and $\alpha_3\beta_1$, are reduced here as they are in epithelial-mesenchymal transition (EMT), a process which is deregulated during metastasis, increasing the migratory potential of the cancerous cells (Toquet et al., 2012).

Primary Melanoma versus Metastatic Melanoma

Melanomas arise from melanocyte cells in the skin which are responsible for melanin production. Primary melanoma has a good survival rate of around 95% when discovered early (2011c). Metastatic melanoma, by comparison, has a survival rate of less than 15% if the metastases are distant. ADAM15 has been shown to be significantly reduced in metastatic melanoma compared to primary melanoma in a manner that can be regulated by TGF-β (Ungerer et al., 2010). Where ADAM15 was expressed, migration and invasion was reduced, implying that ADAM15 is acting in a tumour suppressor role. Although variants A-D are all expressed in melanoma, D is the primary isoform expressed although, as there has been no function established for variant D, why this is the case is unclear (Ungerer et al., 2010). However, contrary to these findings, later stage

melanoma tumours were smaller in ADAM15 null mice compared to wild type along with fewer metastases in the lungs and lymph nodes which implies that ADAM15 is contributing to metastasis formation (Schonefuss et al., 2012). This contradiction, and thus the role of ADAM15 in melanoma, has yet to be resolved.

Intra-tumoral electrotransfer of a plasmid encoding the recombinant disintegrin domain of ADAM15 (pRDD), into B16F10 melanoma-bearing C57BL/6 mice, induced a significant inhibition of tumour growth and, after removal of the primary tumour, an 84% reduction of tumour metastasis. Additionally, pRDD decreased cell proliferation in B16F10 primary tumours while not affecting normal skin blood flow (Daugimont et al., 2011).

Prostate Cancer

Levels of ADAM15 expression have been linked to the progression of metastatic prostate cancer as have the loss of a type of structural junctional complex, desmosomes. A key component of desmosomes is Dsg-2, a substrate of ADAM15 (Shiina et al., 2005). The cleavage of ADAM15 substrates, E-cadherin and N-cadherin has been demonstrated in prostate cancer cell lines, reducing cell-cell interaction and encouraging metastasis (Lucas and Day, 2009).

Angiogenesis is vital for tumour growth beyond 1 mm and prostate cancer is no exception (Lucas and Day, 2009). As previously discussed, ADAM15 increases angiogenesis in a VEGF- and angiopoetin-1-dependent manner but, additionally and specifically in prostate cancer, ADAM15 up-regulation increases production of the pro-angiogenic MMP9 (Bergers et al., 2000). Increased MMP9 has separately been linked to increased invasiveness in prostate cancer.

Finally, when ADAM15 is knocked down in the prostate cancer cell line, PC-3, adhesion to laminin, vitronectin and fibronectin is reduced (Lucas and Day, 2009).

Pancreatic Cancer

When considering pancreatic ductal adenocarcinoma tissue samples, two proteins, ADAM15 and MHC class 1 polypeptide-related sequence B (MICB), were found to be expressed at higher levels than in normal pancreatic tissue. MICB is a ligand for the NKG2D type II receptor and thus induces a cytolytic response. MICB expression was

inversely correlated to ADAM15 expression, with higher ADAM15 expression in the more advanced cases of the disease. When ADAM15 was knocked down, the concentration of MICB on the cell surface increased and the concentration of soluble, cleaved ectodomain form of MICB (sMICB), which has been previously linked to poor differentiation and high tumour stage cells, was reduced in the culture supernatants but mRNA levels for the protein remained unchanged. It was concluded that ADAM15 was involved in the shedding of MICB in PANC-1 cells, thus decreasing MICB NKG1D-mediated toxicity (Xiaohui Duan, 2013).

Breast Cancer

ADAM15 expression levels are significantly raised throughout the progression of breast cancer pathogenesis, with the highest levels in the most aggressive tumours (Kuefer et al., 2006). Loss of the ADAM15 substrate, E-cadherin, has been used as an indicator of poor prognosis in breast cancer, encouraging migration and reducing cell adhesion, and the soluble form, sE-cad, inhibits cell aggregation and increases cell invasion. Additionally sE-cad can interact with HER2 and HER3, under conditions of growth factor deprivation, leading to their dimerisation and initiation of ERK signalling. The downstream effects of ERK signalling are increased cell survival, proliferation and migration, all of which promote tumour growth. ADAM15, alongside ADAM17, mediates another mechanism involving ErbB receptors, that of thrombin-induced EGFR signalling (Najy et al., 2008b).

Recently, a link between the ADAM15 splice variants and prognoses in certain subtypes of breast cancer have been described, Variants B and C were more highly expressed in breast cancer tissue compared to normal, but A and D levels were unaffected. In a longer term study, following up patients over a period of approximately 15 years, those patients suffering from node-negative cancer but whose primary tumours expressed higher levels of A and B, appeared to have a poorer prognosis whereas the levels of C had little difference. By comparison, in those patients suffering from node positive cancers, the expression levels of A and B in tumours had no effect on prognosis but higher levels of C correlated with an improved prognosis (Zhong et al., 2008), as can be seen in figure 1.10.

It has been suggested that the preferential interaction profiles of the splice variants with proteins that contain SH3 domains could be responsible for the correlation between prognosis and expression level. This is further supported by the significant role of some of the SH3 domain containing proteins that show such preferential interactions. The manner in which these interactions take place will be investigated in this thesis.

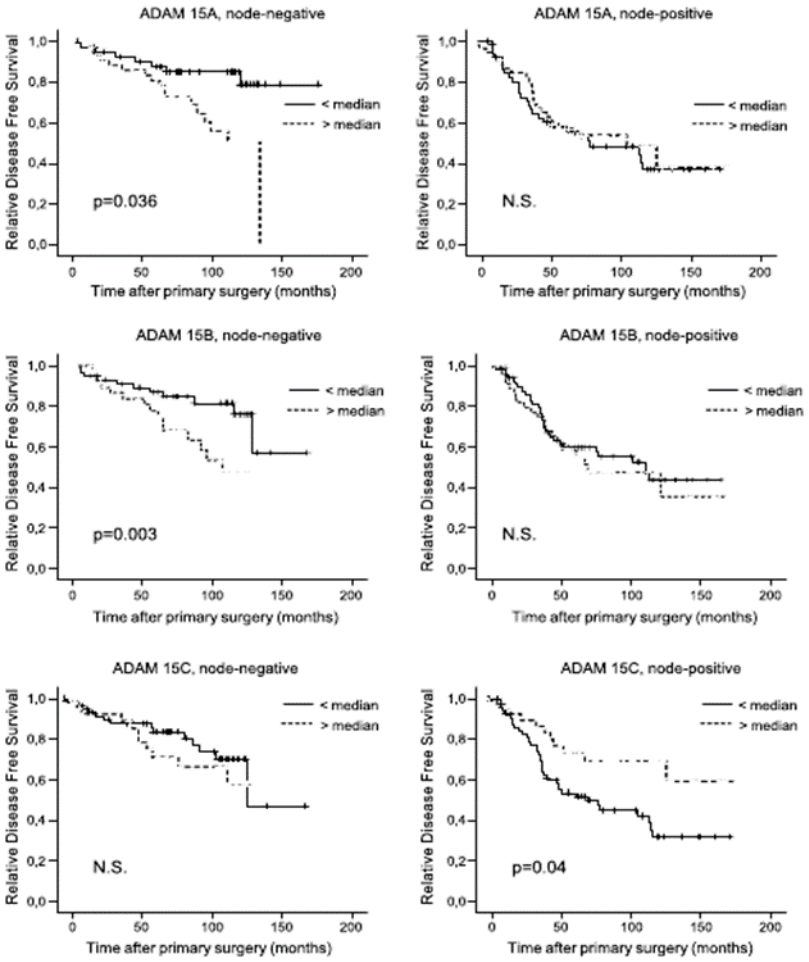

Figure 1.10 Relationship between ADAM15 splice variants expression levels and disease-free survival in non-negative and node-positive tumours. The mRNA for each variant was quantified for 229 patients and the clinical outcome studied. The cohort was split into <median and > median expression levels and then the time after surgery was plotted against disease free survival. Taken from *Zhong et al* (2008, (Zhong et al., 2008))

1.4 SH3 domain containing proteins

Due to their strong, independent links to breast cancer and their interactions with the splice variants of the ICD of ADAM15, three SH3 domain containing proteins have been selected for further study here. These are Grb2, Src and Brk.

1.4.1 Growth Factor Receptor-Bound Protein 2 (Grb2)

Grb2 is a ubiquitously expressed adapter protein consisting of an SH2 domain flanked by two SH3 domains, as can be seen in figure 1.11, that is involved in multiple signalling transduction pathways and is encoded by the *GRB2* gene. Ablation of this gene in mice is embryonic lethal at an early stage highlighting roles for the protein in development and cell proliferation (Jang et al., 2009). Highly conserved across multiple species, the human *GRB2* gene and its Drosphilia *drk* homologue, can be used to replace the *sem-5* gene in *Caenorhabditis elegans* cell signalling (Tari and Lopez-Berestein, 2001).

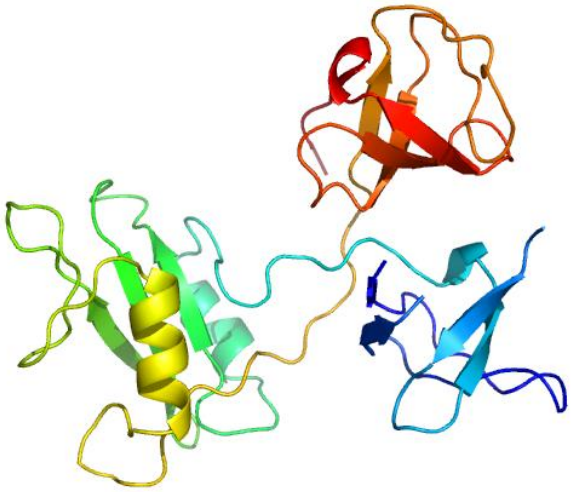

Figure 1.11 Structure of Grb2 based on the crystal structure pdb 1GRI with N-terminal SH3 domain in blue, the central SH2 domain in green and the C-terminal SH3 domain in red (Maignan et al., 1995).

Functions of Grb2

The primary, and most well-known, function of Grb2 is as an adapter protein working to bring Son of Sevenless 1(Sos1), a guanine nucleotide exchange factor, and Ras to within spatial proximity. This allows GDP-GTP exchange to be undertaken by Sos1, this activating Ras (Giubellino et al., 2008). Sos1 and Ras are localised to different regions of the cell when Grb2 is lacking. The central SH2 domain of Grb2 interacts with pYXRX

motifs on the intracellular domain of various receptor tyrosine kinases, such as EGFR, hepatocyte growth factor receptor (HGFR) and platelet-derived growth factor receptor (PDGFR) and with Sos1 via the N-terminal SH3 domain in a 2:1 ratio of Grb2 to Sos1 (McDonald et al., 2012a). Once activated, Ras signalling is responsible for cell growth, proliferation, apoptosis, actin cytoskeleton integrity changes, cell adhesion changes and migration, thus making Grb2 influential in cell processes (Tari and Lopez-Berestein, 2001).

The SH3 domains of Grb2 can be phosphorylated, the physiological context of which is yet to be fully explored. This phosphorylation was required for the inhibitor effect of prolactin on EGF signalling to MAPK activation and cell proliferation. Prolactin is a differentiation factor in mammary epithelial cells so, if Grb2 is not phosphorylated, mammary precursor cells are not capable of differentiation in response to prolactin (Haines et al., 2009).

Grb2 has also been shown to have a role in T and B cell antigen receptor stimulation. In thymocytes, which are hematopoietic progenitor cells which differentiate into mature lymphocytes, Grb2 regulates T-Cell receptor (TCR) induced activation of MAPKs p38 and JNK via control of Lck signalling (Jang et al., 2009). In the absence of Grb2, Lck signalling is dramatically reduced although the mechanism by which this control is conducted is unclear. Influence over TCR signalling cascades in thymocytes grants Grb2 some measure of control over positive and negative cascades that result in cell proliferation, differentiation, cytokine production, T-cell development and homeostasis.

The ability of SH3 domains, such as those in Grb2, to interact with proline-rich motifs is employed in the clathrin-dependent internalisation of ADAM12. Ablation of Grb2 markedly reduces this internalisation thus regulating ADAM12 behaviour in ectodomain shedding, cell-adhesion and signalling (Stautz et al., 2012a).

It has also been shown that dimeric Grb2 will bind to two Fibroblast Growth Factor Receptor 2 (FGFR2) molecules, thus forming a 2:2 heterodimer. The proximity generated allows FGF binding and the FGFR2 cytoplasmic tail kinase domains to cross-phosphorylate themselves and cause a conformational shift, thus causing Grb2

phosphorylation and release. The FGFR2 kinase domains can then transphosphorylate themselves further and initiate downstream signalling (Lin et al., 2012).

Grb2 in Cancer

Grb2 has been linked to cancer in many ways, a selection of which will be discussed here. On a genetic level, the location of the human *grb2* gene, chromosome 17 (q22) is within a region known to be highly duplicated in solid tumours and leukaemias. In chronic myeloid leukaemia (CML), the oncoprotein, Bcr-Abl, will bind to the SH2 domain of Grb2, linking this mutant protein to the Ras pathway, thus initiating cell processes such as proliferation, adhesion, apoptosis and migration which are all manipulated during cancer development (Huebner et al., 1994).

The SH2 domain of Grb2 can also bind to FAK, once it has been phosphorylated by Src, leading to integrin adhesion and deregulation of E-cadherin (Schlaepfer et al., 1994). The subsequent E-cadherin/N-cadherin switch is a hallmark of epithelial-mesenchymal transistion which is necessary for cancer progression (Hazan et al., 2004). Repression of the ability of the SH2 domain to interact with pYXRX motifs inhibits migration *in vitro* and tumour dissemination in animal models, thus corroborating Grb2 SH2 domain involvement. Interacting with FAK also enables FAK to initiate Ras and ERK2 pathways, the downstream effects of which include the ability of cells to spread through actin cytoskeleton rearrangement (Schlaepfer et al., 1998).

This is not the only connection of Grb2 to the actin cytoskeleton as it can interact directly with the actin filament machinery via a regulator of actin cytoskeleton rearrangement, WASp (She et al., 1997). Patients with mutations in WASp possess functional defects in their platelets, T and B cell polarisation and the ability of cells to migrate in response to external stimuli. Binding of WASp to Grb2, via the SH2 domain, translocates cytosolic WASp to the membrane where it can interact with Rac, Cdc45 and EGFR and stimulate signalling. When in a heterotrimer with Nck, the complex stabilises actin-nucleating complexes, a process which promotes cell migration via lamellipodia (Scaplehorn et al., 2002). Another heterotrimer including Grb2, that of EGFR-Grb2-PAK1, is also required to EGFR-induced lamellipodia formation (Puto et al., 2003).

An important process in the metastasis of solid tumours to secondary locations is the process by which cancerous cells exit capillaries (extravasation). Grb2 is associated with this process by interactions with L-Selectin (Brenner et al., 1996). Selectins mediate adhesion of cancer cells to endothelial cell luminal surfaces, allowing the cells to lodge at a secondary location and exit the blood vessel in a process more typically used by lymphocytes (Witz, 2006). Increased selectin ligands and upregulation of L-Selectin expression have been linked to increased metastasis to the lymph nodes (Qian et al., 2001).

In breast cancer, Grb2 is upregulated in several breast cancer cell lines, including MCF-7, MDA-MB-361 and -435 cells, enhancing Ras signalling to modify behaviour of the cells. In primary breast tumours, there is a two fold increase in Grb2 mRNA compared to normal breast tissue. The overexpression of Grb2 mRNA is even more pronounced in primary breast cancer tissue that express low levels of EGFR, implying that Grb2 amplifies signalling downstream from the receptor (Kairouz and Daly, 2000).

Also in breast cancer, Grb2 is required for transforming growth factor β (TGF-β) stimulation of EMT and invasion in mammary epithelial cells (MECs). The TGFβ type II receptor (TβR-II) is phosphorylated on tyrosine 284 by Src, providing a binding site for the SH2 domain of Grb2. Ablation of this interaction impaired stimulation of p38 MAPK in MECs but not Smad3 and prevented cells from undergoing EMT or invade synthetic basement membranes. In mice models, TβR-II phosphorylation of Y284 is necessary for TGFβ stimulation of breast cancer growth and pulmonary metastasis via p38 MAPK (Galliher-Beckley and Schiemann, 2008).

In a final example, lemur tyrosine kinase 3 (LMTK3) –induced CDC45 activation requires the interaction of LMTK3 with Grb2. LMTK3 promotes metastasis in breast cancer by inducing transcription of genes encoding integrin subunits, leading to an increase in actin cytoskeleton remodelling, focal adhesion formation and adhesion to collagen and fibronectin in culture (Xu et al., 2014b).

Grb2 as a therapeutic target

Due to the diverse links between Grb2 and various forms of cancer, it is unsurprising that Grb2 makes a tempting therapeutic target and a number of approaches have been

undertaken. The majority of these focus on interfering with the function of the SH2 domain interacting with RTKs. For example, the general transcription inhibitor, actinomycin D prevents the interaction of the Grb2 SH2 domain with Shc and thus reducing tumour cell cycle progression (Kim et al., 2005b; Kim et al., 1999). Blocking the SH2 domain with recombinant peptide ligands or synthetic small molecules that mimic the target binding motif of RTKs has proven to be effective in some cases. Unlike other SH2 domains in the Src family, Grb2 preferentially binds to motifs that include an arginine at the pY+2 position in the recognition site and that also have a β-bend configuration (Kessels et al., 2002) which reduces the cross-reactivity of potential therapeutics. Such antagonists have been shown to potently block HGF-stimulated cell motility and matrix invasion along with morphogenetic events required for angiogenesis (Atabey et al., 2001). In a murine syngeneic melanoma cell line (B16-F1) metastasis model, there was a significant reduction in metastatic burden in the presence of a prototypical Grb2 SH2 domain binding antagonist (Giubellino et al., 2007). Also recombinant forms of the SH2 domain have been used to competitively inhibit the full length Grb2 protein function with regards to RTKs and thus suppressed breast cancer cells growth and migration (Yin et al., 2013).

Due to low affinities between SH3 domains and their target proteins and the strong overlap of target proteins for SH3 domains in different proteins, it is more difficult to design inhibitors specifically to the SH3 domains of Grb2. However, the function of the SH2 domain does require Grb2 to be localised to the membrane edge. This does reduce the number of practical targets. Some synthetic peptides have been designed to reduce the influence of Grb2 in cancer progression with mixed success although it was possible to reduce proliferation of cells in CML. In terms of small molecules, a selection have been identified that compatibly interfere with the interaction of the C-terminal SH3 domain of Grb2 and Shc with moderate to low affinities. Of those molecules, those based upon dihydro-s-thrazine scaffold are the most successful (Simister et al., 2013).

As can be see here, Grb2 is an important protein in both healthy and cancerous cells and so any interactions with the ADAM15 ICDs could be playing a role in signalling that can allow cells to survive apoptosis and cell precipitation and thus are worthy of further study.

1.4.2 The proto-oncogene, tyrosine kinase Src

A key protein superfamily in cell signalling is that of the Src family tyrosine kinases. Members of this family engage with receptor tyrosine kinases and integrins and are involved in signalling via both potential partners. Src, named for the viral counterpart's ability to cause sarcomas in chickens (Src Rous sarcoma virus) is a cytoplasmic tyrosine kinase with a length of 536 residues in the human form encoded at the chromosomal locus 20q11. It is ubiquitously expressed, with comparative genes across the range of metazoan evolution, and contains two phosphorylation sites at tyrosines 419 and 527 crucial to the activation of the kinase. Beginning at the N-terminus, Src contains a unique domain, sometimes called an SH4 domain, an Src Homology 3 (SH3) domain, an SH2 domain, a proline-rich linker sequence, a tyrosine kinase domain, also known as an SH1 domain, and a C-terminal tail (Wheeler et al., 2009). The unique (SH4) domain acts as a target for myristolation thus targeting it to the cytoplasmic membrane where it is anchored by the C-terminal tail. The SH3 and SH2 domains work together to regulate the catalytic activity of the tyrosine kinase domain through their ability to interact with proline-rich sequences and phosphotyrosine containing short motifs respectively. The phosphorylation site at Tyr527 is phosphorylated which then internally interacts with the SH2 domain which positions the SH3 domain to interact with the proline-rich linker region. This "closed" conformation prevents catalytic activity of the tyrosine kinase domain. If Tyr527 is dephosphorylated, the protein "opens" which allows the autophosphorylation of Tyr419, activating the kinase and freeing the other domains for their functional interactions (Okada and Nakagawa, 1989). This process is illustrated in figure 1.12.

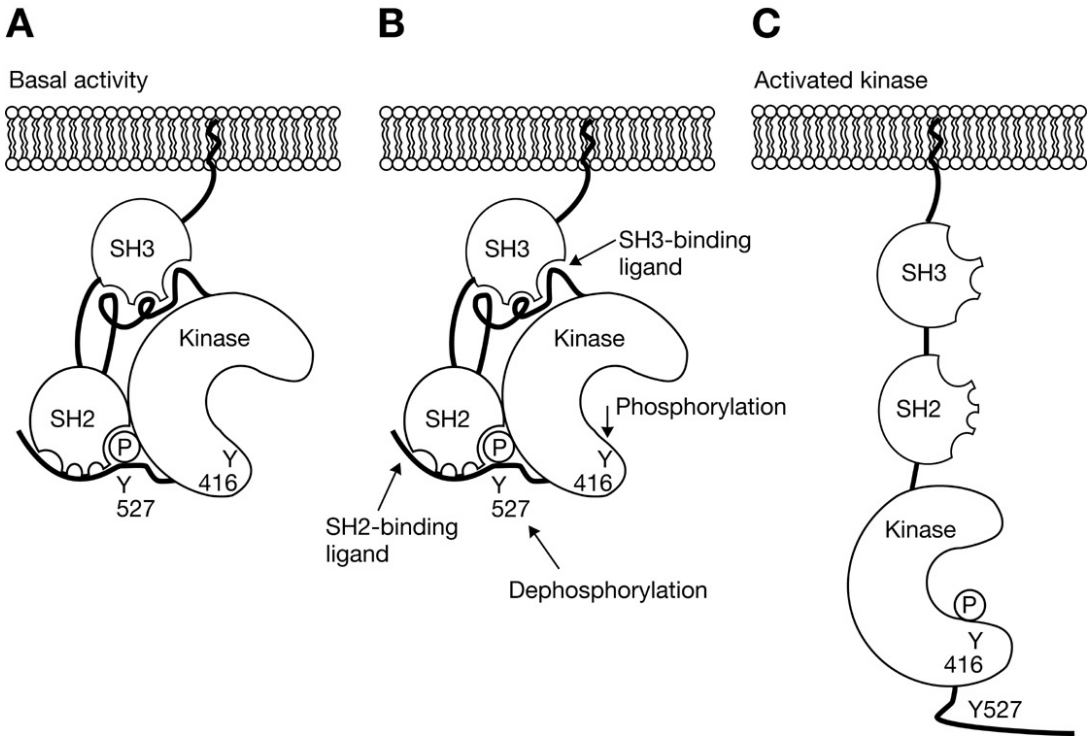

Figure 1.12 Structural changes during Src activation, A) Inactive Src, held in the "closed" conformation by phosphorylated Tyr527 interacting with the SH2 domain allowing the SH3 domain interaction with the linker region. B) Dephosphorylation of Tyr527 leads to autophosphorylation of Tyr416, releasing the SH2 domain and thus the SH3 domain. C) Active Src in the open conformation. Taken from (Elsberger et al., 2009)

Functions of Src

The kinase domain of Src catalyses the following reaction:

$$MgATP^{1-} + \text{protein} - O{:}H \longrightarrow \text{protein} - O{:}PO_3^{2-} + MgADP + H^+$$

The introduction of a phosphoryl group can activate other signalling proteins and initiate signalling with a variety of downstream effects (Roskoski, 2015). Dephosphorylation of the C-terminal tyrosine in Src can be achieved by a range of tyrosine phosphatases (Alonso et al., 2004) or the requirement for dephosphorylation of Tyr527 can be over-ridden by phosphorylation of Tyr213 in the SH2 domain, removing the inhibitory effects of pTyr527 and allowing activation. This second pathway can be achieved by the interaction of the SH2 domain of Src with the intracellular kinase domains of a range of receptor tyrosine kinases such as PDGFR, VEGFR, EGFR, HER-2 and -3, mitogen-activated protein kinase extracellular signal-regulated kinase -2 and colony-stimulating factor 1

receptor, thus allowing external stimuli to initiate internal signalling pathways (Stover et al., 1996).

Due to the wide range of proteins with which Src can interact, along with the variety of cell mechanisms which Src can activate, Src has been described as a "signal-transduction hub" co-ordinating intracellular responses to extracellular stimuli. Some examples of these cell mechanisms can be seen in figure 1.13 and a selection will be discussed here.

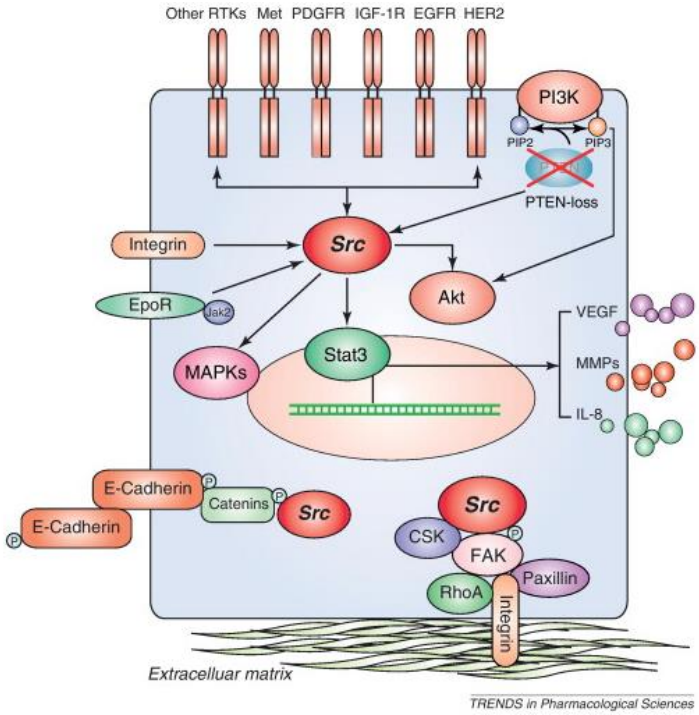

Figure 1.13 Examples of the signalling pathways in which Src plays a pivotal role including cell adhesion, receptor tyrosine kinase signalling and the Akt pathway leading to downstream events such as angiogenesis and inflammation. Taken from (Zhang and Yu, 2012).

Src is able to regulate the cell cycle and proliferation by suppressing regulators such as $p27^{KIP1}$, otherwise known as cyclin-dependent kinase inhibitor 1B, which prevents activation of cyclinE-CDK2 or cyclinD-CDK4 complexes, retaining cells in the G1 phase and preventing cell division (Riley et al., 2001). Additionally, in normally quiescent cells, signalling downstream from Src can induce the expression of cyclins D1, E and A which progress cells through the S and G2 phases of cell division. In addition to regulating cell proliferation, Src protects cells from apoptosis by activating anti-apoptotic signalling proteins such as PI3K and ERK1/2 (Johnson et al., 2000).

Cell-cell adherens junctions and cell matrix focal adhesions can also be negatively regulated by Src signalling via the redistribution of component proteins including FAK, cadherins and catenins (Fincham and Frame, 1998; Sheppard, 2000), thus destabilising focal adhesions and the suppression of E-cadherin localisation to adherens junctions (Serrels et al., 2009).

Negative regulation of cell adhesion by Src is complemented by the roles Src plays in the promotion of cell migration. Firstly, Src can promote the expression of cortactin through interactions with FAK (Kanner et al., 1990). Cortactin promotes migration by recruiting Arp2/3 complex proteins to the actin filaments, stabilising nucleation sites for actin branching within the cytoskeleton at the leading edge of migrating cells. These form invadopodia and facilitate cell migration (Chan et al., 2009; Weaver et al., 2001).

A final example of the diverse functions of Src is that of angiogenesis. Src can regulate VEGF expression via STAT3 thus increasing migration of endothelial cells, mitosis of endothelial cells, MMP activity and $\alpha_v\beta_3$ expression thus creating fenestrations and blood vessel lumens and the generation of new blood vessels (Cheranov et al., 2008).

The interaction of ADAM15 and Src has been shown to be important in conferring the ability of ADAM15 to initiate shedding of FGFR2iiib. ADAM15 variants A and B were compared for their ability to shed FGFR2iiib (Maretzky et al., 2009a). While Cos7 cells transfected with ADAM15 A displayed an increased ability to shed FGFR2iiib when compared to a proteolytically inactive mutant, ADAM15 B showed even higher levels of shedding ability, despite equal protein expression levels of each variant. This effect was confirmed as direct as knocking out ADAM9, which can also shed FGFR2, had no effect. The interaction of ADAM15 with Src was shown to be necessary for this shedding to occur as inhibiting Src with dasatinib or PPI reduced the ADAM15 B dependent shedding of FGFR2 in a dose-dependent manner. When repeated in Src -/- mouse embryonic fibroblasts (mEFs) the shedding of FGFR2 was comparable for both ADAM15 variants A and B. Also, if tyrosine 735 of ADAM15 B was removed, it was not possible for Src to activate ADAM15 mediated shedding. If this tyrosine residue was removed, the shedding ability of ADAM15 B was reduced to the levels of ADAM15 A.

Src in Cancer

All of the cell mechanisms in which Src plays a role, as discussed above, are deregulated in cancerous cells which heavily implicates Src in the development of cancer. As with the functions of Src, these are too varied to discuss in full here but a few examples will be considered focusing particularly on the role of Src in breast cancer.

Elevated Src levels have been observed in glioblastoma (Kleber et al., 2008) and cancers of the prostate (Posadas et al., 2009), pancreas (Fu et al., 2006), lung (Mazurenko et al., 1992) and breast (Verbeek et al., 1996), with some cancers demonstrating increased activity of Src with normal protein levels and others demonstrating increased protein levels (Cartwright et al., 1989). Higher expression of Src has been correlated with malignancy, especially in tumours with a high metastatic potential, with expression being inversely correlated with proliferative stage, size and grade of tumour (Boyer et al., 2002). For example, increased expression of Src correlates with progression of colonic polyps to primary lesions and liver metastases and indicates a poor prognosis in colon carcinoma (Talamonti et al., 1993).

The impact of Src expression on breast cancer has been shown to be varied and important. High expression levels of Src have been linked to a poor prognosis for patients with metastatic disease. In Src-null mice and cell lines, MAPK signalling is no activated in response to estrogen (Kim et al., 2005a). Breast cancer cell lines with increased expression of EGFR and Src also exhibit increased phosphorylated Shc, activation of MAPK and tumorigenicity compared to those cells that either do not overexpress EGFR or only overexpress Src (Biscardi et al., 1998). Additionally, EGF-induced DNA synthesis is dependent on the kinase domain of Src being functional in some breast cancer cell lines (Wilson et al., 1989).

The phosphorylation state of Src in tumours also impacts upon the survival of breast cancer patients. Patients with high cytoplasmic expression of Src phosphorylated at Tyr215 displayed a significant survival advantage compared to those possessing high levels of the autophosphorylated, constitutively active, Tyr419 phosphorylated, membrane bound Src. This constitutively active form of Src is the form expressed in triple negative tumours, those tumours that do not express either the ER, PgR or HER-2

receptor and have a significantly poorer prognosis due to a lack of effective treatments (Kanomata et al., 2011).

Finally, Src is used as an independent predictor of disease specific survival of breast cancer that has metastasised to the bone (Zhang et al., 2009). Deficient bone remodelling is prevalent in Src- null mice leading to osteoporosis (Soriano et al., 1991). Osteoclasts with disrupted Src expression suffer from reduced migration leading them to be unable to form ruffled membranes. Mice infected with MDA-MB-231 breast cancer cells with constitutively active Src suffered from increased osteolytic bone metastases (Zhang et al., 2009).

Src as a therapeutic target

Although Src has several functional roles in the promotion of cancer progression, this is due to its normal role in a number of pathways commandeered within cancerous cells and not due to it being a primary driver of tumourigenesis. It is very rare for mutant forms of Src to exist; involvement is primarily due to overexpression or constitutive activation rather than mutation. As such, monotherapy targeting of Src is unlikely to be successful in treating cancer but it does make Src an appealing target as an auxiliary treatment to current therapies (Roskoski, 2015).

Due to the strong sequence homology within the Src Family Kinases, there are no Src-specific treatments currently under trial in the clinic, with those drugs being tested targeting a range of similar proteins at once. Those already approved for medical use by the United States Food and Drug Administration (FDA) are for use in hematologic cancers such as chronic myelogenous leukaemia (CML) and acute lymphoblastic leukaemia (ALL) and are currently in clinical trials in a number of solid tumours, with the exception of vandetanib which has been approved for medullary thyroid carcinoma. Such drugs include Bosutinib which targets BCR-Abl, Src, Lyn and Hck, amongst others, which is in trials for breast cancer and glioblastoma (Puls et al., 2011). Dasatinib targets BCR-Abl, Src, Lck, Fyn, Yes and PDGFR and is in trials for breast cancer and other solid tumours along with ALL (Araujo and Logothetis, 2010). Ponatinib targets all Src family kinases along with BCR-Abl, PDGFR and VEGFR (Cortes et al., 2013). Saracatinib (Laurie et al., 2014) and AZD0424 (Nowak et al., 2007) are more specific, only targeting Src and

BCR-Abl and are not yet approved for use but as in trials for a range of solid tumours. All of these target the glycine-rich loop, containing a GxGxΦG, which is very mobile and acts as a lid to the ATP binding pocket of the kinase domain, and thus act as ATP-competitive inhibitors (Johnson et al., 2001). AZD0530 is a selective inhibitor of Src and Abl and blocks Src phosphorylation and has been shown to be effective against ER positive breast cancer cells *in vitro* (Herynk et al., 2006). All of these drugs are designed to enhance chemosensitivity and complement endocrine therapy.

These treatments have also been considered as an option for treating triple negative breast cancers which are difficult to treat as they exhibit high levels of constitutively active Src (Herynk et al., 2006). Similarly, these drugs have shown some potential when combined with bisphosphates in patients with breast cancer that has metastasised into bone (Zhang et al., 2009).

Unfortunately, there are no suitable biomarkers with which to identify which tumours would benefit from treatment involving specific Src inhibitor therapies.

1.4.3 Breast Tumour Kinase, Brk, also known as Protein-Tyrosine Kinase 6 (PTK6)

Brk is a non-receptor tyrosine kinase with an ancestral connection to the Src family (D'Aniello et al., 2008). It is encoded by a gene at locus 20q13.3 (Park et al., 1997) downstream from promoters sensitive to NFκB and SP1 (Kang et al., 2002). The full length 451 amino acid protein has a similar structure to that of Src but lacking the myristoylation site, demonstrating a functional divergence from members of the Src family kinases such that Brk is a cytoplasmic, rather than membrane-bound, protein and containing an SH3 domain, an SH2 domain and a protein kinase domain (Lee et al., 1998). It exists in two splice variants, one of which excludes exon 2 of 8 thus removing the SH2 and protein kinase domains and introducing a novel C-terminal region (Mitchell et al., 1997). Activation of Brk also follows a similar pathway to that of Src whereby the phosphorylated Tyr447 residue binds to the SH2 domain and stabilises interactions between a linker region and the SH3 domain, rendering the protein inactive and requiring a phosphatase enzyme to activate (Derry et al., 2000). It also contains

phosphorylation sites at tyrosines 13, 61, 66, 114, 342 and 351. Tyr342 exists within the kinase activation loop and phosphorylation of this residue has been shown to increase catalytic activity of the enzyme (Qiu and Miller, 2002). Brk is expressed in healthy, differentiated epithelial cells of the intestine (Vasioukhin et al., 1995), skin (Wang et al., 2005), prostate (Lee et al., 1998) and oral epithelium (Petro et al., 2004). Despite the protein's early links to breast cancer, it is only expressed in cancerous breast tissue. In healthy mammary glands and ovary tissue, expression levels of Brk are very low to undetectable (Mitchell et al., 1994).

Functions of Brk

Brk has been shown to be able to phosphorylate a number of proteins, although some have not yet been confirmed to be substrates *in vitro*. Most of these potential substrates are involved in the EGF signalling pathway and include the RNA-binding proteins Sam68, SLM-1, SLM-2 and PSF, the transcription factors STAT3 and STAT5a/b and signalling proteins p190RhoGAP, paxillin, Akt, IRS-4, BKS/STAP1 and KAP3A (Ostrander et al., 2010). These substrates link Brk to multiple downstream mechanisms, the most prominent of which include epithelial cell differentiation, migration and apoptosis.

In the skin and intestinal tissues, Brk functions as an inducer of cellular differentiation in both normal and cancerous cells. Increased levels have been observed in differentiating, non-dividing epithelial cells. In human and mouse keratinocytes, differentiation was induced by Brk expression and was required for expression of Keratin 10 and filaggrin, epidermal differentiation markers (Vasioukhin and Tyner, 1997; Wang et al., 2005). Brk is also required for the transcriptional activity of STAT3 and STAT5a/b via their phosphorylation on Y705 and Y694/699 respectively which can, in turn, promote differentiation (Liu et al., 2006; Weaver and Silva, 2007).

Activation of Rac1 signalling has also been linked to Brk expression (Chen et al., 2004). Phosphorylation of the substrate paxillin at tyrosines 31 and 118 creates binding sites for CrkII can activate cellular migration via Rac1 signalling particularly in skin cell lines and breast cancer cell lines (Petit et al., 2000). Heregulin (HRG)-induced Rac1 activity is dependent on Brk expression as is HRG induced activation of p38MAPK and ERK5

(Ostrander et al., 2007). In mouse embryonic fibroblasts (MEFs), EGF induction of Brk is required for migration and proliferation (Shen et al., 2008).

Brk in Cancer

Despite low to undetectable levels of Brk in normal mammary tissue, Brk is highly expressed in 60 % of breast tumours and breast cancer cell lines (Mitchell et al., 1994) and in 86 % of invasive ductal breast cancer (Ostrander et al., 2007). It is also overexpressed in ovarian tumours despite no expression in normal ovary cells (Schmandt et al., 2006). Increased levels have additionally been documented in primary and metastasised colon tumours, head and neck squamous cell carcinoma, prostate tumours, B- and T- cell lymphomas and prostate tumours. Gene expression of Brk is also increased in lung, bladder, pancreatic and gastric cancers but the functions here are yet to be established (Brauer and Tyner, 2010).

In U2OS human osteosarcoma cells, overexpression of Brk increases phosphorylation of PSF, thus reducing its RNA-binding ability, altering the subcellular location of PSF and inducing S-phase cell cycle arrest and reducing proliferation (Lukong et al., 2009). This is counter to the effect of overexpression of Brk in breast cancer, where proliferation is reinitiated in response by inducing expression of Cyclin E and reducing p27 and a transformed phenotype develops (Xiang et al., 2008).

In addition to reducing proliferation in breast cancer, Brk plays a role in migration of tumour cells. T47D and MDA-MB231 breast cancer cell lines required Brk expression for a migratory response to EGF and heregulin-β1 in a kinase independent fashion (Castro and Lange, 2010). In BT20 cells, migration in transwell assays was induced by phosphorylation of KAP3A by constitutively active Brk (Lukong and Richard, 2008). Another Brk substrate, STAT5, encourages a proliferative signal in breast cancer cell lines.

Mutation of Brk is relatively unusual in cancerous tissues. No specific mutations have ever been established in breast cancer (Mitchell et al., 1997). Some mutations have been found in RT-4 bladder and SW900 lung cancer cells lines and in 2.5 % of melanomas (Prickett et al., 2009; Ruhe et al., 2007). More common is gene amplification and

polysomy of chromosome 20 although the *PTK6* gene is amplified to a much lower extent than that of *ErbB2* (Aubele et al., 2009).

Brk as a therapeutic target

Due to the widely increased expression in such a large proportion of breast cancer cells, Brk is an attractive target for therapy, particularly as a cooperative partner in therapy. Altered sensitivity to targeted therapy correlates with Brk expression (Xiang et al., 2008). Inhibition of Brk expression leads to a 50 % suppression of proliferation in breast cancer cells *in vitro* (Harvey and Crompton, 2004). If this could be adapted to delay growth of secondary tumours that arise after primary treatment, it could lead to a significant improvement in patient prognosis.

Currently, the primary focus of tyrosine kinase inhibitory drugs are small molecule inhibitors. An example of this is STI571 which targets a range of tyrosine kinases including Abl, Arg, Kit, PDGFR and BCR-Abl and is surprisingly well tolerated given its diverse inhibitory capabilities (Druker, 2002). Unfortunately, not all Brk function is kinase dependent. In fact, kinase inactivity in Brk in T47D cells actually promoted proliferation thus demonstrating that this may not be the most effective path in Brk inhibition (Harvey and Crompton, 2003).

Alternatively, regulated protein-protein interactions are pivotal to Brk activities via its SH2 and SH3 domains. An example of this is the kinase-independent interaction with Sam68 (Src-associated substrate in mitosis of 68kDa), also known as KHDRBS1 (KH domain containing, RNA binding, signal transduction associated 1). Sam68 is an RNA binding protein with roles in post-translational regulation whose overexpression leads to a reduced tumour burden and lower metastasis. Brk inhibits Sam68 via phosphorylation and the interaction requires the SH2 and SH3 domains (Derry et al., 2000). Blocking these domains could be a more successful path in the inhibition of Brk.

1.5 Nuclear Magnetic Resonance (NMR)

Nuclear magnetic resonance (NMR) spectroscopy is used to study the structure of molecules by capitalising on a physical phenomenon whereby nuclei in a magnetic field can absorb and then re-emit electromagnetic energy, radiofrequency in the case of NMR. At equilibrium magnetisation, the nuclei will either align with the field, at low energy, or against the field at high energy (Hore, 1995a). The initial splitting of these energy states generated by the application of the magnetic field is known as the Nuclear Zeeman Effect (Levitt, 2009d). The NMR signal is generated by the perturbation of the nuclei from the ground state to a higher energy state via the application of a radiofrequency pulse and the electromagnetic radiation released as the nuclei relaxes to the ground state (Hore, 1995a). NMR requires the use of nuclei with a half-integer spin quantum number. Examples of such nuclei include ^{1}H, ^{15}N and ^{13}C. As the ^{15}N and ^{13}C isotopes account for such small percentages of the naturally occurring forms of these elements, any recombinant proteins produced for study by NMR must be isotopically labelled with magnetically active isotopes in order to be detected by NMR (Levitt, 2009c).

1.5.1 A Simple Pulse Sequence

In order to perturb the nuclei into a high energy state, radiofrequency pulses are applied to the sample. A pulse sequence can be thought of as the program that is used by the spectrometer to describe when to apply a pulse, at which frequency, the length of the pulse, the length of time delays and the detection time. A simple pulse sequence combines a series of pulses with time delays (Levitt, 2009b), a schematic diagram of which can be seen in figure 1.14. Initially there is a delay during which equilibrium magnetisation is reached which is known as the relaxation delay and indicated in the figure as t_r. A radiofrequency pulse, close to the appropriate resonant frequency of that nucleus, is then applied in order to disturb the population equilibrium magnetisation away from the ground state into a high energy state. A free induction decay, FID, which is the fluctuating signal generated by the relaxation of the nuclei to their ground state, is generated and acquired during the acquisition time, t_{acq}. This sequence is repeated many times over and the resulting FIDs are added together. This is called time averaging and increases the signal-to-noise ratio (Becker, 1999). As the signal is consistent, the

accumulation of the signal is much stronger than that of the cumulative noise, which is random and adds together very slowly. Thus the difference between the signal and noise is increased and the signal is more obvious.

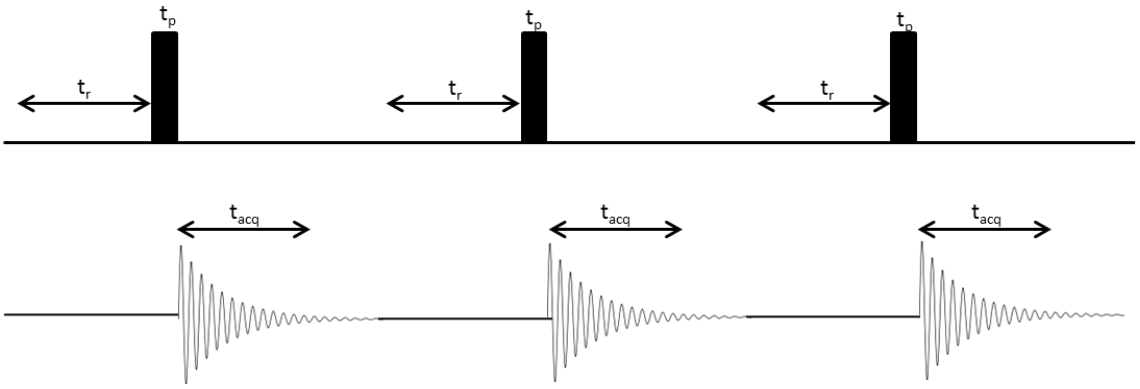

Figure 1.14 A basic pulse sequence and the resulting FID acquired.

Now that an FID has been acquired, conversion to a useable spectrum is required. The acquired FID is first digitised by the spectrometer software, in this case Topspin. The signal is sampled as regular time intervals and the size of the signal is stored. These digital points from the FID are then submitted to a fourier transformation. This mathematical process multiples the FID by cosine waves of different frequencies. The net area under the resulting curve calculated is the height of the peak at that wavelength. This is repeated for all frequencies across an appropriate range. If there is no net area under the curve then there is no peak at that frequency (Keeler, 2006). This results in a spectrum with peaks given in terms of frequency. As these frequencies will vary depending on the size of the magnetic field and the radiofrequency of the spectrometer used, to allow comparison of data from different spectrometers, the chemical shift scale is used. An example of the type of spectrum produced by a one-dimensional ^{1}H NMR experiment is shown in figure 1.15.

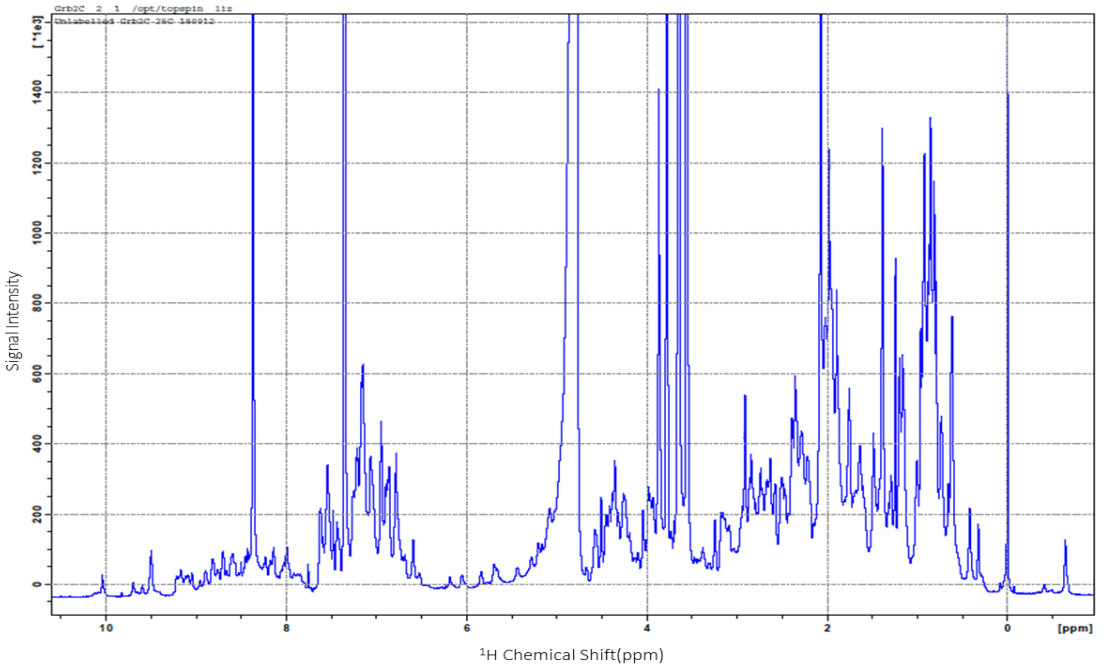

Figure 1.15 1H spectrum of unlabelled C-terminal SH3 domain of Grb2. Each peak represents nuclei in a different environment thus giving a specific chemical shift.

1.5.2 Chemical Shift

If atoms were bare nuclei, each nuclear isotope type would give rise to a single narrow peak reflecting the resonant frequency of that isotope in that magnetic field. However, electrons are magnetic particles and thus bring about a local magnetic field which can add or subtract from the external magnetic field (Levitt, 2009a). This can affect the local environment of the nucleus in question and thus change the chemical shift of a peak for that nucleus in a diamagnetic material. Additionally, if a molecule is considered, the presence of other magnetic spins within the same molecule and their magnetisation also contribute to the local magnetic field and affect the emitted frequency of the nuclei relaxing to ground state. As such, nuclear magnetic signals can reveal the electronic and nuclear environment of the observed spins. The emitted frequency of a given nucleus is proportional to the local value of the magnetic field, thus depends on the location of a nucleus in the molecule and the details of the local electronic structure and is referred to as the chemical shift, δ (Hore, 1995b). Due to this being field dependent, the frequency value for a chemical shift will depend on the spectrometer used to detect it. In order to remove field dependency from the spectrum, an alternative scale, which uses the difference in the frequencies of the peak in question and that of a reference nucleus

(which has a very consistent chemical shift) thus normalising the scale and is quoted in parts per million. The equation used to calculate the chemical shift, δ, using this scale is as follows:

$$\delta = 10^6 \frac{(\nu - \nu_{ref})}{\nu_{ref}} \qquad \text{(Equation 1)}$$

Where v is the frequency of the sample nucleus and v_{ref} is the frequency of the reference nucleus in that field (Hore, 1995b).

1.5.3 Two-Dimensional Pulse Sequences

Two-dimensional pulse sequences, such as that used in heteronuclear single-quantum coherence (HSQC) experiments in this thesis, follow a general scheme as shown in figure 1.16 (Keeler, 2006). The sample magnetisation is allowed to reach thermal equilibrium before a preparation phase, during which the sample is excited by one or more pulses. An evolution time, t_1, follows, during which the magnetisation is allowed to evolve prior to a mixing time containing further pulses. Finally the signal is recorded as a function of the second time variable, t_2.

A two-dimensional data set involves repeating the pulse sequence with increasing values of t_1 and recording the FIDs as a function of t_2 for each value of t_1.

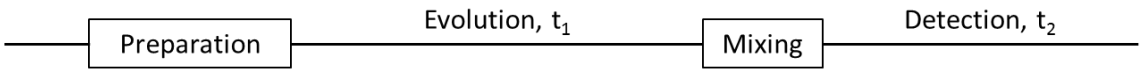

Figure 1.16 General schematic of two dimensional NMR experiments. Adapted from *Understanding NMR Spectroscopy*, James Keeler, Lecture 7, 2004 (Keeler, 2006).

The pulse sequence for the HSQC, as can be seen in figure 1.17, is a complicated two-dimensional pulse sequence which can be used for studying large molecules such as proteins. The pulse sequence has been divided into three periods and affects the two spins (I and S) which are bonded to each other. Period A is the preparation stage for this pulse sequence where magnetisation is transferred from the I nucleus to the S nucleus. Period B is the evolution time and includes a pulse applied exclusively to the I nucleus in order to refocus its offset meaning that only the offset of the S nucleus affects the evolution of the coupling. Then in Period C, the mixing time, the magnetisation is transferred back from the S spin back to the I spin where it is then detected (Keeler, 2006). A two-dimensional Fourier transform is then applied to the acquired FIDs.

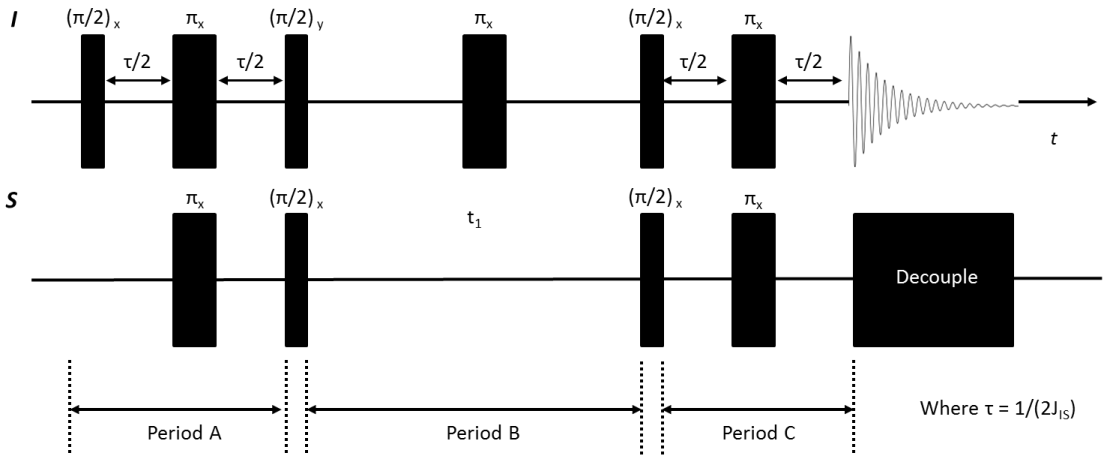

Figure 1.17 Example of a HSQC pulse sequence divided into three periods. Adapted from *Understanding NMR Spectroscopy*, James Keeler, Lecture 7, 2004 (Keeler, 2006).

As t_1 is incrementally increased with each repetition of the HSQC pulse sequence, an FID for each increment is acquired in t_2 but these are each slightly out of phase with each other. If each t_2 FID is individually Fourier transformed, the peaks calculated would have the same chemical shift but vary in intensity and whether they are positive or negative. A schematic of this effect is shown in figure 1.18. The amplitude of the resonance signal varies periodically as a function of t_1 and this amplitude also have a frequency. When this frequency is Fourier transformed, the subsequent chemical shift is for the second dimension (Levitt, 2009e). In the case of the HSQC pulse sequence above, the Fourier transforms of the t_2 FIDs calculate the chemical shift in the I dimension as it is this

nucleus on which magnetisation is detected. The chemical shift of the S dimension is calculated from the frequency of the I dimension signal variation for the chemical shift in question, representing the evolution of coupling during the t_1 period on the S nucleus. In the case of the proteins, I is the ^{1}H nuclei and S is the ^{15}N nuclei.

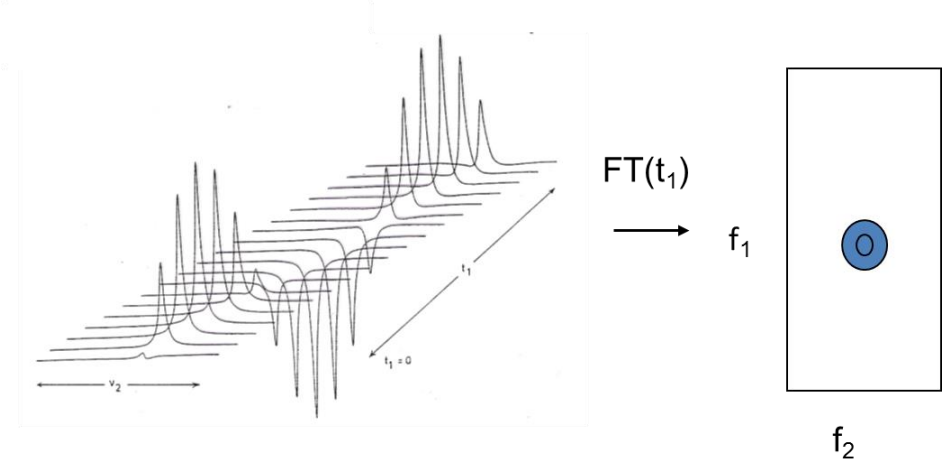

Figure 1.18 Fourier transformed peaks for a given chemical shift calculated from the t_2 FIDs from a HSQC. The frequency of the amplitude variation of these peaks is Fourier transformed to give the other dimension of the two-dimensional spectra. This second dimension is a function of t_1 (Levitt, 2009e).

The [^{1}H-^{15}N]-HSQC experiments conducted in this thesis will give rise to a peak for every NH bond within the sample. In the case of a protein, most of these peaks will correspond to the NH bond within the backbone of the peptide chain for each amino acid in the chain. There are some exceptions to this. For example, proline residues within a peptide chain do not have an NH bond to detect. Additionally, some peaks on the spectrum will account for the NH bonds that exist within the side chains of certain amino acids such as tryptophan and glutamine. As the chemical shift of a peak is dependent on the environment of the nuclei in question, these spectra can be considered a "fingerprint" of the protein in question.

1.5.4 Triple Resonance Experiments

The triple resonance experiments discussed here work in a similar fashion to two-dimensional HSQC experiments by transferring magnetisation between nuclei via covalent bonds such that structural information can be determined. The two

experiments used within this thesis are the HNCACB and the CBCACONH which can be used along with HSQC spectra to assign the backbone of a protein.

Triple resonance experiments are possible due to the large single bond heteronuclear couplings between carbon, nitrogen and hydrogen residues within a protein meaning magnetisation transfer times are shorter and there are fewer losses due to relaxation. Also, the chemical shift of Cα nucleus and that of the CO nucleus within a peptide backbone are sufficiently different for it to be possible to manipulate their magnetisation independently (Ikura et al., 1990).

The nomenclature for triple resonance experiments indicates the magnetisation pathway. For example, when considering the current residue, i, and the previous residue, i-1, the HNCACB experiment follows the transfer of magnetisation from the ^{1}HN through the ^{15}NH through the ^{13}Cα to the ^{1}Hα and ^{1}Hβ and back again to the ^{1}HN for detection. Transfer can occur through the $^{13}C\alpha_{i-1}$ to both the $^{15}N_{i-1}$ and $^{15}N_{i}$ (Grzesiek and Bax, 1992b). Thus for each NH chemical shift, there will be signal for the $C\alpha_i$, $C\alpha_{i-1}$, $C\beta_i$ and $C\beta_{i-1}$ but, as the Cα and Cβ chemical shifts evolve simultaneously, they exist in the same dimension. Figure 1.19 B shows a similar schematic for the CBCACONH experiment. This experiment begins with the ^{1}Hα and ^{1}Hβ of the i-1 residue transferring their magnetisation energy to the appropriate ^{13}C (Grzesiek and Bax, 1992a). But from here, the magnetisation is transferred to the CO. The magnetisation is transferred through this carbon to the $^{15}N_{i}$ and then the $^{1}HN_{i}$ residue for detection. Thus the shifts for the Cα and Cβ residues from the i-1 residue are viewed from the i perspective.

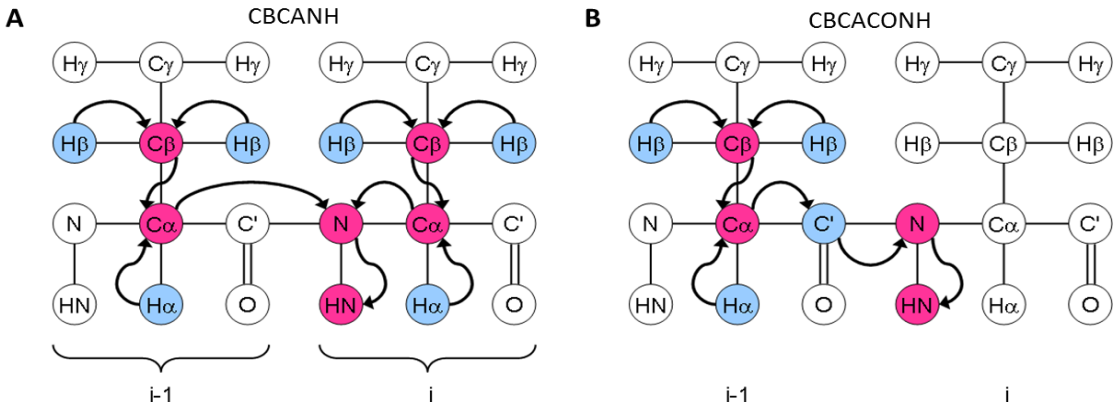

Figure 1.19 A) Schematic of the magnetisation transfer pathway for the CBCANH experiment, an analog of the HNCACB, which correlates the same atoms. B) Schematic of the magnetisation transfer pathway for the CβCαCONH experiment (Highman, 2012).

As such, the HNCACB will have peaks for the $^{13}C\alpha$ and $^{13}C\beta$ nuclei from the perspective of the $^{15}NH_i$ and $^{15}NH_{i-1}$. For each nitrogen and hydrogen shift, there will be 4 peaks in the carbon dimension (apart from glycine residues which have no Cβ and proline which will have no shift at all as they have no ^{1}HN to be detected through). The CBCACONH spectrum will have $^{13}C\alpha$ and $^{13}C\beta$ peaks from the perspective of $^{15}NH_{i-1}$ only. When these are overlaid, those peaks which appear in both the HNCACB and CBCACONH are those for the $^{13}C\alpha$ and $^{13}C\beta$ from the i-1 residue and those that only appear in the HNCACB are those for the i residue (Highman, 2012).

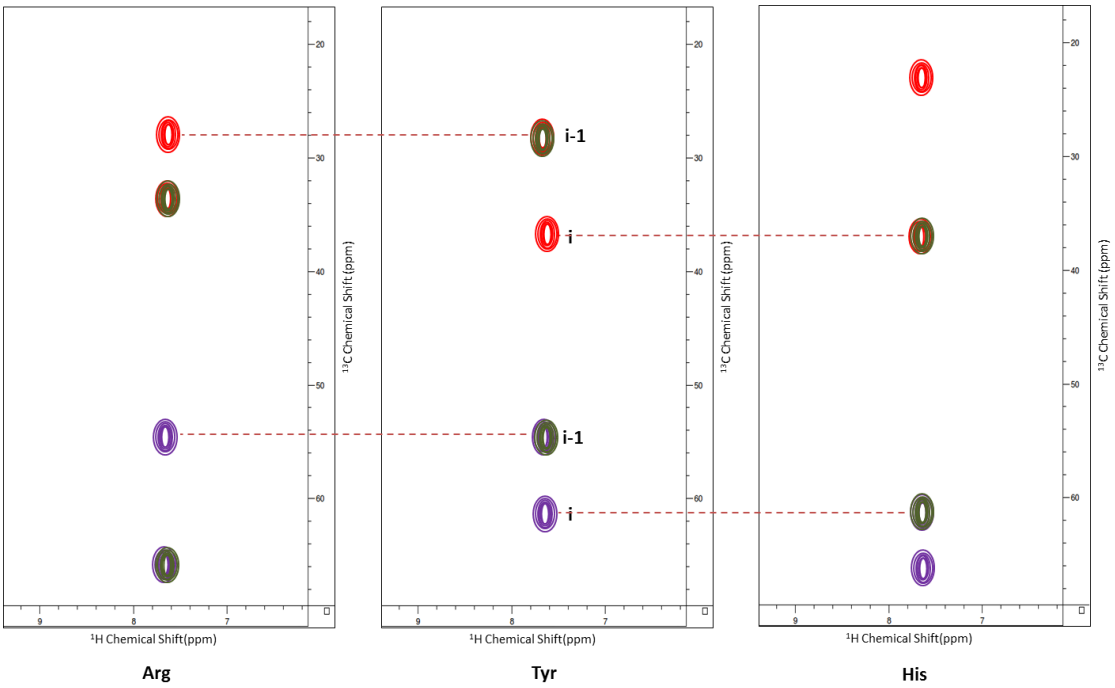

Figure 1.20 Three strips showing the overlaid spectra of a HNCACB and a CBCACONH at the same hydrogen and carbon chemical shifts but with different nitrogen shifts. The positive Cβ peaks in the HNCACB are shown in red and the negative Cα in purple. The CBCACONH peaks are showing in green. Adapted from *Protein NMR: A Practical Guide*, (Highman, 2012).

Given that the carbon chemical shifts for the Cα and Cβ nuclei for each amino acid are characteristic within a certain range (with some limitations), it is possible to deduce the type of amino acid the peaks in a given strip represent. Those Cα and Cβ peaks within a strip that are present on both HNCACB and CBCACONH spectra correspond to the previous residue to i. If Cα and Cβ peaks with the same carbon chemical shifts from the initial strip, but different hydrogen and nitrogen shifts, can be found only on the

HNCACB, these peaks in the new strip will correspond to the i-1 amino acid but now this residue can be considered as i. These amino acids are connected within a peptide sequence and the type of amino acid of this second residue can be deduced as before as can be seen in figure 1.20. Once a small chain of connected residues has been established, this can be linked to the amino acid sequence of the protein in question and the specific residue of that type can be assigned (Highman, 2012). This system can be used in tandem with [^{1}H-^{15}N]-HSQC experiments to assign the backbone of a protein.

1.5.5 Using NMR Titrations to Study Protein-Protein Interactions

As discussed in 1.5.3, the chemical shift of an NH peak in a HSQC spectrum is dependent on the environment of the nuclei within that bond and is affected by other nuclei within the environment of the nitrogen and hydrogen in question. So, if this environment is changed, the chemical shift for the NH bond on the HSQC spectrum will also change. The environment of the nuclei can be changed in in several ways, for example, if the conformation of the protein changed and new local bonds are formed (Williamson, 2013). Here, this principle will be used to study which residues from one protein are involved in an interaction with another protein. When a second protein is introduced, those residues most affected by any interaction will find their environment changed and thus their chemical shifts will change as the concentration of the ligand protein increases until the interaction is fully saturated at which point the chemical shift will settle. An example of this can be seen in figure 1.21 (Garner et al., 2011). The magnitude of the peak movement can be quantified and used to establish which residues are involved in any interaction which can be mapped onto a model of the protein.

This also profits from the requirement for half integer spin quantum number isotopes for detection by NMR. If both proteins were detectable via NMR, peaks accounting for the increasing concentration of the ligand protein would appear on the spectrum making reliable assignment much more difficult. However, if the target protein is isotopically labelled and the ligand protein is not, only the target protein will be detected during the titration. This means that the effect of the increasing concentration of the ligand protein will be observed but the actual ligand protein itself will not (Williamson, 2013). In order to produce a full model, the titration would be repeated but with the

previous ligand protein now isotopically labelled and the previous target protein undetectable.

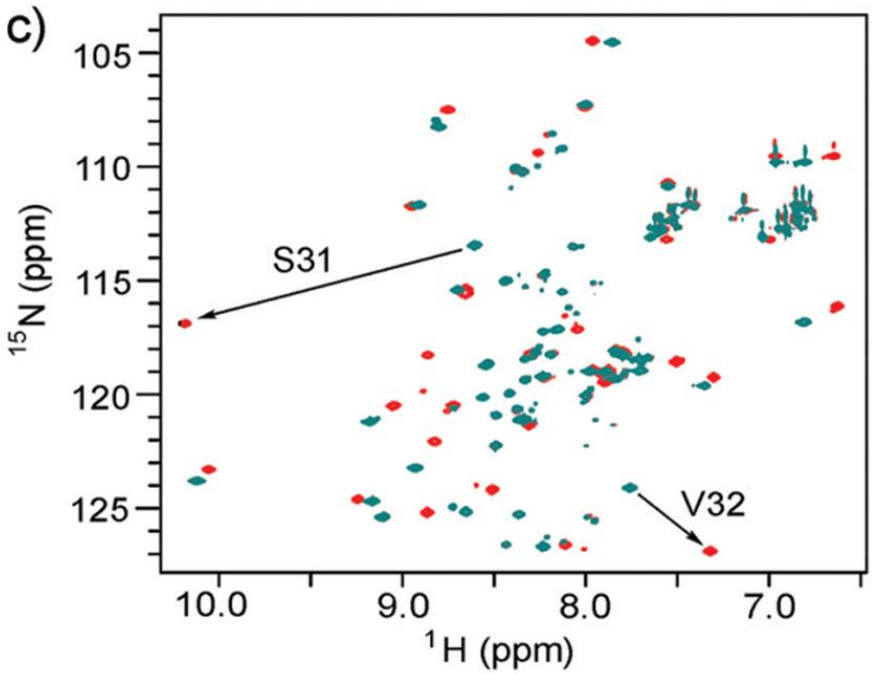

Figure 1.21 Example of chemical shift perturbations in a [^{1}H-^{15}N]-HSQC showing ^{15}N labelled ubiquitin in green and again in the presence of the unlabelled Znf216 A20 domain at a ratio of 1:1 in red. Highlighted are the residues which are perturbed to the greatest extent by the interaction. Taken from (Garner et al., 2011).

1.6 Aims of this Project

As discussed in this chapter, the ADAM15 splice variants have been linked to different prognoses in early stage breast cancer. This reasons for this are unclear but this could be due to the ADAM15 splice variant intracellular domains interacting with various SH3 domain containing proteins in a preferential manner. Several of these SH3 domain containing proteins have been independently linked to breast cancer disease progression and so these provide a potential mechanism for the influence of the ADAM15 splice variants on breast cancer development.

To this end, this project will investigate the interactions of the ADAM15 ICDs with the SH3 domains of Grb2, Src and Brk in order to attempt to establish the source of the preferential binding and potentially the biological relevance of these interactions. This will be achieved by pull down assay and NMR spectroscopy. This will require the optimisation of the purifications of the SH3 domains, altering the ADAM15 ICD fusion tag in order to retain solubility and tumbling rate for NMR and the optimisation of the purification of the ADAM15 ICDs. NMR spectroscopy titrations will be used to attempt to establish the binding interfaces and any variation is the interaction pattern or intensity between the SH3 domains and the various ADAM15 ICDs.

Chapter 2: Materials and Methods

2.1 Materials

Table 2.1 lists the suppliers for the chemicals used in this thesis.

Table 2.1 Suppliers for the chemicals used in this thesis.

Reagent/Chemical	Source
Tryptone	Fisher Scientific (BP9726-5)
Yeast Extract	Oxoid (LP0021)
NaCl	Fisher Scientific (BP358-212)
Agar Bacteriological	Oxoid (LP0011)
Ampicillin sodium	Formedium (AMP100)
Kanamycin Monosulphate	Formedium (KAN0025)
Chloramphenicol	Fisher Bioreagents (10255203)
Isopropyl β-D-1-thiogalactopyranoside (IPTG)	Sigma-Aldritch (I6758-5G)
Na_2HPO_4	Sigma-Aldritch (255793)
$NaH_2PO_4.7H_20$	Sigma-Aldritch (S9638)
KH_2PO_4	Fisher Scientific (P285)
NH_4Cl	Fisher Scientific (A661)
$MgSO_4$	Fisher Scientific (M65)
$CaCl_2$	Fisher Scientific (C614)
$FeSO_4.7H_20$	Acros Organic (201390051)
^{13}C glucose	Sigma-Aldritch (389374)
glucose	Fisher Scientific (10141520)
^{15}N NH_4Cl	Sigma-Aldritch (299251)
KCl	Fisher Bioreagents (BP366)
Tris base	Fisher Scientific (BP152)
Sodium Dodecyl sulphate (SDS)	Fisher Bioreagents (BPE166-5)
beta-mercaptoethanol	Gibco (21985-023)
Bromophenol Blue	Sigma-Aldritch (B0126)
Instant Blue Stain	Expedeon (ISB1L)
Methanol	Fisher Scientific (A412)
Glacial cetic acid	Fisher Scientific (A38SI)
Coomassie Brilliant Blue R250	ThermoScientific (20278)
PonceauS	Electran (44083)
Bovine Serum Albumin (BSA)	Fisher Scientific (BPE9701)
Polysorbate 20 (Tween-20)	Promega (H5151)
HEPES	Fisher Bioreagents (BP310)
L-glutathione reduced	Sigma-Aldritch (G4251)
Tetramethylethylenediamine (TEMED)	ThermoScientific (17919)
Ammonium Persulphate	Sigma-Aldritch (A3678)
Human alpha thrombin	Enzyme Research Laboratories (HT 1002a)
Phenylmethylsulfonyl fluoride (PMSF)	Sigma-Aldritch (P7626)
Factor Xa	Qiagen (33223)
Urea	Fisher Scientific (BP169)
Imidazole	Fisher Bioreagents (BP30550)
D_2O	Sigma-Aldritch (151882)
DSS	ThermoScientific (PI-21555)
NaN_3	Fisher Chemical (S227I)

2.2 Cell Culture

2.2.1 Cell Culture of MCF-7 cells

MCF-7 breast cancer cells were cultured in Roswell Park Memorial Institute (RPMI) 1640 media (with added L-glutamine) (Gibco) with 10% FCS (foetal calf serum) (Hyclone) with 1000 units/ml penicillin and 1000 ug/ml streptomycin (Gibco). These were grown in 75 cm^2 tissue culture grade flasks at 37 °C with 5% (v/v) CO_2. Twice a week, cells were passaged once they had reached 80-90% confluency using 0.25% Trypsin-EDTA (Gibco).

2.2.2 MCF-7 Cell Lysis Protocol

MCF-7 cells were cultured as above in 10 cm^2 cell culture petri dishes for 5 days until they reached 90% confluency and numbered approximately 2 x 10^6 cells. The media was removed and the cells washed with 1 x PBS (phosphate-buffered saline: 137 mM NaCl, 2.7 mM HCl, 2 mM KH_2PO_4, 10 mM Na_2HPO_4 pH7.4) followed by the addition of 1.5 ml of NP-40 buffer (50 mM Tris.HCl pH 7.5, 150 mM NaCl, 1.5 mM $MgCl_2$, 10% glycerol, 1% NP-40 (Roche Applied Science) and 1 x protease inhibitors (Roche Applied Science). The cells were incubated on ice for 5 minutes, scraped from the surface, and incubated on ice for 2 further minutes. The suspended cells were pipetted into 1.5 ml eppendorf tubes and incubated on ice for a further 5 minutes. After micro-centrifugation at 14000 rpm for 15 minutes at 4 °C, the supernatant was kept on ice for further use and the pellet discarded.

2.3 Bacterial Cell Cultures for Protein Purification

GST-tagged ADAM15 A-C constructs were generated by Dr Zaruhi Poghosyan (Zhong et al., 2008). GST-tagged ADAM15 D and E constructs were generated by Dr Christian Roghi (unpublished). These constructs were within a pGEX-5X1 plasmid with resistance to ampicillin. All GB1-tagged constructs were generated via the introduction of restriction sites at the end of the genes by Polymerase Chain Reaction (PCR), digestion of the gene from the pGEX-5X1 vector and ligation into the new vector using T4 ligase. These constructs were within a pSK-Duet01 plasmid with resistance to kanamycin (Iwai et al., 2006), a plasmid map of which can be seen in figure 2.1.

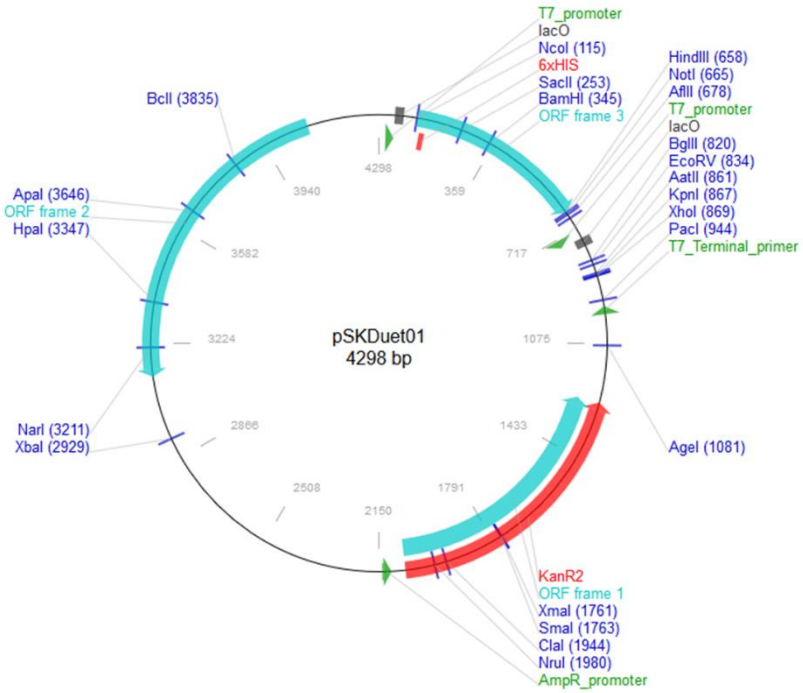

Figure 2.1 Plasmid map for the vector pSKDuet01 as provided by (Iwai et al., 2006) highlighting restriction sites and the location of the His tag (upstream from the GB1 tag) and the site of the kanamycin resistance gene.

2.3.1 Transformation of Bacterial Cells

Due to the presence of human specific codons in the ADAM15 ICD sequence, a variant of BL21 (DE3) cells, Rosetta 2 (Merck Millipore) or an alternative variant, Codon + RP (Agilent Technologies), were used for any culture or transformation involving these constructs. Then 200 µl of calcium-competent Rosetta 2 cells were incubated, on ice for 30 minutes with 2 µl plasmid DNA. The cells were heat shocked at 42 °C for 60 seconds in a water bath and returned to ice for 10 minutes and then 800 µl of 2YT broth (10 g tryptone, 10 g yeast extract and 5 g NaCl in 1 L water and autoclaved) was added and the cells were incubated for 1 hour at 37 °C, then microcentrifuged at 14,000 rpm for 1 minute. Next 800 µl of the supernatant was removed, the cell pellet was resuspended in the remaining supernatant and this was plated on 2YT agar plates (2YT as previously with 15 g agar per litre) containing the appropriate antibiotic for the plasmid (ampicillin at 100 µg/ml for GST-tagged constructs and kanamycin at 50 µg/ml for GB1-tagged constructs) and coated with chloramphenicol at 35 µg/ml. The chloramphenicol was necessary to retain the Rosetta 2 plasmid which allows the translation of human specific codons. The plates were incubated overnight at 37 °C. The SH3 domain constructs were

transformed using a similar protocol but into BL21 (DE3) cells and were selected for using 100 µg/ml ampicillin.

2.3.2 Protein Expression in 2YT

Bacteria were transformed as described and a colony from the transformation was used to inoculate 100 ml 2YT containing kanamycin, or ampicillin, and chloramphenicol at working concentrations described previously. The culture was incubated overnight at 37 °C, shaking at 200 rpm. This saturated culture was then added to 900 ml 2YT with kanamycin, or ampicillin, and chloramphenicol and incubated at 37 °C until the OD reached 0.6-0.8. At this point, the cultures were induced with 0.1 mM IPTG and returned to incubation for 4 hours, unless stated otherwise. After incubation, the cultures were centrifuged at 5000 rpm (Beckman rotor JLA 9.1000) for 15 minutes at 4 °C. The supernatant was discarded and the pellets were either frozen at -70 °C for further use or resuspended in 30ml of the correct buffer for the purification to follow, in the presence of protease inhibitors (Roche Applied Science EDTA-free protease inhibitor cocktail tablets). Once resuspended, the cells were sonicated using a Sonics Vibracell 130 watt, 20 kHz sonicator for 2 minutes with an amplitude of 80%. This was repeated a further four times with 5 minute incubations on ice before each repetition. The lysate was clarified by centrifugation at 12000 x g 4 °C for 20 minutes (Beckman rotor JA 12). The pellet was discarded. Cultures for pull downs were performed as above but using 500 ml 2YT rather than 1000 ml.

2.3.3 Protein Expression in Minimal Media

Bacteria were transformed as described and a colony from the transformation was used to inoculate 10 ml 2YT containing kanamycin, or ampicillin (and chloramphenicol if required) at the working concentrations described previously. The culture was incubated overnight at 37 °C, shaking at 200 rpm. The following morning, 8 ml of this culture was added to 100 ml enhanced MEM (6 g Na_2HPO_4, 3 g KH_2PO_4, 0.5 g NaCl, 1 g NH_4Cl, adjusted to pH 7.2 and autoclaved, then added 13.33 ml 30% glucose, 1 ml 2 M $MgSO_4$, 100 µl 100 mM $CaCl_2$, 500 µl 20 mM $FeSO_4$, 1 ml 1000x micronutrients solution, 10 ml MEM Vitamin Solution 100x (Sigma)). This culture was incubated at 37 °C until it

was saturated; approximately 2 hours. The cells were collected by centrifugation in a sterile centrifuge flask at 5000 rpm (Beckman rotor JLA 16.250) for 10 minutes at 25 °C. The supernatant was discarded and the cells were resuspended in 10 ml fresh enhanced minimal media and added to the main 1000 ml MEM culture (if labelled protein is required, use ^{15}N labelled NH_4Cl or ^{13}C labelled glucose). The culture was incubated at 37 °C until an OD of 06.-0.8 had been achieved. The production of the protein in question was then induced with 0.1 mM IPTG. The cells were incubated at 37 °C for 4 hours, except for Brk and ADAM15 B which were incubated at 28 °C overnight. The cells were harvested by centrifugation at 5000 rpm (Beckman rotor JLA 9.1000) for 15 minutes at 4 °C and the pellets were either frozen at -70 °C for further use or resuspended in 30ml of the correct buffer for the purification to follow, in the presence of protease inhibitors (Roche Applied Science EDTA-free protease inhibitor cocktail tablets). Once resuspended, the cells were sonicated for 2 minutes for four repetitions at 80% amplitude using a 130 watt, 20 kHz Sonics Vibracell with 5 minute ice incubations between each repetition. The lysate was clarified by centrifugation at 12000 x g 4 °C for 20 minutes (Beckman rotor JA 12). The pellet was discarded.

2.4 Protein Concentration Determination

2.4.1 BCA Assays

BCA assays rely on the change in valence state of copper in the presence of a protein in an alkaline environment. The protein chelates Cu^{2+} and reduces it to Cu^{1+}. This then interacts with bicinchoninic acid (BCA) and generates a dark purple colour which absorbs at 562 nm in a linear correlation with protein concentration. Standards of bovine serum albumin (BSA) as provided by the BCA protein assay kit from Pierce Protein Research Products were made with concentrations of 2000, 1000, 500, 250, 125, 62.5 and 31.25 µg/ml. Samples of MCF-7 lysate were diluted 1/5 and 1/10 with ddH_2O and 20 µl of each sample and the standards was pipetted into the wells of a 96 well plate. A blank water sample was included and each sample was pipetted in duplicate. The BCA solution was made using 10 ml Solution A and 200 µl Solution B from the kit. Finally, 200 µl of this solution was added to each well and the plate was incubated for 30 minutes at 37 °C. After measuring the absorbance at 562 nm using a plate reader, the standards were

used to generate a standard curve from which the concentration of the MCF-7 lysate was calculated.

2.4.2 Bradford assay

This assay is based upon the interaction of Coomassie Brilliant Blue G-250 with proteins in a 1:1 fashion. The unbound form of Coomassie Brilliant Blue is dark red whereas the bound version is blue and absorbs at 595 nm. The increasing absorbance is proportional to the protein concentration. Standards were made as for the BCA assay and 5 µl of each was pipetted, in duplicate, into a 96 well plate, along with a water control. To each well, 5 µl of blank affinity sepharose beads were added then 5 µl samples of sepharose bound to protein were pipetted into wells in duplicate and 5 µl water added to compensate for volume. Next, 250 µl Bradford Solution was added and the plate was incubated at room temperature for 5 minutes. After detection at 595 nm, the standards were used to generate a standard curve and, from this, the concentration of the protein bound to the sepharose was calculated as required for the pull down experiments.

2.4.3 Beer-Lambert Law

When calculating the amount of pure protein, the Beer-Lambert method was also used. The absorbance of the protein sample was taken at 280 nm (compared to a blank of the same buffer) and the Beer-Lambert law used to calculate the concentration. The extinction coefficients used were calculated based upon the amino acid sequence of the protein involved using the ProtParam Tool by ExPASy Bioinformatics Resource Portal (Gasteiger E., 2005). The Beer-Lambert Law equation is as follows:

$$A = \varepsilon c l \qquad \text{(Equation 1)}$$

Where A is the absorbance, ε is the extinction coefficient of the protein, c is the concentration of the protein and l is the path length of the sample.

2.5 Pull Downs

2.5.1 GST-ADAM15 ICD Affinity Pull Downs

GST-tagged ADAM15 ICDs, along with a GST tag control, were expressed in Codon + RP cells as described above. After sonication, the bacterial cell lysate (40ml) was incubated with 1 ml (500 µl beads in suspension) of glutathione sepharose slurry (Generon), which had been pre-equilibrated into 1 x PBS (137 mM NaCl, 2.7 mM KCl, 10 mM Na_2HPO_4, 1.8 mM KH_2PO_4 pH 7.2) with protease inhibitors (Roche Applied Science EDTA-free mini protease inhibitor cocktail tablets) by washing 3 times with centrifugation at 1300 x g for 3 minutes. The slurry of beads and lysate was incubated at 4 °C overnight on a rocker and then the beads were collected by centrifugation at 1300 x g for 3 minutes. Once the beads were resuspended in 500 µl 1 x PBS with protease inhibitors, they were kept on ice.

The concentrations of protein bound to the beads and total protein in the MCF-7 lysate, generated as described above, were determined by Bradford assay and BCA Assay respectively. 30 µg/ml of ADAM15 ICD bound to beads was added to MCF-7 lysate at 1 mg/ml and mixed on a rotator at 4 °C for 1 hour. The beads were collected by centrifugation at 13,000 x g for 2 minutes at 4 °C and the supernatant removed and kept on ice. After the beads were washed as previously, with each wash kept on ice, they were resuspended in 100 µl SDS loading buffer (0.312 M Tris pH 6.8, 10% SDS, 25% β-mercaptoethanol, 0.05% Bromophenol Blue) and 100 µl water and heated for 10 minutes at 100 °C. These were then frozen at -20 °C.

2.5.2 GST-SH3 Domain Affinity Pull Downs

Each SH3 domain, along with a GST tag control, was expressed in a bacterial cell culture as described above. Once sonicated, the bacterial cell lysate (12 ml) was incubated with 1 ml (500 µl beads in suspension) of glutathione sepharose beads (Generon). The beads had been pre-equilibrated into 1 x PBS by washing 3 times with centrifugation at 1300 x g for 3 minutes. The lysate and beads slurry were incubated at 4 °C on a rotator overnight, then centrifuged at 1300 x g for 3 minutes. The supernatant was removed and the beads were washed 3 times with 1 ml 1 x PBS and protease inhibitors by

centrifugation at 1300 x g for 3 minutes. The beads were then resuspended in 500 µl PBS with protease inhibitors and kept on ice. The concentration of protein on the beads was established by Bradford assay. The beads were then incubated with 1 ml bacterial cell lysate from Rosetta 2 cells that were over-expressing a GB1-ADAM15 variant. These cell lysates were generated as described above. After incubation for 1 hour at 4 °C on a rotator, this slurry was centrifuged at 1300 x g and the supernatant removed and kept on ice. The beads were washed as previously, with each wash kept on ice. Finally, the beads were resuspended in 100 µl SDS loading buffer and 100 µl water. This was heated to 100 °C for 10 minutes and frozen at -20 °C.

2.5.3 His-GB1 Affinity Pull Downs

These pull downs were achieved with the same protocol as for the GST affinity with some small changes. The initial incubation of the bacterial cell lysate with the beads involves an incubation of 1 hour rather than overnight. The beads used were Ni sepharose (Generon) which interact with the poly-His tag at the N-terminus of the GB1 tag. Once the concentration of protein on the beads had been established by Bradford assay and a 10 cm^2 dish of MCF-7 cells had been lysed per ADAM15 construct, the concentration of the protein in the MCF-7 lysate was established by BCA Assay. This was equalised to 1 ml of 1000 µg of MCF-7 protein per construct and aliquoted. Approximately 20 µl of beads was added to each 1 ml aliquot of MCF-7 lysate for each ADAM15 construct. The volume of beads required was adjusted for the concentration of ADAM15 on the beads based upon the results of the Bradford assay. After incubation for 1 hour at 4 °C on a rotator, this was centrifuged at 1300 x g and the supernatant removed and kept on ice. The beads were washed as previously, with each wash kept on ice, with one of the washes including 10 mM imidazole to remove any non-specific interactions of proteins from the bacteria or MCF-7 cells.

2.5.4 IgG Affinity Pull Downs

This protocol also followed a similar protocol to that of the His-GB1 affinity pull downs, again with a few differences. The IgG sepharose beads (Generon) were incubated with the bacterial cell lysate for 1 hour, as for the His-GB1 affinity. After washing, some beads

were then incubated with MCF-7 lysate, as for the His-GB1 affinity pull down. The beads were washed as previously and the beads resuspended in SDS loading buffer, heated to 100 °C and frozen as previously.

Once the pull down samples were prepared, they were separated by SDS gel electrophoresis. One gel was stained with Instant Blue stain in order to confirm the presence of ADAM15 constructs and that they were intact. The other was used for Western blotting in order to detect whether or not selected proteins were pulled down by the ADAM15 ICD.

2.6 SDS PAGE Gel Electrophoresis

Samples were prepared by dilution with SDS loading buffer and heated for 10 minutes at 100 °C. After microcentrifugation at 14,000 rpm for 1 minute, the desired volume was loaded onto a poly-acrylamide gel and separated at 180 V until the dye band had reached the bottom of the gel. The gel was then stained with either Instant Blue (Expedeon) or fixed with 10% v/v acetic acid for 30 minutes, stained for 1 hour in Coomassie Brilliant Blue stain (1% Coomassie Brilliant Blue R250, 20% v/v Methanol. 10% v/v Acetic acid) and destained overnight in 10% v/v acetic acid and 50% v/v Methanol.

The gels were made as described in table 2.2:

	Resolving Gel (ml)			**Stacking Gel (ml)**
	10%	**12%**	**15%**	**5%**
dH_2O	5	4.2	3	2.43
Acrylamide	4	4.8	6	0.5
Gel Buffer	2	3	3	1
10% w/v APS	0.072	0.072	0.072	0.072
TEMED	0.014	0.014	0.014	0.007

Table 2.2 SDS-PAGE gel protocol. The table shows the volumes of each solution required to make each gel in millilitres. The gel buffers used were appropriate to the gel being made. For example, when making the resolving gel, the resolving gel buffer was used (181.5 g/l Tris, HCl pH 8.8, 4 g/l SDS in a 4 x stock solution) and for stacking gels, the stacking buffer was used (60.5 g/l Tris.HCl pH 6.8, 4 g/l SDS in a 4 x stock solution). All resolving gels used the same 5 % acrylamide stacking gel.

The acrylamide used to make the gels is manufactured by Protogel (30 % w/v acrylamide, 0.8 % w/v bis-acrylamide stock solution 37.5:1)

2.7 Western blotting

Protein from the poly-acrylamide gel was transferred onto nitrocellulose membrane (GE Healthcare Amersham Hybond-ECL) via wet transfer at 25 V for 1 hour and 30 minutes. The membrane was temporarily stained with Ponceau Red in order to highlight proteins bands in order that the membrane could be cut to size. Once the Ponceau Red had been rinsed away with water, the membrane was blocked with 5% BSA in 1 x TBS (Tris Buffered Saline: 150 mM NaCl, 2 mM KCl, 25 mM Tris pH 7.4) with 0.1% Tween-20 for 1 hour. The membrane was then incubated overnight at 4 °C in the same BSA/TBS solution containing the primary antibody at a dilution of 1:1000. The antibody used for detecting Src was #2108 by Cell Signalling and the antibody used for detecting Grb2 was #3972, also from Cell Signalling. The antibody for detecting the poly-His tag was #2365 by Cell Signalling. After this incubation, the membrane was washed 3 times in 1 x TBS with 0.1 % Tween-20 for 10 minutes at room temperature with gentle shaking. Incubation with the secondary antibody was for 1 hour at room temperature with the same BSA/TBS

buffer as for the primary with gentle shaking. The secondary antibody used was goat anti-rabbit polyclonal HRP-linked immunoglobulin (Dako Denmark) for all primaries as they were all rabbit monoclonals. After incubation with the secondary antibody, the membrane was washed as previously. Finally, the membrane was developed with Pierce Protein Research ECL Western blotting Substrate. This membrane was imaged using a FujiFilm Intelligent Dark Box LAS-3000.

2.8 SH3 Domain Purification

2.8.1 GST Affinity Purification of Fusion Proteins

BL21 (DE3) cells were transformed with the appropriate plasmid for the desired SH3 domain. The SH3 domains of Grb2 and that of Src were expressed from pGEX-2T plasmids and the SH3 domain of Brk was expressed from a pGEX-3X plasmid. All plasmids contained resistance to ampicillin. If unlabelled protein was required, the cells were cultured as in the 2YT culture method described; labelled protein was produced using the Minimal Media protocol. After harvesting, the cells were resuspended in 30 ml of the appropriate buffer for the SH3 domain with protease inhibitors. For Grb2C/N and Src, this was 20 mM sodium phosphate, 0.15 M NaCl pH 7.2 (hereafter known as SPB or sodium phosphate buffer) and for Brk, this was 25 mM HEPES, 0.1 M NaCl pH 7.0. The cells were sonicated as described above and incubated on ice for 30 minutes. The lysate was clarified with centrifugation as previously. The pellet was discarded. Meanwhile, the glutathione sepharose beads (Generon) were equilibrated into the appropriate buffer by washing with ~ 40 ml water and 5 column volumes (CV) of buffer. The column volume used was 4 ml. Once the lysate had been clarified by centrifugation, it was syringe filtered through a 0.45 µm membrane and the beads were added to the lysate. The beads and lysate were incubated together overnight on a rotator at 4 °C or for 1 hour at 4 °C in the case of Brk. Next, the lysate-beads mix was returned to the PD-10 column and the flow through was collected. The beads are washed 4 times with 10 ml buffer and each wash flow through was collected. The protein was eluted with 5 times 2 CV buffer with 300 mM glutathione. Each elution was collected separately. Gel samples were taken (20 µl), to which SDS loading buffer was added (20 µl) and they were then heated to 100 °C for 10 minutes and run on 15% SDS PAGE gels as described above. The

fractions shown to be containing the desired SH3 domain were kept on ice or frozen at -20 °C for further use.

2.8.2 Thrombin Digestion

The constructs for the C-terminal domain of Grb2 (known here as Grb2C), the N-terminal domain of Grb2 (known here as Grb2N) and the SH3 domain of Src contained a thrombin cleavage site (LVPRGSAMV) between the GST tag and the SH3 domain construct allowing the removal of the GST tag. The relevant fractions from the GST affinity column were combined and the amount of desired protein present was calculated using the Beer-Lambert method as described previously. In order to establish how many units (based upon the activity) of thrombin was required to completely digest 1 mg of protein during the first purification, 1 ml of sample was incubated overnight with varying numbers of thrombin units per mg protein either at room temperature or at 4 °C. It was established that 5 units of thrombin would completely digest 1 mg Grb2C overnight at room temperature whereas 3 units was insufficient and 7 units was wasteful. For all further reactions, 5 units of thrombin was used per mg desired protein. Based upon the recommended resuspension of thrombin by the manufacturers (HT 1002a, lot 398L, Enzyme Research Laboratories), 1 unit of thrombin equates to 0.092 µl of solution. The required volume of thrombin was added to the sample and incubated overnight at room temperature. After incubation for approximately 16 hours, sample was run on a 15% SDS-PAGE gel as described above to confirm complete digestion. Upon confirmation, the digestion was ended by the application of 1 mM PMSF (phenylmethanesulphonyl fluoride). Following similar optimisation, Grb2N required 7.5 units of thrombin per 1 mg of protein and the Src SH3 domain required 5 units of thrombin.

2.8.3 Factor Xa Digestion

Unlike the other SH3 domains studied here, the GST tag was fused to Brk with a linker region containing a Factor Xa cleavage motif (IEGR). As with thrombin digestions, the amount of enzyme required to digest 1 mg of Brk SH3 domain was optimised and it was found that 7.5 units of Factor Xa is required to digest 1 mg of protein overnight at 37 °C. The fractions shown by SDS-PAGE to contain the GST tagged Brk were combined and the

protein concentration calculated using the Beer-Lambert law and thus the number of units of Factor Xa required was determined. This was incubated with the protein sample overnight at 37 °C and a sample taken the following morning and run on a 15% SDS-PAGE gel. Upon confirmation of complete digestion, the digestion was stopped using PMSF as above.

2.8.4 Spin Concentration of Protein Samples

Spin concentration is the process by which the volume of a sample is reduced by centrifugation through a membrane with a specific molecular weight pore size while maintaining the protein amount, reducing the volume and thus increasing the concentration. Samples were spin concentrated at 4000 x g at 4 °C until the desired volume was achieved. The concentrators used for all proteins, other than the Brk SH3 domain, were Vivaspin 6 or 20 (Sartorius), dependent on initial volume, with a molecular weight membrane cut off of 5000. In the case of Brk, Amicon Ultra-15 were used due to the Brk SH3 domain adhering to the polyethersulfone (PES) membrane of the Vivaspin concentrators. The Amicon concentrators use a cellulose membrane instead. The samples were centrifuged in 45-60 minute runs until the desired volume was achieved.

2.8.5 Size Exclusion Chromatography for SH3 domain purification

Samples were concentrated down to a volume of 2.5 ml and loaded onto a Superdex^{TM} 75 (GE Healthcare) 330ml gel filtration column, pre-equilibrated with the appropriate buffer. This was run with a flow rate of 1 ml/min and 10 ml fractions were collected. 20 µl gel samples were taken and treated as previously and separated with a 15% SDS-PAGE gel as described previously. Once the fractions containing the SH3 domain, and not the GST tag, were identified in this manner, they were combined and the protein concentration calculated using the Beer-Lambert technique. The fractions were then dialysed into the appropriate NMR buffer using a dialysis membrane of MW limit 3000 over the weekend at 4 °C. This was not necessary for the Brk SH3 domain as spectra were collected in the same HEPES buffer used during purification. Finally, the protein sample was concentrated to approximately 2 mM and frozen at -20 °C until used as an NMR sample.

2.9 ADAM15 ICD Purification

2.9.1 Nickel Affinity Purification

Rosetta 2 cells were transformed as described above and cultured following the 2YT protocol. After harvesting, the pellet was resuspended with 50 mM sodium phosphate, 300 mM NaCl, 8 M urea (unless stated otherwise) pH 7.4 (hereafter known as IMAC buffer) with protease inhibitors (Roche Applied Science EDTA-free protease inhibitor cocktail tablets). The cells were sonicated as described and incubated on ice for 30 minutes. The lysate was then clarified by centrifugation and filtering as previously described. The nickel sepharose gravity column (Ni-NTA sepharose, Generon) was equilibrated into IMAC buffer and the clarified lysate was applied to the column and the flow through collected. This step was repeated so that the lysate passed over the beads twice. The beads were then washed twice with 2 CV of IMAC buffer, with each wash collected separated. Next, the beads were washed with increasing concentrations of imidazole in IMAC buffer. These concentrations of imidazole were 50 mM, 75 mM, 100 mM, 150 mM, 200 mM and 500 mM unless otherwise stated. These washes were collected separately and gel samples were made from each elution as described previously. Those fractions containing the protein of interest were then dialysed into IMAC buffer in order to remove the imidazole and urea. The samples were then frozen at -20 °C until further use.

2.9.2 Size Exclusion Chromatography for ADAM15 Purification

The removal of impurities remaining after Ni-NTA Affinity purification was attempted using size exclusion chromatography. The protocol for this was the same as for SH3 domain purification described previously but with the column pre-equilibrated into IMAC buffer (without urea) prior to use.

2.9.3 Talon Affinity Purification

As an alternative to Ni-NTA affinity purification, Talon (® GE Healthcare) affinity purification was attempted. This works under the same principle as Ni-NTA affinity but

uses Co^{2+} as the affinity ion. This has been shown to interact with poly-histidine tags with a higher specificity than Ni-NTA affinity and so was attempted to try to avoid the impurities which remained after Ni-NTA affinity. The lysate was prepared as previously, using a 2YT culture of the variant in question and sonicated and clarified as previously. The column and Äkta was pre-equilibrated into IMAC buffer with 8 M urea. The sample was loaded onto the 1 ml Talon column at 1 ml/min and then the column was washed with 20 cv of IMAC buffer in order to achieve a stable baseline. The protein was eluted with a gradient over 20 cv at 1 ml/min with the concentration of imidazole increasing over that gradient from 0 mM to a final concentration of 300 mM. Fractions of 1 ml were collected and gel samples prepared. Those fractions containing the protein were identified using a 15 % SDS PAGE gel and dialysed into IMAC buffer to remove the imidazole and urea. After dialysis, the sample was frozen at -20 °C until further use.

2.10 Nuclear Magnetic Resonance

2.10.1 NMR Sample Preparation

All samples for NMR were concentrated using Vivaspin spin concentrators as above, having already been dialysed into the appropriate buffer (50 mM sodium phosphate, 100 mM NaCl pH 7.5 for Grb2C, 50 mM Tris.HCl, 100 mM NaCl pH 8.0 for Grb2N and 100 mM sodium phosphate, 100 mM NaCl pH 6.0 for the Src SH3 domain) until a volume of ~0.4 ml was achieved. Brk was studied in the same HEPES buffer as it was purified in and ADAM15 B was dialysed into the same buffer as used for the Src SH3 domain. The sample was transferred by pipette to a 1.5 ml eppendorf and made up to 0.5 ml with flow through from the concentration (i.e. the same buffer). The samples had been made to have a final concentration of 1 mM. To each sample, 50 µl D_2O, 10 µl DSS and 10 µl NaN_3 were added and the samples were transferred to 5 mm NMR tubes (PP535, Wilmad® or Norell® S-5-600-7).

2.10.2 NMR Data Acquisition

Spectra were acquired using a Bruker Avance I 500 MHz spectrometer with a ^1H operating frequency of 499.6853512 MHz. This spectrometer uses a 5 mm inverse triple resonance (HCN) z-gradient probe. All spectra were acquired at 298 K. The spectra

acquired for backbone assignments were ^{15}N HSQC, ^{13}C HSQC, HNCαCβ and CβCαCONH. Spectral parameters are shown in Table 2.3.

Table 2.3 Acquisition Parameters for NMR experiments at 500 MHz obtained

Experiment	Number of Scans	Complex Points			Spectral Width (Hz)		
		^{1}H	^{15}N	^{13}C	^{1}H	^{15}N	^{13}C
^{15}N HSQC	16	1024	128	-	7507.587	1772.345	-
HNCaCb	32	1024	128	32	6510.417	9425.719	1822.984
CbCaCONH	32	1024	61	32	6510.417	9425.719	1822.984
^{15}N HSQC (long titration data points)	120-240	1024	64	-	7507.507	1772.345	-
^{13}C HSQC *	32	512	-	64	10416.67	-	33332.08

* indicates that this experiment was acquired using the 800 MHz spectrometer

The ^{13}C HSQC was acquired at 298 K using a Bruker Avance III 800 MHz spectrometers with a ^{1}H operating frequency of 800.2337599 MHz. This spectrometer uses a triple resonance inverse TXI probe with z- gradients.

2.10.3 NMR Spectral Processing

The NMRPipe software package (Delaglio et al., 1995) was used to zero-fill, linear predict, Fourier transform and phase all spectra acquired. The DSS standard in each sample was used to reference the respective proton, ^{13}C and ^{15}N chemical shifts using a script written in house by Dr James Tolchard.

2.10.4 Backbone Assignments

Backbone assignments for Grb2C were provided by Prof John E. Ladbury via BMRB entry 18748 (Lin et al., 2012). These were used to assign most residues using the CCPNmr analysis software package (Vranken et al., 2005). Any remaining assignments were made by using the i, i-1 connectivities observed with the HNCαCβ and CβCαCONH spectra. Backbone assignments for Grb2N were provided by Michael Wittekind et al (Wittekind et al., 1997), for Src by Hongtao Yu et al (Yu et al., 1993) and for Brk by Sunggeon Ko et al (Ko et al., 2009).

2.10.5 Titration Spreadsheets

Samples A and B were prepared as indicated in the spreadsheets. Intermediate data points were achieved by the removal of the indicated volume from A and replacing with the same volume of B.

Titrations with Grb2C

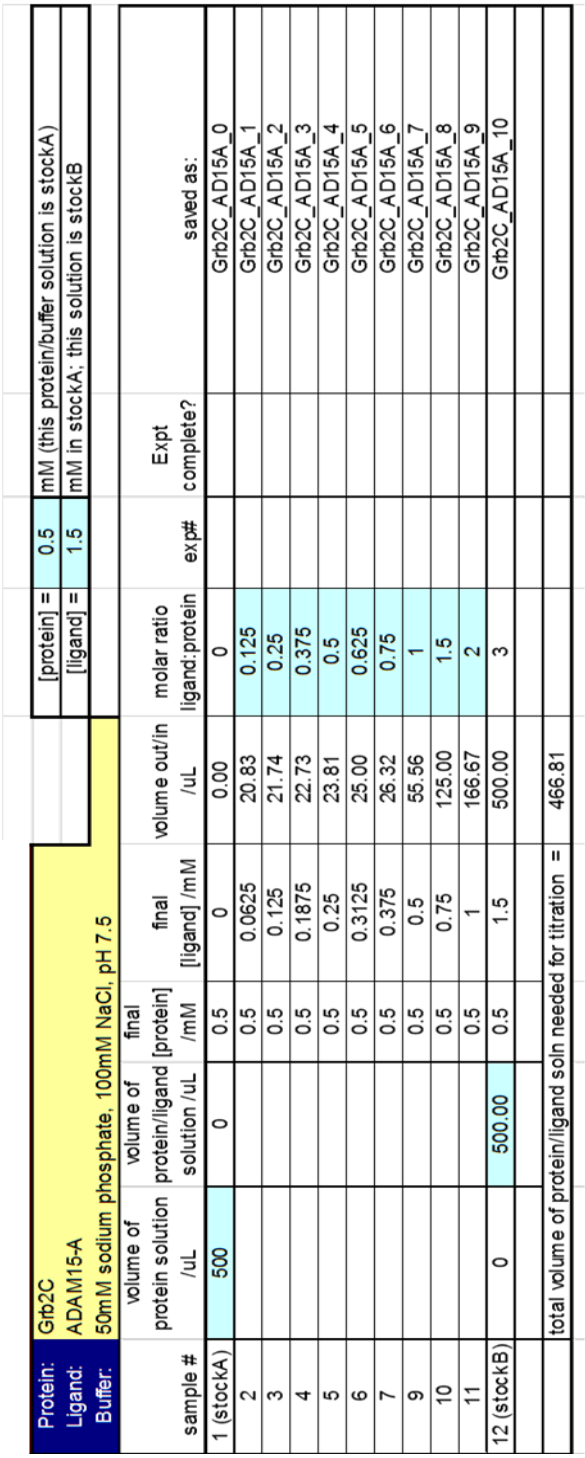

Protein:	Grb2C							[protein] =	0.5	mM (this protein/buffer solution is stockA)
Ligand:	ADAM15-A							[ligand] =	1.5	mM in stockA; this solution is stockB
Buffer:	50mM sodium phosphate, 100mM NaCl, pH 7.5									
sample #	volume of protein solution /uL	volume of protein/ligand solution /uL	final [protein] /mM	final [ligand] /mM	volume out/in /uL	molar ratio ligand:protein	exp#	Expt complete?	saved as:
1 (stockA)	500	0	0.5	0	0.00	0			Grb2C_AD15A_0
2			0.5	0.0625	20.83	0.125			Grb2C_AD15A_1
3			0.5	0.125	21.74	0.25			Grb2C_AD15A_2
4			0.5	0.1875	22.73	0.375			Grb2C_AD15A_3
5			0.5	0.25	23.81	0.5			Grb2C_AD15A_4
6			0.5	0.3125	25.00	0.625			Grb2C_AD15A_5
7			0.5	0.375	26.32	0.75			Grb2C_AD15A_6
9			0.5	0.5	55.56	1			Grb2C_AD15A_7
10			0.5	0.75	125.00	1.5			Grb2C_AD15A_8
11			0.5	1	166.67	2			Grb2C_AD15A_9
12 (stockB)	0	500.00	0.5	1.5	500.00	3			Grb2C_AD15A_10
	total volume of protein/ligand soln needed for titration =				466.81				

Protein:	Grb2C							[protein] =	0.5	mM (this protein/buffer solution is stockA)
Ligand:	ADAM-15 B							[ligand] =	1.6	mM in stockA; this solution is stockB
Buffer:	20mM sodium phosphate, 100mM NaCl, pH 7.5									
sample #	volume of protein solution /uL	volume of protein/ligand solution /uL	final [protein] /mM	final [ligand] /mM	volume out/in /uL	molar ratio ligand:protein	exp#	Expt complete?	saved as:
1 (stockA)	500	0	0.5	0	0.00	0			Grb2C_AD15B_0
2			0.5	0.125	39.06	0.25			Grb2C_AD15B_1
3			0.5	0.25	42.37	0.5			Grb2C_AD15B_2
4			0.5	0.375	46.30	0.75			Grb2C_AD15B_3
5			0.5	0.5	51.02	1			Grb2C_AD15B_4
6			0.5	0.75	113.64	1.5			Grb2C_AD15B_5
7			0.5	1	147.06	2			Grb2C_AD15B_6
9 (stockB)	0	500.00	0.5	1.6	-	3.2			Grb2C_AD15B_7
	total volume of protein/ligand soln needed for titration =				439.45				

Protein:	Grb2C					[protein] =	0.5	mM (this protein/buffer solution is stockA)	
Ligand:	ADAM15-C					[ligand] =	1.5	mM in stockA; this solution is stockB	
Buffer:	50mM sodium phosphate, 100mM NaCl, pH 7.5								
sample #	volume of protein solution /uL	volume of protein/ligand solution /uL	final [protein] /mM	final [ligand] /mM	volume out/in /uL	molar ratio ligand:protein	exp#	Expt complete?	saved as:
1 (stockA)	500	0	0.5	0	0.00	0			Grb2C_AD15C_0
2			0.5	0.0625	20.83	0.125			Grb2C_AD15C_1
3			0.5	0.125	21.74	0.25			Grb2C_AD15C_2
4			0.5	0.1875	22.73	0.375			Grb2C_AD15C_3
5			0.5	0.25	23.81	0.5			Grb2C_AD15C_4
6			0.5	0.3125	25.00	0.625			Grb2C_AD15C_5
7			0.5	0.375	26.32	0.75			Grb2C_AD15C_6
9			0.5	0.5	55.56	1			Grb2C_AD15C_7
10			0.5	0.75	125.00	1.5			Grb2C_AD15C_8
11			0.5	1	166.67	2			Grb2C_AD15C_9
12 (stockB)	0	500.00	0.5	1.5	500.00	3			Grb2C_AD15C_10
	total volume of protein/ligand soln needed for titration =				466.81				

Protein:	Grb2C					[protein] =	0.5	mM (this protein/buffer solution is stockA)	
Ligand:	ADAM15-D					[ligand] =	1.5	mM in stockA; this solution is stockB	
Buffer:	50mM sodium phosphate, 100mM NaCl, pH 7.5								
sample #	volume of protein solution /uL	volume of protein/ligand solution /uL	final [protein] /mM	final [ligand] /mM	volume out/in /uL	molar ratio ligand:protein	exp#	Expt complete?	saved as:
1 (stockA)	500	0	0.5	0	0.00	0			Grb2C_AD15D_0
2			0.5	0.0625	20.83	0.125			Grb2C_AD15D_1
3			0.5	0.125	21.74	0.25			Grb2C_AD15D_2
4			0.5	0.1875	22.73	0.375			Grb2C_AD15D_3
5			0.5	0.25	23.81	0.5			Grb2C_AD15D_4
6			0.5	0.3125	25.00	0.625			Grb2C_AD15D_5
7			0.5	0.375	26.32	0.75			Grb2C_AD15D_6
9			0.5	0.5	55.56	1			Grb2C_AD15D_7
10			0.5	0.75	125.00	1.5			Grb2C_AD15D_8
11			0.5	1	166.67	2			Grb2C_AD15D_9
12 (stockB)	0	500.00	0.5	1.5	500.00	3			Grb2C_AD15D_10
	total volume of protein/ligand soln needed for titration =				466.81				

Protein:	Grb2C					[protein] =	0.5	mM (this protein/buffer solution is stockA)	
Ligand:	ADAM-15 E					[ligand] =	1.58	mM in stockA; this solution is stockB	
Buffer:	50mM sodium phosphate, 100mM NaCl, pH 7.5								
sample #	volume of protein solution /uL	volume of protein/ligand solution /uL	final [protein] /mM	final [ligand] /mM	volume out/in /uL	molar ratio ligand:protein	exp#	Expt complete?	saved as:
1 (stockA)	500	0	0.5	0	0.00	0			Grb2C_AD15E_0
2			0.5	0.0625	19.78	0.125			Grb2C_AD15E_1
3			0.5	0.125	20.59	0.25			Grb2C_AD15E_2
4			0.5	0.1875	21.48	0.375			Grb2C_AD15E_3
5			0.5	0.25	22.44	0.5			Grb2C_AD15E_4
6			0.5	0.3125	23.50	0.625			Grb2C_AD15E_5
7			0.5	0.375	24.65	0.75			Grb2C_AD15E_6
9			0.5	0.5	51.87	1			Grb2C_AD15E_7
10			0.5	0.75	115.74	1.5			Grb2C_AD15E_8
11			0.5	1	150.60	2			Grb2C_AD15E_9
12 (stockB)	0	500.00	0.5	1.58	500.00	3.16			Grb2C_AD15E_10
	total volume of protein/ligand soln needed for titration =				430.87				

Protein:	Grb2C					[protein] =	0.5	mM (this protein/buffer solution is stockA)	
Ligand:	GB1 tag only					[ligand] =	1.5	mM in stockA; this solution is stockB	
Buffer:	50mM sodium phosphate, 100mM NaCl, pH 7.5								
sample #	volume of protein solution /uL	volume of protein/ligand solution /uL	final [protein] /mM	final [ligand] /mM	volume out/in /uL	molar ratio ligand:protein	exp#	Expt complete?	saved as:
1 (stockA)	500	0	0.5	0	0.00	0			Grb2C_GB1_0
9			0.5	0.5	166.67	1			Grb2C_GB1_7
	total volume of protein/ligand soln needed for titration =				166.67				

Protein:	Grb2C					[protein] =	0.5	mM (this protein/buffer solution is stockA)		
Ligand:	ADAM-15 B AGTA					[ligand] =	1.5	mM in stockA; this solution is stockB		
Buffer:	50mM sodium phosphate, 100mM NaCl, pH 7.5									
sample #	volume of protein solution /uL	volume of protein/ligand solution /uL	final [protein] /mM	final [ligand] /mM	volume out/in /uL	molar ratio ligand:protein	exp#	Expt complete?	saved as:	
1 (stockA)	500	0	0.5	0	0.00	0			Grb2C_AD15BM_0	
2			0.5	0.0625	20.83	0.125			Grb2C_AD15BM_1	
3			0.5	0.125	21.74	0.25			Grb2C_AD15BM_2	
4			0.5	0.1875	22.73	0.375			Grb2C_AD15BM_3	
5			0.5	0.25	23.81	0.5			Grb2C_AD15BM_4	
6			0.5	0.3125	25.00	0.625			Grb2C_AD15BM_5	
7			0.5	0.375	26.32	0.75			Grb2C_AD15BM_6	
9			0.5	0.5	55.56	1			Grb2C_AD15BM_7	
10			0.5	0.75	125.00	1.5			Grb2C_AD15BM_8	
11			0.5	1	166.67	2			Grb2C_AD15BM_9	
12 (stockB)	0	500.00	0.5	1.5	500.00	3			Grb2C_AD15BM_10	
	total volume of protein/ligand soln needed for titration =				466.81					

Protein:	Src					[protein] =	0.5	mM (this protein/buffer solution is stockA)	
Ligand:	ADAM15-A					[ligand] =	1.5	mM in stockA; this solution is stockB	
Buffer:	100mM sodium phosphate, 100mM NaCl, pH 6.0								
sample #	volume of protein solution /uL	volume of protein/ligand solution /uL	final [protein] /mM	final [ligand] /mM	volume out/in /uL	molar ratio ligand:protein	exp#	Expt complete?	saved as:
1 (stockA)	500	0	0.5	0	0.00	0			Src_AD15A_0
2			0.5	0.0625	20.83	0.125			Src_AD15A_1
3			0.5	0.125	21.74	0.25			Src_AD15A_2
4			0.5	0.1875	22.73	0.375			Src_AD15A_3
5			0.5	0.25	23.81	0.5			Src_AD15A_4
6			0.5	0.3125	25.00	0.625			Src_AD15A_5
7			0.5	0.375	26.32	0.75			Src_AD15A_6
9			0.5	0.5	55.56	1			Src_AD15A_7
10			0.5	0.75	125.00	1.5			Src_AD15A_8
11			0.5	1	166.67	2			Src_AD15A_9
12 (stockB)	0	500.00	0.5	1.5	500.00	3			Src_AD15A_10
	total volume of protein/ligand soln needed for titration =				466.81				

Protein:	Src					[protein] =	0.5	mM (this protein/buffer solution is stockA)	
Ligand:	ADAM15-B					[ligand] =	1.5	mM in stockA; this solution is stockB	
Buffer:	100mM sodium phosphate, 100mM NaCl, pH 6.0								
sample #	volume of protein solution /uL	volume of protein/ligand solution /uL	final [protein] /mM	final [ligand] /mM	volume out/in /uL	molar ratio ligand:protein	exp#	Expt complete?	saved as:
1 (stockA)	500	0	0.5	0	0.00	0			Src_AD15B_0
2			0.5	0.0625	20.83	0.125			Src_AD15B_1
3			0.5	0.125	21.74	0.25			Src_AD15B_2
4			0.5	0.1875	22.73	0.375			Src_AD15B_3
5			0.5	0.25	23.81	0.5			Src_AD15B_4
6			0.5	0.3125	25.00	0.625			Src_AD15B_5
7			0.5	0.375	26.32	0.75			Src_AD15B_6
9			0.5	0.5	55.56	1			Src_AD15B_7
10			0.5	0.75	125.00	1.5			Src_AD15B_8
11			0.5	1	166.67	2			Src_AD15B_9
12 (stockB)	0	500.00	0.5	1.5	500.00	3			Src_AD15B_10
	total volume of protein/ligand soln needed for titration =				466.81				

Protein:	Src					[protein] =	0.5	mM (this protein/buffer solution is stockA)	
Ligand:	ADAM15-C					[ligand] =	1.5	mM in stockA; this solution is stockB	
Buffer:	100mM sodium phosphate, 100mM NaCl, pH 6.0								
sample #	volume of protein solution /uL	volume of protein/ligand solution /uL	final [protein] /mM	final [ligand] /mM	volume out/in /uL	molar ratio ligand:protein	exp#	Expt complete?	saved as:
1 (stockA)	500	0	0.5	0	0.00	0			Src_AD15C_0
2			0.5	0.0625	20.83	0.125			Src_AD15C_1
3			0.5	0.125	21.74	0.25			Src_AD15C_2
4			0.5	0.1875	22.73	0.375			Src_AD15C_3
5			0.5	0.25	23.81	0.5			Src_AD15C_4
6			0.5	0.3125	25.00	0.625			Src_AD15C_5
7			0.5	0.375	26.32	0.75			Src_AD15C_6
9			0.5	0.5	55.56	1			Src_AD15C_7
10			0.5	0.75	125.00	1.5			Src_AD15C_8
11			0.5	1	166.67	2			Src_AD15C_9
12 (stockB)	0	500.00	0.5	1.5	500.00	3			Src_AD15C_10
	total volume of protein/ligand soln needed for titration =				466.81				

Protein:	Src					[protein] =	0.5	mM (this protein/buffer solution is stockA)	
Ligand:	ADAM15-D					[ligand] =	1.5	mM in stockA; this solution is stockB	
Buffer:	100mM sodium phosphate, 100mM NaCl, pH 6.0								
sample #	volume of protein solution /uL	volume of protein/ligand solution /uL	final [protein] /mM	final [ligand] /mM	volume out/in /uL	molar ratio ligand:protein	exp#	Expt complete?	saved as:
1 (stockA)	500	0	0.5	0	0.00	0			Src_AD15D_0
2			0.5	0.0625	20.83	0.125			Src_AD15D_1
3			0.5	0.125	21.74	0.25			Src_AD15D_2
4			0.5	0.1875	22.73	0.375			Src_AD15D_3
5			0.5	0.25	23.81	0.5			Src_AD15D_4
6			0.5	0.3125	25.00	0.625			Src_AD15D_5
7			0.5	0.375	26.32	0.75			Src_AD15D_6
9			0.5	0.5	55.56	1			Src_AD15D_7
10			0.5	0.75	125.00	1.5			Src_AD15D_8
11			0.5	1	166.67	2			Src_AD15D_9
12 (stockB)	0	500.00	0.5	1.5	500.00	3			Src_AD15D_10
	total volume of protein/ligand soln needed for titration =				466.81				

Protein:	Src					[protein] =	0.5	mM (this protein/buffer solution is stockA)	
Ligand:	ADAM15-E					[ligand] =	1.5	mM in stockA; this solution is stockB	
Buffer:	100mM sodium phosphate, 100mM NaCl, pH 6.0								
sample #	volume of protein solution /uL	volume of protein/ligand solution /uL	final [protein] /mM	final [ligand] /mM	volume out/in /uL	molar ratio ligand:protein	exp#	Expt complete?	saved as:
1 (stockA)	500	0	0.5	0	0.00	0			Src_AD15E_0
2			0.5	0.0625	20.83	0.125			Src_AD15E_1
3			0.5	0.125	21.74	0.25			Src_AD15E_2
4			0.5	0.1875	22.73	0.375			Src_AD15E_3
5			0.5	0.25	23.81	0.5			Src_AD15E_4
6			0.5	0.3125	25.00	0.625			Src_AD15E_5
7			0.5	0.375	26.32	0.75			Src_AD15E_6
9			0.5	0.5	55.56	1			Src_AD15E_7
10			0.5	0.75	125.00	1.5			Src_AD15E_8
11			0.5	1	166.67	2			Src_AD15E_9
12 (stockB)	0	500.00	0.5	1.5	500.00	3			Src_AD15E_10
	total volume of protein/ligand soln needed for titration =				466.81				

Protein:	Src					[protein] =	0.5	mM (this protein/buffer solution is stockA)	
Ligand:	GB1					[ligand] =	1.5	mM in stockA; this solution is stockB	
Buffer:	100mM sodium phosphate, 100mM NaCl, pH 6.0								
sample #	volume of protein solution /uL	volume of protein/ligand solution /uL	final [protein] /mM	final [ligand] /mM	volume out/in /uL	molar ratio ligand:protein	exp#	Expt complete?	saved as:
1 (stockA)	500	0	0.5	0	0.00	0			Src_GB1_0
9			0.5	0.5	166.67	1			Src_GB1_7
12 (stockB)	0	500.00	0.5	1.5	500.00	3			Src_GB1_10
	total volume of protein/ligand soln needed for titration =				166.67				

Protein:	Brk					[protein] =	0.1	mM (this protein/buffer solution is stockA)	
Ligand:	ADAM15-B					[ligand] =	1	mM in stockA; this solution is stockB	
Buffer:	25mM HEPES, 100mM NaCl, pH 7.0								
sample #	volume of protein solution /uL	volume of protein/ligand solution /uL	final [protein] /mM	final [ligand] /mM	volume out/in /uL	molar ratio ligand:protein	exp#	Expt complete?	saved as:
1 (stockA)	500	0	0.1	0	0.00	0			Brk_AD15B_0
2			0.1	0.0125	6.25	0.125			Brk_AD15B_1
3			0.1	0.025	6.33	0.25			Brk_AD15B_2
4			0.1	0.0375	6.41	0.375			Brk_AD15B_3
5			0.1	0.05	6.49	0.5			Brk_AD15B_4
6			0.1	0.0625	6.58	0.625			Brk_AD15B_5
7			0.1	0.075	6.67	0.75			Brk_AD15B_6
8			0.1	0.1	13.51	1			Brk_AD15B_7
9			0.1	0.2	55.56	2			Brk_AD15B_8
10			0.1	0.5	187.50	5			Brk_AD15B_9
11			0.1	0.7	200.00	7			Brk_AD15B_10
12 (stockB)	0	500.00	0.1	1	500.00	10			Brk_AD15B_11
	total volume of protein/ligand soln needed for titration =				489.05				

Protein:	Brk					[protein] =	0.1	mM (this protein/buffer solution is stockA)	
Ligand:	GB1					[ligand] =	1	mM in stockA; this solution is stockB	
Buffer:	2mM HEPES, 100mM NaCl, pH 7.0								
sample #	volume of protein solution /uL	volume of protein/ligand solution /uL	final [protein] /mM	final [ligand] /mM	volume out/in /uL	molar ratio ligand:protein	exp#	Expt complete?	saved as:
1 (stockA)	500	0	0.1	0	0.00	0			Brk_GB1_0
9			0.1	0.1	50.00	1			Brk_GB1_1
12 (stockB)	0	500.00	0.1	1	500.00	10			Brk_GB1_2
	total volume of protein/ligand soln needed for titration =				50.00				

Chapter 3: Studying the ADAM15 Intracellular Domains

3.1 Introduction

As discussed in chapter 1, the ADAM15 intracellular domain is encoded by exons 18-23 of the *ADAM15* gene with the splice variants involving exons 19-22 (Kleino et al., 2007). As shown in figure 3.1, ADAM15 A is missing exons 20 and 21 and is 97 residues long, whereas ADAM15 B is missing exon 21 and is 122 residues long. ADAM15 C is the longest ICD variant, at 145 residues long, as it includes all potential exons and thus all of the potential proline-rich regions that the gene translates to. ADAM15 D includes a frameshift at tyrosine 735 which is encoded for at the end of exon 18 and thus has no polyproline regions(Poghosyan, 2001). Additionally, exons 19-21 and 23 are spliced out of this variant rendering ADAM15 D as the shortest variant at only 56 residues. Finally, ADAM15 E excludes exon 20 and is 121 residues in total. The potential proline-rich regions available here include potential binding sites for SH3 domains whereby the **ΦPpΦP** motif (where Φ is a hydrophobic residue and p can be a proline) folds into the hydrophobic cleft of the SH3 domain and specificity is provided by the residues surrounding the motif (Kaneko et al., 2008). Due to the variations in behaviour displayed by cells overexpressing each ICD (Zhong et al., 2008), along with the correlation to differing prognoses in breast cancer patients (Zhong et al., 2008), and the prospective specificity of each ICD with different SH3 domains (Kärkkäinen et al., 2006; Kleino et al., 2009; Zhong et al., 2008), it is of value to study how these splice variants behave with regards to their interactions with SH3 domains.

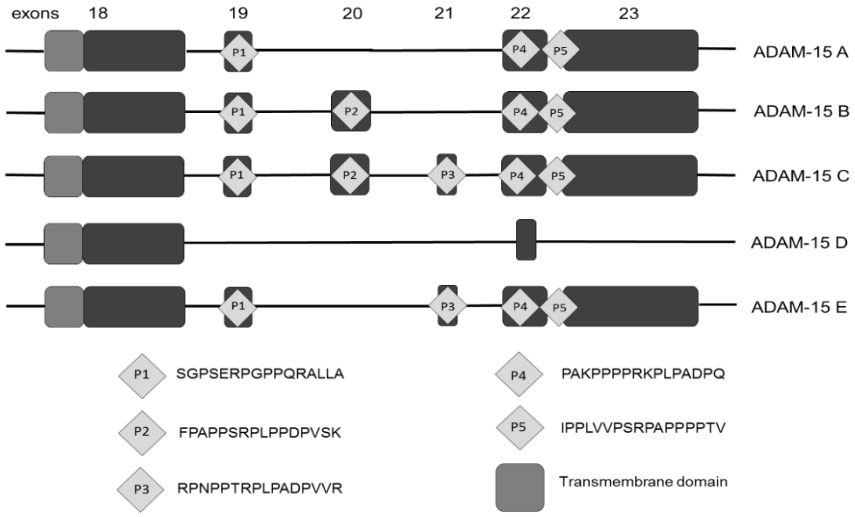

Figure 3.1 Schematic showing the ADAM15 splicing locations and the proline-rich regions that they are translated to. Adapted from Zhong et al (Zhong et al., 2008).

Due to the high proportion of glycine, arginine, proline, serine, glutamine and glutamic acid residues within all of the ADAM15 ICDs, it has been predicted that the proteins are intrinsically disordered and lack consistent secondary structure. Although this renders NMR studies of the proteins more difficult, as intrinsically disordered residues have amide ^{1}H chemical shifts between 8.0 and 8.5 ppm leading to overlapping peaks which can be more difficult to assign, it has been achieved in the past (Kosol et al., 2013). Any potential NMR studies are, however, complicated by the high number of proline residues present as these do not contain an N-H bond when in a peptide chain and so do not have a peak on a standard [^{1}H-^{15}N]-HSQC spectrum. When the importance of the proline residues with regards to interactions with any SH3 domains is considered, this is a significant hindrance although alternative pulse sequences can be used here instead. Additional problems arise due to the insolubility of the recombinant ICDs when not fusion-tagged to a more soluble protein as established by a previous summer project student in the lab, Alex Carey-Hulyer.

3.2 Interactions of the SH3 domain-containing proteins with GST-tagged ADAM15 ICDs via GST Affinity Pull Down Assay

Previously it has been shown by pull down assay that the ADAM15 ICD variants interact preferentially with different proteins that contain SH3-domains (Poghosyan, 2001). In these studies, the MDA-MB-435 cell line was used to provide the endogenous SH3 domain proteins. To confirm that these results could be reproduced in the breast cancer MCF-7 cell line, these experiments were repeated. Since the publication of the previous pull down studies, it has also been shown that FAK can act as an intermediary in interactions between ADAM15 A and some SH3 domain containing proteins (Fried et al., 2012) providing additional reasons for repetition of the assay, as FAK is present in MCF-7 cells but not in MDA-MB-435 cells. Finally, there has been some debate as to the lineage of MDA-MB-435 cells recently due to their expression of melanocyte-specific markers along with the expected breast cell-specific markers. As other aggressive breast cancer cell line have shown similar expression profiles, it has been suggested that these lines did originate from breast tumours but have experienced some lineage infidelity (Sellappan et al., 2004).

A Bicinchoninic acid (BCA) assay was initially used to establish the total protein concentration of the MCF-7 cell lysate but unfortunately, the presence of the sepharose beads interfered with the reaction involved, rendering it not suitable. The Bradford assayAssay was chosen for this purpose as it is not sensitive to the presence of sepharose. Additionally, the first anti-Src antibody used was later discovered to be specific for an epitope of Src that is conserved across many members of the Src homology family including Lyn and Hck which are of a similar molecular weight to Src and thus could be contributing to the results for Src on a Western blot.

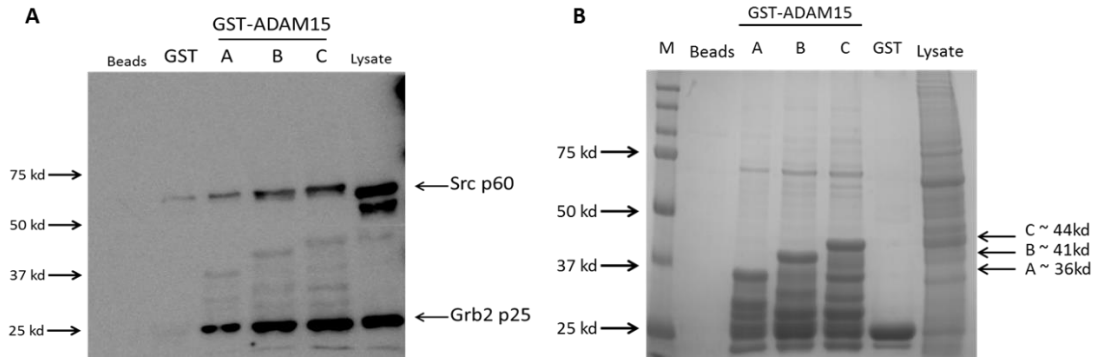

Figure 3.2 SH3 domain-containing proteins pulled down from MCF-7 cell lysate by recombinant GST fusion ADAM15 ICD variants. Glutathione sepharose beads with no covalently bound protein was presented as a negative control. GST fusion ADAM15 ICD variants used as bait proteins as indicated. GST bound to sepharose without an ADAM15 ICD was used to indicate a lack of interaction between the tag and the SH3 domains directly. Src and Grb2 were detectable at endogenous levels from the MCF-7 lysate. A) Western blots probing for Src or Grb2. B) Equal loading of proteins confirmed by Coomassie Blue stained SDS-PAGE poly-acrylamide gels.

Both Src and Grb2 were equally pulled down by all of the ADAM15 ICDs, as seen in figure 3.2 which is, in the case of ADAM15 B and C, consistent with the results achieved in previous publications using MDA-MB-435 cells. However, Src was shown to interact with ADAM15 A here which is contrary to previous studies. This difference could be due to the presence of FAK in the lysate of MCF-7 cells acting as an intermediate in the interaction. These results are also consistent with data collected by Dr Christian Roghi through in cell localisation studies using proximity ligation studies (personal communication). Although this difference occurs, it is clear that the MCF-7 cells show a similar pattern of interactions to previous research and are of a more reliable breast cancer lineage so are suitable for continued use here.

3.3 Test Purifications of Recombinant GB1 Fusion Proteins

As mentioned in section 3.1, the ADAM15 ICDs were found to be insoluble when the GST fusion tag, intended for purification purposes, was removed. Unfortunately, retaining the GST fusion tag for use in the later NMR studies was not feasible due to the large size of the final fusion proteins having too large a molecular weight and slow tumbling time to be practical. For this reason, the fusion tag used for purification purposes needed to be of a size small enough to be retained for the NMR titrations later. Due to its small size and consistent, clear [^{1}H-^{15}N]-HSQC spectrum, the immunoglobulin binding domain 1 of Protein G from group C and G Streptococcal bacteria (GB1) was chosen (Sommer et al., 2012; Xu et al., 2014a). A vector, based upon pRSFDuet from Novagen, was purchased and contained DnaE N-intein with a His-GB1 fusion tag. This was called pSKDuet01 and was produced by Hideo Iwai et al (Iwai et al., 2006) and provided an N-terminal GB1 tag for solubility purposes and an associated His tag for purification purposes. The DnaE N-intein gene was removed using restriction sites for BamHI and HindIII which were also introduced to the 5' and 3' ends of the genes for the ADAM15 ICDs by polymerase chain reaction (PCR). The ADAM15 ICD genes were ligated into the pSKDuet01 and validated by sequencing. This vector was then transformed into Codon + RP cells for protein expression tests.

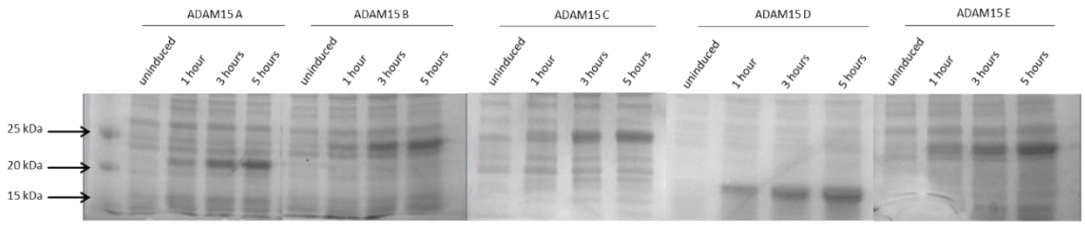

Figure 3.3 SDS-PAGE gel electrophoresis of a time course test expression of each of the GB1-tagged ADAM15 ICDs in Codon + RP bacterial cells.

A time course expression test, shown in figure 3.3, was conducted using E.coli Codon + RP (Agilent Technologies) at 37 °C over 5 hours. Human specific codons are used in these genes; and therefore they required adapted bacterial strains, such as Codon + RP, for successful expression. All the ADAM15 ICDs expressed well at 37 °C and expression continued over time so there was no evidence of toxic over-expression if incubated for

too long. Test purification via nickel affinity chromatography was possible due to the poly-histidine tag but the low concentration of the eluted bands for all the ICDs compared to the concentration of the proteins seen in the Codon + RP lysate, demonstrated a need for further optimisation of the purification protocol. However weak, this test experiment did prove that the His-GB1 tagged ADAM15 ICDs do bind to Ni sepharose which was capitalised on for future purifications and in further pull down assays.

3.4 Interactions of the SH3 domain-containing proteins with GB1-tagged ADAM15 ICDs via His Affinity Pull Down Assay

The GST-based pull down assay was repeated using the newly made His-GB1 fusion ADAM15 ICDs to study the interactions of ADAM15 D and E, which were not available as GST fusion proteins previously, and to confirm that the GB1 tag did not affect the interactions of the ADAM15 ICDs with SH3 domain-containing proteins. Ni-NTA sepharose was used to bind to the His tag of the new fusion proteins, as in the test purification, and the concentration of ADAM15 ICD bound to the sepharose beads was determined by Bradford assay as previously, prior to their exposure to MCF-7 cell lysate.

Unfortunately, test pull down assays using GB1 tagged ADAM15 B and D as bait proteins, showed that there was a strong interaction between the SH3 domain-containing proteins and the Ni-NTA sepharose beads directly. In the case of Brk and Grb2, the beads actually led to the apparent enrichment of the SH3 protein compared to the concentration of the proteins in the MCF-7 lysate as seen in figure 3.4 A. The presence of the GB1 tag or GB1-ADAM15 B or D actually inhibited the interaction of the SH3 domain-containing proteins with the Ni sepharose beads in certain cases. It was not possible to confirm a lack of interference from the GB1 tag in any interaction from this study in advance of later NMR titrations due to the non-specific binding seen. However, one possible explanation is that this non-specific binding could be between the Ni^{2+} ions on the sepharose beads rather than the sepharose beads themselves. If this was the case, the GB1-ADAM15 bait protein would need to saturate all the available Ni^{2+} ions on the sepharose, so that any SH3 domain-containing protein pulled down by this mixture

could be guaranted to have been pulled down by the bait protein. Figure 3.4 B attempts to resolve this issue by introducing a second negative control of sepharose beads that had been entirely stripped of Ni^{2+} ions by exposure to EDTA prior to pre-equilibration into the appropriate buffer as with the other sepharose samples.

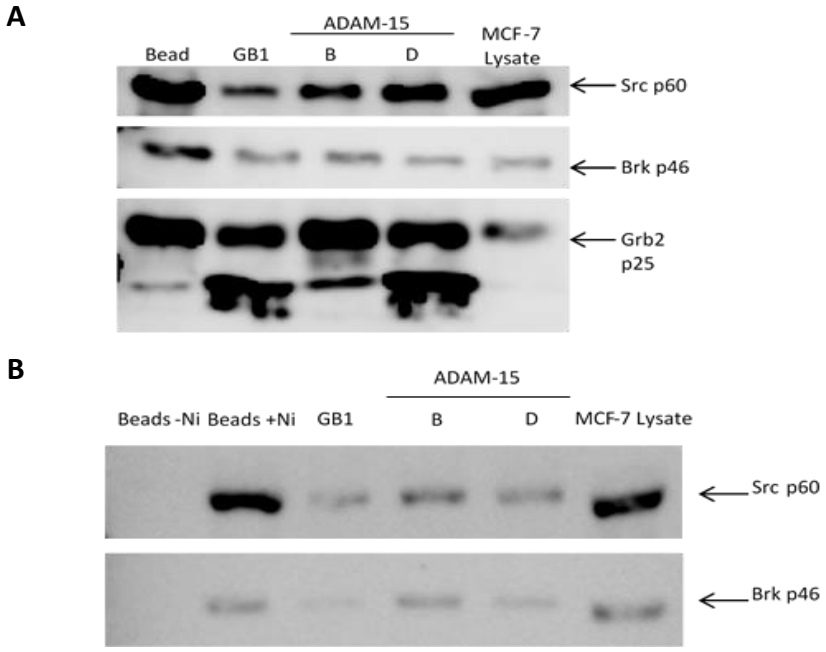

Figure 3.4 A) Western blot of the test pull down of Src, Grb2 and Brk by GB1 tagged ADAM15 B and D including a Ni sepharose negative control and the MCF-7 cell lysate to confirm the presence of endogenous protein. B) Western blot of the test pull down of Src and Brk by GB1 tagged ADAM15 B and D with two negative controls; Ni sepharose beads that have been stripped of Ni^{2+} and the Ni sepharose that is not bound to any bait protein as in A.

This control showed no interaction with either Src or Brk which confirms that the interactions between the SH3 domain-containing proteins with the negative sepharose control were via the Ni^{2+} ions and not the sepharose beads themselves. While this did imply that any interaction was between the ADAM15 ICD bait proteins and the SH3 domain-containing proteins rather than any non-specific interaction, it introduced a lack of reliability to the experiment. The Bradford assay results did confirm that the concentration of ADAM15 ICD bait proteins bound to the Ni-NTA sepharose was at least equal to the potential binding capacity of the sepharose as provided by manufacturer but this value is theoretical and so saturation of the Ni^{2+} ions could not be guaranteed. An alternative technique would need to be attempted in order to confirm that the GB1

tag does not affect the interactions of the ADAM15 ICDs with proteins containing SH3 domains.

3.5 Interactions of the SH3 domain-containing proteins with GB1-tagged ADAM15 ICDs via IgG Affinity Pull Down Assays

As mentioned above, the GB1 tag is derived from the immunoglobulin binding domain 1 of Protein G from group C and G Streptococcal bacteria and is capable of interacting with IgG molecules. As such, sepharose coated in IgG molecules can be used in place of Ni^{2+} sepharose. IgG is a complex, multi-chain, folded protein (Vidarsson et al., 2014) and not a small molecule or simple protein, requiring very specific conditions to function. While these properties had the potential to be prohibitive, it was hoped that this technique would eradicate the non-specific interactions seen in section 3.4.

On experimentation with this more sensitive technique, it became clear that success would be mixed as seen in figure 3.5. When probing for Src, the protein was shown to be present in the MCF-7 lysate and pulled down by ADAM15 B. Src was not pulled down by ADAM15 D or the GB1 tag, although there was a larger protein pulled down by both to which the anti-Src antibody interacts. Src has significant sequence identity with many other members of the Src homology family and this band may be one of these. Unfortunately here, the anti-Brk antibody (ICR-100 (Kamalati et al., 1996)) did not detect any Brk and only non-specific sensitivity to the antibody was seen.

However, the major issue presented was in the case of Grb2. There was significant interference with the signal from the anti-Grb2 antibody and a positive signal in all lanes. Potentially, there could have been a direct interaction between the IgG molecules and the Grb2 protein which would explain Grb2 being pulled down by both the ADAM15 D ICD, which should not be able to interact at all with SH3 domains as it lacks any proline rich regions, and by the GB1 tag and the IgG sepharose which had not been exposed to any bait protein. It was unlikely that the SH3 domain-containing proteins were binding directly to the sepharose beads as the IgG is conjugated to the same type of sepharose as the Ni-NTA sepharose used in section 3.4. In that figure, the SH3 domain-containing proteins were not pulled down by unconjugated sepharose beads. An alternative

explanation is that the Grb2 antibody was sensitive to one of the protein chains of the IgG molecule. When making the SDS-PAGE gel samples, the sepharose beads, having been washed and being conjugated to IgG – GB1-ADAM15 ICD – Grb2, were heated to 100 °C to remove the proteins from the beads. The sample was loaded from this supernatant which means that the loaded sample included denatured IgG protein chains. The light chains of IgG have a molecular weight of approximately 25 kDa, similar to Grb2 and thus could potentially have been interfering with the signal here. This interference rendered this pull down assay technique impractical in confirming that the biological interactions seen in previous pull down studies were unaffected by altering the fusion tag on each ADAM15 ICD from GST to GB1.

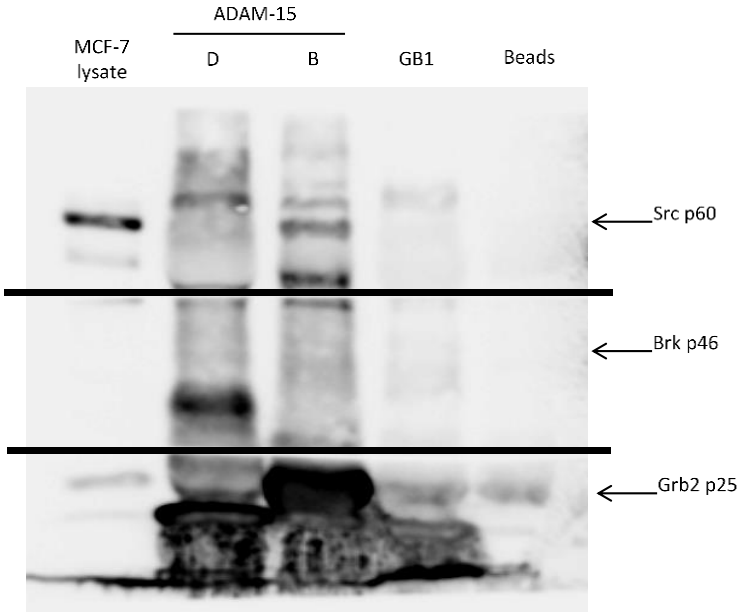

Figure 3.5 Western blots probing for the SH3 domain-containing proteins pulled down by ADAM15 B or D by the trial IgG pull downs. The top panel has been probed for Src, the middle panel for Brk and the bottom panel for Grb2. From the left: a positive control of the MCF-7 lysate, results for those proteins pulled down by ADAM15 B, D and the GB1 tag and finally the negative control of the IgG sepharose conjugated to no bait ADAM15 ICD protein.

3.6 Interactions of the recombinant SH3 domains with the GB1-tagged ADAM15 ICDs

All studies involved recombinant forms of the ADAM15 ICDs and endogenous, full length forms of the SH3 domain-containing proteins. However, the full length versions of these ADAM15-interactors are too large for practical use in NMR titration experiments. The molecular tumbling of proteins in the spectrometer lead to microscopic changes in the local magnetic fields which affect the rate at which nuclei in the high energy state return to the low energy state. Larger molecules tumble much slower and thus return to population equilibrium more quickly and the FID signal decays much more quickly until it is difficult to detect. The viable limit of sensitivity of the NMR experiments to be used here is approximately 25-30 kDa (Keeler, 2006) and both Src and Brk surpass this in their full length forms. Although Grb2 would be small enough to study alone, interactions with the ADAM15 ICDs would increase the overall molecular mass and reduce the tumbling to an undetectable rate. Additionally, Grb2 contains two SH3 domains and they could compete with each other in vitro. As such, recombinant proteins accounting for each individual SH3 domain and the recombinant GB1-ADAM15 ICD proteins were used in NMR titration studies of the interactions. In order to confirm that it is indeed the SH3 domains of the signalling proteins that are responsible for the previous pull down interactions observed, a similar pull down assay was used which also served to establish that the recombinant domains behave similarly to the full length endogenous proteins.

In this experiment, instead of using MCF-7 breast cancer cell lysate, lysates of bacterial cells which were overexpressing the recombinant target protein were incubated with the sepharose. Given the issues of specificity encountered in section 3.5, the SH3 domains were employed as the bait proteins in this pull down assay and the His-GB1-ADAM15 ICDs were detected by Western blot. This removed interactions of potential non-specific bacterial bait proteins competing with the recombinant SH3 domains for the Ni-NTA sepharose. As no antibody against either the GB1 tag or any of the ADAM15 ICDs available, the membrane was probed using a poly-His specific antibody.

As can be seen in figure 3.6 A, there was some non-specific interaction observed between the GST tag control with each of the GB1-ADAM15 ICDs. This did not present a significant problem with regards to future NMR titrations however as the GST fusion tag was used to purify the SH3 domains and will have been cleaved and removed prior to acquisition of the NMR experiments. In this case, the level of interaction seen between the GST fusion tag and the GB1-ADAM15 ICDs can be viewed as a background level for that GB1-ADAM15 ICD being detected. The same can be said for any direct interaction seen with the glutathione sepharose beads and the GB1-ADAM15 ICD, as the beads were not present in the titrations.

A

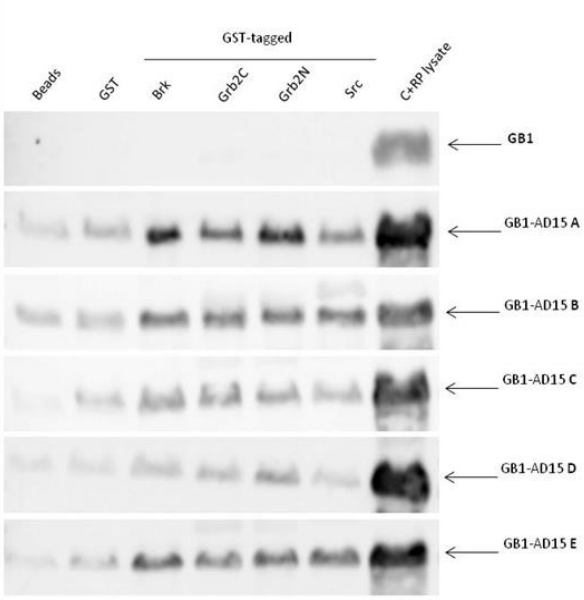

B

	GB1	A15A	A15B	A15C	A15D	A15E
Beads	✗	✗	✗	✗	✗	✗
GST	✗	✗	✗	✗	✗	✗
Src	✗	✓	✓	✓	✗	✓
Brk	✗	✓	✓	✓	✓	✓
Grb2C	✗	✓	✓	✓	✓	✓
Grb2N	✗	✓	✓	✓	✓	✓

✗ No Interaction
✓ Low Level Interaction
✓ Positive Interaction

Figure 3.6 A) Western blots showing the ADAM15 ICDs pulled down by each of the recombinant GST-tagged SH3 domain including a GST negative control, a non-baited sepharose negative control and a positive Codon + RP (C+RP) lysate sample, along with a GB1 negative control in the top panel. B) Summary table of the interactions seen in A. Results are respresentative for three biological replicates.

GB1-ADAM15 A appeared to be pulled down equally by Brk and the N-terminal SH3 domain of Grb2 (Grb2N), less so by the C-terminal SH3 domain of Grb2 (Grb2C) and even less so again by Src. In fact, the band representing the relative amount of ADAM15 A pulled down by the Src SH3 domain was barely more intense than that of the background level seen with GST. This weak interaction was potentially due to the high concentrations used in this experiment compared to the endogenous levels relevant in previous studies here such as figure 3.2. GB1-ADAM15 B was pulled down equally by all the SH3 domains investigated here which agreed with previous studies (Zhong et al., 2008). GB1-ADAM15 C was pulled down by the SH3 domain of Brk, Grb2C and Grb2N with equal intensity but the interaction observed with the Src SH3 domain was minimal compared to the background level. This was not dissimilar to the results seen in the GST pull down assays where little Grb2 was pulled down by GST-ADAM15 C (see figure 3.2). GB1-ADAM15 D was only marginally pulled down by any of the SH3 domains which confirmed expectations as the ADAM15 D ICD does not contain any motifs previously described as capable of interaction with SH3 domains. Any interaction seen could also potentially be due to the relatively high concentrations used in this type of assay compared to endogenous levels of these proteins. Finally, ADAM15 E interacted equally with all the SH3 domains available as did ADAM15 B. Importantly, the GB1 tag alone did not interact with any of the SH3 domains. This was crucial for the NMR titrations as the GB1 tag would be present as a fusion tag on the ADAM15 ICDs during the experiments in order to maintain solubility of these recombinant proteins.

This experiment confirmed that the recombinant forms of the GB1-ADAM15 ICDs and the SH3 domains did interact with each other *in vitro* ensuring the viability of the planned NMR titrations.

3.7 Optimisation of the Purification of the ADAM15 ICD variants

3.7.1 Purification of His-GB1 tagged ADAM15 ICDs by Ni Affinity

As the recombinant ADAM15 ICDs have a poly-histidine tag, in addition to the GB1 tag, initial purification was performed via Ni affinity. As can be seen in figure 3.7 A, two proteins of similar molecular weight were eluted at different imidazole concentrations

during purification of GB1-ADAM15 B; more specifically, one protein of approximately 25 kDa was eluted at 50 mM imidazole and then a slightly larger protein was eluted between 100 mM and 300 mM imidazole. When the GB1 tag is analysed by SDS PAGE, it appears to have a molecular weight of approximately 13 kDa despite having an actual molecular weight of 8.4 kDa. Combined with the molecular weight of the ADAM15 B of 12.8 kDa, the GB1-ADAM15 B recombinant protein could appear to be slightly larger than its actual molecular weight on a polyacrylamide gel. Due to this, it was not immediately clear as to which of the eluted proteins with the approximate molecular weight of 25 kDa was that of GB1-ADAM15 B. If one of the eluted proteins was a bacterial protein endogenous to the Codon + RP cells used to express the protein rather than that of the desired GB1-ADAM15 B, this protein should be present when purifying other ADAM15 ICDs. To this end, the purification of GB1-ADAM15 D was attempted as the combined molecular weight of GB1-ADAM15 D is only 14.6 kDa and so, even with the apparent inflation of the molecular weight of the GB1 tag on polyacrylamide gels, it would be clear which elutions contained the desired recombinant protein. As can be seen in figure 3.7 B, GB1-ADAM15 D was eluted by imidazole concentrations between 100 mM and 300 mM which demonstrated that the protein eluted at 50 mM imidazole was likely a bacterial protein interacting with the Ni-NTA sepharose and as such the elutions at 50 mM imidazole were not taken forward to later stages of the purification protocol.

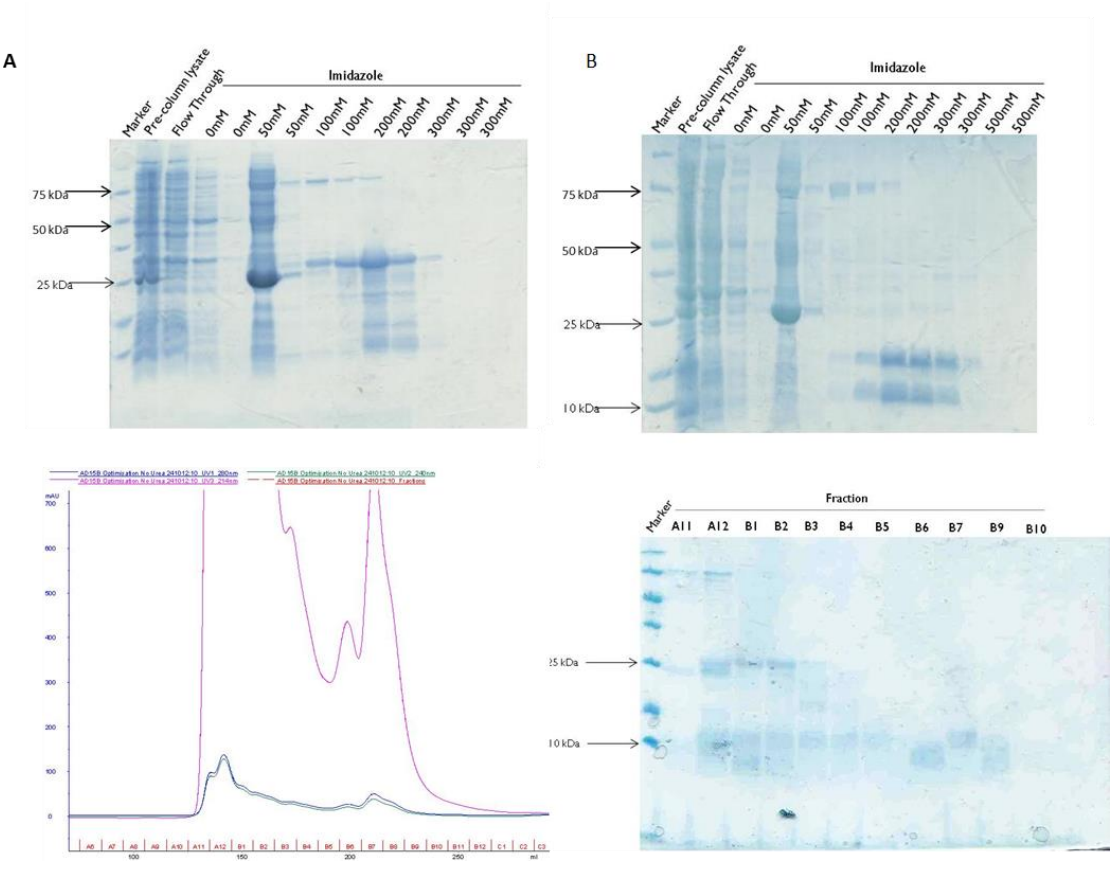

Figure 3.7 A) SDS PAGE gel electrophoresis of Ni Affinity purification of GB1-ADAM15 B with the protein eluting when exposed to more than 100 mM imidazole. B) SDS PAGE gel electrophoresis of Ni Affinity purification of GB1-ADAM15 D with the protein eluting when exposed to more than 100 mM imidazole. C) Chromatogram of size exclusion chromatography purification of GB1-ADAM15 B. D) SDS PAGE gel electrophoresis of fraction from the size exclusion chromatography purification of GB1-ADAM15 B.

Subsequently to the Ni affinity purification, removal of the large protein of approximately 50 kDa, along with the small contaminants eluted with the GB1-ADAM15 B, was attempted by size exclusion chromatography. As can be seen in the chromatogram in figure 3.7 C and the subsequent SDS PAGE gel in D, the similar size of the smaller contaminants were too close to that of the desired GB1-ADAM15 B and they could not be separated this way.

3.7.2 Purification of the His-GB1 tagged ADAM15 ICDs by Ion Exchange Chromatography

As size exclusion chromatography had been unable to remove the small contaminant proteins from the GB1-ADAM15 B, ion exchange chromatography was attempted. The fractions from the Ni affinity purification were combined and dialysed into either 50 mM sodium acetate pH 5 or 100 mM sodium acetate pH 5. Unfortunately, after 48 hours of dialysis, a precipitate had formed in both samples. Figure 3.8 A shows a gel of the sample prior to dialysis in acetate buffer and from the supernatants of the samples from after dialysis and it is clear that it is indeed the GB1-ADAM15 B protein that has been precipitating, ruling out the use of these buffers.

3.7.3 Purification of the His-GB1 tagged ADAM15 ICDs by Ni affinity in the presence of 6 M Urea

A disadvantage of using Ni affinity for purification purposes, as opposed to GST affinity for example, is that the affinity of the Ni^{2+} ions for polyhistidine tags is not as specific as other techniques. Ni affinity columns can potentially interact with any protein exhibiting a sufficient localised negative charge, at the pH used. This could account for the contaminant proteins that were eluted at similar imidazole concentrations to the desired GB1-ADAM15 ICD. Denaturation of all the proteins present would reduce the likelihood of localised negative charge and thus avoid non-specific interactions whereas the sequential nature of the polyHis-tag will still retain its localised charge and so the cluster is not reliant on correct folding. To achieve denaturation, 6 M urea was added to all the buffers involved in the Ni affinity purification.

As can be seen in figure 3.8 B, the addition of urea was successful in the removal the larger, 50 kDa protein from the elutions at high imidazole concentrations but did little to reduce the presence of the smaller contaminants from the same elutions as the desired GB1-ADAM15 B. Also shown in figure 3.8 B is a sample of the eluted GB1-ADAM15 B with the urea removed to confirm that it was not degraded by exposure to high concentrations of urea. Although the contamination issues where not entirely solved by the presence of urea, this did go some way to aid the purity of the final sample and so was used for all future Ni affinity purifications of the GB1-ADAM15 ICDs.

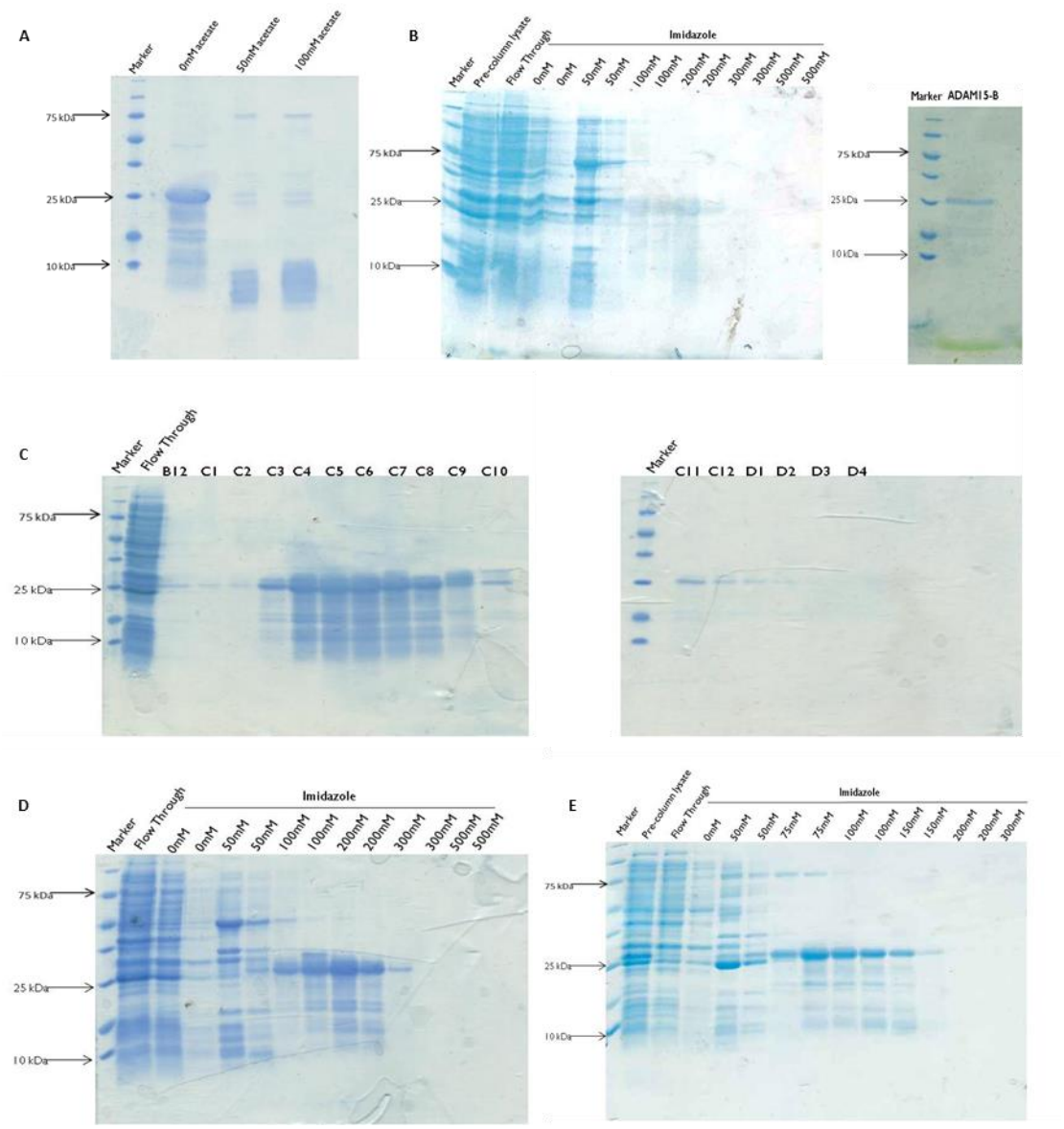

Figure 3.8 A) SDS PAGE gel electrophoresis of GB1-ADAM15 B sample before and after dialysis into acetate buffer. The protein has precipitated due to exposure to sodium acetate solutions. B) SDS PAGE gel electrophoresis of fractions from the Ni Affinity purification of GB1-ADAM15 B in the presence of 6 M urea along with a gel of the sample after dialysis to remove the urea to confirm the protein had not degraded. The protein eluted at concentrations of more than 100 mM imidazole as previously. C) SDS PAGE gel electrophoresis of the fractions from the Talon™ purification of GB1-ADAM15 B. The concentration of imidazole that caused protein elution was 75 mM. D) SDS PAGE gel electrophoresis of the fractions from the Ni affinity purification of the same expression of GB1-ADAM15 B. E) SDS PAGE gel electrophoresis of the fractions from the Ni Affinity purification of GB1-ADAM15 B at 4 °C after a shorter, 3 hour induction.

3.7.4 Purification of the GB1-ADAM15 ICDs via alternative protocols utilising the His-tag

While nickel ions are the ion of choice for use in purifications of His-tagged proteins, due to their strong affinity even at low protein concentrations, other ions, including cobalt can also be used. Cobalt has six coordination sites, like nickel, but has a lower affinity for His-tags, especially if the His-tag is not fully exposed or if the protein concentration is lower. The benefit here is that this means that there are fewer non-specific interactions with the Co sepharose (Jiang et al., 2004). A lower concentration may not be ideal but samples purified this way are often less contaminated.

In order to compare the efficacy of Ni affinity compared to Co affinity, the pellet from a 1 L culture was split in half and one half purified by each technique using the same buffers and both in the presence of urea. The cobalt sepharose used here was Talon™ (GE Healthcare) and it was used with the Äkta purification system. The results of this column can be seen in figure 3.8 C and the Ni affinity purification of the same expression in D. Unfortunately, using Co affinity did not reduce the contaminants of smaller size any more effectively than Ni affinity. This implied that the bands seen on the gels are not non-specific contaminants but either degraded or truncated forms of the desired GB1-ADAM15 ICD that retains the N-terminal His-tag.

3.7.5 Ni Affinity Purification of GB1-ADAM15 B at low temperature with a shorter induction culture

It is possible that the small contaminant bands are in fact degraded or truncated forms of the desired GB1-ADAM15 ICD and therefore modifications to the culture and purification were considered. The induction length of the culture was reduced from 4 hours to 3 hours to avoid a toxic response from the bacterial cells to the high concentrations of the GB1-ADAM15 ICD and the Ni affinity purification was conducted at 4 °C to reduce degradation, the results of which can be seen in figure 3.8 E. However, these steps did not reduce the level of degraded protein bands. Further optimisation was therefore required.

3.7.6 Low Temperature Culture of GB1-ADAM15 B

An effective method for reducing in-cell degradation or truncation is to induce production of the desired protein at a lower temperature for a longer time. Rather than induce the bacteria to produce GB1-ADAM15 B at 37 °C for 4 hours, the cells were induced at 28 °C overnight which slows protein production, allowing the bacterial ribosomes to respond to clusters of rare codon tRNAs or to cope with any rare codon tRNAs which are still at a relatively low copy number, despite the use of specialised cells equipped with extra copies of rare codons. Potential protein misfolding is also reduced in long, cool inductions. The results of the subsequent Ni affinity purification can be seen in figure 3.9 A and show that the degradation/truncation issue had been significantly reduced but not entirely resolved and thus further modifications to the purification protocol were required.

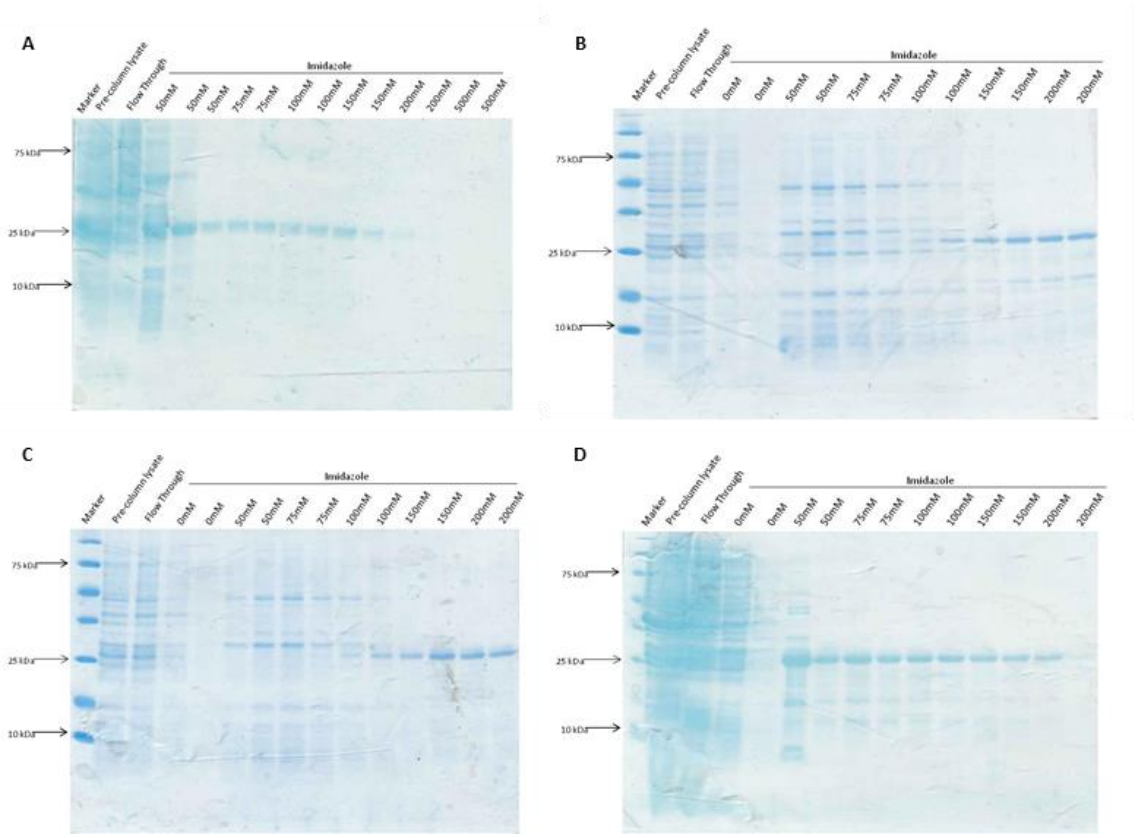

Figure 3.9 A) SDS PAGE gel electrophoresis of NI affinity purification of GB1-ADAM15 B expressed at 28 °C overnight in Codon + RP cells. B) SDS PAGE gel electrophoresis of Ni affinity purification of small scale expression of GB1-ADAM15 expressed in Codon + RP cells at 28 °C overnight. C) SDS PAGE gel electrophoresis of Ni affinity purification of small scale expression of GB1-ADAM15 B expressed in Rosetta 2 cells at 28 °C overnight. D) SDS PAGE gel electrophoresis of Ni affinity of purification of GB1-ADAM15 B expressed in large scale, 28 °C overnight culture in Rosetta 2 cells.

3.7.7 Comparison of Expression of GB1-ADAM15 ICDs in Codon + RP cells and Rosetta 2 cells

If the issue seen here was not degradation but truncation, this could be due to the rare codons required for the translation of the GB1-ADAM15 ICDs. The Codon + RP cells used to express the GB1-ADAM15 ICDs thus far have extra copies of the *argU* and *proL* codons but lack extra copies of either *ileY* or *leuW* codons. As all of these rare codons are required for the expression of the ADAM15 ICDs, an alternative cell line which contains extra copies of all of these codons was evaluated. The Rosetta 2 cell line, another variation on the BL21 (DE3) cell line, containing all of the rare codons required was trialled. Small scale cultures of both the Rosetta 2 and Codon + RP cell lines were grown and GB1-ADAM15 B expressed in both. Ni affinity purifications from these cultures can be seen in figure 3.8 B and C and the purification from the Rosetta 2 cell culture demonstrated fewer of the small contaminant proteins than that of the Codon + RP cells although they were not removed entirely.

3.7.8 Large Scale Culture and Purification of GB1-ADAM15 B using Rosetta 2 cells

As the small scale production of the GB1-ADAM15 ICDs using Rosetta 2 cells produced fewer contaminants than that of Codon + RP cells, and the low temperature overnight culture generated fewer contaminants in Codon + RP cells, the next stage of optimisation was to combine these and attempt production of GB1-ADAM15 B in Rosetta 2 cells at low temperature overnight. The results of the Ni affinity purification of that culture can be seen in figure 3.9 D and showed a significant reduction in the contaminant bands compared to previous purifications and this improvement was seen in the case of all the GB1-ADAM15 ICDs. Ideally, NMR experiments would use proteins of the highest purity possible as NMR spectra represent the net behaviour of the nuclei generating a given chemical shift. This was not possible here but the purity level demonstrated was enough to attempt NMR experiments and was pure enough to act as the ligand protein in a titration experiment.

3.8 Nuclear Magnetic Resonance Studies of GB1-ADAM15 B

As it had proven difficult to purify the ADAM15 ICDs to the preferred level of purity required for NMR studies, it was decided that the interactions between the ADAM15 ICDs and the SH3 domains should initially be studied from the perspective of the SH3 domains. There are assignments available for all of the SH3 domains being studied here (Lin et al., 2012; Wittekind et al., 1997; Yu et al., 1993) which will be covered in later chapters. Additionally, the high number of proline residues present in the ADAM15 ICDs, which are likely to be directly relevant to any potential interaction, would require the use of less common NMR pulse sequences for detection from the ADAM15 ICD perspective.

Single labelled, ^{15}N GB1-ADAM15 B was produced using the optimised protocol described above. A [^{1}H-^{15}N]-HSQC was acquired for this to establish how much the contaminants affect the spectrum of the protein, which can be seen in figure 3.10.

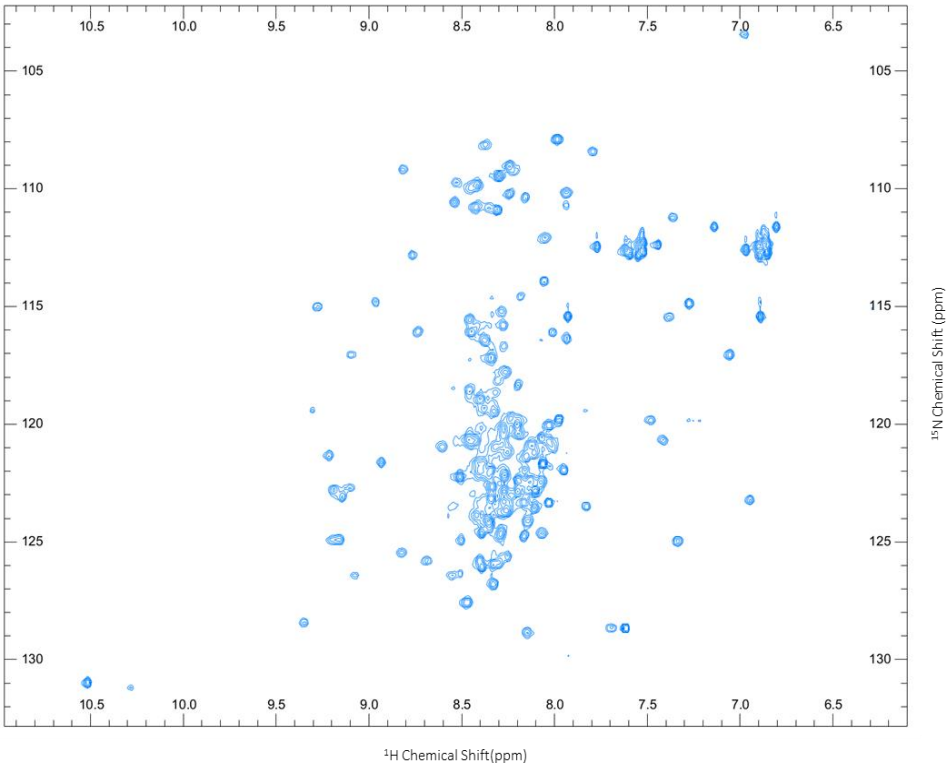

Figure 3.10 [^{1}H-^{15}N]-HSQC of ^{15}N labelled GB1-ADAM15 B

The spectrum for GB1-ADAM15 B proved to be better resolved than expected. The high level of contaminants with potentially similar sequences to the GB1-ADAM15 ICD, with several potential versions of the same residue in slightly different environments due to variable truncation, had the potential to present a significant level of interference. Sufficient concentrations of the truncated proteins would add to the signal of residues unaffected by the truncation while providing new peaks for those that are affected. However, this was not seen here. The level of purity attained was enough to overcome this and presented a clear spectrum. The majority of the peaks are positioned between 8.0 ppm and 8.5 ppm in the ^{1}H dimension which is consistent with amino acids residing in regions of disorder in proteins (Uversky, 2011). This is likely to represent the majority of the residues from the ADAM15 B ICD. The peaks spread out through the rest of the spectrum correlate strongly with the published spectrum of the GB1 tag (Sun et al., 2005).

3.9 Conclusions and Discussion

It has already been shown in a number of studies that the ADAM15 ICDs interact with proteins that contain SH3 domains (Zhong et al., 2008). It has also been shown that the proline-rich regions play a large part in those interactions (Kleino et al., 2009). This chapter attempted to validate these studies and ensure that alterations, necessary for the planned NMR experiments, do not affect those results.

Previously used as a model of metastatic breast cancer, the MDA-MB-435 cell line is now suspected to have been cross-contaminated with the M14 melanoma cell line (Rae et al., 2007) and expresses markers for both breast cancer and melanoma. Here, it was demonstrated that the interaction profile previously observed in this melanoma line could be reproduced in the breast cancer cell line, MCF-7. This would suggest that the interactions of the ADAM15 ICD with intracellular proteins that contain an SH3 domain are not restricted by tissue type and thus could potentially have a function beyond that of cancerous disease. Since ADAM15 has also been heavily implicated in inflammatory conditions such as arthritis and in atherosclerosis (Bohm et al., 2013; Sun et al., 2012),

any interactions observed throughout this thesis could have an impact in such conditions beyond breast cancer.

Previously, the interactions of ADAM15 variants D and E have not been discussed. Although the interactions viewed here are using recombinant domains rather than full length endogenous proteins, these have the potential to have a biological function. ADAM15 D did not interact with Src or Brk as expected, due to the lack of proline-rich motifs with which to bind to canonical SH3 domains. The lack of interaction partners discovered for ADAM15 D does not explain why this variant is the most widely expressed variant across a wide selection of healthy tissues, after that of ADAM15 A (Kleino et al., 2007). However, it did interact at the low level with the N-terminal SH3 domain of Grb2. This was unexpected and may go some way to completing the functional roles of the ADAM15 D variant.

The interaction profile of ADAM15 E was very similar to that of ADAM15 B. In previous studies it was not possible to differentiate between expression of the ADAM15 E and ADAM15 B variants due to their very similar molecular weight and sequence length (Kleino et al., 2007). There is only one polyproline region differing between these two variants. Although the biological function of each of the variants remains unclear, it is intriguing that these two variants behave in such a redundant manner.

In summary, this chapter has shown that:

- MCF-7 breast cancer cells displayed a similar interaction profile to that of MDA-MB-435 cells.
- Expression and purification of the newly GB1-tagged ADAM15 ICDs was possible.
- Ni affinity based pull down assays were not possible due to non-specific interactions of the SH3 domain-containing proteins with the Ni ions.
- IgG affinity based pull down assays were problematic due to the interference of the IgG light chain with the Grb2 antibody.
- Src was not pulled down from MCF-7 cell lysate by GB1-tagged ADAM15 D.
- Recombinant SH3 domains from Grb2, Src and Brk do interact with the GB1-tagged ADAM15 ICDs but did not interact with the GB1 tag alone.
- Production of the GB1-tagged ADAM15 ICD was optimised to use Rosetta 2 cells for expression and purification by Ni affinity in the presence of urea.
- NMR studies of GB1-tagged ADAM15 B are possible but due to the existence of backbone assignments for the SH3 domains and high proline concentration in the ADAM15 ICDs, the titrations were studied from the perspective of the SH3 domains primarily.

Chapter 4: Interactions of Grb2 with ADAM15 ICDs

4.1 Introduction

Growth factor receptor-bound protein 2 (Grb2) is 217 residues long and contains an N-terminal SH3 domain from residues 1-58, a central SH2 domain from residues 60-152 and a C-terminal SH3 domain from residues 156-215 (Uniprot ID: P62993 (Magrane and Consortium, 2011)). The SH2 domain binds to tyrosine phosphorylated sequences containing the motif pY-X-N-X where X is a hydrophobic residue, most commonly valine (Vidal et al., 2001). Both the N-terminal and C-terminal SH3 domains have been shown to interact with proline-rich regions (Simon and Schreiber, 1995). For example, the N-terminal SH3 domain (Grb2N) interacts with Ras-guanine exchange factor SOS and the C-terminal SH3 domain (Grb2C) interacts with proline-rich motifs such as those which contain the motif P-X-I/L/V-D/N-R-X-X-K-P (Berry et al., 2002; Simon and Schreiber, 1995).

Both SH3 domains will be considered as potential interaction partners in this chapter, using recombinant proteins for each specific domain. Both Grb2N and Grb2C follow the general structural pattern for SH3 domains. Both Grb2N and Grb2C contain 8 β-strands, an n-Src loop, a RT loop, a distal loop and an α-turn as shown in Figure 4.1.

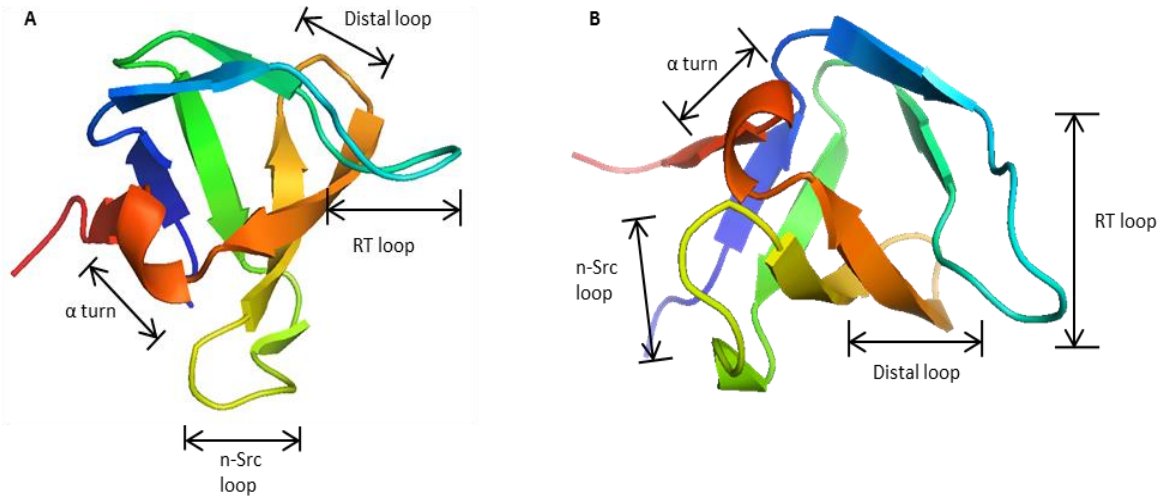

Figure 4.1 A) The NMR structure of Grb2C based on the pdb 1GFC (Kohda et al., 1994). B) The structure of Grb2N based on the pdb 3GBQ (Wittekind et al., 1997). Highlighted on each are the standard features of an SH3 domain, the n-Src loop, the RT loop, the distal loop and the α-turn.

As shown previously, Grb2 has been shown to interact with ADAM15 variants A-C in various published studies (Kärkkäinen et al., 2006; Zhong et al., 2008). The previous chapter has shown that ADAM15 E can also bind to Grb2 but ADAM15 D does not. However, as there are two SH3 domains present in full length Grb2, it is not known which domain is involved in the ADAM15 interactions and this will be addressed here. Grb2C was chosen to be studied first due to the full ^{1}H, ^{15}N and α and β ^{13}C assignments having been published along with the PDB structure used here (1GFC (Kohda et al., 1994)) and an article demonstrated that the Grb2C was responsible for the interaction with the cytoplasmic domain of FGFR2 Bii and that the Grb2N acted to dimerise with the parallel domain of second Grb2 molecule (Lin et al., 2012).

Due to the purification issues described in the previous chapter and the high number of prolines present in the ADAM15 ICDs, the interactions will be studied from the perspective of the SH3 domains. The ADAM15 ICDs were purified as discussed and dialysed into the appropriate NMR buffer for the labelled SH3 domain in question.

4.2 Optimisation of the Purification of Grb2C

During the optimisation of the pull downs, the DNA sequence of the Grb2C was confirmed and the expression was optimised in BL21 (DE3) cells. This construct has a GST fusion tag and, after cell lysis by sonication and clarification by centrifugation, glutathione sepharose was used to extract the fusion protein from the lysate. This was eluted with 300 mM reduced glutathione and the fractions containing eluted protein were combined, once identified by gel electrophoresis shown in figure 4.2 A. As previously discussed, the GST tag is too cumbersome for NMR spectroscopy (Zhou and Wagner, 2010) and so it was removed from the Grb2C construct via thrombin digestion. This was optimised by digesting 1 ml of the protein overnight at either room temperature or at 4 °C with either 1.5, 3, 5 or 7.5 units of thrombin per mg of protein. The results were analysed by gel electrophoresis, shown in figure 4.2 B, and 5 units of thrombin per mg of protein was used for further purification. Once the thrombin reaction was stopped with 100 mM PMSF, separation of the GST tag was initially attempted via the use of a second glutathione sepharose column. Unfortunately, as

shown in the figure 4.2 C, this failed to remove all of the tag. The flow through sample which contained Grb2C with some remaining GST tag was concentrated by centrifugation to a volume of less than 3 ml and then the GST tag was separated from the Grb2C protein by size exclusion chromatography, using the same SPB buffer, as previously used for the glutathione affinity column, with a flow rate of 1 ml/min. The resulting chromatogram is shown in figure 4.2 E with the SDS-PAGE gel of the peaks shown in figure 4.2 D. As size exclusion chromatography was more successful at removing the tag, the second glutathione sepharose column was omitted from further purification attempts and size exclusion chromatography was used to remove all of the tag in a single step. Finally, the sample was dialysed into Grb2C NMR buffer and concentrated to 2 mM.

In order to confirm that the purification of the protein yielded folded protein, a one dimensional ^{1}H NMR experiment was acquired. The presence of a peak (highlighted in red in Figure 4.3) with a chemical shift lower than 0 ppm indicated that a methyl group was shielded from the magnetisation by the electron cloud of a ring in an aromatic residue. In order for this to be possible, the protein must have been folded in such a way as to bring these two functional groups in close proximity in the hydrophobic core. Also, there were peaks in the high ppm region additional to the characteristic tryptophan residue peaks, further confirming that the protein was produced and folded correctly as such peaks would only occur due to protein folding.

Based on the success of producing unlabelled Grb2C, ^{15}N and ^{15}N, ^{13}C labelled versions of the protein were generated using the same protocol, without the second GST affinity column.

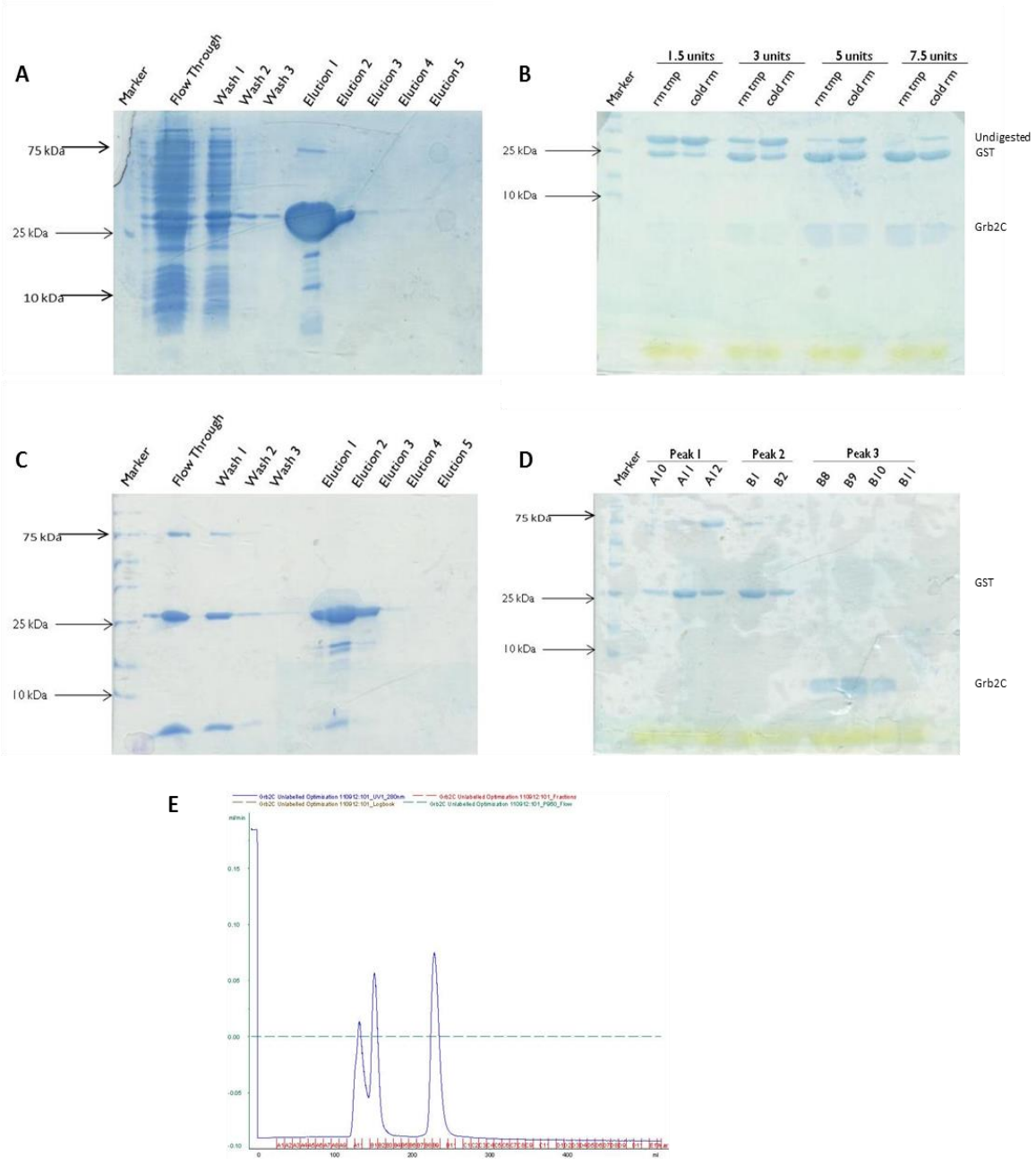

Figure 4.2 A) The first GST affinity column performed. The band eluted in elution 1, at 300 mM glutathione, is GST-Grb2C. B) Optimisation of thrombin cleavage of the tag from Grb2C. Thrombin as used in the indicated amount (from 1.5 units to 7 units per milligram of protein) and temperatures (4 °C or room temperature) C) The second GST affinity column attempted. The Grb2C should be in the flow through with all GST retained until the elutions. D) SDS PAGE gel of the fractions from the size exclusion column with those fractions from peak 3 containing the desired Grb2C. E) Chromatogram of this size exclusion column with three clear peaks.

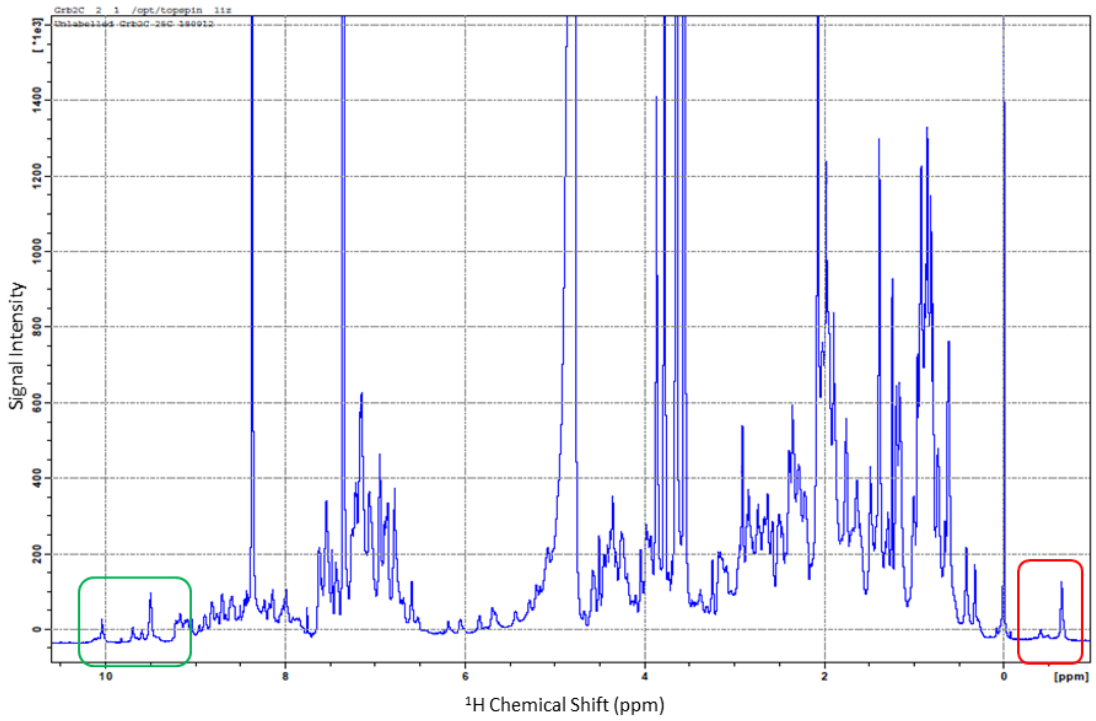

Figure 4.3 ^{1}H NMR spectra of unlabelled Grb2C. The red square highlights a hydroxyl group with a ppm shift of less than 0 indicates that it is shielded from magnetisation by its proximity to an aromatic ring. The green box highlights peaks characteristic of tryptophan residues along with additional peaks characteristic of a folded protein.

4.3 Assignment of Grb2C backbone using NMR

Using the ^{13}C, ^{15}N labelled recombinant protein produced above, HSQC, HNCACB and CBCACONH spectra were collected using the 500 MHz spectrometer. Using the ^{1}H, ^{13}C and ^{15}N assignments from Chi-Chuan Lin et al (Lin et al., 2012), 76% of the backbone of Grb2C was assigned with the exception of the proline residues and 1Gly, 2Ser, 3Ala, 5Val, 8Gln, 50His, 51Gly, 65Asn, 66Arg and 67Asn. The assignments are shown in figure 4.4.

4.4 Titrations of Grb2C with the cytoplasmic domains of ADAM15

Although it was not possible to purify the ADAM15 cytoplasmic domains to a sufficient level in order to begin structural analysis, due to in cell degradation of the protein during expression, it was possible to purify the ADAM15 ICDs to a suitable degree in order to use them as the ligand protein in a titration experiment. As NMR data uses the net signal

produced, small signals caused by low level contaminants of the ligand protein will be negligible in comparison to the overall signal caused by the effects of the ligand.

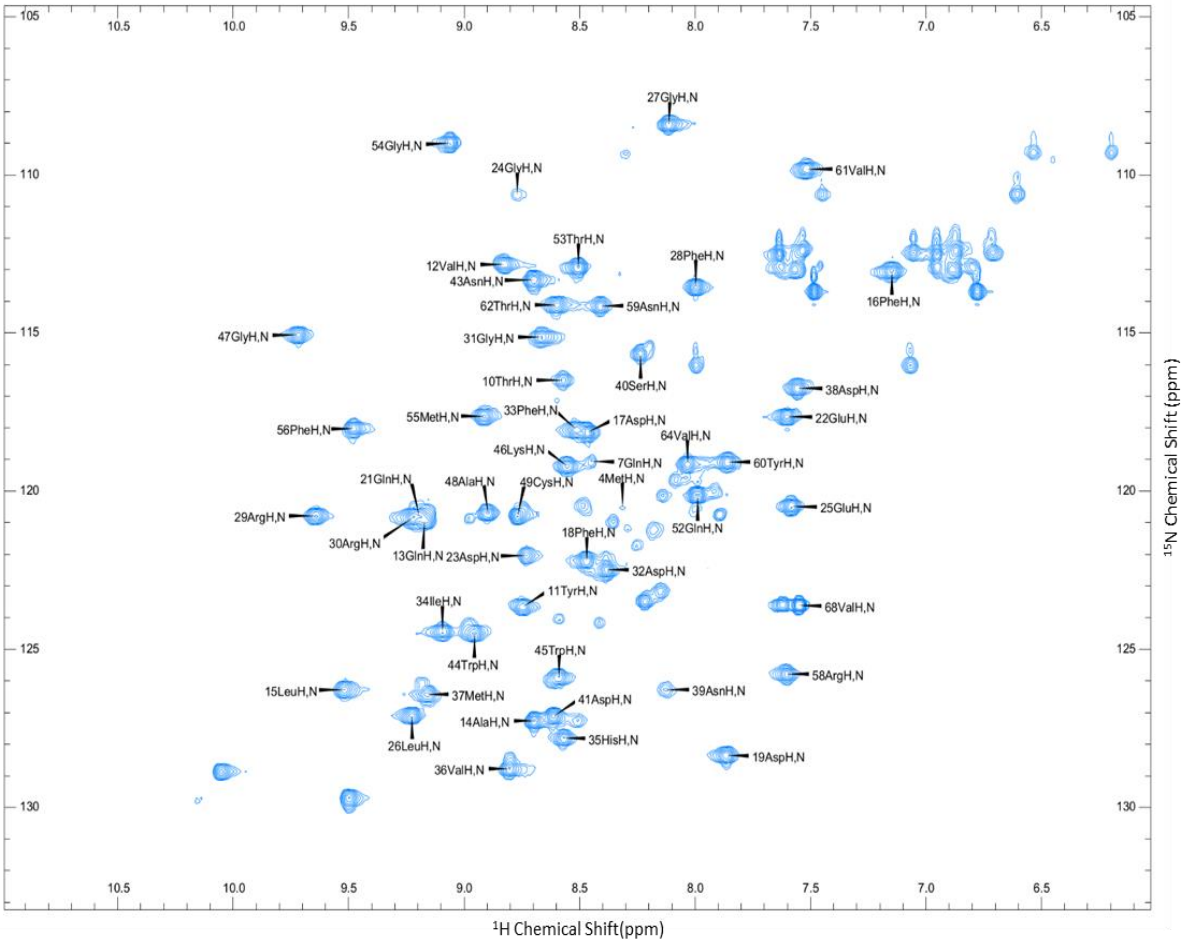

Figure 4.4 shows the ^{1}H, ^{15}N HSQC spectrum of the Grb2C SH3 domain with peak assignments

As long as a clear majority of the ligand sample is the full length ADAM15 cytoplasmic domain construct, the effects seen in the spectrum for GrbC2C will be those caused by the main ADAM15 ICD construct and not the contaminants.

In order to study the interaction of Grb2C with each ADAM15 ICD, two NMR samples were made. For each titration, sample A contained 0.5 mM ^{15}N Grb2C in NMR buffer. Sample B contained 0.5 mM ^{15}N Grb2C and 1.5 mM ADAM15 ICD in NMR buffer. HSQC experiments were acquired for both samples and these represent the first and last data points for a titration. The intermediate data points were collected by transferring a small volume of sample B into sample A, increasing the concentration of ADAM15 ICD in

sample A while maintaining the Grb2C concentration. Those peaks that are affected by any interaction between the two proteins will appear to "move" across the spectra. This is called the chemical shift perturbation (CSP) and it was calculated for each peak using the following equation:

$$\text{CSP (}\Delta\text{ppm)} = \sqrt{(\Delta\delta_{HN})^2 + (\Delta\delta_N * 0.15)^2} \qquad \text{(Equation 2)}$$

Where 0.15 is a scaling factor to compensate for the difference in ppm scale for ^{15}N compared to ^{1}H and Δδ is the change in chemical shift (Takahashi et al., 2000).

Firstly, a titration of ^{15}N Grb2C with the unlabelled GB1 tag was conducted as a control and to establish a baseline. As can be seen in Figure 4.5, there was negligible perturbation of peaks when the GB1 tag was added thus confirming that any chemical shift perturbations seen in further titrations with each ADAM15 ICD would be attributable to the ADAM15 ICD in question and not the presence of the GB1 tag.

Despite being minimal, the chemical shift perturbations caused by the presence of the GB1 tag were subtracted from the CSPs caused by each GB1-tagged ADAM15 ICD prior to further analysis. All the ADAM15 IDs, other than variant D, showed some interaction with the Grb2C SH3 domain, with perturbations of Grb2C residues 22Glu, 44Trp and 56Phe common to all of the interactions. In figure 4.6, the quantification of the perturbations caused by ADAM15 A, shown in figure 4.6 B, were calculated from the spectra in figure 4.6 A. Other residues affected by the presence of the variant A ICD include 13Gln, 18Phe and 55Met, though to a significantly lower extent.

The perturbations caused by the presence of ADAM15 B include 22Glu, 44Trp and 56Phe, as for the other ICD interactions, but 58Arg was also affected here. Unlike in the case of ADAM15 A, 13Gln was not affected at all by the presence of ADAM15 B, whereas 19Asp was. Residues 18Phe and 55Met were perturbed to a similar extent here as in the interaction of Grb2C with ADAM15 A. This can be seen in Figure 4.7 B.

In Figure 4.8, the effect of the introduction of ADAM15 C on the chemical shift of the residues of Grb2C can be seen. As in the cases of ADAM15 A and B, residues 22Glu, 44Trp, 56Phe and 58Arg were shifted most dramatically by the introduction of ADAM15 C but by a smaller margin than was the case for the previous ADAM15 ICDs. Unlike the

introduction of ADAM15 A or B, 13Gln, 18Phe and 55Met were either unaffected entirely or shifted by a less than 0.02. In this case, only the residues mentioned above and 17Asp, 19Asp and 46Lys were shifted by more than 0.02.

As can be seen in Figure 4.9, the chemical shift perturbations of the residues of Grb2C caused by the presence of ADAM15 D were negligible. The largest shift observed was for residue 22Glu but this was still only 0.015. This is consistent with predictions that ADAM15 D would not interact with the SH3 domains as it lacks proline-rich motifs.

Finally, Figure 4.10 shows the results for the titration of Grb2C with ADAM15 E. As for the titrations with ADAM15 A-C, residue 22Glu, 44Trp and 56Phe of Grb2C were the most affected by the introduction of ADAM15 E. Additionally, 12Val, 13Gln, 15Leu, 17Asp, 19Asp, 45Trp, 55Met, 58Arg and 59Asn show significant movement upon interaction with ADAM15 E.

Additionally, it is important to note that as the concentration of each ADAM15 ICD increased in the titration sample, a precipitate formed. This happened in all cases, except for ADAM15 D, once the ratio of Grb2C to ADAM15 was above 1:1.5. However in the cases of ADAM15 B and E, this occurred at lower concentrations of ADAM15 than for ADAM15 A and C, beginning at concentrations of 0.5 mM: 0.5 mM in the cases of variants B and E and at 0.5 mM: 0.75 mM for variants A and C. As the intensity of the peaks for Grb2C decreased dramatically once the precipitate started to form, it can be argued that the concentration of ^{15}N Grb2C in solution was reducing as the concentration of ADAM15 ICD increases. Additionally, peak broadening in an indicator of intermediate exchange whereby the exchange rate between the bound and unbound forms of the protein is of the same order as the frequency difference and thus the chemical shift of the peak is an average based upon the time spent in the unbound form with a lower intensity. This sort of exchange can also be seen when there are multi-binding events occurring such as non-specific interactions due to the high concentrations of the proteins present in the sample (Kovrigin, 2012). Thus the interactions of the SH3 domain with the ADAM15 ICD causes aggregation and precipitation *in vitro*.

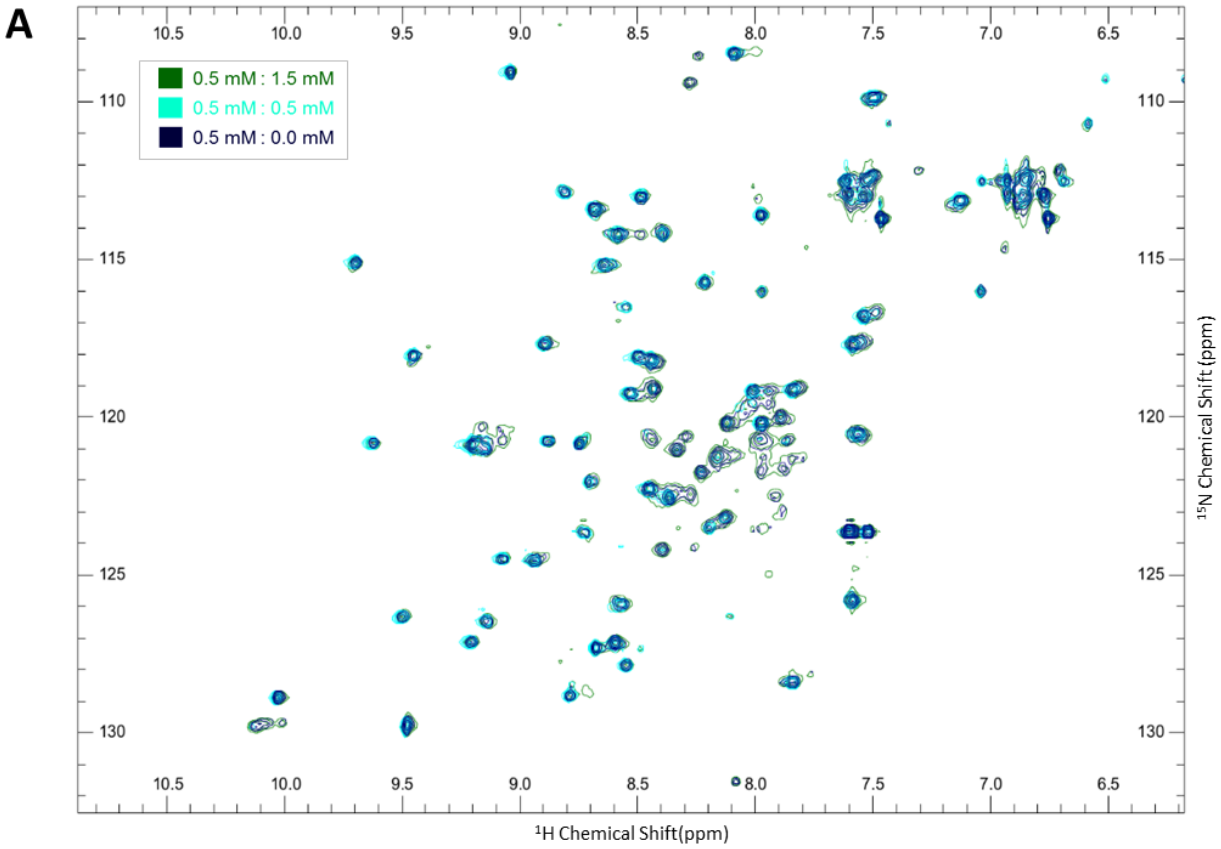

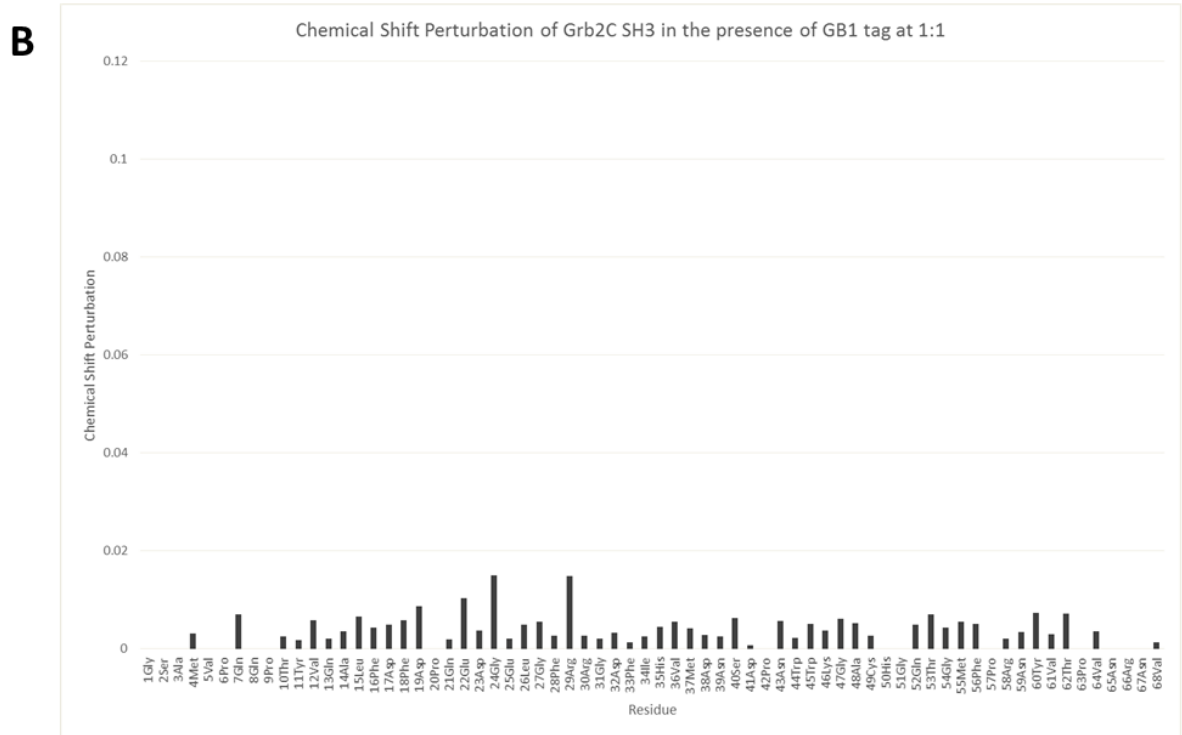

Figure 4.5 A) [^{1}H-^{15}N]-HSQC spectra for the ^{15}N Grb2C SH3 domain by itself (navy blue), in the presence of 0.5 mM GB1 tag (cyan) and in the presence of 1.5 mM GB1 tag (green) and the intermediates in intermediate shades as indicated in the key. The concentration of 15N Grb2C SH3 domain was 0.5 mM in all spectra. B) Chemical shift perturbations caused by the presence of the GB1 tag on the spectrum of the Grb2C SH3 domain at 0.5 mM of each protein.

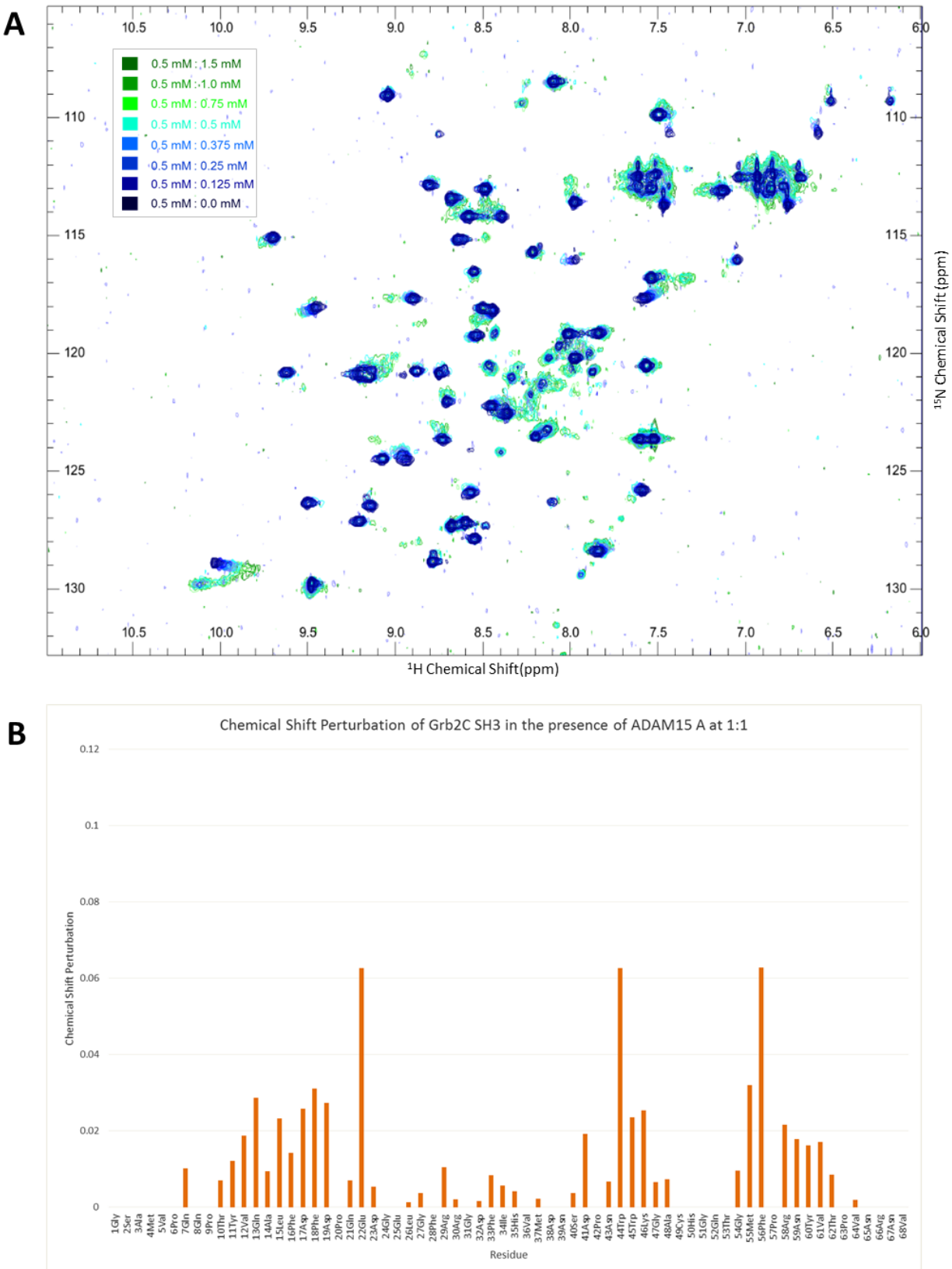

Figure 4.6 A) [^{1}H-^{15}N]-HSQC spectra for the ^{15}N Grb2C SH3 domain by itself (navy blue), in the presence of 0.5 mM ADAM15 A (cyan) and in the presence of 1.5 mM ADAM15 A (green) and the intermediates in intermediate shades as indicated in the key. The concentration of 15N Grb2C SH3 domain was 0.5 mM in all spectra and intermediate concentrations are also shown. B) Chemical shift perturbations caused by the presence of the ADAM15 A on the spectrum of the Grb2C SH3 domain at 0.5 mM of each protein.

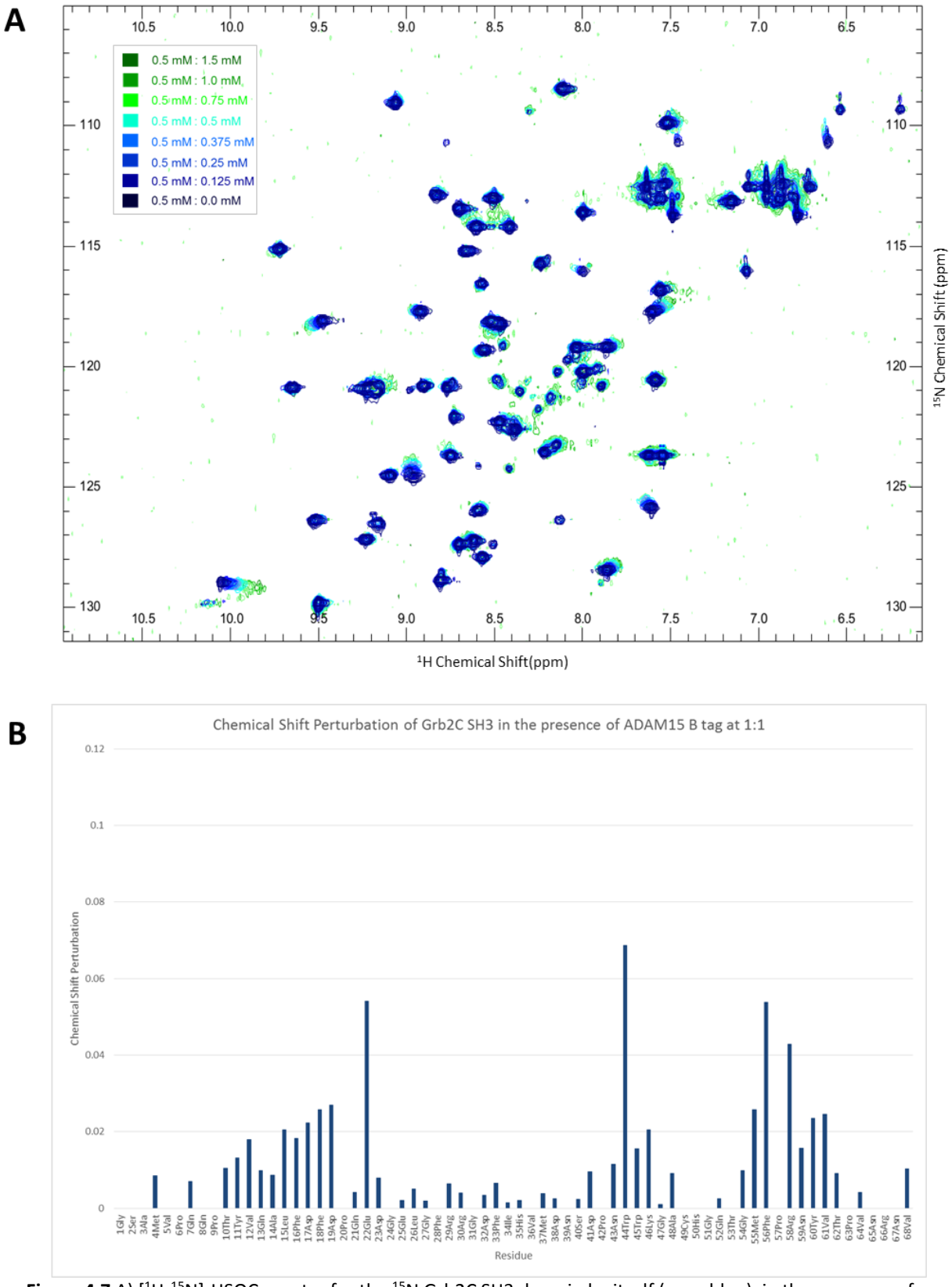

Figure 4.7 A) [^{1}H-^{15}N]-HSQC spectra for the ^{15}N Grb2C SH3 domain by itself (navy blue), in the presence of 0.5 mM ADAM15 B (cyan) and in the presence of 1.5 mM ADAM15 B (green) and the intermediates in intermediate shades as indicated in the key. The concentration of 15N Grb2C SH3 domain was 0.5 mM in all spectra and intermediate concentrations are also shown. B) Chemical shift perturbations caused by the presence of the ADAM15 B on the spectrum of the Grb2C SH3 domain at 0.5 mM of each protein.

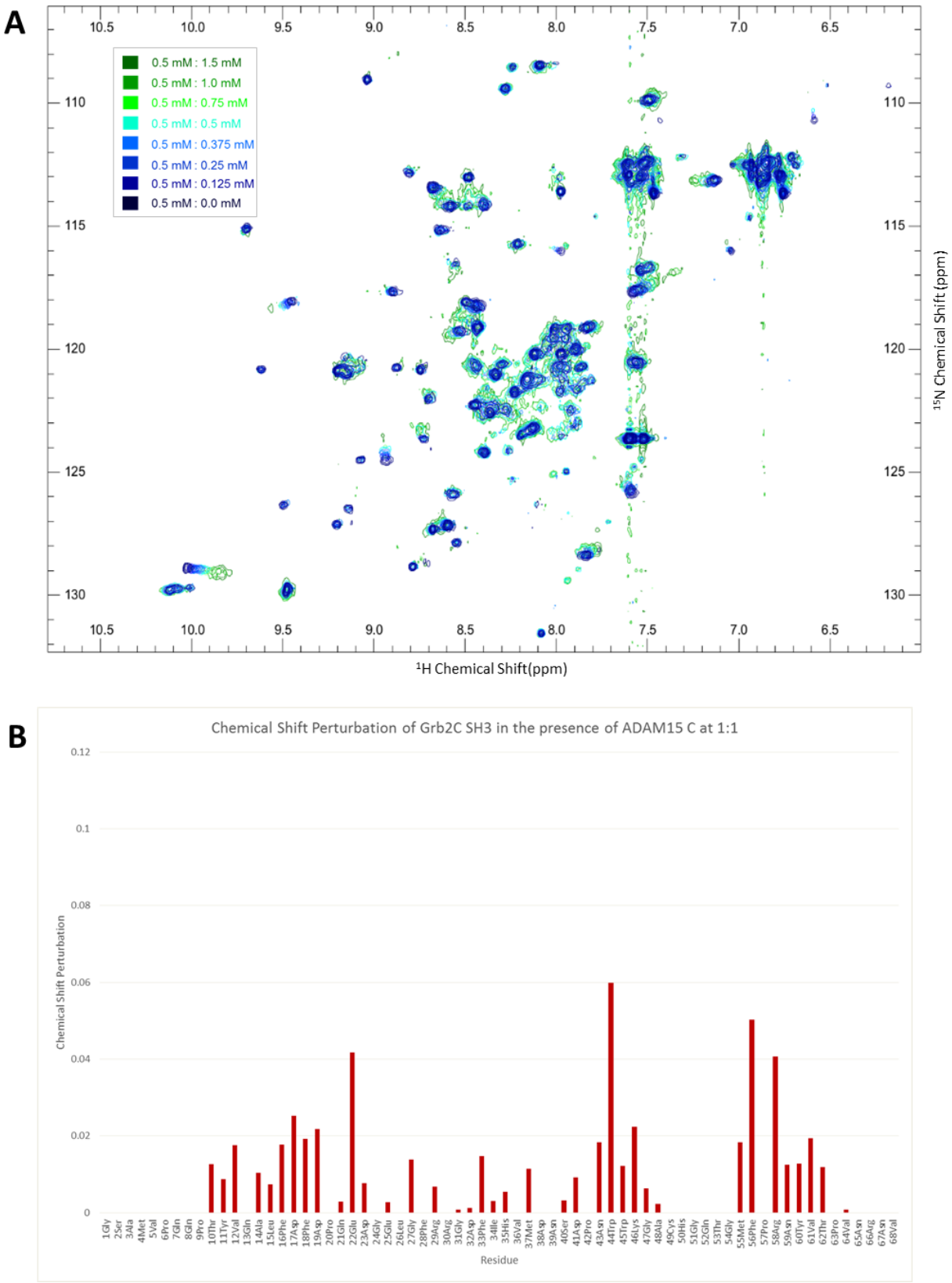

Figure 4.8 A) [^{1}H-^{15}N]-HSQC spectra for the ^{15}N Grb2C SH3 domain by itself (navy blue), in the presence of 0.5 mM ADAM15 C (cyan) and in the presence of 1.5 mM ADAM15 C (green) and the intermediates in intermediate shades as indicated in the key. The concentration of 15N Grb2C SH3 domain was 0.5 mM in all spectra and intermediate concentrations are also shown. B) Chemical shift perturbations caused by the presence of the ADAM15 C on the spectrum of the Grb2C SH3 domain at 0.5 mM of each protein.

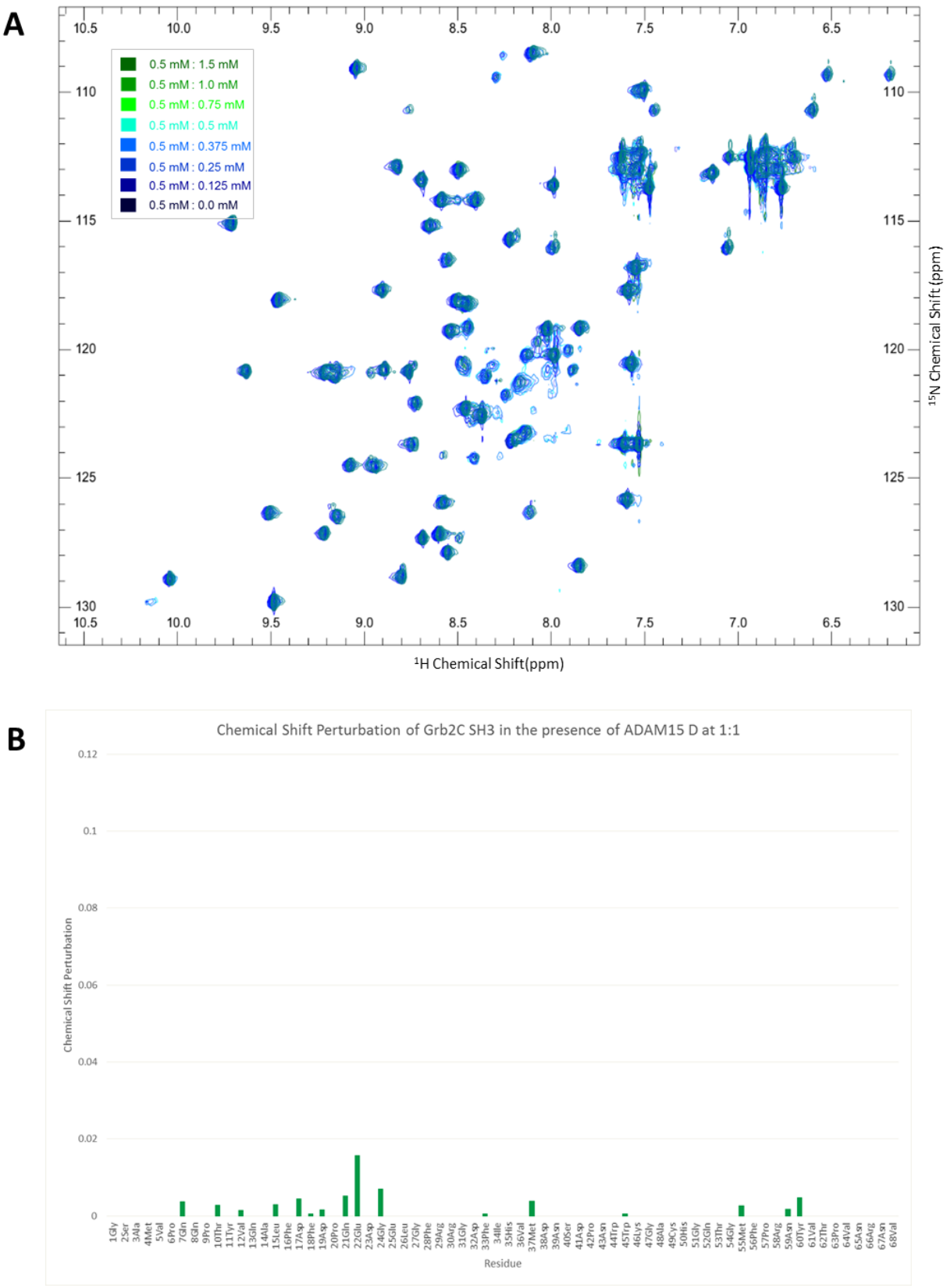

Figure 4.9 A) [^{1}H-^{15}N]-HSQC spectra for the ^{15}N Grb2C SH3 domain by itself (navy blue), in the presence of 0.5 mM ADAM15 D (cyan) and in the presence of 1.5 mM ADAM15 D (green) and the intermediates in intermediate shades as indicated in the key. The concentration of 15N Grb2C SH3 domain was 0.5 mM in all spectra and intermediate concentrations were also shown. B) Chemical shift perturbations caused by the presence of the ADAM15 D on the spectrum of the Grb2C SH3 domain at 0.5 mM of each protein.

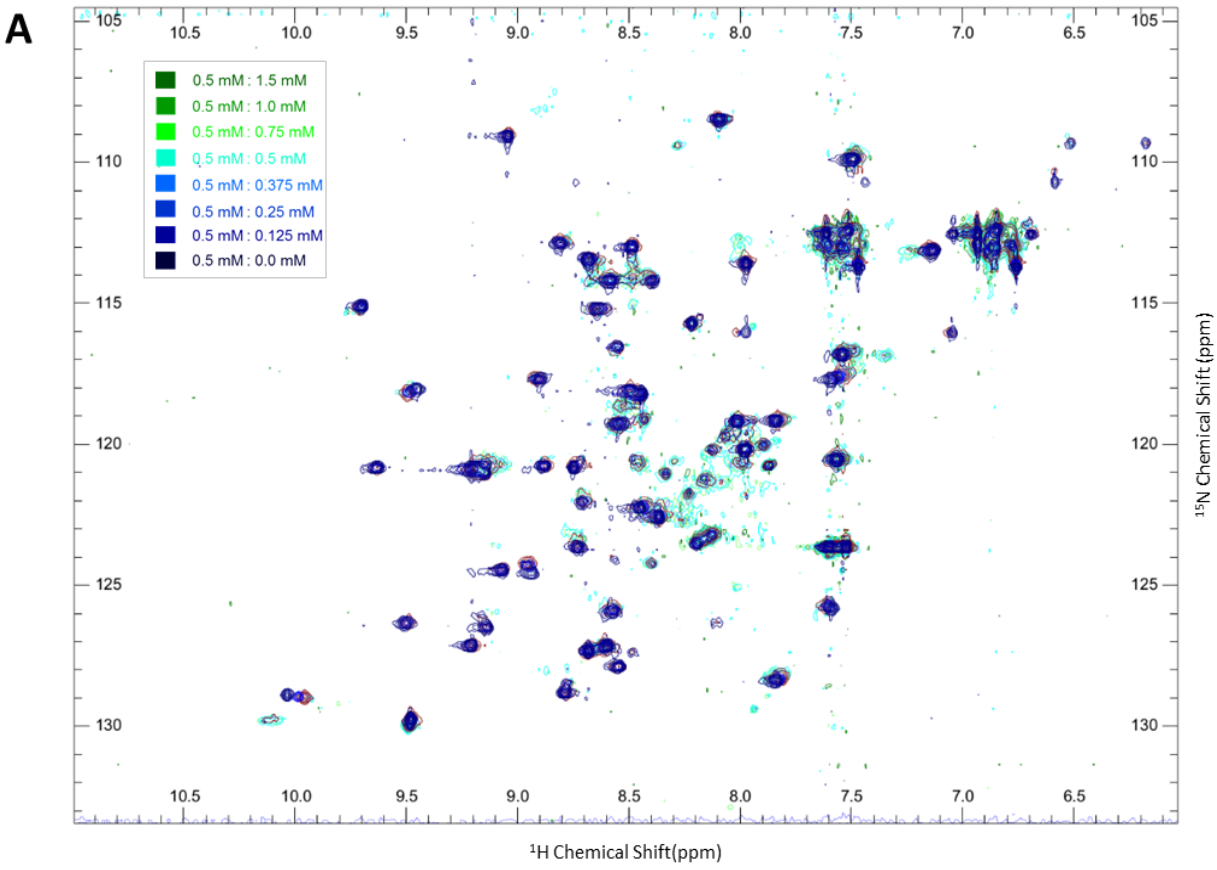

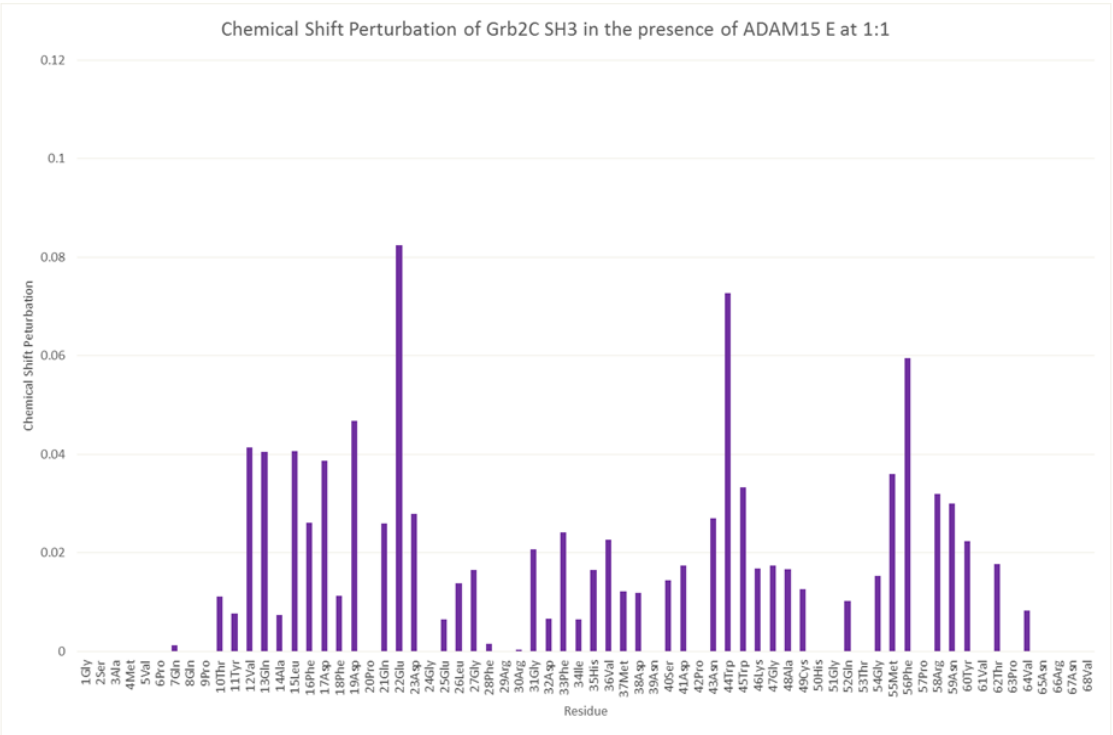

Figure 4.10 A) [^{1}H-^{15}N]-HSQC spectra for the ^{15}N Grb2C SH3 domain by itself (navy blue), in the presence of 0.5 mM ADAM15 E (cyan) and in the presence of 1.5 mM ADAM15 E (green) and the intermediates in intermediate shades as indicated in the key. The concentration of 15N Grb2C SH3 domain was 0.5 mM in all spectra and intermediate concentrations were also shown. B) Chemical shift perturbations caused by the presence of the ADAM15 E on the spectrum of the Grb2C SH3 domain at 0.5 mM of each protein.

4.5 Comparison of the CSPs of Grb2C caused by each ADAM15 ICD

When the results of the Grb2C-ADAM15 ICD titrations were compared, as shown in Figure 4.12, the differences in CSP intensity were emphasised. When considering only those residues with a CSP above the average + 2x standard deviation, residues 22Glu, 44Trp and 56Phe were consistently affected although there was some variation in the intensity of the CSP, particularly in the case of 22Glu which ranges from a CSP of 0.07 when in the presence of ADAM15 E to ~0.045 in the presence of the other ICDs. The residue 13Gln was affected by the presence of ADAM15 A and E but not any of the others. The titrations of ADAM15 B and C followed very similar patterns with 58Arg also displaying shifts larger than the average + 2 standard deviations. However, the CSPs caused by ADAM15 B were consistently slightly larger than those caused by ADAM15 C which implies a slightly tighter interaction. Larger chemical shift perturbations correlate with stronger binding affinities, although the exact proportion of the relationship between these depends on the proteins involved (Williamson, 2013). ADAM15 E caused significantly larger chemical shift perturbations over the whole of the Grb2C SH3 domain which also strongly implies that the interaction between these two proteins is tighter than for the other ICDs.

In Figure 4.13, the chemical shift perturbations have been mapped onto the structure of Grb2C, as shown in Figure 4.1A. Mapped were those residues which exhibit the greatest chemical shift perturbation when the appropriate ADAM15 ICD is introduced.

The models make it very clear that the interaction interface between Grb2C and all of the ADAM15 ICDs, except D, are consistent with the many of the same key residues involved in all of the interactions albeit to differing extents. This implies two things: firstly, there is variation in the binding intensities of the each of the ADAM15 ICDs with Grb2C based upon the intensity of the chemical shift perturbations of those residues involved. This was supported by the rate of precipitation of the protein in the NMR tube during the titrations. As the concentration of the ADAM15 ICDs was increased, a precipitate began to form. This likely occurred at a lower concentration of ADAM15 B and E likely due to their binding more tightly to Grb2C than the other ADAM15 ICDs. Unfortunately, it was not possible to measure the dissociation constant by NMR as the

reaction did not saturate before precipitation began. It is likely that non-specific interactions aided earlier precipitation.

Secondly, it is clear that the same face of the SH3 domain is involved in all of the interactions which suggests that those ICDs which interact with Grb2C (ADAM15 A, B, C and E) do so in a similar manner. A common element between each ICD must be involved. Studying the sequences of the ADAM15 ICDs, shown in Figure 4.11, there were only two characteristics common in all of the Grb2C-interacting ADAM15 ICDs and thus potential motifs involved in the interaction investigated here.

Figure 4.11 The sequence alignment of the ADAM15 ICDs A-E with the proline-rich regions highlighted and the GRTK/RSPK motifs underlined.

The three proline-rich regions common to all the ADAM15 ICDs, except D for the case of this discussion, were regions P1, P4 and P5. Any of these could be responsible for the interactions, individually or in combination. Additionally, it has been demonstrated previously that the C-terminal SH3 domain of Grb2 can interact with proteins that contain the motif RGTK (Simister et al., 2013). This alternative sequence is present in all the ADAM15 ICDs as well and will be further investigated.

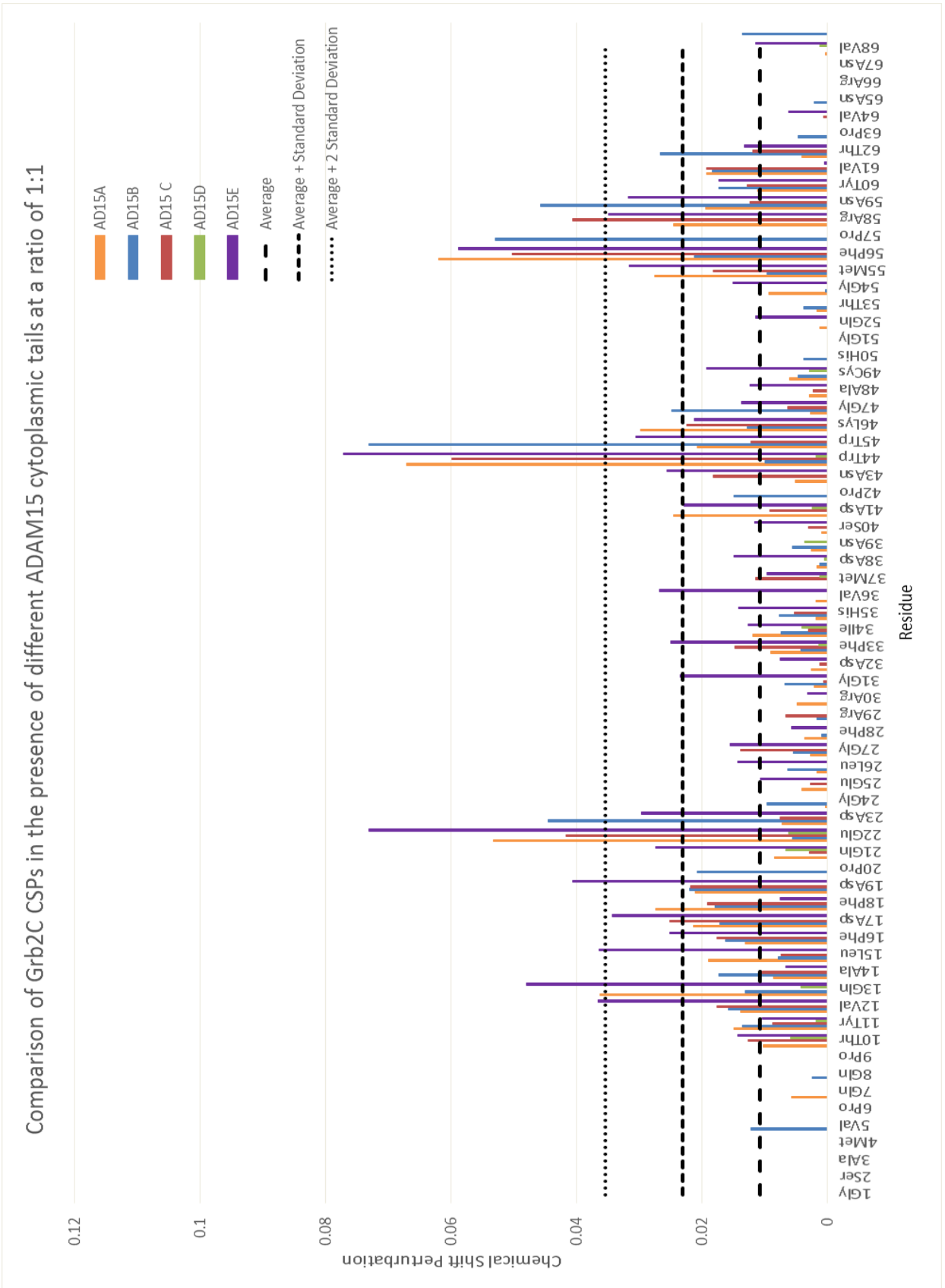

Figure 4.12 Chemical Shift Perturbations of Grb2C caused by each of the ADAM15 ICDs. Also highlighted were the average CSP across all five titrations, the average + standard deviation and the average + 2x standard deviation.

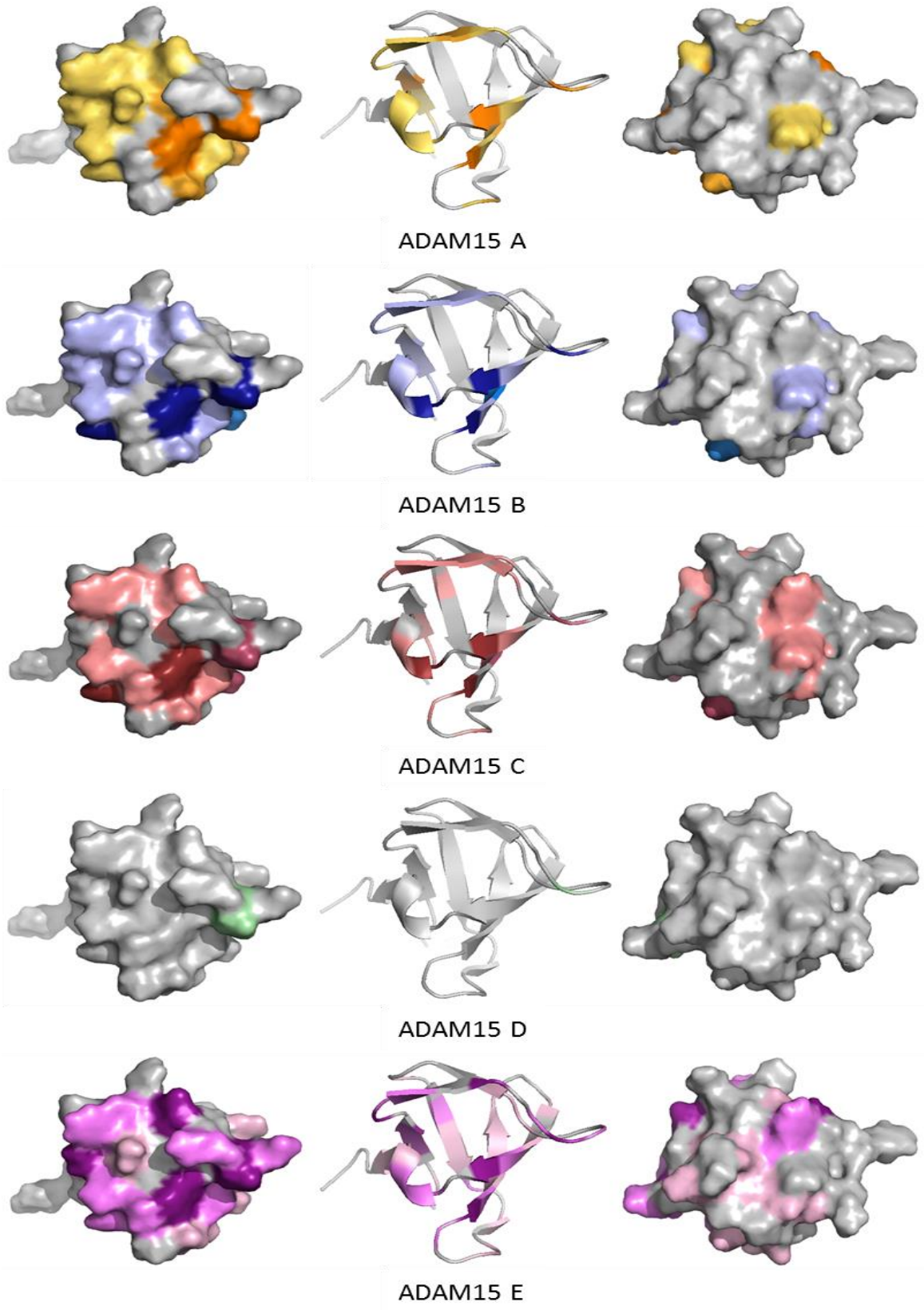

Figure 4.13 Chemical Shift Perturbations caused by each ADAM15 ICD mapped on to the structure of Grb2C (1GFC) where the darkest shading indicates the CSPs above average + 2x standard deviation, the middle shading for those CSPs above average + standard deviation and the lightest shading for CSPs above average. Grey residues were unaffected or shifted by less than the average CSP. The model on the left and the central model show the same perspective of the protein; the right model was rotated 180°.

4.6 Titration of 15N Grb2C with mutated ADAM15 B

To determine whether the interaction of the ADAM15 ICDs with the C-terminal SH3 domain of Grb2 required one of the proline-rich motifs 1, 4 and 5 of the ICDs or the alternative RGTK sequence, the RGTK sequence was mutated in the ICD of ADAM15 B and the titration with ^{15}N Grb2C was repeated. The mutated gene was synthesised by GenScript in order to include the BamHI and HindIII restriction sites which were used when generating the previous GB1-tagged ADAM15 ICD constructs. This allowed the gene to be ligated into the pSKDuet01 vector thus GB1-tagging the mutant (Iwai et al., 2006). No further optimisation of the purification was required. The mutant, henceforth known as ADAM15 BM, included the altered RGTK motif, now an AGTA sequence, which should have removed any interaction present if this was the motif required.

As with the titration with ADAM15 B, protein began to precipitate at a ratio of 1:1. Additionally, the same residues of Grb2C that exhibited movement in the presence of ADAM15 B still exhibited movement in the presence of ADAM15 BM as can be seen in figure 4.14. In fact, those residues affected by the presence of the ADAM15 B ICD were affected more so in the presence of ADAM15 BM. Removal of the RGTK motif did not reduce the ability of the B variant ICD to interact with the Grb2C SH3 domain thus confirming that the alternative RGTK motif was not necessary here.

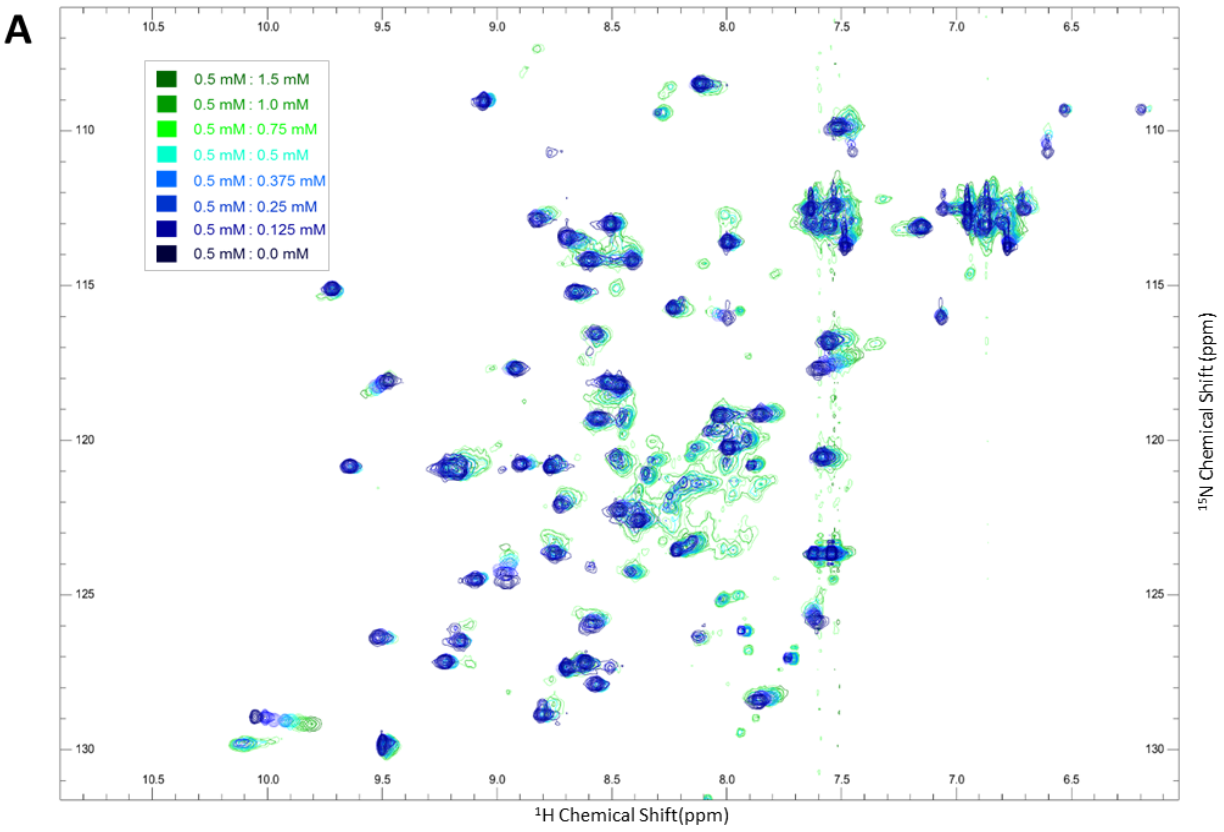

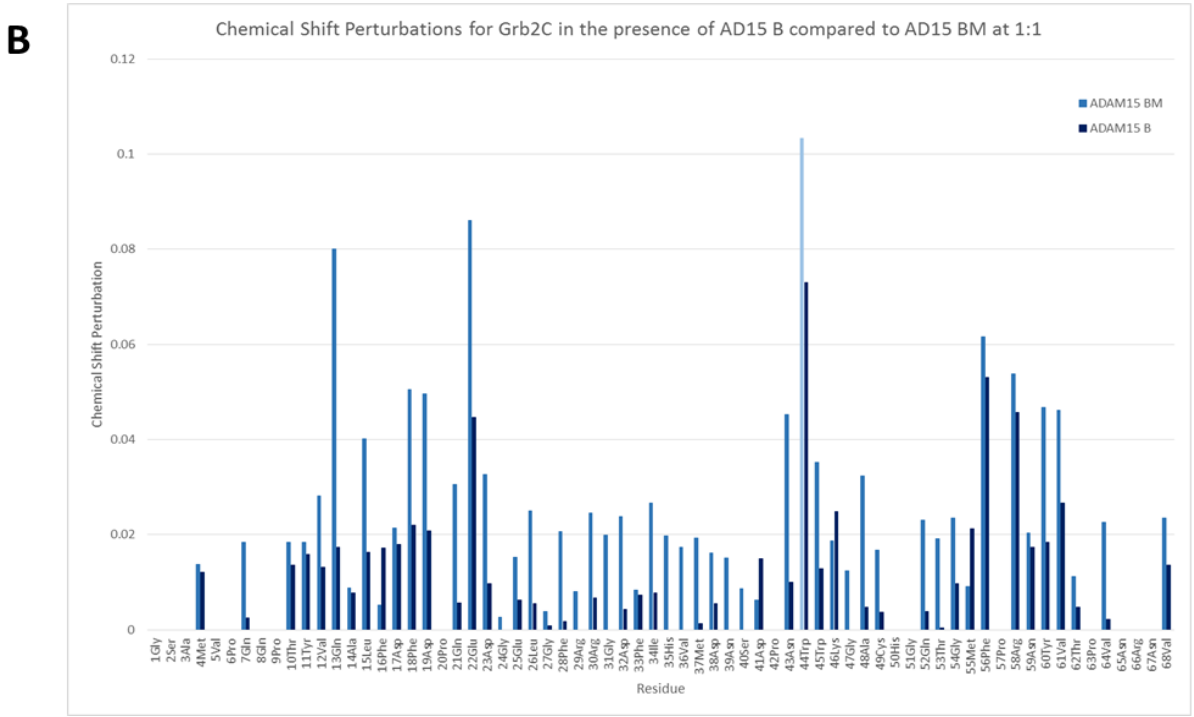

Figure 4.14 A) [^{1}H-^{15}N]-HSQC spectra for the ^{15}N Grb2C SH3 domain by itself (navy blue), in the presence of 0.5 mM ADAM15 BM (cyan) and in the presence of 1.5 mM ADAM15 BM (green) and the intermediates in intermediate shades as indicated in the key. The concentration of 15N Grb2C SH3 domain was 0.5 mM in all spectra and intermediate concentrations were also shown. B) Chemical shift perturbations caused by the presence of the ADAM15 BM on the spectrum of the Grb2C SH3 domain at 0.5 mM of each protein alongside those for the CSPs caused by ADAM15 B.

4.7 Optimisation of the purification of Grb2N

The purification of Grb2N was attempted using the same protocol as for Grb2C, as they were both GST fusion tagged. After clarification of the bacterial lysate, the GST-tagged protein was purified by glutathione sepharose and eluted with 300 mM reduced glutathione in SPB pH 7.2, as can be seen in Figure 4.15 A. Thrombin digestion was optimised to 7.5 units as can be seen in Figure 4.15 B. Finally, the GST tag and Grb2N were separated by size exclusion chromatography. The purified protein was then dialysed into 50 mM sodium phosphate, 100 mM sodium chloride pH 6.0, the buffer used when acquiring the assignments (Wittekind et al., 1997). A selection of NMR experiments including [^{1}H-^{15}N] HSQC, HNCACB and CBCACONH were acquired. With the aid of a summer project student, Sam Walpole, it was possible to assign the majority of the backbone of Grb2N as shown in Figure 4.16 A (Wittekind et al., 1997).

However, as has been highlighted in Figure 4.16 B, there were several residues for which there were two peaks appearing on the HSQC spectrum. The corresponding peaks in the HNCACB and CBCACONH spectra for the HSQC peaks, were equally duplicated. There are two possible explanations for this. Firstly, it has been shown that Grb2N dimerises with itself *in vitro* and *in vivo* (Lin et al., 2012). Secondly, it could be that Grb2N exists in two forms here, a full folded form and a partially, or entirely, unfolded form. Half of the duplicated peaks reside between 8.0 ppm and 8.5 ppm in the ^{1}H dimension which is characteristic of unfolded residues making the second explanation more likely here (Kosol et al., 2013).

In order to improve folding in future experiments, the purification protocol was altered to include an incubation step in the presence of 8 M urea and 1 mM DTT for 4-5 hours at 25 °C after the size exclusion step. The urea was removed by dialysis but the DTT concentration was maintained in order to prevent possible dimerisation of the Grb2N with itself. The urea incubation was intended to unfold all the protein in the sample and allow it to refold as the urea was removed. However, this did not improve the peak duplication in the HSQC.

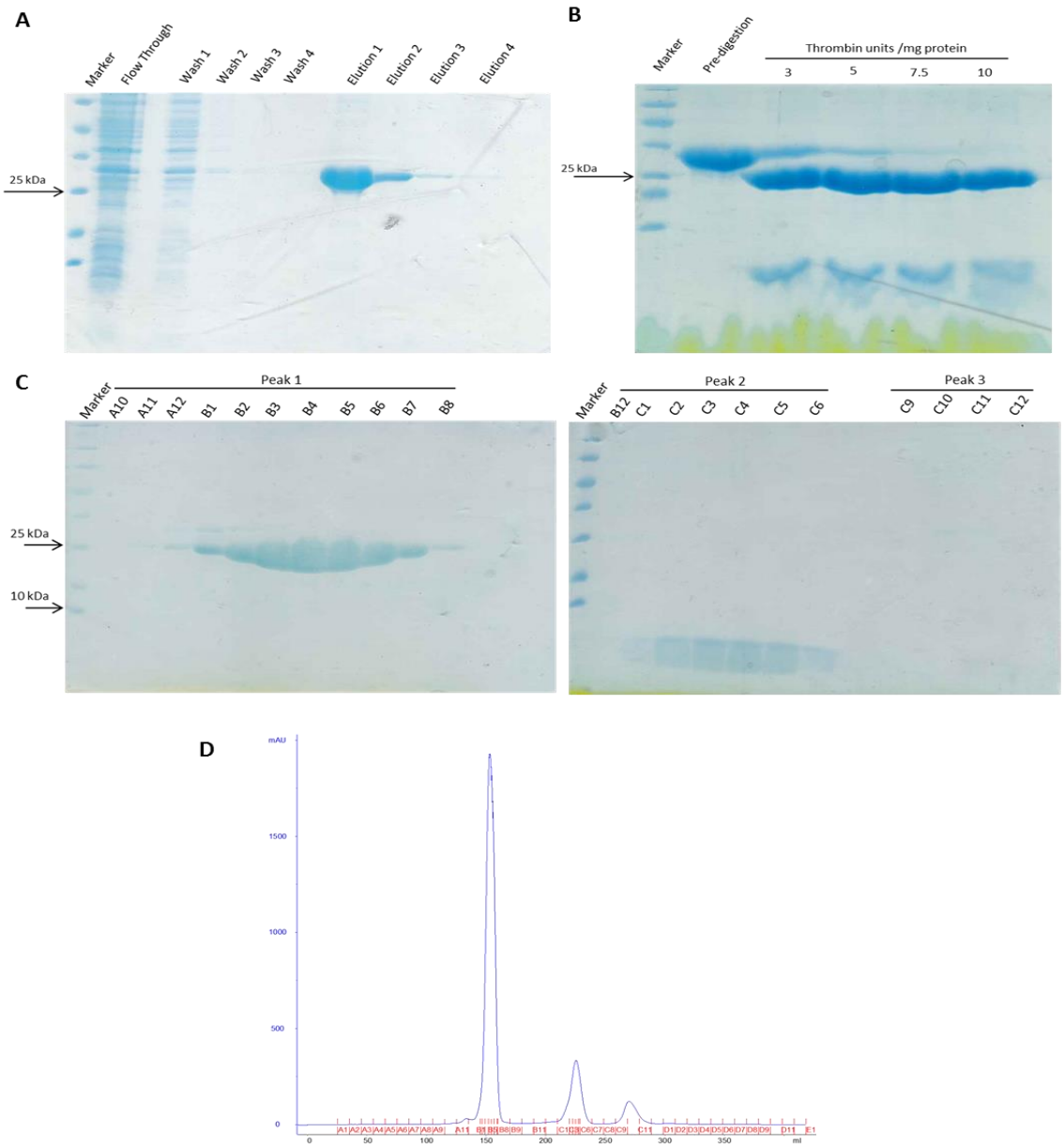

Figure 4.15 A) Glutathione sepharose purification of GST-tagged Grb2N. B) Thrombin digestion optimisation to remove GST tag. C) SDS PAGE gel of peaks from the size exclusion separation of GST and Grb2N. D) Chromatogram of the size exclusion column.

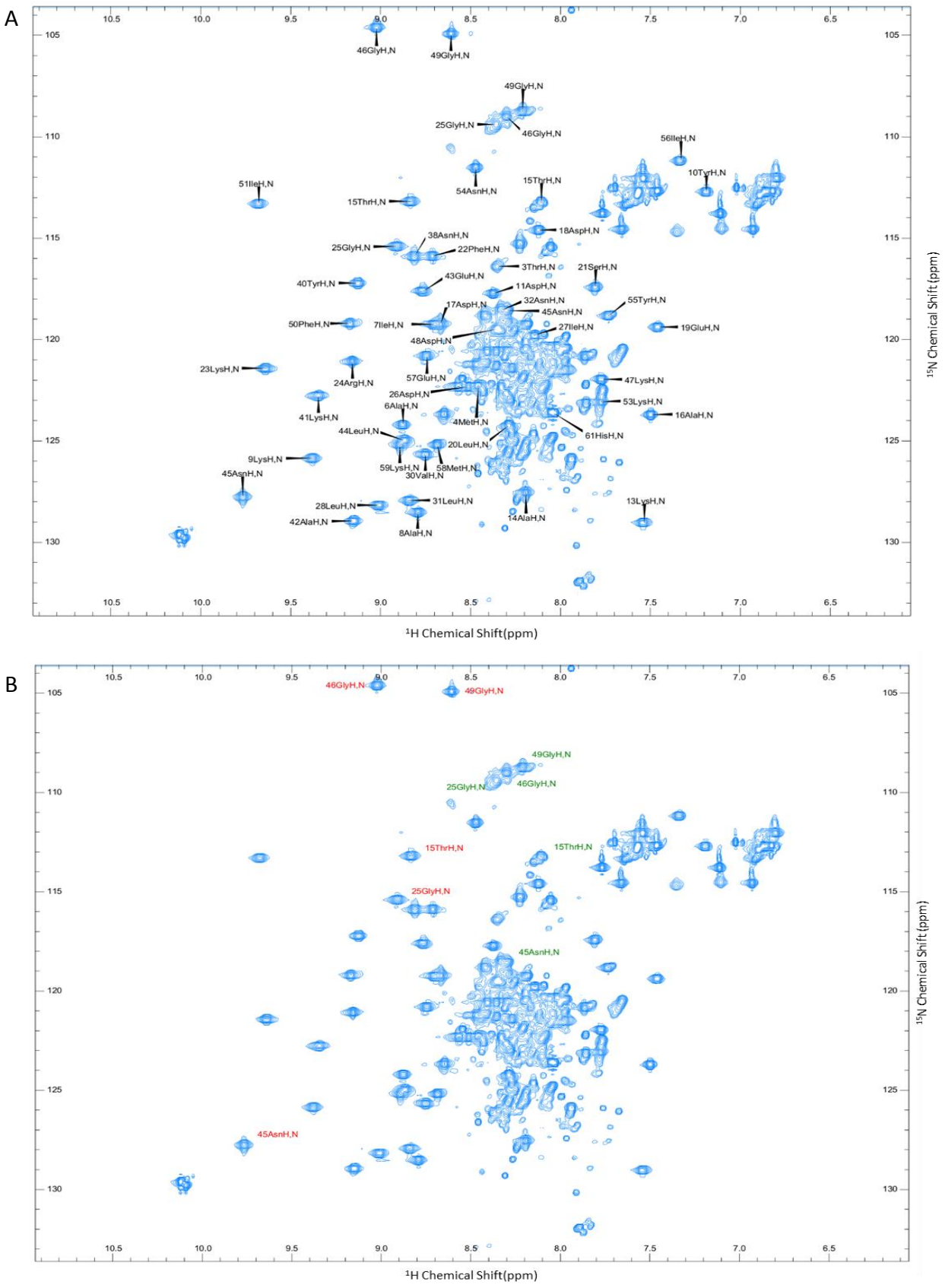

Figure 4.16 A) [^{1}H-^{15}N] HSQC of Grb2N showing backbone assignments. B) [^{1}H-^{15}N] HSQC highlighting those peaks which were duplicated. Peaks highlighted with red assignments are located in positions expected from residues within a folded region. The peaks highlighted with green assignments are for the same residues but residing within a region which implies disordered residues.

Based upon the purification technique from a different Grb2N publication (Wittekind et al., 1997), the purification was repeated but in 50 mM Tris.HCl pH 8.0 rather than SPB. When the sample was separated by size exclusion chromatography, a small shoulder appeared on one of the peaks as shown in Figure 4.17 B. When a sample of each fraction was analysed by SDS PAGE gel electrophoresis (Figure 4.17 A), both the shoulder and the main peak appeared to contain Grb2N, although to a much smaller extent in the shoulder. In order to investigate whether this shoulder represented a partially unfolded version of the SH3 domain, each fraction was concentrated separately and [^{1}H-^{15}N] HSQC were collected for each. Figure 4.17 C shows these spectra overlaid with an example of the HSQC prior to the Tris.HCl purification. Although there were some differences between the spectra, neither set of the duplicated peaks is removed entirely, confirming that the current purification protocol was not specific enough to separate the folded and unfolded forms of Grb2N.

Finally, ion exchange chromatography was attempted in order to try to purify only the folded form of Grb2N as this technique had been used in the purification of the domain in previous publications. Unfortunately, the chromatogram and subsequent SDS PAGE gel electrophoresis, shown in Figure 4.18, show that this technique was also unable to separate the folded and unfolded forms of this protein nor remove the cleaved GST tag.

4.9 Conclusions and Discussion

This chapter has discussed the interactions of the scaffolding protein, Grb2, with the splice variant intracellular domains of ADAM15. Initially the results demonstrated that, in the case of the C-terminal SH3 domain of Grb2 and given that the interactions observed were not dependent on the RGTK motif, one of proline-rich region 1, 4 or 5, from the ADAM15 ICDs is responsible and thus follows a more traditional interaction pathway. Unfortunately, it is not possible to say which exactly region is responsible here or if multiple polyproline region cooperate to facilitate binding without further mutation studies. However, previous truncation studies using ADAM15 A, have shown that the N-terminal proline-rich region (proline-rich region 1), inhibited interaction with full length Grb2, although this was relaxed upon phosphorylation of the ADAM15 A ICD

(Poghosyan, 2001). Pull down studies showed that proline-rich region 4, which is the second motif of ADAM15 A, held considerable importance for interactions with endogenous Grb2, as removal of this motif dramatically reduced the amount of Grb2 pulled down from breast cancer cell lysate. Mutants with the final proline-rich region, P5, removed, showed some reduced interaction but not to the same extent as when P4 was removed (Poghosyan, 2001). Combining this with the NMR data discussed in this chapter, it is highly likely that P4 is the primary proline-rich region of the ADAM15 ICDs involved in the interaction with Grb2C.

Unfortunately, the inability to produce entirely folded Grb2N presented a number of issues with regards to collecting titration data to study the interaction of the ADAM15 ICDs. Although the peak intensity of the duplicated peaks implies that the proportions of unfolded and folded were fairly equal, it would not be possible to quantifiably study any potential interaction exhibited. Additionally, there may have been some interaction between the ADAM15 ICDs and the unfolded protein which would render the results unreliable. This means it was not possible to study the potential interactions between Grb2N and the ADAM15 ICDs despite it being shown by pull down in chapter 3 that Grb2N had the ability to interact with the ADAM15 ICDs, apart from variant D. This is disappointing as it means it was not possible to entirely confirm which SH3 domain from Grb2 provides the primary mechanism of interaction with ADAM15 in a biological setting.

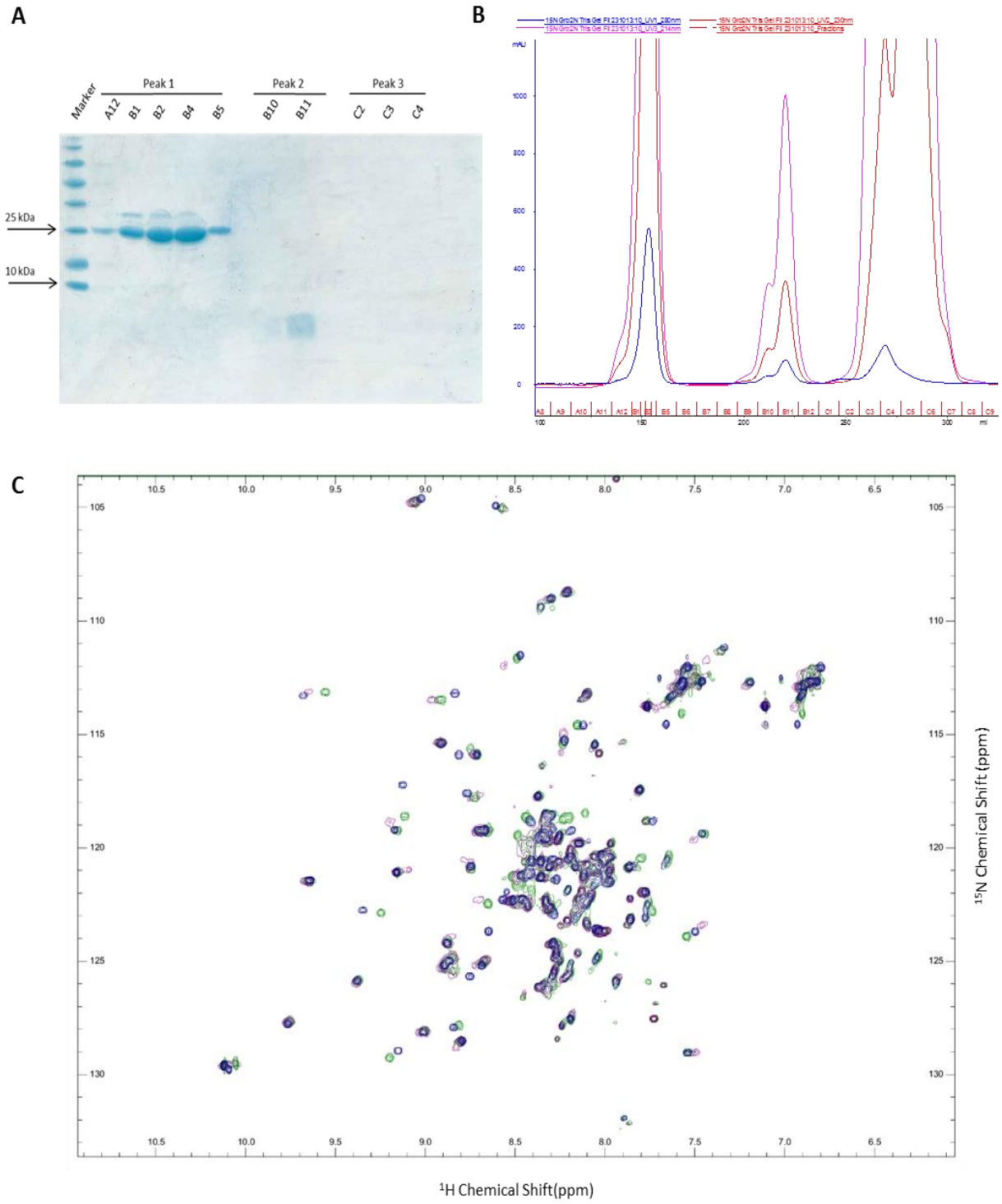

Figure 4.17 A) SDS PAGE gel electrophoresis of the size exclusion chromatography column. B) Chromatogram of the size exclusion chromatography column showing the shoulder on peak 2. C) [^{1}H-^{15}N] HSQC spectra of ^{15}N Grb2N. The blue spectrum is an example of Grb2N using the previous purification protocol. In purple is the spectrum of the main peak containing Grb2N from the size exclusion column and the green spectrum shows the protein purified from the shoulder of this peak.

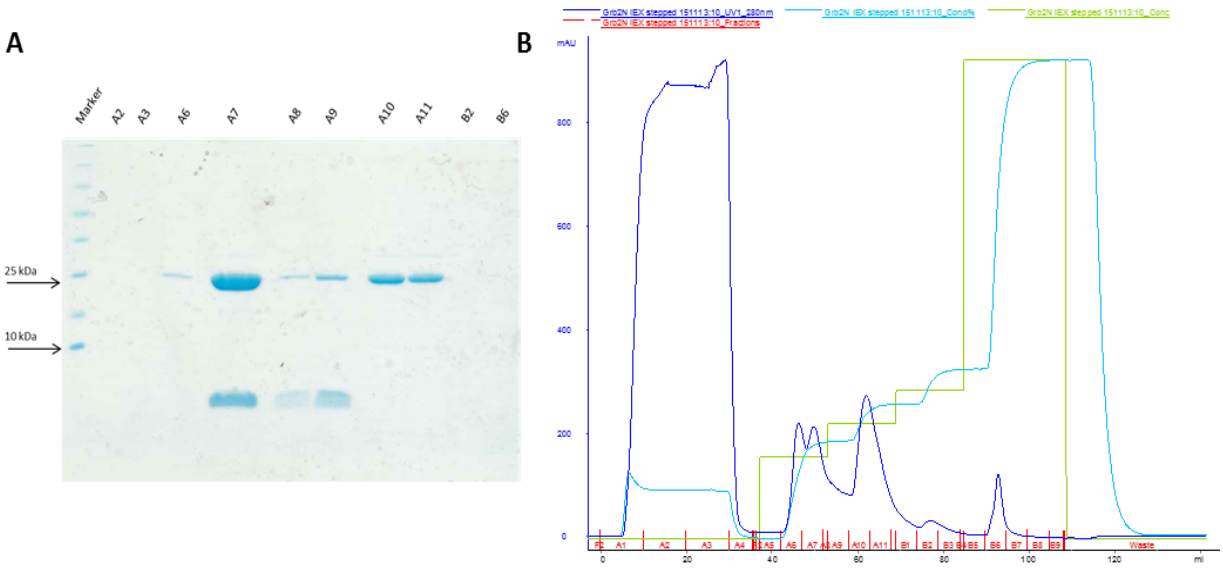

Figure 4.18 A) SDS PAGE gel electrophoresis of the fractions from the anion exchange chromatography. B) Chromatogram of the anion exchange chromatography.

In a biological setting, the N-terminal SH3 domain is responsible for the primary function of Grb2, namely interactions with Son of Sevenless (SoS) (McDonald et al., 2012a), the guanine nucleotide exchange factor responsible for GTP hydrolysis of Ras, thus initiating the MAPK cascade. This relies upon recruitment of Grb2 by phosphorylated Receptor Tyrosine Kinases (pRTKs) by the central SH2 domain (Belov and Mohammadi, 2012). By contrast, the C-terminal SH3 domain interacts with Gab1, via the non-canonical RxxK motif (McDonald et al., 2012b), and to proteins such as mutant Huntingtin (Baksi et al., 2014) and UVRAG (Roy et al., 2014). It is currently unclear as to how the interaction of Grb2 with ADAM15 plays a role in cell function. However, Grb2 has been shown to be required for FGF7 (also known as Keratinocyte Growth Factor) induced motility in MCF-7 breast cancer cells via the activation of ERK 1/2 (Zang et al., 2004). It has also been shown that ADAM15 increases migration and proliferation in breast cancer in an ERK 1/2 phosphorylation dependent manner (Sun et al., 2010) so there could potentially be crossover in these pathways. As mentioned previously, Grb2 inhibits FGFR2 until the introduction of a growth factor, such as FGF7, at which point, the conformational change in FGFR2 leads to the cross-phosphorylation of Grb2 and subsequent release thus activating FGFR2 (Lin et al., 2012). ADAM15 B has also been shown to shed a splice variant of FGFR2, specifically FGFR2iiib, in an apparently Src dependent manner

(Maretzky et al., 2009b). ADAM15 B expression is linked to more aggressive forms of node negative breast cancer (Zhong et al., 2008). Although it is unclear precisely how the interaction of Grb2 and ADAM15 is relevant to their biological functions, there is significant overlap of pathways in which both proteins are involved and even greater correlation of the phenotypic behaviour of breast cancer cells exposed to high levels of these proteins, which lends credence to their connected role in breast cancer progression and is likely reliant upon the P4 region of the ADAM15 ICD.

In summary, this chapter has shown that:

- Purification of the Grb2C domain was optimised.
- The backbone of ^{13}C, ^{15}N Grb2C was assigned.
- Titrations of the ^{15}N Grb2C domain with the ADAM15 ICDs demonstrated a consistent binding interface including 22Glu, 44Trp and 56Phe;
    - Also 13Gln in the presence of ADAM15 A and E;
    - Also 58Arg in the presence of ADAM15 B and C;
    - Larger CSPs imply a stronger interaction with ADAM15 E.
- ADAM15 D does not interact with ^{15}N Grb2C.
- Non-specific interactions between the ADAM15 ICDs and ^{15}N Grb2C caused protein aggregation and precipitation at higher concentrations.
- A proposed RXXK motif was not responsible for any interaction observed.
- Highly likely that the polyproline region 4 of the ADAM15 ICDs is responsible for the observed interactions with 15N Grb2C.
- Grb2N proved difficult to purify due to partially folded and unfolded states;
    - Exposure to urea did not aid refolding;
    - Size exclusion could not separate the folded and unfolded forms;
    - Ion exchange chromatography was unsuccessful despite success in previous publications.

Chapter 5: Interactions of Src and Brk with the ICDs of ADAM15

5.1 Introduction to Src

The human protein tyrosine kinase Src is 536 residues long and contains, starting from the N-terminus, a long unfolded region, an SH3 domain, a SH2 domain, a proline-rich linker sequence, a tyrosine kinase domain and a C-terminal tail (Wheeler et al., 2009). The SH3 and SH2 domains work together to regulate the catalytic activity of the tyrosine kinase domain through their ability to interact with proline-rich sequences and phosphotyrosine containing short motifs respectively. The SH3 domain of Src follows the same structural pattern as other SH3 domains (Saksela and Permi, 2012). It contains five β-strands, a RT loop, a distal loop, an n-Src loop and a short α-turn as shown in figure 5.1 (Yu et al., 1993).

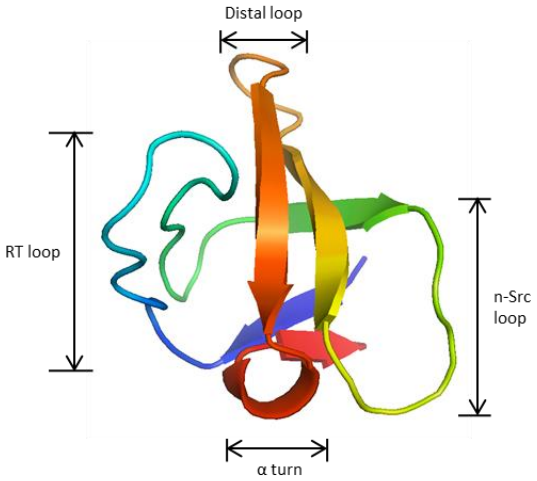

Figure 5.1 Structure of the SH3 domain of Src (1SRL (Yu et al., 1993)) with the RT loop, the distal loop, the n-Src loop and the α-turn highlighted.

Src has been shown previously to interact with the ICDs of ADAM 15 variants B and C but not with variant A (Zhong et al., 2008). This was reinforced in the data presented in chapter 3. In this chapter, each ADAM15 ICD was titrated into the SH3 domain of Src and the interaction studied by HSQC NMR experiments.

5.2 Purification of the Src SH3 domain

As our construct for the Src SH3 domain has a GST fusion tag, the protocol used was based upon the same principles as for the purification of Grb2C as can be seen in figure 5.2. Affinity purification was used to separate the protein from the cell lysate. After enzymatic digestion with thrombin to remove the GST fusion tag, these were separated using size exclusion chromatography. The concentrated sample was stored at -20 °C.

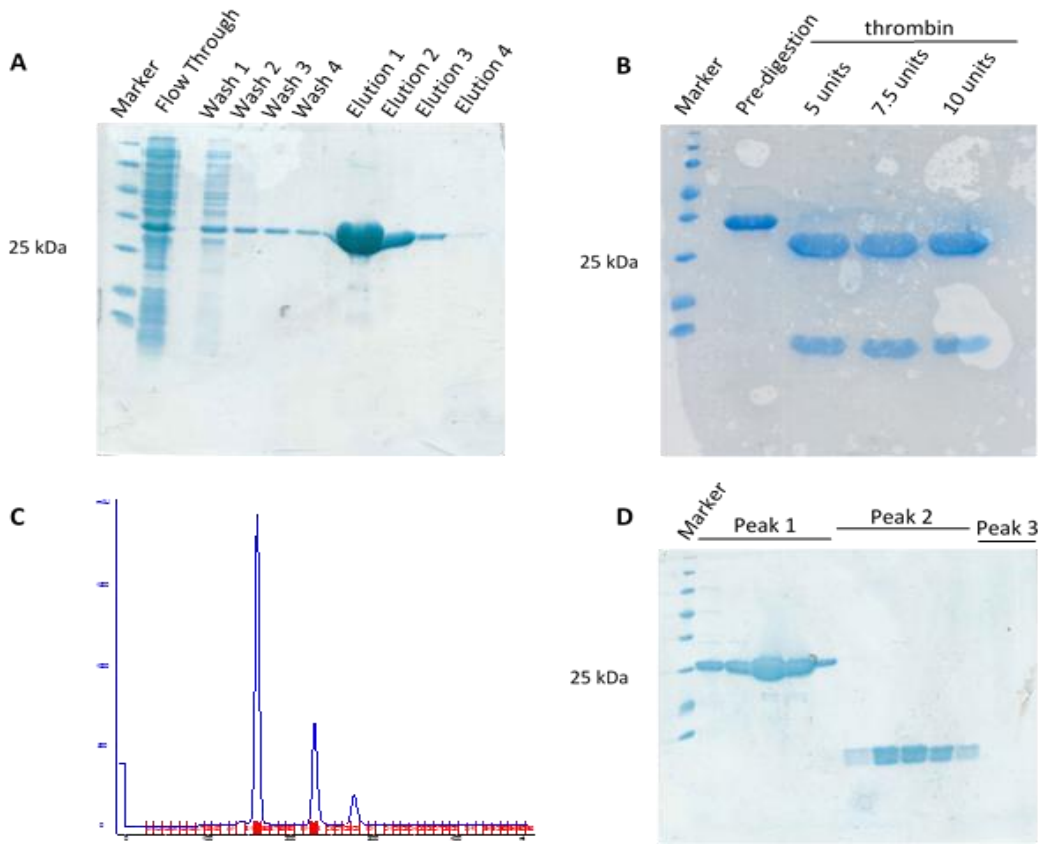

Figure 5.2 SDS PAGE gels for the purification of the Src SH3 domain. A) Glutathione sepharose column fractions with the GST-Src SH3 domain eluted at 300 mM glutathione in elution 1. B) Thrombin digestion optimisation with various thrombin amounts at room temperature. C) Akta chromatogram for the size exclusion showing 3 peaks D) SDS PAGE gel of the fractions of the size exclusion column with the peaks from which they originated highlighted. Peak 1 contained the GST fusion tag, peak 2 the Src SH3 domain and peak 3 containing no protein.

5.3 Assignment of Src SH3 domain

In order to assign the backbone of the Src SH3 domain, ^{13}C-, ^{15}N-labelled recombinant protein was produced as described above. HSQC, HNCαCβ and CβCαCONH spectra were acquired. Along with ^{1}H and ^{15}N assignments from Yu and colleagues (Yu et al., 1993),

these were used to assign the full ^{1}H, ^{15}N, $^{13}C\alpha$ and $^{13}C\beta$ of the Src SH3 domain with the exception of Gly1, Ser2, Pro55 and Pro61 ($^{13}C\alpha$ and $^{13}C\beta$ assigned for Pro55 and 61). The successfully assigned peaks are shown on a HSQC spectrum in figure 5.3.

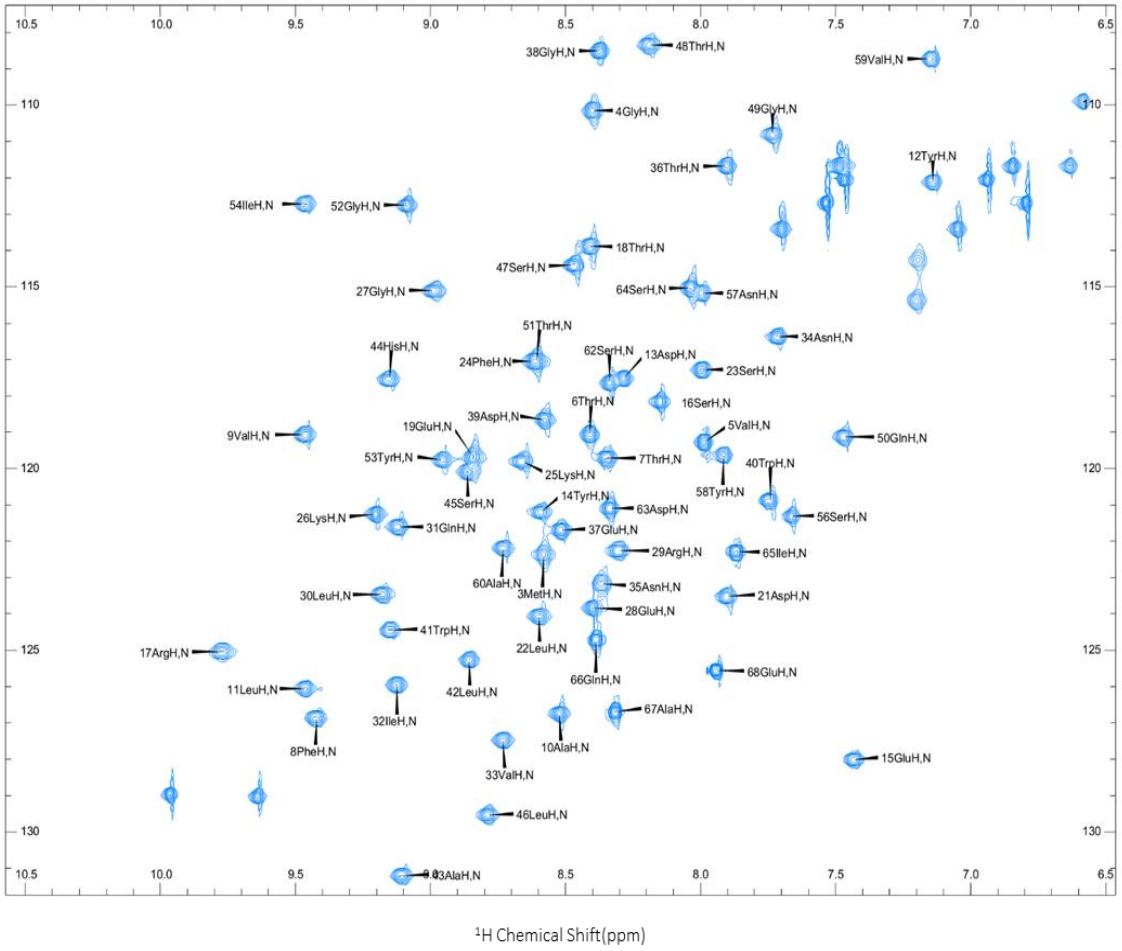

Figure 5.3 ^{1}H, ^{15}N HSQC spectrum of the Src SH3 domain with peak assignments

5.4 Titrations of Src SH3 domain with the cytoplasmic domains of ADAM15

As with the titrations of the Grb2C with the ADAM15 ICDs, two NMR samples were made for each titration with sample A containing 0.5 mM ^{15}N Src SH3 domain and sample B containing 0.5 mM ^{15}N Src SH3 domain and 1.5 mM of the appropriate ADAM15 ICD. After acquiring HSQC spectra for these data points, small volumes were removed from sample A and replaced with the same volume from sample B which maintained the concentration of the labelled Src SH3 domain while providing intermediate concentrations of the ADAM15 ICD. In order to ensure that all the chemical shift

perturbations observed are exclusively due to the interaction of the Src SH3 domain with the ADAM15 ICD involved, the SH3 domain was also titrated with the GB1 tag. The small chemical shift perturbations (CSPs) caused by the presence of the tag were subtracted from further titration CSPs when the ADAM15 ICDs were involved.

As shown in figure 5.4 A, there were very small changes between the spectrum for 0.5 mM Src SH3 alone and the spectrum for 0.5 mM Src SH3 in the presence of 0.5 mM GB1 tag. These were quantified using the same calculation for chemical shift perturbation as for Grb2C as shown below:

$$\text{CSP } (\Delta\text{ppm}) = \sqrt{(\Delta\delta_{HN})^2 + (\Delta\delta_N * 0.15)^2} \qquad \text{(Equation 2)}$$

The CSPs caused by the presence of the GB1 tag are shown in figure 5.4 B.

As can be seen in figure 5.5 A, several peaks in the spectrum for the ^{15}N Src SH3 domain undergo chemical shift perturbations indicating that there is an interaction between the ADAM15 A ICD and the Src SH3 domain. The chemical shift perturbations observed at a ratio of 0.5 mM Src SH3 to 0.5 mM ADAM15 A (with the CSPs caused by the GB1 tag subtracted) are lower than those observed for the interaction of Grb2C with ADAM15 A and do not follow the usual pattern of interaction shown by the Src SH3 domain with other proline-rich motifs. The biggest movements displayed are 17Arg, 20Thr, 53Tyr, 54Ile and 57Asn.

Unlabelled ADAM15 B was titrated into 0.5 mM ^{15}N Src SH3 to a final concentration of 1.5 mM ADAM15 B as previously. The spectra for this titration can be seen in figure 5.6 A with the chemical shift perturbations shown in figure 5.6 B. The shifts caused by the presence of ADAM15 B were much greater than those caused by ADAM15 A with some CSPs caused by ADAM15 B being more than double those caused by ADAM15 A. Although the reaction does not saturate at these concentrations, larger chemical shift perturbations implied a tighter interaction between the Src SH3 domain and ADAM15 B than with ADAM15 A. The residues most affected by the interaction are 17Arg, 19Glu, 22Leu, 36Thr, 40Trp, 41Trp, 53Tyr and 57Asn.

The spectra for the titration of ^{15}N Src with ADAM15 C are shown in figure 5.7 A and the quantification of the chemical shift perturbations are shown in B. The CSPs here are

lower than those caused by ADAM15 B but still much higher than for the interaction with ADAM15 A. The residues most involved in the interaction are 17Arg, 19Glu, 36Thr, 40Trp, 56Ser and 57Asn. This interaction follows a similar pattern to that of the interaction of the Src SH3 domain with ADAM15 B.

ADAM15 D was titrated into 0.5 mM ^{15}N Src SH3 domain to a final concentration of 1.5 mM and observed by HSQC as for the previous titrations which can be seen in figure 5.8 A. There were very few changes between the spectra for 0.5 mM Src SH3 domain alone and in the presence of 0.5 mM ADAM15 D and any peak movements observed were very small in comparison to those caused by the other ADAM15 ICDs, even ADAM15 A. This would imply that ADAM15 D does not interact with the SH3 domain of Src. This is expected since ADAM15 D does not contain any proline-rich motifs and the Src SH3 domain has not been shown to interact with any other motifs.

Figure 5.9 A shows the chemical shift perturbations of the ^{15}N Src SH3 domain caused by the presence of ADAM15 E, with the quantification of these shown in B. A similar pattern of peak movements to those caused by ADAM15 B and C can be observed, implying that there is a similar interaction, although these were smaller than those of ADAM15 B. The residues most affected are 17Arg, 19Glu, 22Leu, 36Thr, 40Trp, 41Trp, 53Tyr, 56Ser and 57Asn.

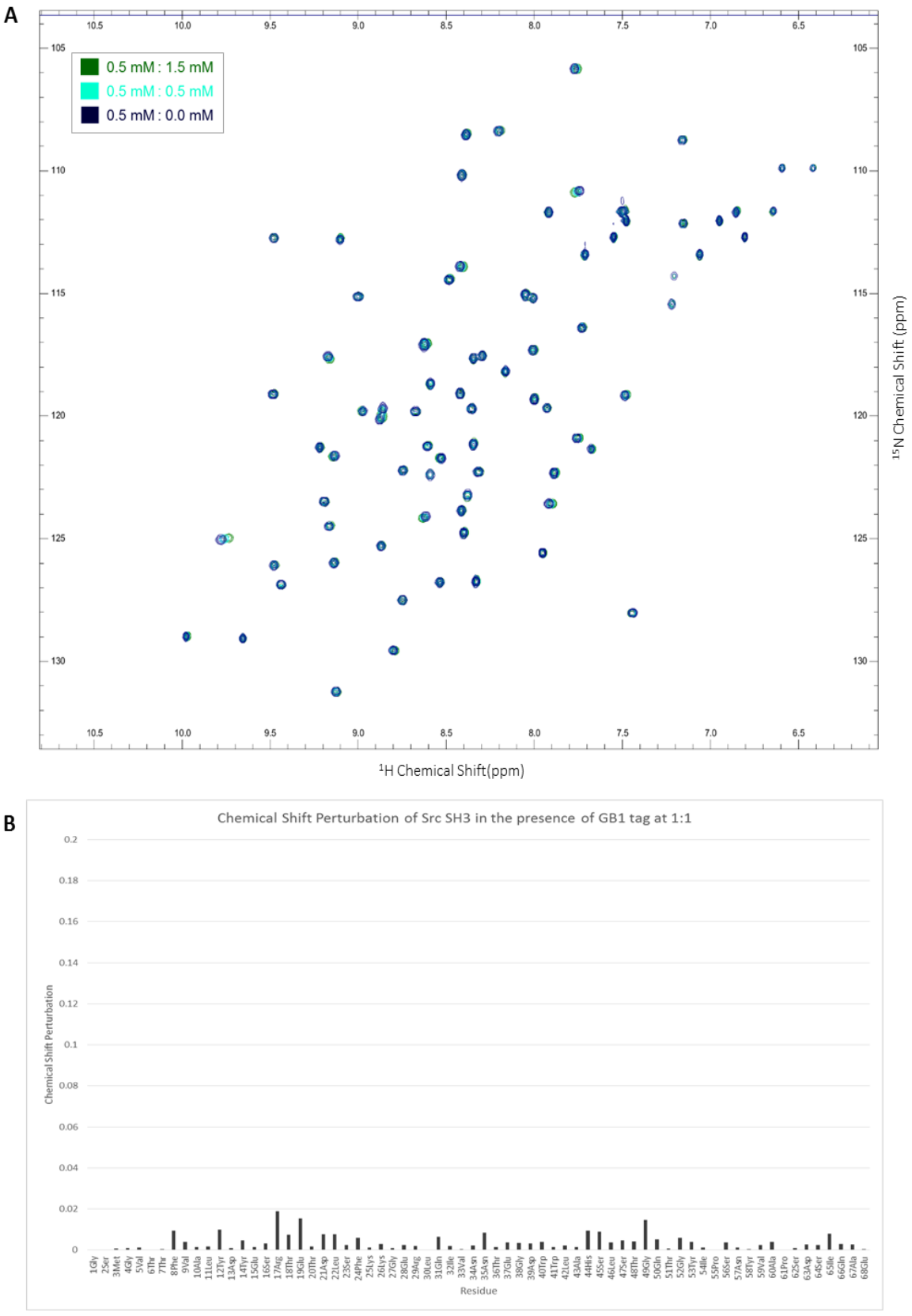

Figure 5.4 A) ^{1}H, ^{15}N HSQC spectra for the ^{15}N Src SH3 domain by itself (navy blue), in the presence of 0.5 mM GB1 tag (cyan) and in the presence of 1.5 mM GB1 tag (green). Concentration of the Src SH3 domain was 0.5 mM in all spectra. B) Chemical shift perturbations caused by the presence of GB1 tag on the spectrum of the Src SH3 domain at 0.5 mM of each protein.

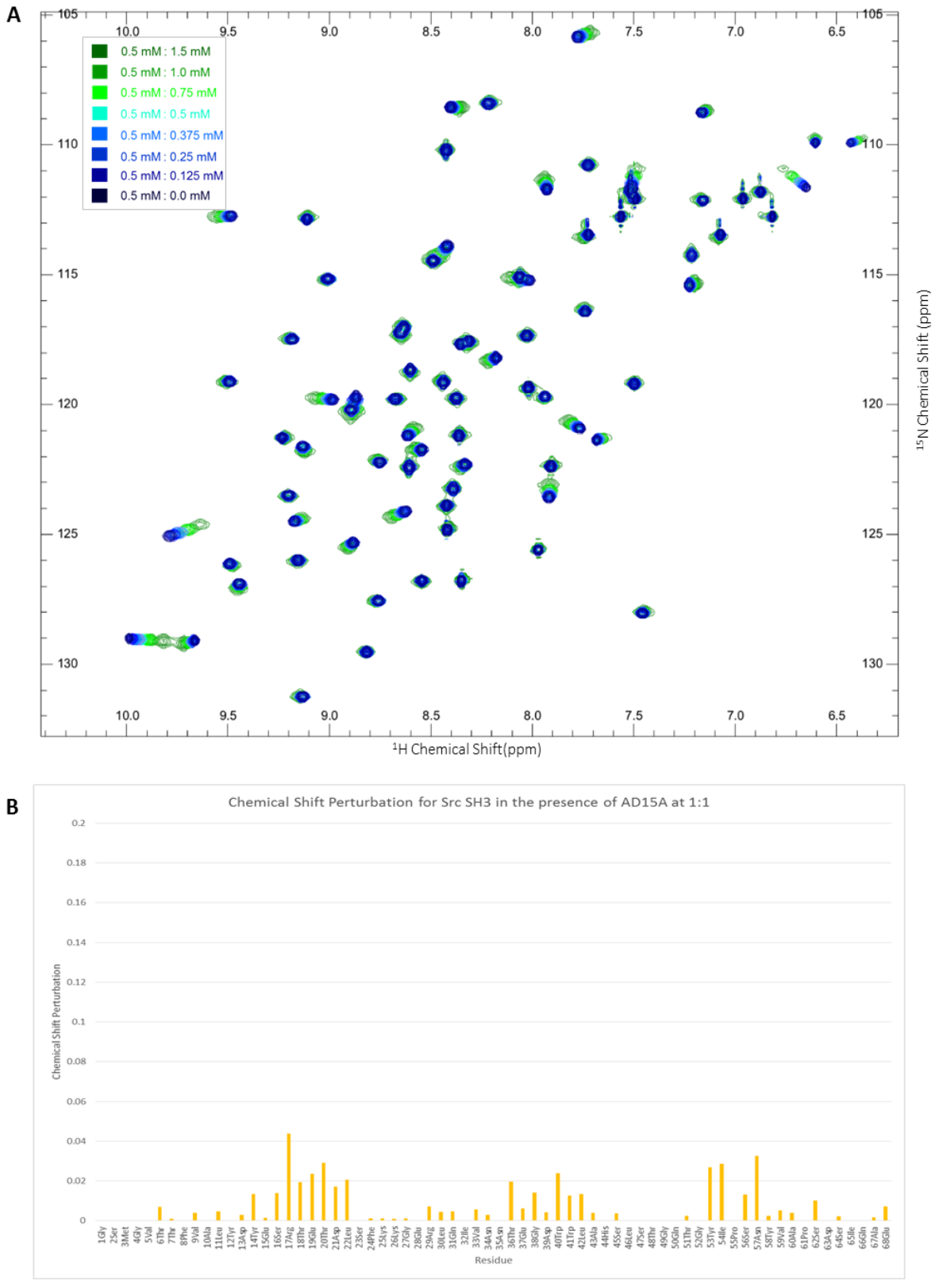

Figure 5.5 A) ^{1}H, ^{15}N HSQC spectra for the ^{15}N Src SH3 domain by itself (navy blue), in the presence of 0.5 mM ADAM15 A (cyan) and in the presence of 1.5 mM ADAM15 A (green) and the intermediates in intermediate shades as indicated in the key. Concentration of the Src SH3 domain was 0.5 mM in all spectra. B) Chemical shift perturbations caused by the presence of ADAM15 A on the spectrum of the Src SH3 domain at 0.5 mM of each protein.

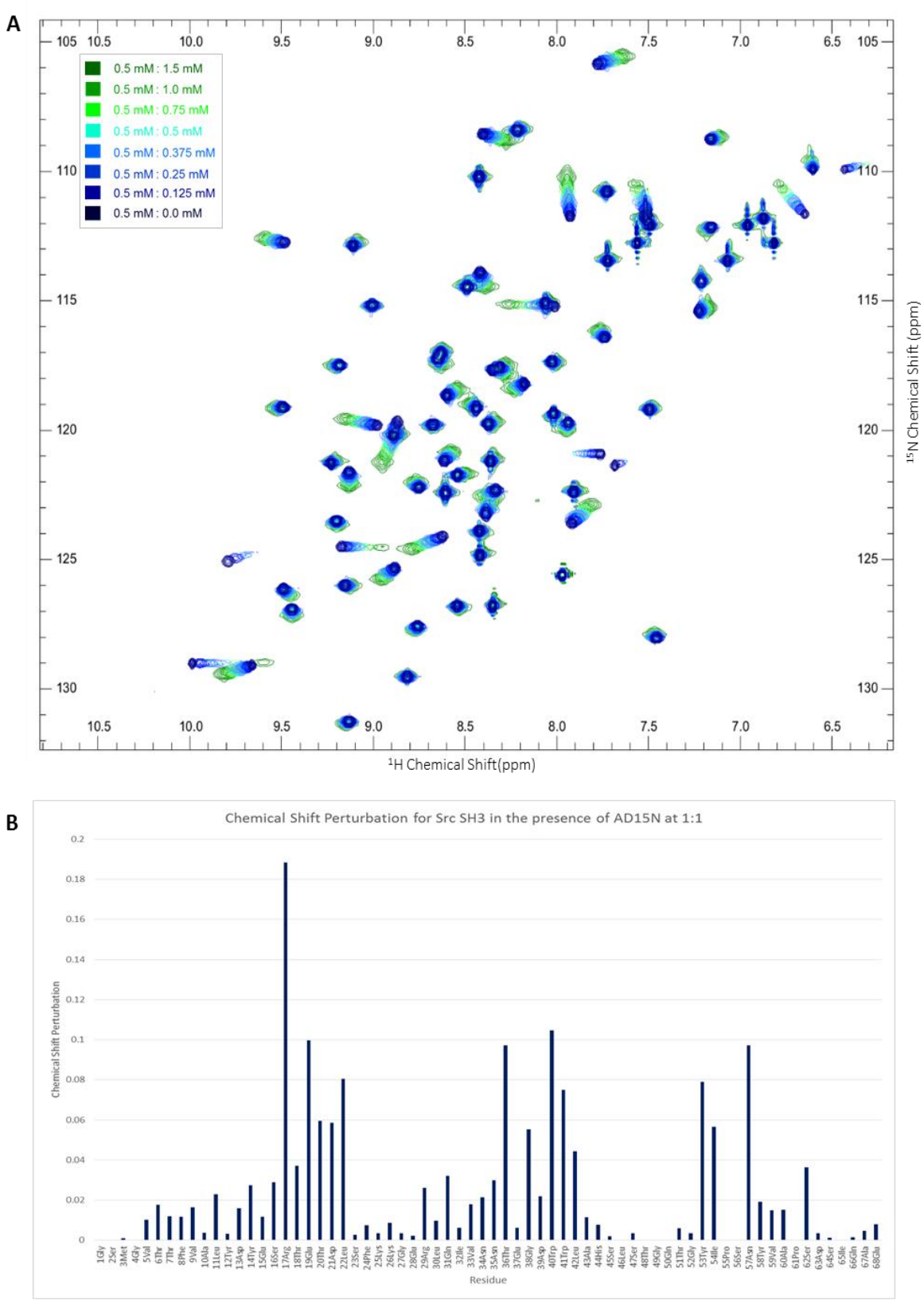

Figure 5.6 A) ^{1}H, ^{15}N HSQC spectra for the ^{15}N Src SH3 domain by itself (navy blue), in the presence of 0.5 mM ADAM15 B (cyan) and in the presence of 1.5 mM ADAM15 B (green) and the intermediates in intermediate shades as indicated in the key. Concentration of the Src SH3 domain was 0.5 mM in all spectra. B) Chemical shift perturbations caused by the presence of ADAM15 B on the spectrum of the Src SH3 domain at 0.5 mM of each protein.

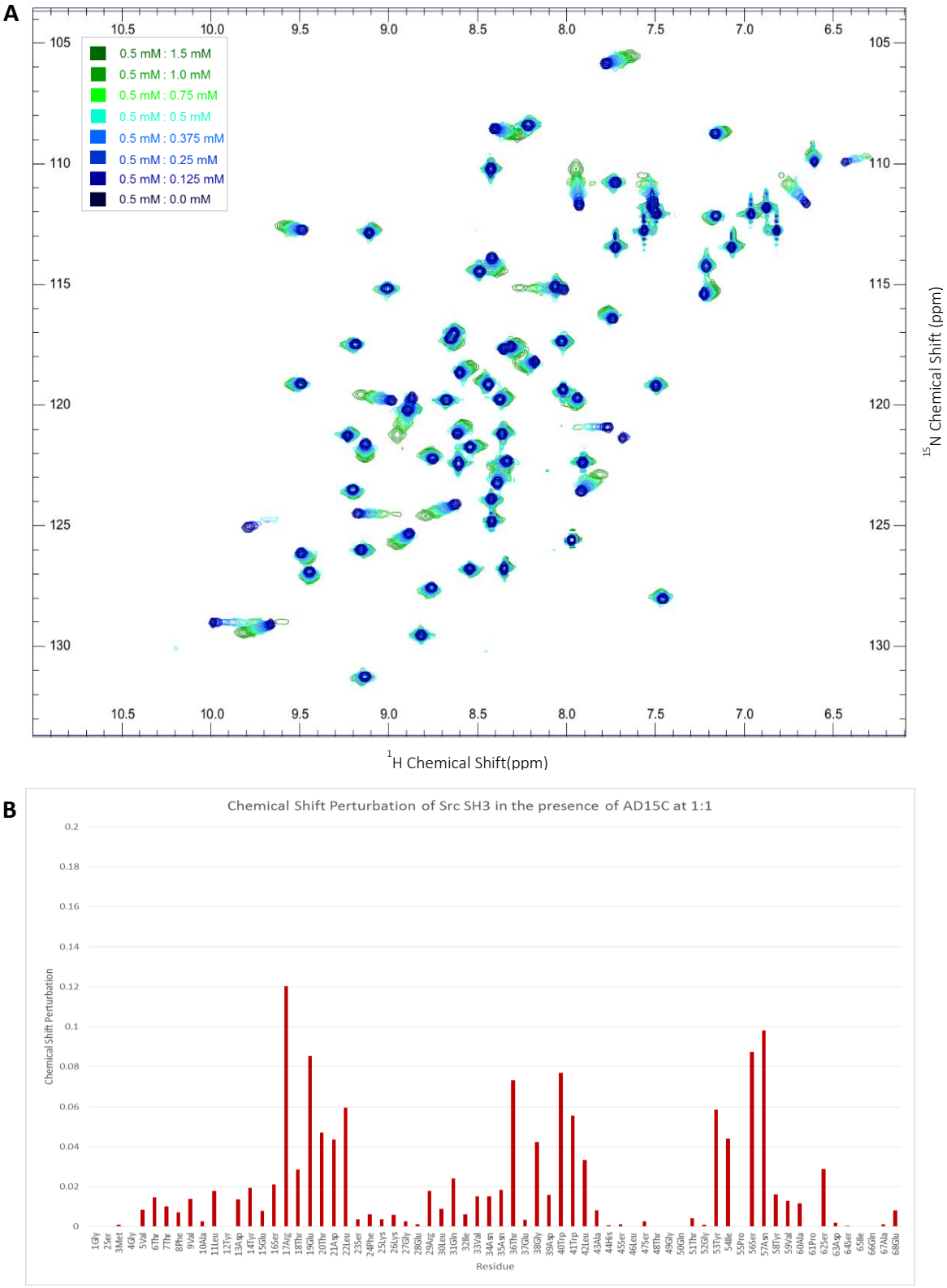

Figure 5.7 A) ^{1}H, ^{15}N HSQC spectra for the ^{15}N Src SH3 domain by itself (navy blue), in the presence of 0.5 mM ADAM15 C (cyan) and in the presence of 1.5 mM ADAM15 C (green) and the intermediates in intermediate shades as indicated in the key. Concentration of the Src SH3 domain was 0.5 mM in all spectra. B) Chemical shift perturbations caused by the presence of ADAM15 C on the spectrum of the Src SH3 domain at 0.5 mM of each protein.

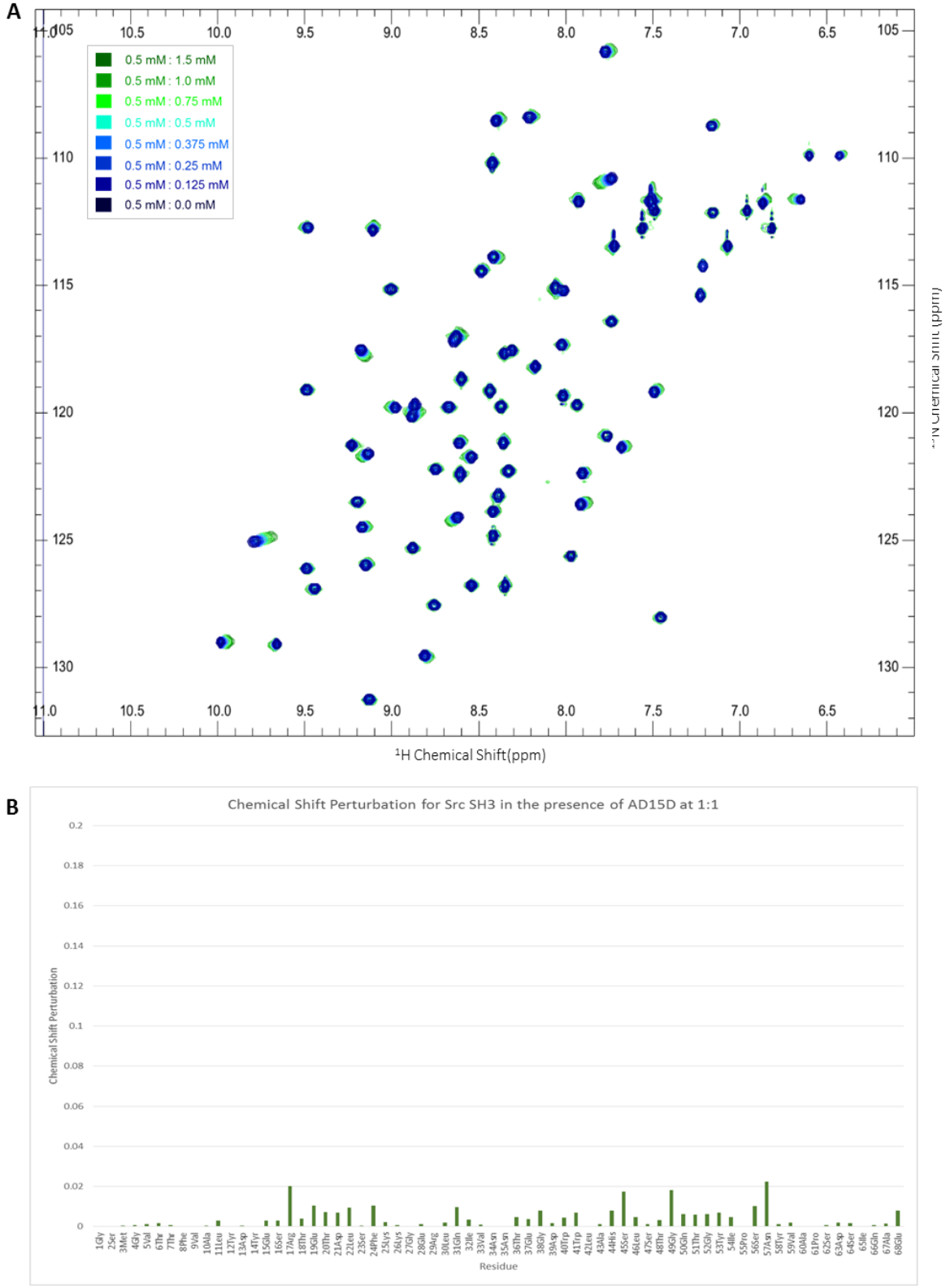

Figure 5.8 A) ^{1}H, ^{15}N HSQC spectra for the ^{15}N Src SH3 domain by itself (navy blue), in the presence of 0.5 mM ADAM15 D (cyan) and in the presence of 1.5 mM ADAM15 D (green) and the intermediates in intermediate shades as indicated in the key. Concentration of the Src SH3 domain was 0.5 mM in all spectra. B) Chemical shift perturbations caused by the presence of ADAM15 D on the spectrum of the Src SH3 domain at 0.5 mM of each protein.

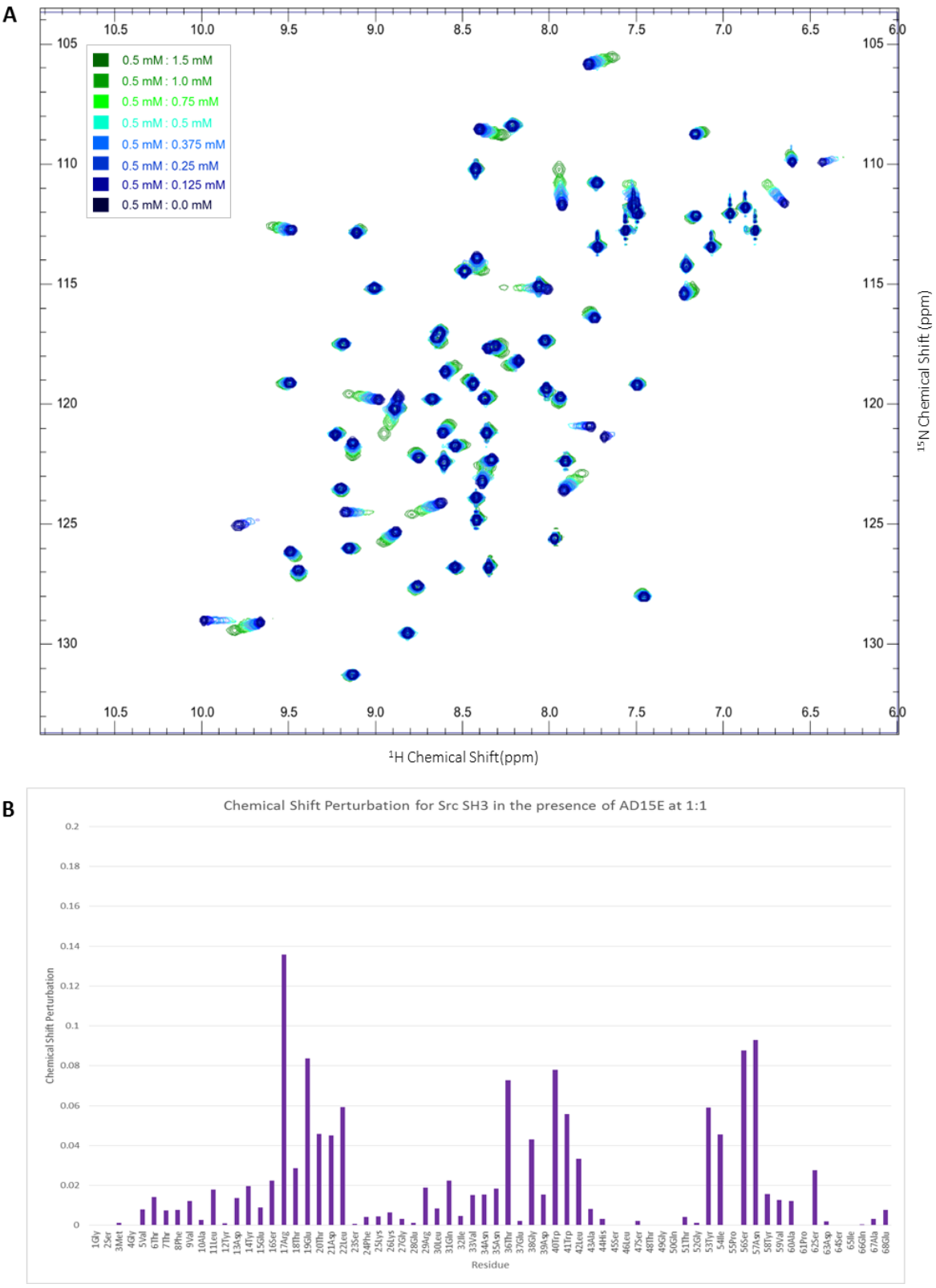

.

Figure 5.9 A) ^{1}H, ^{15}N HSQC spectra for the ^{15}N Src SH3 domain by itself (navy blue), in the presence of 0.5 mM ADAM15 E (cyan) and in the presence of 1.5 mM ADAM15 E (green) and the intermediates in intermediate shades as indicated in the key. Concentration of the Src SH3 domain was 0.5 mM in all spectra. B) Chemical shift perturbations caused by the presence of ADAM15 E on the spectrum of the Src SH3 domain at 0.5 mM of each protein.

5.5 Comparison of the Binding Interface of the Src SH3 domain with different ADAM15 ICDs

In order to compare directly the effects of the interaction of each ADAM15 ICD with the Src SH3 domain, the chemical shift perturbations caused by each ICD (with the CSPs for GB1 subtracted) were combined onto one graph, shown in figure 5.10. The average CSP for all the titrations was calculated and are shown, along with the average plus the standard deviation and the average plus half of the standard deviation. These limits were used to define the boundaries mapped onto the structure of the Src SH3 domains seen in figure 5.11, with those residues with CSPs that were greater than the average plus the standard deviation highlighted in the darkest colour, with progressively lighter colours for the other boundaries. Those values below average are not significantly affected by the interactions.

From this analysis, it is even clearer that ADAM15 D does not interact with the Src SH3 domain. Only two residues of the Src SH3 domain display movements large enough to be above average when in the presence of ADAM15 D and, when the CSPs caused by ADAM5 D are removed from the average calculation, the average value shifts up and no ADAM 15 D caused shifts reach this value. It is likely that there is no interaction between ADAM15 D and the Src SH3 domain due to ADAM15 D's lack of any proline-rich motifs.

The chemical shift perturbations caused by ADAM15 B, C and E are all fairly similar in their magnitude and follow an almost identical pattern in terms of which residues are involved in the interactions. This would imply that they all interact with the Src SH3 domain through a consistent motif across all three ADAM15 ICDs. When compared to those resides shown to be involved in other interactions of the Src SH3 domain, highlighted in figure 5.10 with green boxes (Sparks et al., 1994), there are strong correlations, especially at residues 17Arg, 21Asp, 40Trp and 56Ser – 58Tyr. Although residues 12Try – 15Glu from the RT loop have been shown to be involved in previous studies, they are not here with the possible exception of 14Tyr to a small extent. Residues 16Ser – 22Leu are involved and this string of amino acids also reside on the RT loop of the domain. This means that the interface displayed here is consistent with those seen in the literature and also involves the α-turn portion of the protein.

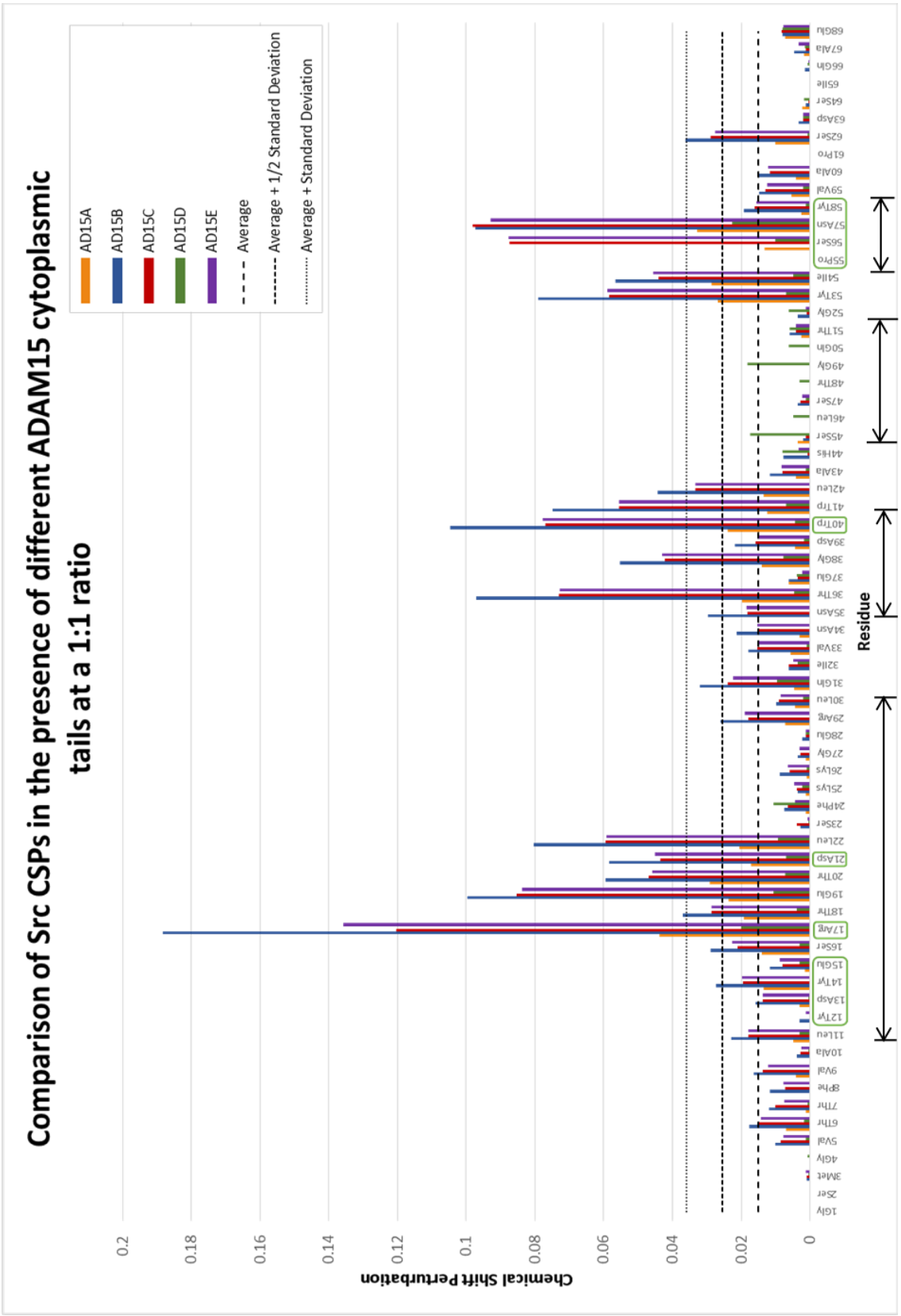

Figure 5.10 Chemical shift perturbations caused by each ADAM15 ICD, with those caused by ADAM15 A in orange, B in blue, C in red, D in green and E in purple, on the Src SH3 domain. The residues highlighted in green boxes have been shown to be involved in the interaction of the domain with other proline-rich motifs. Also highlighted are some structural features of the domain.

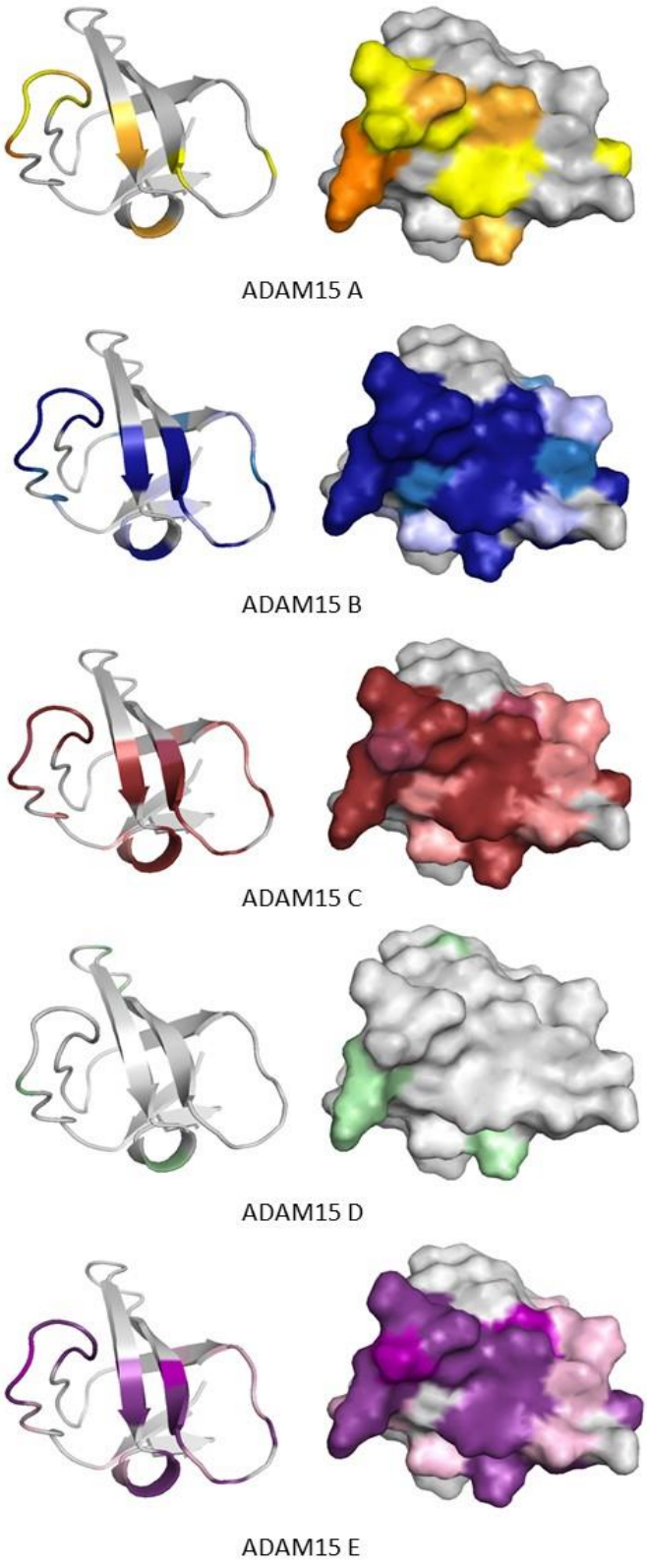

Figure 5.11 Chemical shift perturbations caused by each ADAM ICD, displayed on the 3D structure of the Src SH3 domain (PDB code 1SRL (Yu et al., 1993)). The darkest colour for each indicates those CSPs larger than the average plus the standard deviation. The middle colour indicates the residues with a CSP higher than the average plus half of the standard deviation and the lightest colour shows those residues with CSPs above average.

Unfortunately, as with the titrations of Grb2C, the interactions between the Src SH3 domain and the ADAM15 ICDs do not saturate even at the highest concentrations involved. As the ADAM15 ICDs precipitate at more than 1.5-2 mM, it was not possible to increase the final concentrations of the titration to saturate the binding and calculate the K_d accurately. However, as discussed in chapter 4, the larger chemical shift perturbations are an indicator of a tighter interaction as they represent interactions that are closer to the saturation chemical shift (Williamson, 2013). In this case, that would be those caused by ADAM15 B, by a significant margin. The CSPs caused by ADAM15 C and E are extremely similar in magnitude which would imply they have bind to the Src SH3 domain with a similar strength.

5.6 Introduction to Brk

Breast tumour kinase, Brk, (also known as Protein-Tyrosine Kinase 6, PTK6) is a non-receptor tyrosine kinase in a similar, but distinct, family to that of the Src family of tyrosine kinases. It contains an SH3 domain from residues 11-72, an SH2 domain from residues 78-170 and a protein kinase domain from residues 191-445 (Lee et al., 1998). The myristolation site required for the Src family kinases to be membrane-bound is not included in Brk thus allowing it to exist as a cytoplasmic protein. As discussed in chapter 1, Brk exists in two splice variants, with one variant excluding exon 2 creating a unique C-terminal region but both variants include the SH3 domain (Mitchell et al., 1997). Dephosphorylation of Tyr 447 is required for release of the SH2 domain and destabilisation of interactions between the SH3 domain and the linker domain, which maintains the "closed", inactive conformation of Brk, in order to active the "open" conformation of the enzyme (Qiu and Miller, 2002). This is an activation pathway that Brk shared with Src. The linker region of Brk contains a type II polyproline helix with the sequence HEPEPLPHW which sits within the hydrophobic pocket of the SH3 domain when Brk is in the "closed" conformation consisting of Phe19, Trp44, Pro63 and Tyr66 which follows the canonical interaction of SH3 domains with polyproline motifs (Ko et al., 2009). The SH3 domain has also been shown to interact with the $P_{424}XXP_{427}$ sequence within the C-terminal region of Akt and thus contributes to the regulation of the phosphorylation and activation of Akt (Zheng et al., 2010).

The structure of the Brk SH3 domain follows a similar structural arrangement as the other SH3 domains discussed in this thesis with the exception of the α-turn which is missing here and is shown in figure 5.12 (Ko et al., 2009).

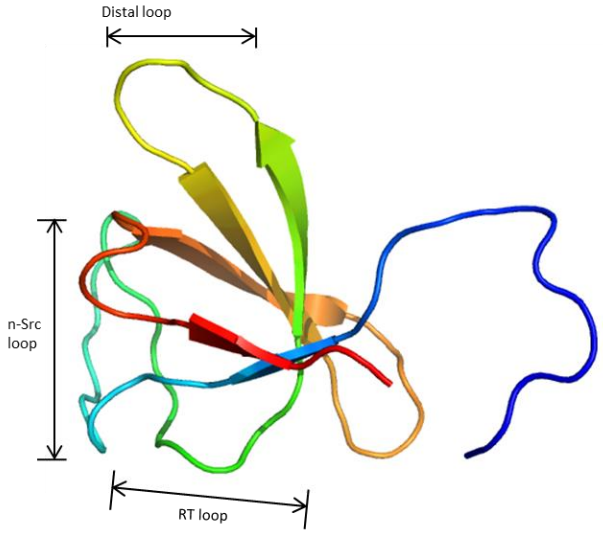

Figure 5.12 Structure of the SH3 domain of Brk (2KGT (Ko et al., 2009)) with the RT loop, n-Src loop and distal loop highlighted. This SH3 domain lacks the α-turn.

5.7 Optimisation of the purification of the Brk SH3 domain

As with the other SH3 domains studied in this thesis, the Brk SH3 domain had a GST fusion tag for purification purposes. As can be seen in figure 5.13, a small scale expression test of the Brk SH3 domain demonstrated that the protein could be expressed well in BL21 (DE3) cells for up to 3 hours at 37 °C but that the protein began to degrade in-cell when induced for longer than this and so initial investigations began with the comparison of the expression of the recombinant domain at either 37 °C for 3 hours of at 28 °C overnight in order to gain the maximum expression and minimum degradation. These can be seen in figure 5.14 A and B. Expression was significantly higher in the culture that had been induced at 28 °C overnight and so this culture technique was used in all further purifications.

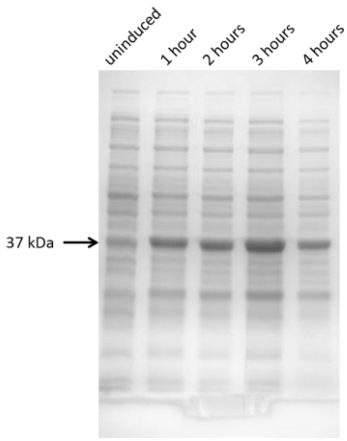

Figure 5.13 Test expression of the Brk SH3 domain in BL21 (DE3) cells with induction for the indicated times at 37 °C.

Unlike the other SH3 domains studied, the linker region between the GST fusion tag and the Brk SH3 domain was sensitive to digestion by the enzyme Factor Xa, rather than thrombin. Optimisation of the digestion was undertaken by the incubation of 1 mg of the recombinant fusion protein with either 1, 3, 5, 7.5 or 10 units of Factor Xa at 25 °C overnight. The results of this can be seen in figure 5.14 C and 7.5 units per mg protein was selected for future use in the purification process. The digested protein sample was then concentrated to approximately 2.5 ml and then loaded onto the gel filtration column in order to separate the now cleaved GST fusion tag from the Brk SH3 domain. Unfortunately, as can be seen in figure 5.14 D, separation was unsuccessful and a large portion of the Brk SH3 domain has been lost while the amount of GST fusion tag appears to have remained the same. It was suggested that this could be due to the recombinant SH3 domain sticking to the membrane of the spin concentrator used to reduce the sample volume after digestion to a more suitable volume for size exclusion chromatography. The membrane in the Vivaspin spin concentrators used previously is made from polyethersulfone (PES). While this is usually a suitable membrane material for use in spin concentrators, a small number of proteins will bind to this membrane and very little will be released by washing of the membrane when the concentrated sample is removed. In order to confirm if this is indeed an issue, another digested sample was concentrated for size exclusion using a spin concentrator with a cellulose rather than PES membrane. Once concentrated, a sample was studied by SDS PAGE gel

electrophoresis to confirm that the protein was still present and not bound to the membrane. This can be seen in figure 5.15, and due to the success seen here, the Amicon Ultra-15 spin concentrators were used whenever the volume of the Brk SH3 domain required reducing in future purifications. When this sample was separated by size exclusion chromatography, separation was significantly improved and no further Brk was lost during this stage of purification.

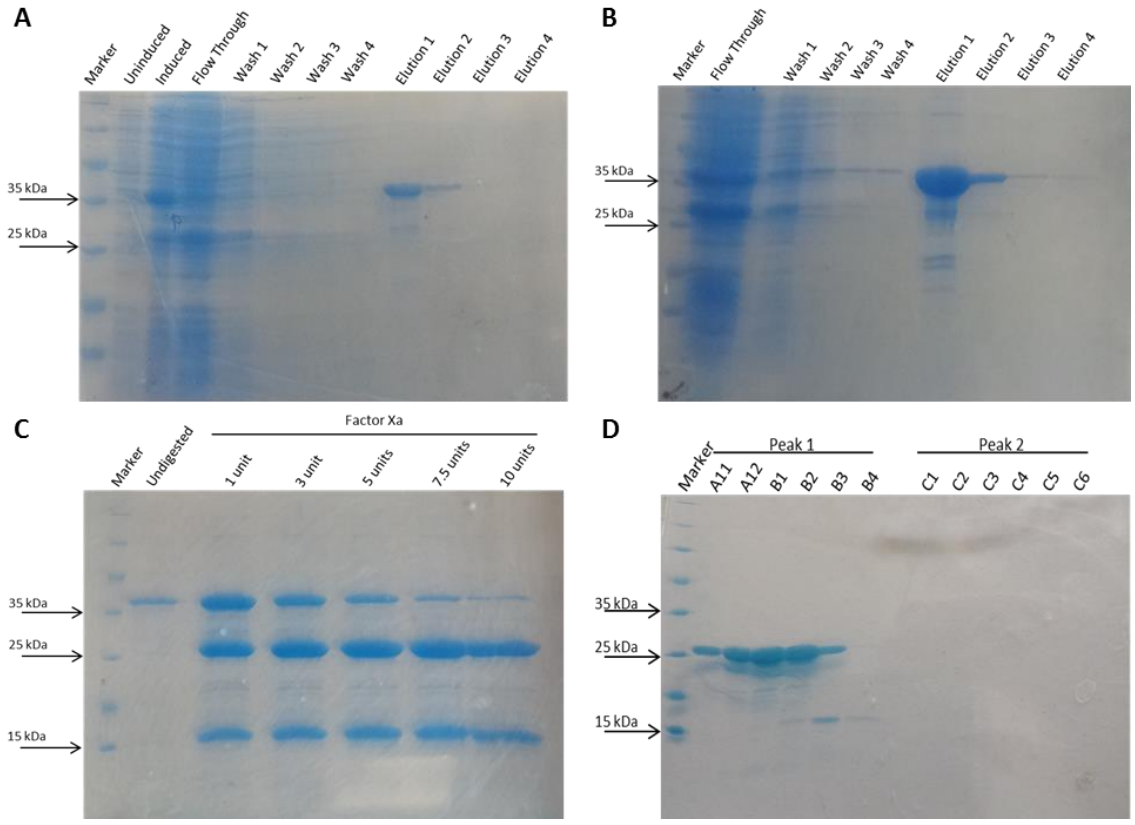

Figure 5.14 SDS PAGE gel electrophoresis of A) Glutathione sepharose purification of GST-fusion Brk SH3 domain expressed at 37 °C for 3 hours. B) Glutathione sepharose purification of GST-fusion Brk SH3 domain expressed at 28 °C overnight. C) Optimisation of the digestion of the GST fusion tag from the Brk SH3 domain by Factor Xa using varied amounts of the enzyme as indicated at 25 °C overnight. D) First failed separation of cleaved GST fusion tag from the Brk SH3 domain by size exclusion chromatography.

Unfortunately, when expression of the Brk SH3 domain was attempted with ^{13}C and ^{15}N labelling, the expression was significantly reduced compared to unlabelled expression. While some reduction in expression is expected due to the use of minimal media in order to limit the sources of these isotopes to only the labelled forms provided causing a harsher environment for the bacterial cells to grow in, reductions of this level were unexpected. Unfortunately, due to time restraints, it was not possible to confirm exactly

what was causing this poor expression in minimal media and so NMR experiments were conducted using a lower concentration of labelled SH3 domain than in previous studies.

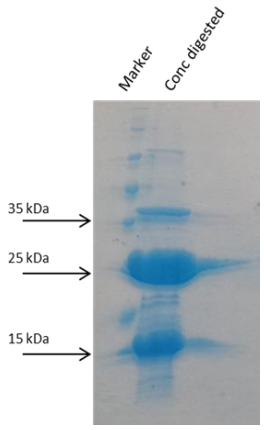

Figure 5.15 SDS PAGE gel electrophoresis of the concentrated digested sample of GST fusion tag and Brk SH3 domain concentrated using an Amicon Ultra-15 spin concentrator with a cellulose membrane.

5.8 Assignment of the Brk SH3 domain backbone

Recombinant Brk SH3 domain, labelled with ^{13}C and ^{15}N isotopes, was purified. HSQC, HNCACB and CBCACONH experiments spectra were acquired using the 500 MHz spectrometer. Along with the ^{1}H and ^{15}N assignments from Lee and Sunggeon (Ko et al., 2009), it was possible to assign 65% of the recombinant Brk SH3 domain. This included the sequence of the entire Brk SH3 domain but did not include the extensions included in the protein construct that arise from the linker region between the domain and the GST fusion tag at the N-terminus and the vector sequence at the C-terminus of the desired SH3 domain. These extra residues within the recombinant protein are predicted to be disordered, using PONDR Disorder Predictor (Li et al., 1999; Romero et al., 1997; Romero et al., 2001), and could account for the high number of overlapping peaks between 8.0 and 8.5ppm in the ^{1}H dimension. Due to the low concentration of the sample, many of these peaks did not have corresponding signals in the triple resonance HNCACB or CACBCONH resulting in those peaks were very difficult to reliably assign. The HSQC spectrum for the Brk SH3 domain is shown in figure 5.16.

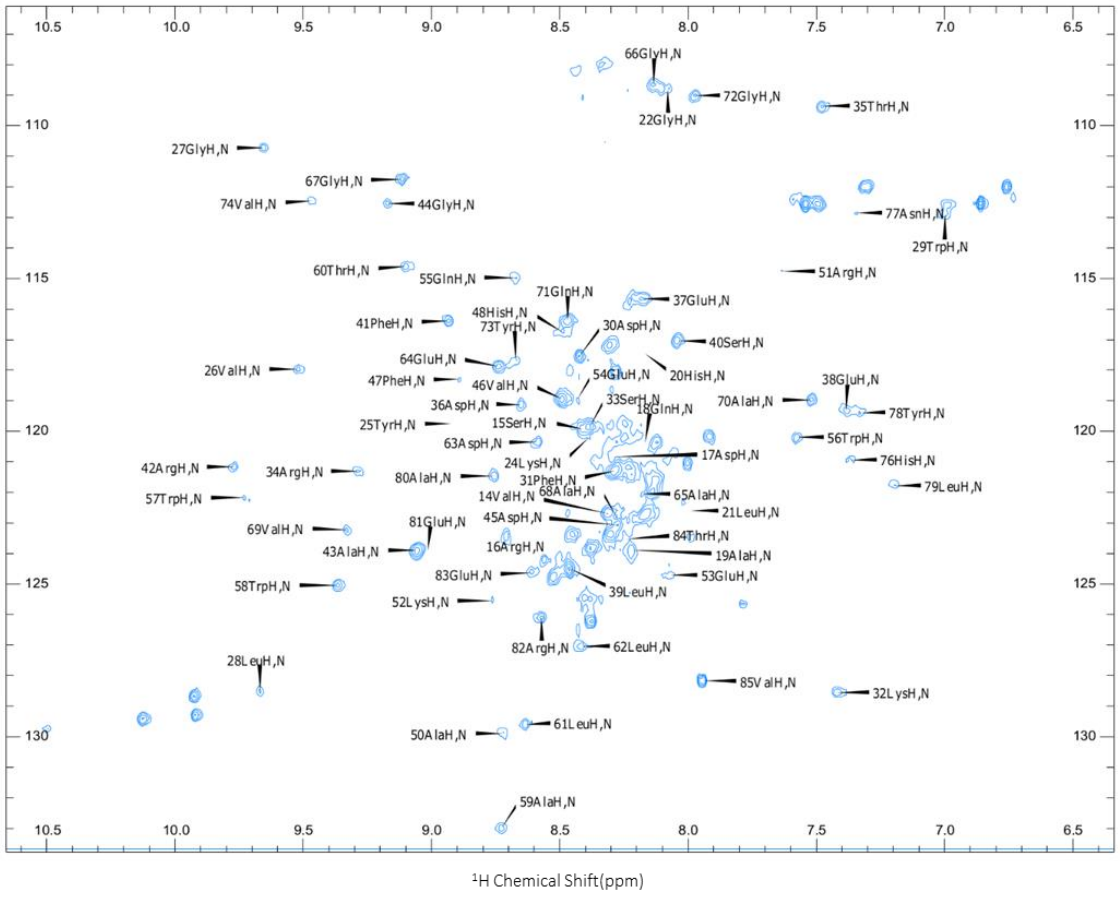

Figure 5.16 ^{1}H, ^{15}N HSQC of the Brk SH3 domain with peak assignments.

5.9 Titration of the Brk SH3 with the cytoplasmic domain of ADAM15 B

As with the previous titrations, two samples were made. Sample A contained 0.1 mM ^{15}N Brk SH3 domain in HEPES buffer. Sample B contained 0.1 mM Brk and 1 mM unlabelled ADAM15 B or the unlabelled GB1 tag. These represented the first and final points of the titration and intermediate data points were achieved by removal of a small volume from sample A and replacing this with an equal volume of sample B, thus maintaining the concentration of the ^{15}N Brk SH3 domain and slowly increasing the concentration of the unlabelled ligand protein in sample A. Due to time constraints, only ADAM15 B was titrated with the Brk SH3 domain as this was representative of all of the interactions exhibited with the Src SH3 domain and the Grb2 C-terminal SH3 domain. As with the previous titrations, the unlabelled GB1 tag was also titrated with the Brk SH3 domain in order to confirm that any chemical shift perturbations observed were due to the presence of ADAM15 B and not the GB1 tag.

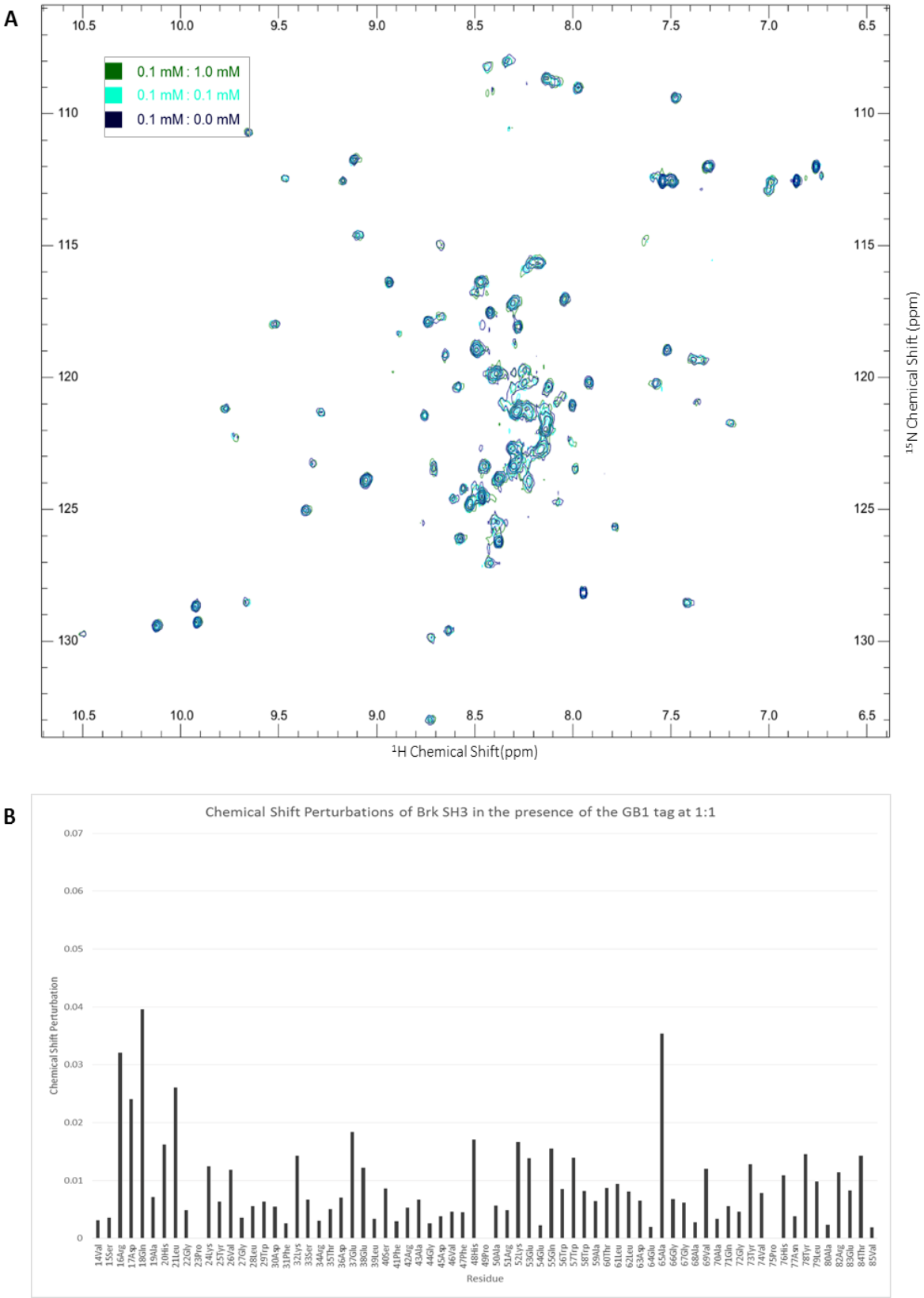

Figure 5.17 A) ^{1}H, ^{15}N HSQC spectra for the ^{15}N Brk SH3 domain by itself (navy blue), in the presence of 0.1 mM GB1 tag (cyan) and in the presence of 1.0 mM GB1 tag (green). Concentration of the Brk SH3 domain was 0.1 mM in all spectra. B) Chemical shift perturbations caused by the presence of the GB1 tag on the spectrum of the Brk SH3 domain at 0.1 mM of each protein.

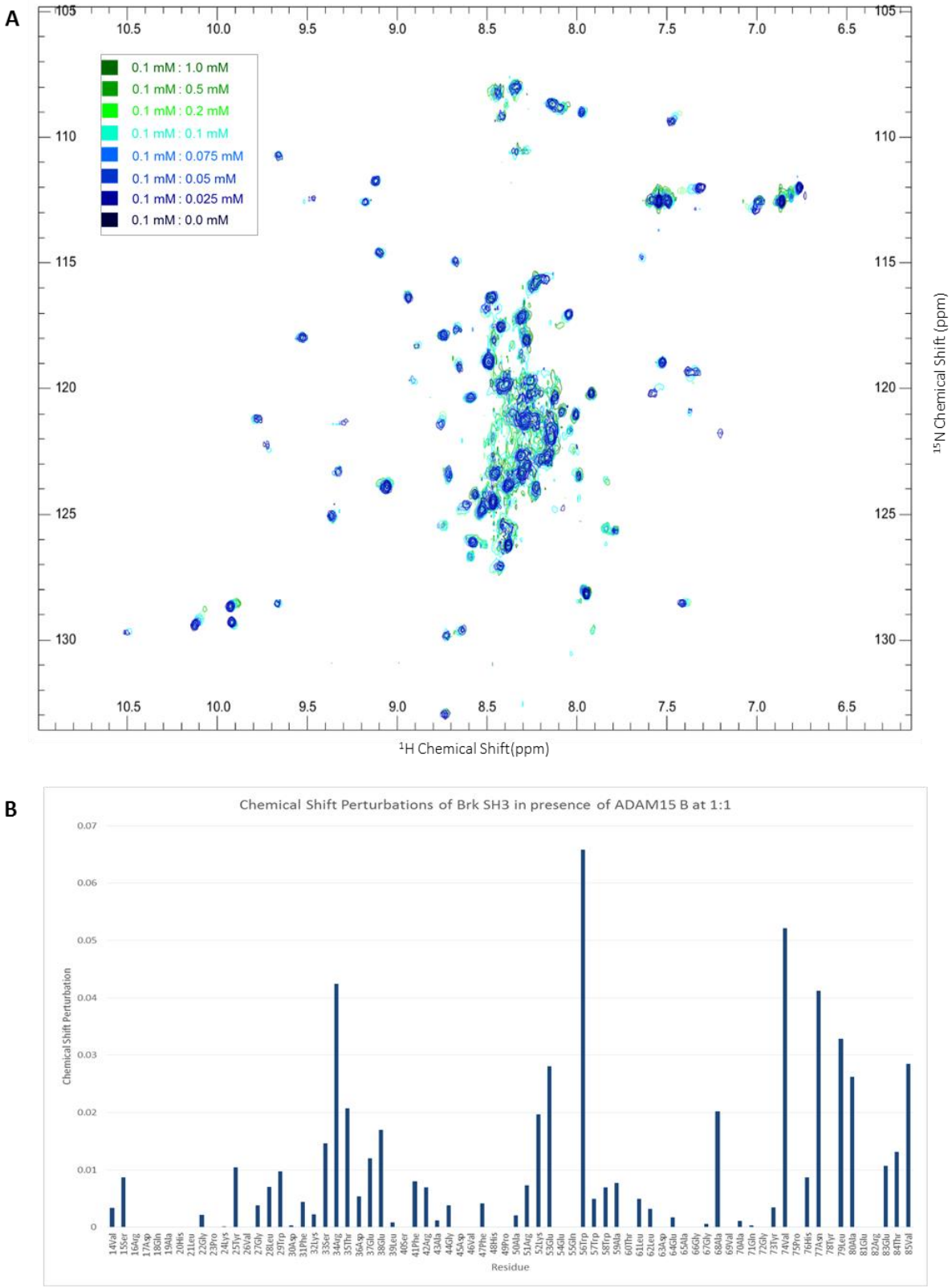

Figure 5.18 A) ^{1}H, ^{15}N HSQC spectra for the ^{15}N Brk SH3 domain by itself (navy blue), in the presence of 0.1 mM ADAM15 B (cyan) and in the presence of 1.0 mM ADAM15 B (green) and the intermediates in intermediate shades as indicated in the key. Concentration of the Brk SH3 domain was 0.1 mM in all spectra. B) Chemical shift perturbations caused by the presence of the ADAM15 B on the spectrum of the Brk SH3 domain at 0.1 mM of each protein.

The chemical shift perturbations were calculated using equation 2 described in section 5.4. As can be seen in figure 5.17 A, there are some chemical shift perturbations in the HSQC of the Brk SH3 domain implying that there is some level of interaction with between the GB1 tag and the SH3 domain. This looks to be a significant interaction in figure 5.17 A but this is due to the scale of the graph, which is the same as that required for the titration with ADAM15 B shown in figure 5.18 B. The CSPs caused by the GB1 tag here are similar in magnitude to those observed with the other SH3 domains in this thesis. However, a few residues are more heavily affected by the presence of the GB1 tag that has been previously seen including 16Arg, 17Asp, 18Gln, 21Leu and 65Ala. As with the previous titrations, the CSPs caused by the presence of the GB1 tag were subtracted from those seen in the titration of the Brk SH3 domain with ADAM15 B, the spectra of which can be seen in figure 5.18 A. Figure 5.18 B shows the quantification of the CSPs of the Brk SH3 domain caused by the presence of ADAM15 B. There is an interaction seen between the Brk SH3 domain and ADAM15 B although the CSPs are not large which implies that the interaction is fairly weak. Those residues most affected include 34Arg, 56Trp, 74Val, 77Asn and 79Leu. The average CSP was calculated along with the standard deviation of the CSPs. The residues which shifted by more than the average CSP was mapped in light blue onto the surface model of the Brk SH3 domain, with those residues that shifted by more than the sum of the average and the standard deviation in middle blue and the residues that shift the most, by more than the sum of the average and 2 standard deviation, in dark blue as can be seen in figure 5.19.

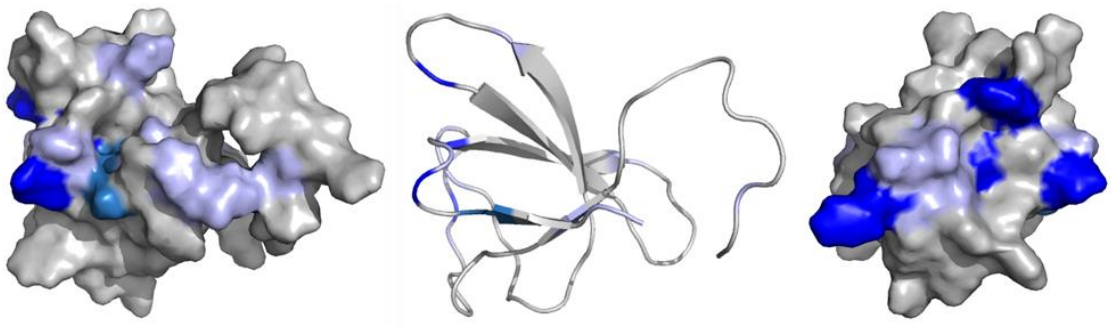

Figure 5.19 Chemical shift perturbations caused by the presence of ADAM15 B mapped onto the structure of the Brk SH3 domain (2KGT (Ko et al., 2009)) with those residues that shifted by more than the average + 2 standard deviation in dark blue, those that shifted by more than the average + standard deviation in middle blue and those that shifted by more than the average in light blue. The centre model is the cartoon model of the same. The right model has been rotated through 90° from the orientation of the left model.

5.10 Conclusions and Discussion

In this chapter, the interactions of the SH3 domains of the tyrosine kinases Src and Brk have been studied. In the case of the Src SH3 domain, ADAM15 D was shown to not interact with the Src SH3 domain at all, likely due to the lack of any polyproline motifs within the ICD of ADAM15 D. ADAM15 B, C and E all interact with Src with similar CSP intensity and with almost identical interaction interfaces. Several common residues are affected by the presence of these ADAM15 ICDs including 17Arg, 21Asp, 40Trp and 56Ser-58Tyr. ADAM15 A also demonstrated some interaction with the Src SH3 domain, involving similar residues as those affected by ADAM15 B, C and E but with significantly smaller chemical shift perturbations.

In order to explain which proline-rich motif from the ADAM15 ICDs is involved in binding to the Src SH3 domain, it is necessary to consider the domains common to ADAM15 B, C and E along with the proline-rich motifs previously shown to interact with the Src SH3 domain. Class I poly-proline motifs follow the pattern of **+ p Ψ P p Ψ P** where + stands for basic residues and Ψ stands for aliphatic residues and p can be a proline. Class II poly-proline motifs follow the pattern of **Ψ P p Ψ P p +**. The SH3 domain of Src has been shown to be capable of interacting with SH3-binding proteins containing poly-proline motifs of both classes (Teyra et al., 2012). For example, CDC42 will interact with the Src SH3 domain through a Class I motif whereas dynamin contains a Class II motif which interacts with the Src SH3 domain (Feng et al., 1994). Each ADAM15 ICD contains a combination of the 5 potential poly-proline regions, apart from ADAM15 D, as has been highlighted in figure 5.20, ADAM15 B contains poly-proline regions 1, 2, 4 and 5, ADAM15 C contains all five regions and ADAM15 E contains regions 1, 3, 4 and 5. As ADAM15 D is a frame-shift variant, it does not contain any proline-rich regions (Zhong et al., 2008).

When these regions are aligned, it is clear that poly-proline region 2 (P2) and poly-proline region 3 (P3) have fairly strong sequence homology across the whole region. However, the sequences in those two regions, underlined in figure 5.20 B, have strong homology with a Class I sequence, RPLPPLP, which has been shown to interact with the Src SH3 domain previously through the residues highlighted in green in figure 5.10 (Sparks et al., 1994). As ADAM15 B, C and E all contain one or both of these poly-proline

regions, it is highly likely that it this sequence that is most strongly involved in the interaction.

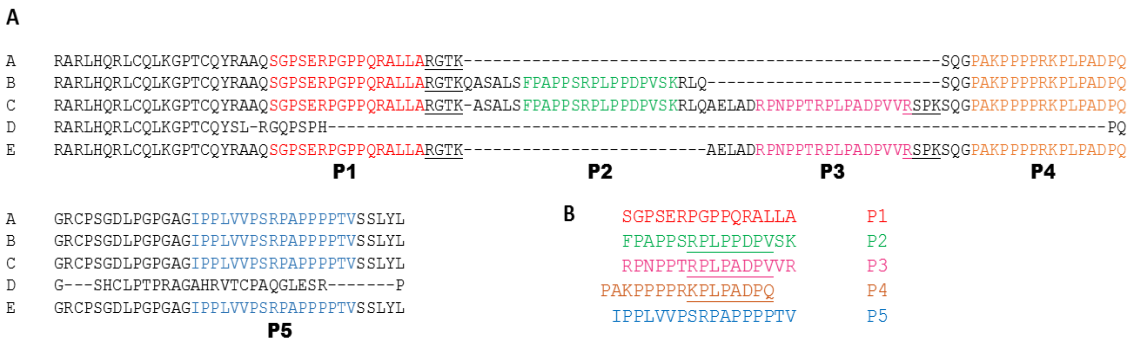

Figure 5.20 Amino acid alignment of the ADAM15 ICDs. A) Full ICDS with the poly-proline regions highlighted. B) The poly-proline regions only aligned in the same colour as in A.

This also goes some way to explain the low level of interaction shown between the Src SH3 domain and ADAM15 A. There is no direct interaction between Src and ADAM15 A in a biological setting (Zhong et al., 2008) but, in the spectrometer, the presence of ADAM15 A does cause some peaks of the Src SH3 domain to shift. Although these are larger than for ADAM15 D and several residues cross the average CSP limit and even the average plus half the standard deviation limit, it is likely that the shifts observed are due to a weak interaction which only occurs due to the high concentration of the proteins in the spectrometer compared to endogenous levels. However, the pattern of CSPs agrees with that of ADAM15 B, C and E which would not occur if it was a non-specific interaction. When the sequence for P4 is compared with that of the RPLPPLP consensus sequence, it is apparent that there is a similar motif, KPLPADPQ, present. It is likely that this is contributing to the interaction observed here but due to the comparatively small interaction seen compared to the other ADAM15 ICDs; however, it is unlikely to have a biological function and is only observed here due to the high concentrations involved. The low intensity of the CSPs observed supports a lack of biological relevance as this implies a weaker binding intensity which would reduce the likelihood of functionality within a cell.

In the case of the interaction observed with the Brk SH3 domain, the residues most involved were those of the 34Arg, 56Trp, 74Val, 77Asn and 79Leu. The magnitude of the chemical shift perturbations implied a fairly weak interaction. Those residues involved

here include several that form the hydrophobic core of the SH3 domain including 56Trp which is necessary for required for the auto-inhibition of full length Brk (Ko et al., 2009). Of the five most affected residues, three are common to those required for an interaction between the SH3 domain and the linker region in full length Brk which forms an important part of the auto-inhibition mechanism. Those residues are 34Arg, 56Trp and 77Asn which correspond to 22Arg, 44Trp and 65Asn in the full length enzyme. This suggests that the interaction between the Brk SH3 domain and ADAM15 B follows a very similar pattern to that of the Brk SH3 domain and Brk linker region. The residues from the linker region, corresponding to residues 175-179 correspond with a common polyproline motif PxPxP, here PEPLP, and it is this region that is required for the auto-inhibition interaction, particularly the proline residues. Also required for the auto-inhibition was 182Asp within the linker region (Ko et al., 2009).

It is still not possible to determine which polyproline region of the ADAM15 ICDs is responsible for the interactions with the Brk SH3 domain. The interaction with ADAM15 B implies a mechanism of interaction similar to that of the interaction between the SH3 domain and the Brk linker region but sequences that include PxPxP motifs with a satellite aspartic acid residue exist in the polyproline regions 2, 3 and 4 of the ADAM15 ICDs. Previous pull down assays have indicated that ADAM15 C does not interact with the Brk SH3 domain (Zhong et al., 2008). As ADAM15 A and B do, this would imply that polyproline region 3 (P3) is not necessary for any potential interaction, as this region is not included in either ADAM15 A or B but is present in C, or perhaps even hinders any interaction. However, as any potential interaction between ADAM15 E, the only other ADAM15 ICD to include P3, and the Brk SH3 domain have yet to be studied, it is impossible to conclude this with any certainty.

In summary this chapter has shown that:

- Purification of the Src SH3 domain was optimised and the Brk SH3 domain partially optimised.
- The [^{1}H-^{15}N]-HSQC of the ^{15}N Src SH3 domain was assigned as with 65% of the peaks on the [^{1}H-^{15}N]-HSQC of the ^{15}N Brk SH3 domain.
- ADAM15 B, C and E cause CSPs in the peaks for 17Arg, 21Asp, 40Trp and 56Ser-58Tyr of the ^{15}N Src SH3 domain.
- ADAM15 D did not interact with the ^{15}N Src SH3 domain.
- ADAM15 B, C and E likely interact with the ^{15}N Src SH3 domain through a RPLPXDPV present in polyproline regions 2 and 3.
- ADAM15 A interacted with the Src ^{15}N SH3 domain to a lesser extent, likely through a similar motif within P4.
- The ^{15}N Brk SH3 domain interacted with ADAM15 B via residues 34Arg, 56Trp, 74Val, 77Asn and 79Leu.
    - Similar interaction pattern to inhibitory interaction of Brk linker region with Brk SH3 domain when in closed conformation.

Chapter 6: General Discussion and Future Work

ADAM15 is a metalloproteinase which is expressed at high levels throughout breast cancer progression, particularly in the most aggressive forms (Kuefer et al., 2006). The expression of different splice variants, with splicing occurring in the intracellular domain as indicated in the schematic in figure 6.1, has been linked to poor prognosis in node-negative breast cancer in the case of ADAM15 A and B whereas ADAM15 C has been correlated with a positive prognosis in node-positive cancer (Zhong et al., 2008). The intracellular domain splice variants can interact preferentially with proteins containing SH3 domains (Kleino et al., 2009; Zhong et al., 2008) and, as many of these proteins have been independently linked to breast cancer, these interactions were investigated here.

The SH3 domains studied included the C-terminal and N-terminal SH3 domains of Grb2 and the SH3 domains of the protein tyrosine kinases Src and Brk. Grb2 interacts with all the ADAM15 variants other than D, whereas the Src SH3 domain interacts with ADAM15 B, C and E (Zhong et al., 2008). The Brk SH3 domain will interact with ADAM15 A and B but not C or D (Kärkkäinen et al., 2006). ADAM15 E has not been studied with regards to potential Brk interactions. Unfortunately, the problematic purifications of the ADAM15 ICDs meant that potential interactions were only studied from the perspective of the SH3 domains but, despite this, it was possible in the case of the C-terminal Grb2 SH3 domain and the Src SH3 domain to theorise the potential ADAM15 ICD motifs involved in the interactions to a greater degree of accuracy.

Firstly, despite lineage doubts with regards to MDA-MB-435 cells used in previous studies (Sellappan et al., 2004), it was confirmed that those interactions observed by pull down assay in those studies were consistent in MCF-7 breast cancer cells. Due to size restrictions for detection by NMR spectroscopy, the GST fusion tag that was linked to the ADAM15 ICDs in the constructs generated by Dr Zaruhi Poghosyan was not suitable and the insolubility of the ADAM15 ICDs alone required the substitution of the GST tag for a smaller fusion tag which could remain tagged to the ADAM15 ICDs during the NMR spectroscopy while maintaining solubility. The immunoglobulin binding 1 domain from group C and G Streptococcal bacteria (GB1) was chosen (Iwai et al., 2006) and the ADAM15 ICD genes were cloned into a vector introducing a His-GB1 tag. This

His-tag was used in an attempt to repeat the GST based pull downs from previous studies but this was unsuccessful due to non-specific interactions of the SH3 domain containing proteins with the Ni ions on the sepharose. Recombinant forms of each of the SH3 domains in question did pull down the recombinant forms of the ADAM15 ICDs which confirmed that *in vitro* studies such as NMR titrations would be possible.

Optimisation of the purification of the GB1-tagged ADAM15 ICDs proved to be problematic due to the in cell degradation or truncation of the proteins prior to purification but samples were of sufficient quality to use as the unlabelled ligand proteins in NMR titrations. The [^{1}H-^{15}N]-HSQC of ADAM15 B was much cleaner than expected and opened the opportunities for potential further study.

The interactions of the C-terminal SH3 domain of Grb2 with the ADAM15 ICDs indicated a consistent interaction interface across ADAM15 A, B, C and E with ADAM15 D demonstrating no interaction. Residues of Grb2C involved included 22Glu, 44Trp and 56Phe in all of the interactions and additionally including 13Gln in the interactions with ADAM15 A and E and 58Arg in the interactions with ADAM15 B and C. As Grb2C had been shown to interact with Gab1 via a non-canonical RxxK motif (McDonald et al., 2012b), an RGTK motif found in ADAM15 B was altered to AGTA by site-directed mutagenesis and the titration with Grb2C was repeated. However this analysis confirmed that this alternative motif is not required for interactions with the ADAM15 ICDs. This supports the conclusion that the interactions observed are due to a more typical poly-proline region within the ADAM15 ICD. Those regions common to ADAM15 A, B, C and E are polyproline regions 1, 4 and 5. As discussed in chapter 4, previous work using ADAM15 A demonstrated that the P1 region inhibited interactions between ADAM15 A and full length Grb2, whereas P4 was heavily required (Poghosyan, 2001). Loss of P5 did reduce the amount of interaction but was not necessary for interaction. Therefore it is likely that the interaction between the ADAM15 ICDs and Grb2C is mediated mainly by polyproline region 4. The precipitations observed during the titrations suggest the formation of aggregates at higher concentrations with other polyproline regions potentially involved.

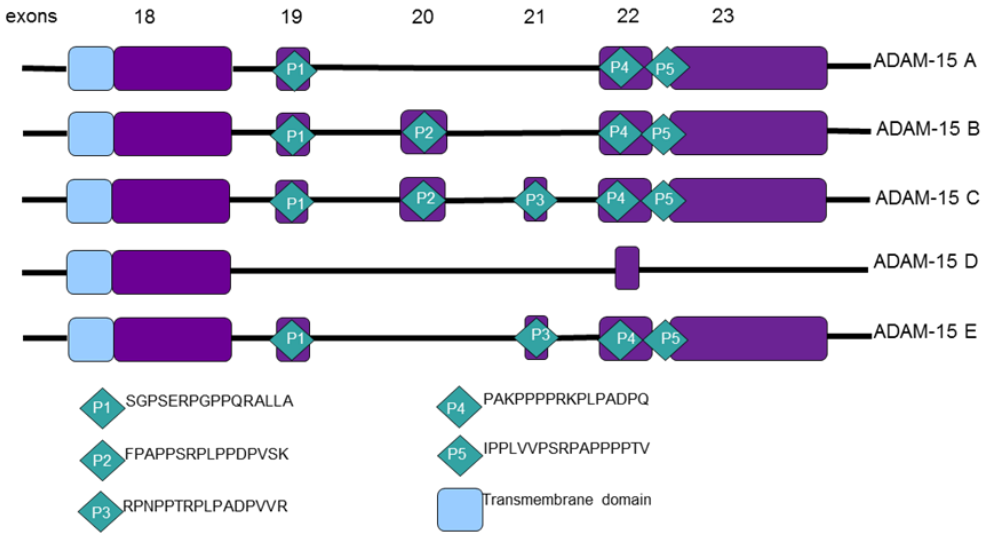

Figure 6.1 Schematic of the proline-rich regions of the ADAM15 ICD splice variants with the exons that encode for them indicated. Adapted from *Zhong et al* (2008, (Zhong et al., 2008)).

Issues with the folding of the N-terminal SH3 domain of Grb2 proved very difficult to solve and, unfortunately, meant that any titrations of this domain with the ADAM15 ICDs were unreliable and thus it was not possible to determine which SH3 domain is responsible for the interactions between the ADAM15 ICDs and the full length Grb2 signalling protein. Preliminarily titration studies (data not shown) suggest that Grb2N binds to ADAM15 A, B and E and does not bind to ADAM15 C or D. In studies of the Grb2 SH3 domains interactions with Sos1 (McDonald et al., 2009), Grb2N was capable of interacting with all four polyproline motifs in Sos1 but the Grb2C domain bound only to the first polyproline region. This region contained a PxΨPxRRR motif. The interaction is possible without the terminal two arginine residues but these form additional salt bridges between the SH3 domain and the polyproline region and further stabilise the interaction. These arginines are not necessary for interactions involving Grb2N (McDonald et al., 2009). None of the ADAM15 ICD polyproline regions include a PxΨPxRRR motif but the P4 region does include a PPPPRKP motif which is similar to other motifs with which Grb2C has been shown to interact, that of PxxxRxxKP. While the motif in P4 of the ADAM15 ICD does not fulfil this theoretical motif exactly, it does contain the residues required for interaction along with an arginine and lysine with the potential to form additional salt bridges to stabilise the interaction.

The biological function of the interaction of ADAM15 ICDs with Grb2 remain unclear but there are overlaps between their separate functions. For example, Grb2 inhibits FGFR2 dimers until their exposure to a growth factor such as FGF7 (Lin et al., 2012) and ADAM15 B can shed a splice variant of FGFR2, specifically FGFR2iiib in a Src dependent manner (Maretzky et al., 2009b). Given their overlapping function and clear roles in breast cancer, there is strong indication of a shared biological function. A schematic showing the interactions between each ADAM15 ICD observed here is shown in figure 6.2 along with some of the pathways Grb2 and Src are involved with.

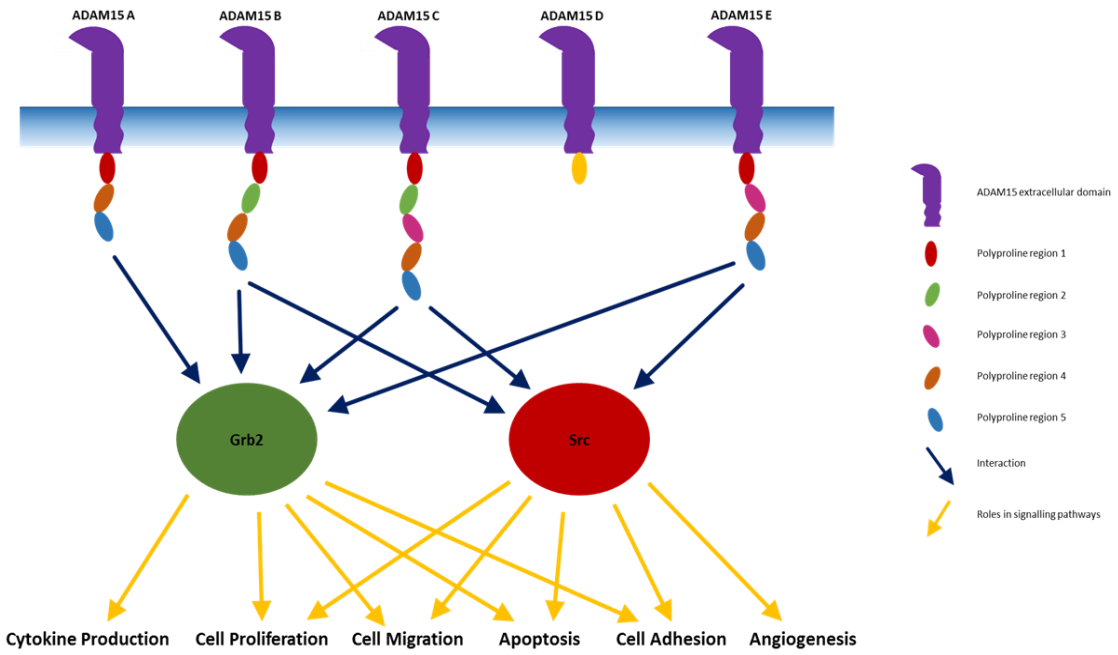

Figure 6.2 Schematic of the interactions observed in this thesis between the ADAM15 splice variants and the intracellular proteins Grb2 and Src which contain SH3 domains. Signalling pathways in which these intracellular proteins have a role in have also been indicated as potential downstream functions of the interactions observed.

In the case of the Src interactions with the ADAM15 ICDs, a consistent interface can be observed when the Src SH3 domains are exposed to ADAM15 B, C and E including the residues 17Arg, 21Asp, 40Trp and 56Ser- 58Tyr. These residues are consistent with previous interactions of the Src SH3 domain with small peptides that include a RPLPPLP motif (Sparks et al., 1994). Additionally, ADAM15 A, which exhibits no direct interaction with Src in a biological setting (Zhong et al., 2008), does interact with the Src SH3 domain

in the spectrometer but with much smaller chemical shift perturbations than those caused by the other ICDs. These weak perturbations are consistent with a low energy interaction that occurs due to the high concentrations of the domains in the spectrometer compared to endogenous levels. When this is considered along with the lack of interaction of ADAM15 D and that ADAM15 A does not interact directly in a biological setting, it is implied that the motif responsible for any interaction with the Src SH3 domain is common to ADAM15 B, C and E but exclusive of motifs available in ADAM15 A. Polyproline regions 2 and 3 are not common across all three ADAM15 B, C and E but there is a common motif across both regions, that of RPLPXDPV. Additionally, polyproline region 4 has a KPLPADPQ sequence which is similar enough to potentially be accounting for the interaction seen between ADAM15 A and the Src SH3 domain in the spectrometer but with no biological relevance.

The functions of ADAM15 have been linked to Src in more than one case. ADAM15 has a role in the regulation of endothelial permeability and neutrophil migration which requires the Src/ ERK1/2 signalling and is independent of the catalytic function of ADAM15 (Sun et al., 2010). Development of atherosclerotic lesions was increased by ADAM15 signalling through Src and Yes leading to the disruption of adherens junction integrity and promoting monocyte migration and required a functional cytoplasmic domain of ADAM15 (Sun et al., 2012). It is unclear which splice variant of ADAM15 is used here but it likely that it was ADAM15 A as this was the first variant of the protein discovered and most commonly used in the literature. ADAM15 also contributes to apoptosis resistance in rheumatoid arthritis synovial fibroblasts by activating the Src/FAK pathway upon exposure to FasL (Bohm et al., 2013). Again, it is likely that this study used ADAM15 A. The exclusive use of ADAM15 A in studies which suggest a function of the splice variants involving the overlapping roles of ADAM15 A with Src, despite a lack of direct interaction between ADAM15 A and Src biologically, means that clarity as to the function of the ADAM15 variants is reduced. Additionally, proximity ligation assays (personal communication, Dr Christian Roghi) have shown that Src and ADAM15 A do localise together. This could be due to the reported ability of FAK to act as an intermediate between these proteins (Fried et al., 2012) but this is unclear. It would be interesting to repeat these experiments while FAK is knocked down as this

would confirm the prediction that FAK is required for functional signalling between ADAM15 A and Src. Additionally, expansion of the study into apoptosis resistance in rheumatoid arthritis using the other ADAM15 variants has the potential to demonstrate whether this effect can be generated by all the variants. If only some of the variants can affect apoptosis, their intracellular binding profiles could lead to greater understanding as to the function of the different ADAM15 splice variants. However, while increased migration and apoptosis resistance are processes common to inflammatory conditions and breast cancer progression, there have been no direct links between ADAM15 and Src function in cancer discovered.

Alternatively to roles with complementary functions within the same pathway, it is possible that the interactions of the ADAM15 ICDs provide competition for interaction with the Src SH3 domain. The Src SH3 domain's primary functions are to bind to substrates and bring them within the vicinity of the kinase domain of Src and as part of the inhibitory folding of Src via interactions with the SH2-linker region (Elsberger et al., 2010). Given that the downstream functions of Src are similar to several of those downstream of ADAM15, such as cell adhesion (Klessner et al., 2009; Serrels et al., 2009), apoptosis resistance (Bohm et al., 2010; Johnson et al., 2000), angiogenesis (Cheranov et al., 2008; Raiter et al., 2010) and FGFR2iib shedding (Maretzky et al., 2009a), it would seem unlikely that any competition provided by the ADAM15 ICDs would be against substrates of the Src protein. However, the SH3 domain of Src is required for Csk to phosphorylate Tyr527, which then finds to the SH2 domain of Src, forming the inactive, "closed" conformation which is stabilised by interactions between the SH3 domain and the linker region (Superti-Furga et al., 1993). If the ADAM15 ICDs provided a form of competitive inhibition to Csk's role in activating Src, the increase in activated Src could explain the cross over in downstream functions between ADAM15 and Src. The variability of interaction potential across the different variants of ADAM15 with Src could also give some indication as to the functional purpose of the splice variants. If confirmed, this would make an interesting therapeutic target, particularly in cancer. Reducing Src activity is already a target for several drugs, such as Bosutinib (Puls et al., 2011) and Dasatinib (Araujo and Logothetis, 2010). Current trial therapies target the kinase domain of Src Family Kinases but, due to strong sequence conservation in this

domain, specificity for one member of the family is difficult. If further studies into the functional relevance of the interactions between the ADAM15 ICDs and the Src SH3 domain prove a link between ADAM15 and constitutive activation of Src via competitive inhibition of Csk, this could provide a new, more specific, therapeutic target.

Brk proved difficult to purify in the quantities desired for NMR spectroscopy, and time restraints meant that only the interaction with ADAM15 B was studied. Residues 34Arg, 56Trp, 74Val, 77Asn and 79Leu were all involved in the interaction and these residues occupy the hydrophobic pocket of the Brk SH3 domain. Three of these residues, 34Arg, 56Trp and 77Asn, correspond to those residues within the full length Brk that are responsible for the inhibitory interaction between the Brk SH3 domain and Brk linker region (Derry et al., 2000). Similar motifs to the Brk linker region exist in polyproline regions 2, 3 and 4 of the ADAM15 ICDs so this titration, and the comparison with the Brk SH3 domain-linker region interaction, is not currently enough to establish exactly which polyproline region from the ADAM15 ICD is responsible for any interaction with the Brk SH3 domain. As ADAM15 C does not interact with the Brk SH3 domain. However ADAM15 A and B do (Zhong et al., 2008), it is implied that P3 is not required but it is not possible to confirm this until studies with ADAM15 E, which also includes P3 are conducted. Given that Brk is overexpressed in 86% of invasive ductal breast carcinomas (Ostrander et al., 2007) and that high ADAM15 A and B expression have been linked to a poorer prognosis in patients with initially non-metastatic breast tumours whereas ADAM15 C has no such correlation in the similar patients (Zhong et al., 2008), it could be suggested that there is a potential cooperation between Brk and the ADAM15 A and B proteins that could be linked to the progression of breast cancer to invasive stages. However, without further study, particularly including ADAM15 C and E, this remains a hypothesis.

When the SH3 domains studied here are compared, the low level of sequence identity within the SH3 domain family is apparent, as can be seen in figure 6.3. There are only 12 residues conserved between all three of the domains successfully studied here although there are several other residues which are conserved across two of the domains or where the sequences include different amino acids of the same type in equivalent locations. Highlighted in red in the figure 6.3 are those residues most involved in the

interaction of that SH3 domain with ADAM15 B. Only the conserved tryptophan residue is consistently involved in all three interactions whereas the interactions with the Brk SH3 domain and Src SH3 domain also involve a conserved arginine and a conserved asparagine. These residues are all part of the hydrophobic pocket of the SH3 domain and suggest a similar interaction mechanism. Indeed, the proposed sequences for the motifs involved in these interactions, RPLPXLPV in the case of the Src SH3 domain and PEPLP in the case of the Brk SH3 domain, are more similar than that proposed for the interaction with Grb2C, that of PXXXRXXKP.

```
Brk             MVSRDQAHLGPKYV-GLWDFKSRTDEELSFRAGDVFHVARKEEQWWWATL
Grb2C           MVPQ-----QPTYVQALFDFDPQEDGELGFRRGDFIHVMDNSDPNWWKGA
Src             MGV-------TTFV-ALYDYESRTETDLSFKKGERLQIVNNTEGDWWLAH
                *          ..:* .*:*:..: : :*.*: *: :::  : :  **

Brk             LDEAGGAVAQGYVPHNYLAERETVESEPAGHAGCAALQDRVDSSGRIVTD
Grb2C           -----CHGQTGMFPRNYVTPVNR-----------------------NV
Src             S---LSTGQTGYIPSNYVAPSDSIQ----------------------AE
                          * .* **::
```

Figure 6.3 Sequence alignment of the SH3 domains of Brk, Grb2C and Src. Highlighted in red are the residues most affected by the interaction with ADAM15 B.

Unfortunately, due to the precipitation of the ADAM15 ICDs at concentrations higher than 1.5 mM, it was not possible to saturate the interactions studied here, which are calculated as a function of the ligand concentration. This means that it was not possible to accurately calculate the dissociation constants, K_d, for any of the residues involved in the interactions. The error values for the calculated K_ds were almost as large as the K_d values themselves. However, the Kd value measured at the conserved tryptophan of Grb2C and the Brk SH3 domain was in the 10^{-5} M range and in the 10^{-6} M range for this residue in the Src SH3 domain. The arginine residues involved in the interactions of the SH3 domains of Brk and Src both have a dissociation constant in the 10^{-5} M range. Finally, the conserved asparagines involved in the interactions with the Brk and Src SH3 domains give dissociation constants in the 10^{-5} and 10^{-4} M range respectively. This is consistent with results obtained by of Briony Keir, an undergraduate project student in our laboratory, who studied the interaction of ^{15}N ADAM15 B with the unlabelled Src SH3 domain (Keir and Blumenschein, Unpublished data, 2015). Although the backbone

assignments for the ADAM15 B protein were not obtained, it was possible to distinguish which peaks corresponded to the GB1 tag and rule these out from any interaction. When the dissociation constants of the residues of ADAM15 B were calculated, although again the interaction was not fully saturated, these were in the 10^{-4} M range. These K_d values indicate that the interactions studied here are fairly weak. Other documented SH3 domain interactions with polyproline regions are in the 10^{-6} M region (Li et al., 2014; Stangler et al., 2007) but these reactions were saturated unlike those here rendering the dissociation constants seen in this study are not entirely reliable. As the dissociation constant is defined as the ligand concentration at which the protein is half saturated, it is not possible to calculate this accurately if the ligand concentration at full saturation is unknown. However, it has been shown previously that low energy interactions can still be biologically relevant if the local concentration environment within the cell is high enough (Mayer, 2001).

The lack of any interaction of ADAM15 D with any intracellular protein in any published literature and this thesis does present an interesting conundrum. As discussed in chapter 1.3.3, ADAM15 D accounts for 11% of the total ADAM15 expressed across a number of healthy tissues, second only to ADAM15 A which accounts for 58.6% of expression across those tissues (Kleino et al., 2009). No function has been found for this splice variant thus far despite its strong expression. There are no motifs within this intracellular domain that correlate with other motifs known to interact with other intracellular proteins which leaves little for speculation unless it is to provide a functioning ADAM15 metalloproteinase which is unaffected by intracellular signalling. Once the primary substrate of the ADAM15 metalloproteinase has been identified, it would be fascinating to see whether the expression pattern of ADAM15 D correlates with this substrate.

Other members of the ADAM family have been shown to interact with SH3 domain-containing proteins including ADAM -7, -10, -12, -19, -22, -29 and -33 (Edwards et al., 2008). The cytoplasmic domain of ADAM10 is required for correct localisation in polarised epithelial cells. This requires the proline-rich regions of the domain which implies that this regulation could involve an interaction with an SH3 domain-containing protein. If incorrectly localised, ADAM10 is rendered incapable of cleaving E-cadherin and thus does not play a role in cell migration (Wild-Bode et al., 2006). An SH3 domain-

containing protein has been proposed as having a potential role in this. Synapse-associated protein 97, SAP97, is responsible for the localisation of ADAM10 in synaptic membranes and additionally promotes α-secretase activity. The intracellular domain of ADAM10 is also involved in the regulation of the constitutive activity of the enzyme, although this does not require the polyproline region which interact with SH3 domains but an endoplasmic reticulum retention motif (Marcello et al., 2007). However, the ICD does not affect the stimulated activity of ADAM10. Although the pathway of ADAM15 localisation has yet to be fully elucidated, the SH3 domain-containing proteins endophilin 1 and SH3PX1, which both have roles in endocytosis and subcellular localisation, only bind to the ICD of the pro-form of ADAM15 (Howard et al., 1999). ADAM10 and ADAM15 have both been shown to target E-cadherin for cleavage, although the evidence is less clear in the case of ADAM15, and both show some interaction preference based upon subcellular localisation. It could be suggested that some interactions of the ADAM15 ICDs with SH3 domain-containing proteins have a regulatory effect on the ADAM in a similar manner to that of ADAM10.

The SH3 domain-containing protein PACSIN3 (protein kinase C and casein kinase substrate in neurons protein 3) has been shown to interact via its SH3 domain to the intracellular domains of ADAMs -9, -10, -12, -15 and -19 and has roles in endocytosis via interactions with dynamin and interacts with N-WASP thus conferring a role in regulation of the actin cytoskeleton (Mori, 2003). PACSIN3 is functionally important for ADAM12 shedding of heparin-binding EGF-like growth factor (HB-EGF) in response to PMA or the GPCR agonist angiotensin II. The function of PACSIN3 with regards to the acitivity of the other ADAMs that it is capable of interaction with has not been expanded upon currently but it has the potential to play a role in ADAM15 activity regulation in a similar fashion to its role in the activity of ADAM12.

The intracellular domain functions of ADAM12, which has 10 potential SH3 domain binding motifs (Seals, 2003), have been studied more extensively than that of the ADAM15 ICD. Trafficking of ADAM12 to the cell membrane in response to PMA stimulation is regulated by its ICD and is also dependent on PKCε (Sundberg et al., 2004). Additionally, the ICD of ADAM12 can act as a retention agent, keeping the ADAM12 protein within the cell and preventing cell surface accumulation via interactions with

PI3K and Src, which is activated upon interactions with the ADAM12 ICD (Maretzky et al., 2015). The ADAM12 ICD interaction with Src has been confirmed to be via the SH3 domain of Src and requires the same conserved tryptophan that is required for interactions with the ADAM15 ICDs as shown in this thesis. The polyproline region 2 of the ADAM12 ICD includes the sequence PSVPARPLPAKP which is not dissimilar to the RPLPXDPV sequence seen in the P2 and P3 regions of the ADAM15 ICD (Stautz et al., 2010). The interaction of Src with ADAM12 is required for the correct subcellular localisation of the ADAM, with this interaction promoting cell surface localisation and has been shown to enhance Src activity at focal adhesions. ADAM15 B, C and E also interact with the Src SH3 domain and has a role in the regulation of cell adhesion, thus presenting a potential mechanism by which ADAM15 can influence cell adhesion in a similar manner to ADAM12.

A further link between the ADAM15 ICDs and cell adhesion has been shown through studies into the phenotype of MCF-7 cells overexpressing each of the full length ADAM15 variants. When ADAM15 E is overexpressed, the amount of the tight junction protein, claudin 1, was also highly increased (personal communication, Dr Christian Roghi). Tight junctions, also known as occluding junctions, are a method by which cells interact with each other and form a virtually impermeable fluid barrier. Claudin 1 also has a role in breast cancer and promotes apoptosis in MCF-7 cells (Liu et al., 2012).

Grb2 also interacts with ADAM12 and is involved in the internalisation of the ADAM via the clathrin-dependent pathway (Stautz et al., 2012a). The function of the interaction between Grb2 and the ADAM15 ICDs is unknown but a similar pathway to endocytosis as followed by ADAM12 is also possible here.

ADAM12, like ADAM15, has also been shown to the linked to breast cancer progression but is not a driver-mutation (Stautz et al., 2012b), that is, it does not cause the progression of breast cancer but arises because of the breast cancer. ADAM12 is more useful as a marker for breast cancer progression and ADAM15 could fill a similar function once ADAM15's role in breast cancer is elucidated.

This thesis has shown how the ADAM15 ICDs interact with three different SH3 domains from the perspective of the SH3 domain. Further study into the interaction from the

perspective of the ADAM15 ICDs would be very useful to extend understanding of these interfaces. An extension of this would include studies of the dissociation constants using surface plasmon resonance and mutation studies to remove the interactions and evaluate the downstream effects of these interaction knock outs in breast cancer cells such as MCF-7 and MDA-MB-231 cells. Isothermal calorimetry would be useful in the case of the interactions with the Src SH3 domain and Brk SH3 domain as these interactions do not cause protein precipitation as the interactions with Grb2C did. Further studies of the subcellular localisation of the ADAM15 variants in response to SH3 domain-containing proteins could expand the potential regulatory role of these interactions on ADAM15 function. This study represents a stepping stone into a deeper understanding of the role of the ADAM15 ICDs in the progression of breast cancer.

Bibliography

2001. Familial breast cancer: collaborative reanalysis of individual data from 52 epidemiological studies including 58 209 women with breast cancer and 101 986 women without the disease. The Lancet 358, 1389-1399.

2011a. Breast Cancer. Cancer Research UK, London.

2011b. Breast Cancer Risk Factors. Cancer Research UK, London.

2011c. Skin Cancer - UK mortaility statistics. Cancer Research UK, London.

2011d. TNM Breast Cancer Staging. Cancer Research UK, London.

Acharya, M., Borland, G., Edkins, A.L., Maclellan, L.M., Matheson, J., Ozanne, B.W., Cushley, W., 2010. CD23/FcepsilonRII: molecular multi-tasking. Clin Exp Immunol 162, 12-23.

Ahmed, S., Maratha, A., Butt, A.Q., Shevlin, E., Miggin, S.M., 2013. TRIF-mediated TLR3 and TLR4 signaling is negatively regulated by ADAM15. Journal of immunology (Baltimore, Md. : 1950) 190, 2217-2228.

Al-Fakhri, N., Wilhelm, J., Hahn, M., Heidt, M., Hehrlein, F.W., Endisch, A.M., Hupp, T., Cherian, S.M., Bobryshev, Y.V., Lord, R.S., Katz, N., 2003. Increased expression of disintegrin-metalloproteinases ADAM-15 and ADAM-9 following upregulation of integrins alpha5beta1 and alphavbeta3 in atherosclerosis. J Cell Biochem 89, 808-823.

Alonso, A., Sasin, J., Bottini, N., Friedberg, I., Friedberg, I., Osterman, A., Godzik, A., Hunter, T., Dixon, J., Mustelin, T., 2004. Protein Tyrosine Phosphatases in the Human Genome. Cell 117, 699-711.

Araujo, J., Logothetis, C., 2010. Dasatinib: A potent SRC inhibitor in clinical development for the treatment of solid tumors. Cancer Treatment Reviews 36, 492-500.

Arribas, J., Esselens, C., 2009. ADAM17 as a therapeutic target in multiple diseases. Curr Pharm Des 15, 2319-2335.

Atabey, N., Gao, Y., Yao, Z.J., Breckenridge, D., Soon, L., Soriano, J.V., Burke, T.R., Jr., Bottaro, D.P., 2001. Potent blockade of hepatocyte growth factor-stimulated cell motility, matrix invasion and branching morphogenesis by antagonists of Grb2 Src homology 2 domain interactions. J Biol Chem 276, 14308-14314.

Aubele, M., Vidojkovic, S., Braselmann, H., Ritterswurden, D., Auer, G., Atkinson, M.J., Tapio, S., Hofler, H., Rauser, S., Bartlett, J.M., 2009. Overexpression of PTK6 (breast tumor kinase) protein--a prognostic factor for long-term breast cancer survival--is not

due to gene amplification. Virchows Archiv : an international journal of pathology 455, 117-123.

Baksi, S., Basu, S., Mukhopadhyay, D., 2014. Mutant huntingtin replaces Gab1 and interacts with C-terminal SH3 domain of growth factor receptor binding protein 2 (Grb2). Neuroscience research 87, 77-83.

Becker, E.D., 1999. High Resolution NMR: Theory and Chemical Applications, 3 ed. Academic Press, p. 79.

Belov, A.A., Mohammadi, M., 2012. Grb2, a double-edged sword of receptor tyrosine kinase signaling. Science signaling 5, pe49.

Bergers, G., Brekken, R., McMahon, G., Vu, T.H., Itoh, T., Tamaki, K., Tanzawa, K., Thorpe, P., Itohara, S., Werb, Z., Hanahan, D., 2000. Matrix metalloproteinase-9 triggers the angiogenic switch during carcinogenesis. Nat Cell Biol 2, 737-744.

Berry, D.M., Nash, P., Liu, S.K., Pawson, T., McGlade, C.J., 2002. A high-affinity Arg-X-X-Lys SH3 binding motif confers specificity for the interaction between Gads and SLP-76 in T cell signaling. Current biology : CB 12, 1336-1341.

Biscardi, J.S., Belsches, A.P., Parsons, S.J., 1998. Characterization of human epidermal growth factor receptor and c-Src interactions in human breast tumor cells. Molecular carcinogenesis 21, 261-272.

Bode, W., Gomis-Rüth, F.-X., Stöckler, W., 1993. Astacins, serralysins, snake venom and matrix metalloproteinases exhibit identical zinc-binding environments (HEXXHXXGXXH and Met-turn) and topologies and should be grouped into a common family, the ‘metzincins’. FEBS Letters 331, 134-140.

Bohm, B., Hess, S., Krause, K., Schirner, A., Ewald, W., Aigner, T., Burkhardt, H., 2010. ADAM15 exerts an antiapoptotic effect on osteoarthritic chondrocytes via up-regulation of the X-linked inhibitor of apoptosis. Arthritis Rheum 62, 1372-1382.

Bohm, B.B., Aigner, T., Blobel, C.P., Kalden, J.R., Burkhardt, H., 2001. Highly enhanced expression of the disintegrin metalloproteinase MDC15 (metargidin) in rheumatoid synovial tissue. Arthritis Rheum 44, 2046-2054.

Bohm, B.B., Aigner, T., Roy, B., Brodie, T.A., Blobel, C.P., Burkhardt, H., 2005. Homeostatic effects of the metalloproteinase disintegrin ADAM15 in degenerative cartilage remodeling. Arthritis & Rheumatism 52, 1100-1109.

Bohm, B.B., Freund, I., Krause, K., Kinne, R.W., Burkhardt, H., 2013. ADAM15 adds to apoptosis resistance of synovial fibroblasts by modulating focal adhesion kinase signaling. Arthritis Rheum 65, 2826-2834.

Bombonati, A., Sgroi, D.C., 2011. The molecular pathology of breast cancer progression. The Journal of Pathology 223, 308-318.

Bonnefoy, J.Y., Plater-Zyberk, C., Lecoanet-Henchoz, S., Gauchat, J.F., Aubry, J.P., Graber, P., 1996. A new role for CD23 in inflammation. Immunol Today 17, 418-420.

Boyer, B., Bourgeois, Y., Poupon, M.F., 2002. Src kinase contributes to the metastatic spread of carcinoma cells. Oncogene 21, 2347-2356.

Brauer, P.M., Tyner, A.L., 2010. Building a better understanding of the intracellular tyrosine kinase PTK6 - BRK by BRK. Biochim Biophys Acta 1806, 66-73.

Brenner, B., Gulbins, E., Schlottmann, K., Koppenhoefer, U., Busch, G.L., Walzog, B., Steinhausen, M., Coggeshall, K.M., Linderkamp, O., Lang, F., 1996. L-selectin activates the Ras pathway via the tyrosine kinase p56lck. Proceedings of the National Academy of Sciences of the United States of America 93, 15376-15381.

Brooke, M.A., Nitoiu, D., Kelsell, D.P., 2012. Cell-cell connectivity: desmosomes and disease. J Pathol 226, 158-171.

Brown, R.V., Gaerig, V.C., Simmons, T., Brooks, T.A., 2013. Helping Eve overcome ADAM: G-quadruplexes in the ADAM-15 promoter as new molecular targets for breast cancer therapeutics. Molecules 18, 15019-15034.

Bultmann, A., Li, Z., Wagner, S., Gawaz, M., Ungerer, M., Langer, H., May, A.E., Munch, G., 2011. Loss of protease activity of ADAM15 abolishes protective effects on plaque progression in atherosclerosis. Int J Cardiol 152, 382-385.

Burstein, H.J., Polyak, K., Wong, J.S., Lester, S.C., Kaelin, C.M., 2004. Ductal carcinoma in situ of the breast. The New England journal of medicine 350, 1430-1441.

Cartwright, C.A., Kamps, M.P., Meisler, A.I., Pipas, J.M., Eckhart, W., 1989. pp60c-src activation in human colon carcinoma. J Clin Invest 83, 2025-2033.

Castro, N.E., Lange, C.A., 2010. Breast tumor kinase and extracellular signal-regulated kinase 5 mediate Met receptor signaling to cell migration in breast cancer cells. Breast Cancer Res 12, R60.

Chan, K.T., Cortesio, C.L., Huttenlocher, A., 2009. FAK alters invadopodia and focal adhesion composition and dynamics to regulate breast cancer invasion. J Cell Biol 185, 357-370.

Charrier-Hisamuddin, L., Laboisse, C.L., Merlin, D., 2007. ADAM-15: a metalloprotease that mediates inflammation. The FASEB Journal 22, 641-653.

Chatterjee, V., Beard, R.S., Jr., Reynolds, J.J., Haines, R., Guo, M., Rubin, M., Guido, J., Wu, M.H., Yuan, S.Y., 2014. MicroRNA-147b regulates vascular endothelial barrier function by targeting ADAM15 expression. PloS one 9, e110286.

Chen, H.Y., Shen, C.H., Tsai, Y.T., Lin, F.C., Huang, Y.P., Chen, R.H., 2004. Brk activates rac1 and promotes cell migration and invasion by phosphorylating paxillin. Mol Cell Biol 24, 10558-10572.

Cheranov, S.Y., Karpurapu, M., Wang, D., Zhang, B., Venema, R.C., Rao, G.N., 2008. An essential role for SRC-activated STAT-3 in 14,15-EET-induced VEGF expression and angiogenesis. Blood 111, 5581-5591.

Cortes, J.E., Kim, D.-W., Pinilla-Ibarz, J., le Coutre, P., Paquette, R., Chuah, C., Nicolini, F.E., Apperley, J.F., Khoury, H.J., Talpaz, M., DiPersio, J., DeAngelo, D.J., Abruzzese, E., Rea, D., Baccarani, M., Müller, M.C., Gambacorti-Passerini, C., Wong, S., Lustgarten, S., Rivera, V.M., Clackson, T., Turner, C.D., Haluska, F.G., Guilhot, F., Deininger, M.W., Hochhaus, A., Hughes, T., Goldman, J.M., Shah, N.P., Kantarjian, H., 2013. A Phase 2 Trial of Ponatinib in Philadelphia Chromosome–Positive Leukemias. New England Journal of Medicine 369, 1783-1796.

D'Aniello, S., Irimia, M., Maeso, I., Pascual-Anaya, J., Jimenez-Delgado, S., Bertrand, S., Garcia-Fernandez, J., 2008. Gene expansion and retention leads to a diverse tyrosine kinase superfamily in amphioxus. Molecular biology and evolution 25, 1841-1854.

Daugimont, L., Vandermeulen, G., Defresne, F., Bouzin, C., Mir, L.M., Bouquet, C., Feron, O., Preat, V., 2011. Antitumoral and antimetastatic effect of antiangiogenic plasmids in B16 melanoma: Higher efficiency of the recombinant disintegrin domain of ADAM 15. European journal of pharmaceutics and biopharmaceutics : official journal of Arbeitsgemeinschaft fur Pharmazeutische Verfahrenstechnik e.V 78, 314-319.

Decock, J., Thirkettle, S., Wagstaff, L., Edwards, D.R., 2011. Matrix metalloproteinases: protective roles in cancer. J Cell Mol Med 15, 1254-1265.

Delaglio, F., Grzesiek, S., Vuister, G.W., Zhu, G., Pfeifer, J., Bax, A., 1995. NMRPipe: a multidimensional spectral processing system based on UNIX pipes. J Biomol NMR 6, 277-293.

Derry, J.J., Richard, S., Valderrama Carvajal, H., Ye, X., Vasioukhin, V., Cochrane, A.W., Chen, T., Tyner, A.L., 2000. Sik (BRK) phosphorylates Sam68 in the nucleus and negatively regulates its RNA binding ability. Mol Cell Biol 20, 6114-6126.

Derycke, L.D., Bracke, M.E., 2004. N-cadherin in the spotlight of cell-cell adhesion, differentiation, embryogenesis, invasion and signalling. Int J Dev Biol 48, 463-476.

Deuss, M., Reiss, K., Hartmann, D., 2008. Part-time alpha-secretases: the functional biology of ADAM 9, 10 and 17. Curr Alzheimer Res 5, 187-201.

Doedens, J.R., Black, R.A., 2000. Stimulation-induced down-regulation of tumor necrosis factor-alpha converting enzyme. J Biol Chem 275, 14598-14607.

Druker, B.J., 2002. STI571 (Gleevec) as a paradigm for cancer therapy. Trends in molecular medicine 8, S14-18.

Edwards, D., Handsley, M., Pennington, C., 2008. The ADAM metalloproteinases. Molecular Aspects of Medicine 29, 258-289.

Elsberger, B., Stewart, B., Tatarov, O., Edwards, J., 2010. Is Src a viable target for treating solid tumours? Current cancer drug targets 10, 683-694.

Elsberger, B., Tan, B.A., Mitchell, T.J., Brown, S.B.F., Mallon, E.A., Tovey, S.M., Cooke, T.G., Brunton, V.G., Edwards, J., 2009. Is Expression or Activation of Src Kinase Associated with Cancer-Specific Survival in ER-, PR- and HER2-Negative Breast Cancer Patients? The American Journal of Pathology 175, 1389-1397.

Endsley, M.A., Somasunderam, A.D., Li, G., Oezguen, N., Thiviyanathan, V., Murray, J.L., Rubin, D.H., Hodge, T.W., O'Brien, W.A., Lewis, B., Ferguson, M.R., 2014. Nuclear trafficking of the HIV-1 pre-integration complex depends on the ADAM10 intracellular domain. Virology 454-455, 60-66.

Eto, K., Huet, C., Tarui, T., Kupriyanov, S., Liu, H.Z., Puzon-McLaughlin, W., Zhang, X.P., Sheppard, D., Engvall, E., Takada, Y., 2002. Functional classification of ADAMs based on a conserved motif for binding to integrin alpha 9beta 1: implications for sperm-egg binding and other cell interactions. J Biol Chem 277, 17804-17810.

Feng, S., Chen, J.K., Yu, H., Simon, J.A., Schreiber, S.L., 1994. Two binding orientations for peptides to the Src SH3 domain: development of a general model for SH3-ligand interactions. Science 266, 1241-1247.

Fincham, V.J., Frame, M.C., 1998. The catalytic activity of Src is dispensable for translocation to focal adhesions but controls the turnover of these structures during cell motility. Embo j 17, 81-92.

Fourie, A.M., Coles, F., Moreno, V., Karlsson, L., 2003. Catalytic activity of ADAM8, ADAM15, and MDC-L (ADAM28) on synthetic peptide substrates and in ectodomain cleavage of CD23. J Biol Chem 278, 30469-30477.

Fried, D., Böhm, B.B., Krause, K., Burkhardt, H., 2012. ADAM15 Protein Amplifies Focal Adhesion Kinase Phosphorylation under Genotoxic Stress Conditions. Journal of Biological Chemistry 287, 21214-21223.

Fu, Y., Zagozdzon, R., Avraham, R., Avraham, H.K., 2006. CHK negatively regulates Lyn kinase and suppresses pancreatic cancer cell invasion. Int J Oncol 29, 1453-1458.

Galliher-Beckley, A.J., Schiemann, W.P., 2008. Grb2 binding to Tyr284 in TbetaR-II is essential for mammary tumor growth and metastasis stimulated by TGF-beta. Carcinogenesis 29, 244-251.

Gao, J., Zheng, W., Wang, L., Song, B., 2015. A disintegrin and metallproteinase 15 knockout decreases migration of fibroblast-like synoviocytes and inflammation in rheumatoid arthritis. Molecular medicine reports 11, 4389-4396.

Garner, T.P., Strachan, J., Shedden, E.C., Long, J.E., Cavey, J.R., Shaw, B., Layfield, R., Searle, M.S., 2011. Independent interactions of ubiquitin-binding domains in a ubiquitin-mediated ternary complex. Biochemistry 50, 9076-9087.

Garton, K.J., Gough, P.J., Raines, E.W., 2006. Emerging roles for ectodomain shedding in the regulation of inflammatory responses. J Leukoc Biol 79, 1105-1116.

Gasteiger E., H.C., Gattiker A., Duvaud S., Wilkins M.R., Appel R.D., Bairoch A., 2005. Protein Identification and Analysis Tools on the ExPASy Server;, in: Walker, J.M. (Ed.), The Proteomics Protocols Handbook. The Humana Press, pp. 571-607.

Giubellino, A., Burke, T.R., Bottaro, D.P., 2008. Grb2 signaling in cell motility and cancer. Expert Opinion on Therapeutic Targets 12, 1021-1033.

Giubellino, A., Gao, Y., Lee, S., Lee, M.J., Vasselli, J.R., Medepalli, S., Trepel, J.B., Burke, T.R., Jr., Bottaro, D.P., 2007. Inhibition of tumor metastasis by a growth factor receptor bound protein 2 Src homology 2 domain-binding antagonist. Cancer Res 67, 6012-6016.

Gomis-Ruth, F.X., 2003. Structural aspects of the metzincin clan of metalloendopeptidases. Mol Biotechnol 24, 157-202.

Gonzales, P.E., Solomon, A., Miller, A.B., Leesnitzer, M.A., Sagi, I., Milla, M.E., 2004. Inhibition of the tumor necrosis factor-alpha-converting enzyme by its pro domain. J Biol Chem 279, 31638-31645.

Gooz, M., 2010. ADAM-17: the enzyme that does it all. Crit Rev Biochem Mol Biol 45, 146-169.

Grzesiek, S., Bax, A., 1992a. Correlating backbone amide and side chain resonances in larger proteins by multiple relayed triple resonance NMR. Journal of the American Chemical Society 114, 6291-6293.

Grzesiek, S., Bax, A., 1992b. An efficient experiment for sequential backbone assignment of medium-sized isotopically enriched proteins. Journal of Magnetic Resonance (1969) 99, 201-207.

Haines, E., Minoo, P., Feng, Z., Resalatpanah, N., Nie, X.M., Campiglio, M., Alvarez, L., Cocolakis, E., Ridha, M., Di Fulvio, M., Gomez-Cambronero, J., Lebrun, J.J., Ali, S., 2009. Tyrosine Phosphorylation of Grb2: Role in Prolactin/Epidermal Growth Factor Cross Talk

in Mammary Epithelial Cell Growth and Differentiation. Molecular and Cellular Biology 29, 2505-2520.

Ham, C., 2002. ADAM15 Is an Adherens Junction Molecule Whose Surface Expression Can Be Driven by VE-Cadherin. Experimental Cell Research 279, 239-247.

Harvey, A.J., Crompton, M.R., 2003. Use of RNA interference to validate Brk as a novel therapeutic target in breast cancer: Brk promotes breast carcinoma cell proliferation. Oncogene 22, 5006-5010.

Harvey, A.J., Crompton, M.R., 2004. The Brk protein tyrosine kinase as a therapeutic target in cancer: opportunities and challenges. Anti-cancer drugs 15, 107-111.

Hazan, R.B., Qiao, R., Keren, R., Badano, I., Suyama, K., 2004. Cadherin switch in tumor progression. Annals of the New York Academy of Sciences 1014, 155-163.

Herynk, M.H., Beyer, A.R., Cui, Y., Weiss, H., Anderson, E., Green, T.P., Fuqua, S.A., 2006. Cooperative action of tamoxifen and c-Src inhibition in preventing the growth of estrogen receptor-positive human breast cancer cells. Mol Cancer Ther 5, 3023-3031.

Highman, V.A., 2012. Protein NMR: A Practical Guide.

Holgate, S.T., 2010. ADAM metallopeptidase domain 33 (ADAM33): identification and role in airways disease. Drug News Perspect 23, 381-387.

Hore, P.J., 1995a. Nuclear Magnetic Resonance. Oxford Science Publications, pp. 2-6.

Hore, P.J., 1995b. Nuclear Magnetic Resonance. Oxford Science Publications, pp. 9-10.

Howard, L., Maciewicz, R.A., Blobel, C.P., 2000. Cloning and characterization of ADAM28: evidence for autocatalytic pro-domain removal and for cell surface localization of mature ADAM28. Biochem J 348 Pt 1, 21-27.

Howard, L., Nelson, K.K., Maciewicz, R.A., Blobel, C.P., 1999. Interaction of the metalloprotease disintegrins MDC9 and MDC15 with two SH3 domain-containing proteins, endophilin I and SH3PX1. J Biol Chem 274, 31693-31699.

Huebner, K., Kastury, K., Druck, T., Salcini, A.E., Lanfrancone, L., Pelicci, G., Lowenstein, E., Li, W., Park, S.H., Cannizzaro, L., et al., 1994. Chromosome locations of genes encoding human signal transduction adapter proteins, Nck (NCK), Shc (SHC1), and Grb2 (GRB2). Genomics 22, 281-287.

Iba, K., Albrechtsen, R., Gilpin, B., Frohlich, C., Loechel, F., Zolkiewska, A., Ishiguro, K., Kojima, T., Liu, W., Langford, J.K., Sanderson, R.D., Brakebusch, C., Fassler, R., Wewer, U.M., 2000. The cysteine-rich domain of human ADAM 12 supports cell adhesion through syndecans and triggers signaling events that lead to beta1 integrin-dependent cell spreading. J Cell Biol 149, 1143-1156.

Ikura, M., Kay, L.E., Bax, A., 1990. A novel approach for sequential assignment of 1H, 13C, and 15N spectra of proteins: heteronuclear triple-resonance three-dimensional NMR spectroscopy. Application to calmodulin. Biochemistry 29, 4659-4667.

Iwai, H., Zuger, S., Jin, J., Tam, P.H., 2006. Highly efficient protein trans-splicing by a naturally split DnaE intein from Nostoc punctiforme. FEBS Lett 580, 1853-1858.

Izumi, Y., Hirata, M., Hasuwa, H., Iwamoto, R., Umata, T., Miyado, K., Tamai, Y., Kurisaki, T., Sehara-Fujisawa, A., Ohno, S., Mekada, E., 1998. A metalloprotease-disintegrin, MDC9/meltrin-gamma/ADAM9 and PKCdelta are involved in TPA-induced ectodomain shedding of membrane-anchored heparin-binding EGF-like growth factor. EMBO J 17, 7260-7272.

Janes, P.W., Saha, N., Barton, W.A., Kolev, M.V., Wimmer-Kleikamp, S.H., Nievergall, E., Blobel, C.P., Himanen, J.P., Lackmann, M., Nikolov, D.B., 2005. Adam meets Eph: an ADAM substrate recognition module acts as a molecular switch for ephrin cleavage in trans. Cell 123, 291-304.

Jang, I.K., Zhang, J., Gu, H., 2009. Grb2, a simple adapter with complex roles in lymphocyte development, function, and signaling. Immunol Rev 232, 150-159.
Jiang, C., Wechuck, J.B., Goins, W.F., Krisky, D.M., Wolfe, D., Ataai, M.M., Glorioso, J.C., 2004. Immobilized Cobalt Affinity Chromatography Provides a Novel, Efficient Method for Herpes Simplex Virus Type 1 Gene Vector Purification. Journal of Virology 78, 8994-9006.

Johnson, D., Agochiya, M., Samejima, K., Earnshaw, W., Frame, M., Wyke, J., 2000. Regulation of both apoptosis and cell survival by the v-Src oncoprotein. Cell death and differentiation 7, 685-696.

Johnson, D.A., Akamine, P., Radzio-Andzelm, E., Madhusudan, Taylor, S.S., 2001. Dynamics of cAMP-Dependent Protein Kinase. Chemical Reviews 101, 2243-2270.

Kairouz, R., Daly, R.J., 2000. Tyrosine kinase signalling in breast cancer: modulation of tyrosine kinase signalling in human breast cancer through altered expression of signalling intermediates. Breast Cancer Res 2, 197-202.

Kamalati, T., Jolin, H.E., Mitchell, P.J., Barker, K.T., Jackson, L.E., Dean, C.J., Page, M.J., Gusterson, B.A., Crompton, M.R., 1996. Brk, a breast tumor-derived non-receptor protein-tyrosine kinase, sensitizes mammary epithelial cells to epidermal growth factor. J Biol Chem 271, 30956-30963.

Kaneko, T., Li, L., Li, S.S., 2008. The SH3 domain--a family of versatile peptide- and protein-recognition module. Front Biosci 13, 4938-4952.

Kang, K.N., Kim, M., Pae, K.M., Lee, S.T., 2002. Characterization of the 5'-flanking region of the human PTK6 gene. Biochim Biophys Acta 1574, 365-369.

Kanner, S.B., Reynolds, A.B., Vines, R.R., Parsons, J.T., 1990. Monoclonal antibodies to individual tyrosine-phosphorylated protein substrates of oncogene-encoded tyrosine kinases. Proceedings of the National Academy of Sciences of the United States of America 87, 3328-3332.

Kanomata, N., Kurebayashi, J., Kozuka, Y., Sonoo, H., Moriya, T., 2011. Clinicopathological significance of Y416Src and Y527Src expression in breast cancer. Journal of Clinical Pathology 64, 578-586.

Kärkkäinen, S., Hiipakka, M., Wang, J.-H., Kleino, I., Vähä-Jaakkola, M., Renkema, G.H., Liss, M., Wagner, R., Saksela, K., 2006. Identification of preferred protein interactions by phage-display of the human Src homology-3 proteome. EMBO reports 7, 186-191.

Keeler, J., 2006. Understanding NMR Spectroscopy. Wiley.
Kessels, H.W., Ward, A.C., Schumacher, T.N., 2002. Specificity and affinity motifs for Grb2 SH2-ligand interactions. Proceedings of the National Academy of Sciences of the United States of America 99, 8524-8529.

Kim, H., Laing, M., Muller, W., 2005a. c-Src-null mice exhibit defects in normal mammary gland development and ERalpha signaling. Oncogene 24, 5629-5636.

Kim, H.K., Kong, M.Y., Jeong, M.J., Han, D.C., Choi, J.D., Kim, H.Y., Yoon, K.S., Kim, J.M., Son, K.H., Kwon, B.M., 2005b. Investigation of cell cycle arrest effects of actinomycin D at G1 phase using proteomic methods in B104-1-1 cells. Int J Biochem Cell Biol 37, 1921-1929.

Kim, H.K., Nam, J.Y., Han, M.Y., Lee, E.K., Choi, J.D., Bok, S.H., Kwon, B.M., 1999. Actinomycin D as a novel SH2 domain ligand inhibits Shc/Grb2 interaction in B104-1-1 (neu*-transformed NIH3T3) and SAA (hEGFR-overexpressed NIH3T3) cells. FEBS Lett 453, 174-178.

Kleber, S., Sancho-Martinez, I., Wiestler, B., Beisel, A., Gieffers, C., Hill, O., Thiemann, M., Mueller, W., Sykora, J., Kuhn, A., Schreglmann, N., Letellier, E., Zuliani, C., Klussmann, S., Teodorczyk, M., Grone, H.J., Ganten, T.M., Sultmann, H., Tuttenberg, J., von Deimling, A., Regnier-Vigouroux, A., Herold-Mende, C., Martin-Villalba, A., 2008. Yes and PI3K bind CD95 to signal invasion of glioblastoma. Cancer Cell 13, 235-248.

Kleino, I., Ortiz, R.M., Huovila, A.P., 2007. ADAM15 gene structure and differential alternative exon use in human tissues. BMC Mol Biol 8, 90.

Kleino, I., Ortiz, R.M., Yritys, M., Huovila, A.-P.J., Saksela, K., 2009. Alternative splicing of ADAM15 regulates its interactions with cellular SH3 proteins. Journal of Cellular Biochemistry 108, 877-885.

Klessner, J.L., Desai, B.V., Amargo, E.V., Getsios, S., Green, K.J., 2009. EGFR and ADAMs cooperate to regulate shedding and endocytic trafficking of the desmosomal cadherin desmoglein 2. Mol Biol Cell 20, 328-337.

Ko, S., Ahn, K.E., Lee, Y.M., Ahn, H.C., Lee, W., 2009. Structural basis of the auto-inhibition mechanism of nonreceptor tyrosine kinase PTK6. Biochem Biophys Res Commun 384, 236-242.

Kohda, D., Terasawa, H., Ichikawa, S., Ogura, K., Hatanaka, H., Mandiyan, V., Ullrich, A., Schlessinger, J., Inagaki, F., 1994. Solution structure and ligand-binding site of the carboxy-terminal SH3 domain of GRB2. Structure (London, England : 1993) 2, 1029-1040.

Kosol, S., Contreras-Martos, S., Cedeño, C., Tompa, P., 2013. Structural Characterization of Intrinsically Disordered Proteins by NMR Spectroscopy. Molecules 18, 10802-10828.

Kovrigin, E., 2012. NMR line shapes and multi-state binding equilibria. Journal of Biomolecular NMR 53, 257-270.

Kratzschmar, J., Lum, L., Blobel, C.P., 1996. Metargidin, a membrane-anchored metalloprotease-disintegrin protein with an RGD integrin binding sequence. J Biol Chem 271, 4593-4596.

Kuefer, R., Day, K.C., Kleer, C.G., Sabel, M.S., Hofer, M.D., Varambally, S., Zorn, C.S., Chinnaiyan, A.M., Rubin, M.A., Day, M.L., 2006. ADAM15 Disintegrin Is Associated with Aggressive Prostate and Breast Cancer Disease. Neoplasia 8, 319-329.

Laurie, S.A., Goss, G.D., Shepherd, F.A., Reaume, M.N., Nicholas, G., Philip, L., Wang, L., Schwock, J., Hirsh, V., Oza, A., Tsao, M.-S., Wright, J.J., Leighl, N.B., 2014. A Phase II Trial of Saracatinib, an Inhibitor of src Kinases, in Previously-Treated Advanced Non–Small-Cell Lung Cancer: The Princess Margaret Hospital Phase II Consortium. Clinical Lung Cancer 15, 52-57.

Lee, H., Kim, M., Lee, K.H., Kang, K.N., Lee, S.T., 1998. Exon-intron structure of the human PTK6 gene demonstrates that PTK6 constitutes a distinct family of non-receptor tyrosine kinase. Molecules and cells 8, 401-407.

Lee, H., Sodek, K.L., Hwang, Q., Brown, T.J., Ringuette, M., Sodek, J., 2007. Phagocytosis of collagen by fibroblasts and invasive cancer cells is mediated by MT1-MMP. Biochem Soc Trans 35, 704-706.

Lee, H.D., Kim, Y.H., Koo, B.H., Kim, D.S., 2014. Ectodomain of ADAM15 is shed from secretory exosomes. BMB reports.

Lee, H.D., Koo, B.H., Kim, Y.H., Jeon, O.H., Kim, D.S., 2012. Exosome release of ADAM15 and the functional implications of human macrophage-derived ADAM15 exosomes. FASEB journal : official publication of the Federation of American Societies for Experimental Biology 26, 3084-3095.

Levitt, M.H., 2009a. Spin Dynamics: Basics Of Nuclear Magnetic Resonance, 2 ed. Wiley, pp. 50-53.

Levitt, M.H., 2009b. Spin Dynamics: Basics Of Nuclear Magnetic Resonance, 2 ed. Wiley, p. 39.

Levitt, M.H., 2009c. Spin Dynamics: Basics Of Nuclear Magnetic Resonance, 2 ed. Wiley, p. 15.

Levitt, M.H., 2009d. Spin Dynamics: Basics Of Nuclear Magnetic Resonance, 2 ed. Wiley, p. 7.

Levitt, M.H., 2009e. Spin Dynamics: Basics Of Nuclear Magnetic Resonance, 2 ed. Wiley, pp. 105-113.

Li, X., Romero, P., Rani, M., Dunker, A.K., Obradovic, Z., 1999. Predicting Protein Disorder for N-, C-, and Internal Regions. Genome informatics. Workshop on Genome Informatics 10, 30-40.

Li, Y., Wei, Z., Yan, Y., Wan, Q., Du, Q., Zhang, M., 2014. Structure of Crumbs tail in complex with the PALS1 PDZ-SH3-GK tandem reveals a highly specific assembly mechanism for the apical Crumbs complex. Proceedings of the National Academy of Sciences of the United States of America 111, 17444-17449.

Lin, C.C., Melo, F.A., Ghosh, R., Suen, K.M., Stagg, L.J., Kirkpatrick, J., Arold, S.T., Ahmed, Z., Ladbury, J.E., 2012. Inhibition of basal FGF receptor signaling by dimeric Grb2. Cell 149, 1514-1524.

Liu, D., Ha, C., Zhang, X., Zhang, Z., Liu, P., 2013. Molecular implication of ADAM-15 and -17 in intrauterine adhesions. European journal of obstetrics, gynecology, and reproductive biology 170, 264-269.

Liu, L., Gao, Y., Qiu, H., Miller, W.T., Poli, V., Reich, N.C., 2006. Identification of STAT3 as a specific substrate of breast tumor kinase. Oncogene 25, 4904-4912.

Liu, Y., Wang, L., Lin, X.Y., Wang, J., Yu, J.H., Miao, Y., Wang, E.H., 2012. Anti-apoptotic effect of claudin-1 on TNF-alpha-induced apoptosis in human breast cancer MCF-7 cells. Tumour biology : the journal of the International Society for Oncodevelopmental Biology and Medicine 33, 2307-2315.

Lu, D., Scully, M., Kakkar, V., Lu, X., 2010. ADAM-15 Disintegrin-Like Domain Structure and Function. Toxins 2, 2411-2427.

Lucas, N., Day, M.L., 2009. The role of the disintegrin metalloproteinase ADAM15 in prostate cancer progression. J Cell Biochem 106, 967-974.

Lucas, N., Najy, A.J., Day, M.L., 2009. The therapeutic potential of ADAM15. Curr Pharm Des 15, 2311-2318.

Lukong, K.E., Huot, M.E., Richard, S., 2009. BRK phosphorylates PSF promoting its cytoplasmic localization and cell cycle arrest. Cellular signalling 21, 1415-1422.

Lukong, K.E., Richard, S., 2008. Breast tumor kinase BRK requires kinesin-2 subunit KAP3A in modulation of cell migration. Cellular signalling 20, 432-442.

Lum, L., Reid, M.S., Blobel, C.P., 1998. Intracellular maturation of the mouse metalloprotease disintegrin MDC15. J Biol Chem 273, 26236-26247.

Magrane, M., Consortium, U., 2011. UniProt Knowledgebase: a hub of integrated protein data. Database : the journal of biological databases and curation 2011, bar009.

Maignan, S., Guilloteau, J.P., Fromage, N., Arnoux, B., Becquart, J., Ducruix, A., 1995. Crystal structure of the mammalian Grb2 adaptor. Science 268, 291-293.

Marcello, E., Gardoni, F., Mauceri, D., Romorini, S., Jeromin, A., Epis, R., Borroni, B., Cattabeni, F., Sala, C., Padovani, A., Di Luca, M., 2007. Synapse-associated protein-97 mediates alpha-secretase ADAM10 trafficking and promotes its activity. The Journal of neuroscience : the official journal of the Society for Neuroscience 27, 1682-1691.

Maretzky, T., Evers, A., Le Gall, S., Alabi, R.O., Speck, N., Reiss, K., Blobel, C.P., 2015. The Cytoplasmic Domain of A Disintegrin and Metalloproteinase 10 (ADAM10) Regulates Its Constitutive Activity but Is Dispensable for Stimulated ADAM10-dependent Shedding. J Biol Chem 290, 7416-7425.

Maretzky, T., Le Gall, S.M., Worpenberg-Pietruk, S., Eder, J., Overall, C.M., Huang, X.Y., Poghosyan, Z., Edwards, D.R., Blobel, C.P., 2009a. Src Stimulates Fibroblast Growth Factor Receptor-2 Shedding by an ADAM15 Splice Variant Linked to Breast Cancer. Cancer Research 69, 4573-4576.

Maretzky, T., Yang, G., Ouerfelli, O., Overall, C.M., Worpenberg, S., Hassiepen, U., Eder, J., Blobel, C.P., 2009b. Characterization of the catalytic activity of the membrane-anchored metalloproteinase ADAM15 in cell-based assays. Biochem J 420, 105-113.

Martin-Garcia, J.M., Ruiz-Sanz, J., Luque, I., 2012. Interfacial water molecules in SH3 interactions: a revised paradigm for polyproline recognition. Biochem J 442, 443-451.

Mayer, B.J., 2001. SH3 domains: complexity in moderation. J Cell Sci 114, 1253-1263.

Mazurenko, N.N., Kogan, E.A., Zborovskaya, I.B., Kisseljov, F.L., 1992. Expression of pp60c-src in human small cell and non-small cell lung carcinomas. European journal of cancer (Oxford, England : 1990) 28, 372-377.

Mazzocca, A., Coppari, R., De Franco, R., Cho, J.Y., Libermann, T.A., Pinzani, M., Toker, A., 2005. A secreted form of ADAM9 promotes carcinoma invasion through tumor-stromal interactions. Cancer Res 65, 4728-4738.

McDonald, C.B., Balke, J.E., Bhat, V., Mikles, D.C., Deegan, B.J., Seldeen, K.L., Farooq, A., 2012a. Multivalent binding and facilitated diffusion account for the formation of the Grb2-Sos1 signaling complex in a cooperative manner. Biochemistry 51, 2122-2135.

McDonald, C.B., Bhat, V., Mikles, D.C., Deegan, B.J., Seldeen, K.L., Farooq, A., 2012b. Bivalent binding drives the formation of the Grb2-Gab1 signaling complex in a noncooperative manner. The FEBS journal 279, 2156-2173.

McDonald, C.B., Seldeen, K.L., Deegan, B.J., Farooq, A., 2009. SH3 Domains of Grb2 Adaptor Bind to PXψPXR Motifs Within the Sos1 Nucleotide Exchange Factor in a Discriminate Manner. Biochemistry 48, 4074-4085.

Mitchell, P.J., Barker, K.T., Martindale, J.E., Kamalati, T., Lowe, P.N., Page, M.J., Gusterson, B.A., Crompton, M.R., 1994. Cloning and characterisation of cDNAs encoding a novel non-receptor tyrosine kinase, brk, expressed in human breast tumours. Oncogene 9, 2383-2390.

Mitchell, P.J., Barker, K.T., Shipley, J., Crompton, M.R., 1997. Characterisation and chromosome mapping of the human non receptor tyrosine kinase gene, brk. Oncogene 15, 1497-1502.

Mori, S., 2003. PACSIN3 Binds ADAM12/Meltrin and Up-regulates Ectodomain Shedding of Heparin-binding Epidermal Growth Factor-like Growth Factor. Journal of Biological Chemistry 278, 46029-46034.

Mosnier, J.F., Jarry, A., Bou-Hanna, C., Denis, M.G., Merlin, D., Laboisse, C.L., 2006. ADAM15 upregulation and interaction with multiple binding partners in inflammatory bowel disease. Lab Invest 86, 1064-1073.

Moss, M.L., Bomar, M., Liu, Q., Sage, H., Dempsey, P., Lenhart, P.M., Gillispie, P.A., Stoeck, A., Wildeboer, D., Bartsch, J.W., Palmisano, R., Zhou, P., 2007. The ADAM10 prodomain is a specific inhibitor of ADAM10 proteolytic activity and inhibits cellular shedding events. J Biol Chem 282, 35712-35721.

Moss, M.L., Stoeck, A., Yan, W., Dempsey, P.J., 2008. ADAM10 as a target for anti-cancer therapy. Curr Pharm Biotechnol 9, 2-8.

Muraguchi, T., Takegami, Y., Ohtsuka, T., Kitajima, S., Chandana, E.P., Omura, A., Miki, T., Takahashi, R., Matsumoto, N., Ludwig, A., Noda, M., Takahashi, C., 2007. RECK modulates Notch signaling during cortical neurogenesis by regulating ADAM10 activity. Nat Neurosci 10, 838-845.

Murphy, G., 2008. The ADAMs: signalling scissors in the tumour microenvironment. Nat Rev Cancer 8, 929-941.

Murphy, G., 2009. Regulation of the proteolytic disintegrin metalloproteinases, the 'Sheddases'. Semin Cell Dev Biol 20, 138-145.

Murphy, G., Murthy, A., Khokha, R., 2008. Clipping, shedding and RIPping keep immunity on cue. Trends Immunol 29, 75-82.

Najy, A.J., Day, K.C., Day, M.L., 2008a. ADAM15 Supports Prostate Cancer Metastasis by Modulating Tumor Cell-Endothelial Cell Interaction. Cancer Research 68, 1092-1099.

Najy, A.J., Day, K.C., Day, M.L., 2008b. The Ectodomain Shedding of E-cadherin by ADAM15 Supports ErbB Receptor Activation. Journal of Biological Chemistry 283, 18393-18401.

Nowak, D., Boehrer, S., Hochmuth, S., Trepohl, B., Hofmann, W., Hoelzer, D., Hofmann, W.K., Mitrou, P.S., Ruthardt, M., Chow, K.U., 2007. Src kinase inhibitors induce apoptosis and mediate cell cycle arrest in lymphoma cells. Anti-cancer drugs 18, 981-995.

Okada, M., Nakagawa, H., 1989. A protein tyrosine kinase involved in regulation of pp60c-src function. J Biol Chem 264, 20886-20893.

Ostrander, J.H., Daniel, A.R., Lange, C.A., 2010. Brk/PTK6 signaling in normal and cancer cell models. Current opinion in pharmacology 10, 662-669.

Ostrander, J.H., Daniel, A.R., Lofgren, K., Kleer, C.G., Lange, C.A., 2007. Breast tumor kinase (protein tyrosine kinase 6) regulates heregulin-induced activation of ERK5 and p38 MAP kinases in breast cancer cells. Cancer Res 67, 4199-4209.

Park, S.H., Lee, K.H., Kim, H., Lee, S.T., 1997. Assignment of the human PTK6 gene encoding a non-receptor protein tyrosine kinase to 20q13.3 by fluorescence in situ hybridization. Cytogenetics and cell genetics 77, 271-272.

Pelisek, J., Pongratz, J., Deutsch, L., Reeps, C., Stadlbauer, T., Eckstein, H.H., 2012. Expression and cellular localization of metalloproteases ADAMs in high graded carotid artery lesions. Scandinavian journal of clinical and laboratory investigation 72, 648-656.

Petit, V., Boyer, B., Lentz, D., Turner, C.E., Thiery, J.P., Valles, A.M., 2000. Phosphorylation of tyrosine residues 31 and 118 on paxillin regulates cell migration through an association with CRK in NBT-II cells. J Cell Biol 148, 957-970.

Petro, B.J., Tan, R.C., Tyner, A.L., Lingen, M.W., Watanabe, K., 2004. Differential expression of the non-receptor tyrosine kinase BRK in oral squamous cell carcinoma and normal oral epithelium. Oral oncology 40, 1040-1047.

Poghosyan, Z., 2001. Phosphorylation-dependent Interactions between ADAM15 Cytoplasmic Domain and Src Family Protein-tyrosine Kinases. Journal of Biological Chemistry 277, 4999-5007.

Ponnuchamy, B., Khalil, R.A., 2008. Role of ADAMs in endothelial cell permeability: cadherin shedding and leukocyte rolling. Circ Res 102, 1139-1142.

Posadas, E.M., Al-Ahmadie, H., Robinson, V.L., Jagadeeswaran, R., Otto, K., Kasza, K.E., Tretiakov, M., Siddiqui, J., Pienta, K.J., Stadler, W.M., Rinker-Schaeffer, C., Salgia, R., 2009. FYN is overexpressed in human prostate cancer. BJU international 103, 171-177.

Prickett, T.D., Agrawal, N.S., Wei, X., Yates, K.E., Lin, J.C., Wunderlich, J.R., Cronin, J.C., Cruz, P., Rosenberg, S.A., Samuels, Y., 2009. Analysis of the tyrosine kinome in melanoma reveals recurrent mutations in ERBB4. Nature genetics 41, 1127-1132.

Puente, X.S., Sanchez, L.M., Overall, C.M., Lopez-Otin, C., 2003. Human and mouse proteases: a comparative genomic approach. Nat Rev Genet 4, 544-558.

Puls, L.N., Eadens, M., Messersmith, W., 2011. Current status of SRC inhibitors in solid tumor malignancies. Oncologist 16, 566-578.

Puto, L.A., Pestonjamasp, K., King, C.C., Bokoch, G.M., 2003. p21-activated kinase 1 (PAK1) interacts with the Grb2 adapter protein to couple to growth factor signaling. J Biol Chem 278, 9388-9393.

Qian, F., Hanahan, D., Weissman, I.L., 2001. L-selectin can facilitate metastasis to lymph nodes in a transgenic mouse model of carcinogenesis. Proceedings of the National Academy of Sciences of the United States of America 98, 3976-3981.

Qiu, H., Miller, W.T., 2002. Regulation of the nonreceptor tyrosine kinase Brk by autophosphorylation and by autoinhibition. J Biol Chem 277, 34634-34641.

Rae, J.M., Creighton, C.J., Meck, J.M., Haddad, B.R., Johnson, M.D., 2007. MDA-MB-435 cells are derived from M14 melanoma cells--a loss for breast cancer, but a boon for melanoma research. Breast cancer research and treatment 104, 13-19.

Raiter, A., Weiss, C., Bechor, Z., Ben-Dor, I., Battler, A., Kaplan, B., Hardy, B., 2010. Activation of GRP78 on endothelial cell membranes by an ADAM15-derived peptide induces angiogenesis. J Vasc Res 47, 399-411.

Rawlings, N.D., Morton, F.R., Kok, C.Y., Kong, J., Barrett, A.J., 2008. MEROPS: the peptidase database. Nucleic Acids Res 36, D320-325.

Reddy, P., Slack, J.L., Davis, R., Cerretti, D.P., Kozlosky, C.J., Blanton, R.A., Shows, D., Peschon, J.J., Black, R.A., 2000. Functional analysis of the domain structure of tumor necrosis factor-alpha converting enzyme. J Biol Chem 275, 14608-14614.

Riley, D., Carragher, N.O., Frame, M.C., Wyke, J.A., 2001. The mechanism of cell cycle regulation by v-Src. Oncogene 20, 5941-5950.

Roghani, M., Becherer, J.D., Moss, M.L., Atherton, R.E., Erdjument-Bromage, H., Arribas, J., Blackburn, R.K., Weskamp, G., Tempst, P., Blobel, C.P., 1999. Metalloprotease-disintegrin MDC9: intracellular maturation and catalytic activity. J Biol Chem 274, 3531-3540.

Romero, Obradovic, Dunker, K., 1997. Sequence Data Analysis for Long Disordered Regions Prediction in the Calcineurin Family. Genome informatics. Workshop on Genome Informatics 8, 110-124.

Romero, P., Obradovic, Z., Li, X., Garner, E.C., Brown, C.J., Dunker, A.K., 2001. Sequence complexity of disordered protein. Proteins 42, 38-48.

Roskoski, R., Jr., 2015. Src protein-tyrosine kinase structure, mechanism, and small molecule inhibitors. Pharmacological research : the official journal of the Italian Pharmacological Society 94c, 9-25.

Roy, K., Chakrabarti, O., Mukhopadhyay, D., 2014. Interaction of Grb2 SH3 domain with UVRAG in an Alzheimer's disease-like scenario. Biochemistry and cell biology = Biochimie et biologie cellulaire 92, 219-225.

Ruhe, J.E., Streit, S., Hart, S., Wong, C.H., Specht, K., Knyazev, P., Knyazeva, T., Tay, L.S., Loo, H.L., Foo, P., Wong, W., Pok, S., Lim, S.J., Ong, H., Luo, M., Ho, H.K., Peng, K., Lee, T.C., Bezler, M., Mann, C., Gaertner, S., Hoefler, H., Iacobelli, S., Peter, S., Tay, A., Brenner, S., Venkatesh, B., Ullrich, A., 2007. Genetic alterations in the tyrosine kinase transcriptome of human cancer cell lines. Cancer Res 67, 11368-11376.

Saksela, K., Permi, P., 2012. SH3 domain ligand binding: What's the consensus and where's the specificity? FEBS Lett 586, 2609-2614.

Scaplehorn, N., Holmstrom, A., Moreau, V., Frischknecht, F., Reckmann, I., Way, M., 2002. Grb2 and Nck act cooperatively to promote actin-based motility of vaccinia virus. Current biology : CB 12, 740-745.

Schlaepfer, D.D., Hanks, S.K., Hunter, T., van der Geer, P., 1994. Integrin-mediated signal transduction linked to Ras pathway by GRB2 binding to focal adhesion kinase. Nature 372, 786-791.

Schlaepfer, D.D., Jones, K.C., Hunter, T., 1998. Multiple Grb2-mediated integrin-stimulated signaling pathways to ERK2/mitogen-activated protein kinase: summation of both c-Src- and focal adhesion kinase-initiated tyrosine phosphorylation events. Mol Cell Biol 18, 2571-2585.

Schlomann, U., Wildeboer, D., Webster, A., Antropova, O., Zeuschner, D., Knight, C.G., Docherty, A.J., Lambert, M., Skelton, L., Jockusch, H., Bartsch, J.W., 2002. The metalloprotease disintegrin ADAM8. Processing by autocatalysis is required for proteolytic activity and cell adhesion. J Biol Chem 277, 48210-48219.

Schmandt, R.E., Bennett, M., Clifford, S., Thornton, A., Jiang, F., Broaddus, R.R., Sun, C.C., Lu, K.H., Sood, A.K., Gershenson, D.M., 2006. The BRK tyrosine kinase is expressed in high-grade serous carcinoma of the ovary. Cancer biology & therapy 5, 1136-1141.

Schonefuss, A., Abety, A.N., Zamek, J., Mauch, C., Zigrino, P., 2012. Role of ADAM-15 in wound healing and melanoma development. Exp Dermatol 21, 437-442.

Seals, D.F., 2003. The ADAMs family of metalloproteases: multidomain proteins with multiple functions. Genes & Development 17, 7-30.

Seals, D.F., Courtneidge, S.A., 2003. The ADAMs family of metalloproteases: multidomain proteins with multiple functions. Genes Dev 17, 7-30.

Sellappan, S., Grijalva, R., Zhou, X., Yang, W., Eli, M.B., Mills, G.B., Yu, D., 2004. Lineage infidelity of MDA-MB-435 cells: expression of melanocyte proteins in a breast cancer cell line. Cancer Res 64, 3479-3485.

Serrels, A., Timpson, P., Canel, M., Schwarz, J.P., Carragher, N.O., Frame, M.C., Brunton, V.G., Anderson, K.I., 2009. Real-time study of E-cadherin and membrane dynamics in living animals: implications for disease modeling and drug development. Cancer Res 69, 2714-2719.

She, H.Y., Rockow, S., Tang, J., Nishimura, R., Skolnik, E.Y., Chen, M., Margolis, B., Li, W., 1997. Wiskott-Aldrich syndrome protein is associated with the adapter protein Grb2 and the epidermal growth factor receptor in living cells. Mol Biol Cell 8, 1709-1721.

Shen, C.H., Chen, H.Y., Lin, M.S., Li, F.Y., Chang, C.C., Kuo, M.L., Settleman, J., Chen, R.H., 2008. Breast tumor kinase phosphorylates p190RhoGAP to regulate rho and ras and promote breast carcinoma growth, migration, and invasion. Cancer Res 68, 7779-7787.

Sheppard, D., 2000. In vivo functions of integrins: lessons from null mutations in mice. Matrix biology : journal of the International Society for Matrix Biology 19, 203-209.

Shiina, H., Breault, J.E., Basset, W.W., Enokida, H., Urakami, S., Li, L.C., Okino, S.T., Deguchi, M., Kaneuchi, M., Terashima, M., Yoneda, T., Shigeno, K., Carroll, P.R., Igawa, M., Dahiya, R., 2005. Functional Loss of the gamma-catenin gene through epigenetic and genetic pathways in human prostate cancer. Cancer Res 65, 2130-2138.

Simister, P.C., Luccarelli, J., Thompson, S., Appella, D.H., Feller, S.M., Hamilton, A.D., 2013. Novel inhibitors of a Grb2 SH3C domain interaction identified by a virtual screen. Bioorganic & medicinal chemistry 21, 4027-4033.

Simon, J.A., Schreiber, S.L., 1995. Grb2 SH3 binding to peptides from Sos: evaluation of a general model for SH3-ligand interactions. Chemistry & Biology 2, 53-60.

Smith, K.M., Gaultier, A., Cousin, H., Alfandari, D., White, J.M., DeSimone, D.W., 2002. The cysteine-rich domain regulates ADAM protease function in vivo. J Cell Biol 159, 893-902.

Sommer, L.A., Meier, M.A., Dames, S.A., 2012. A fast and simple method for probing the interaction of peptides and proteins with lipids and membrane-mimetics using GB1 fusion proteins and NMR spectroscopy. Protein Sci 21, 1566-1570.

Soriano, P., Montgomery, C., Geske, R., Bradley, A., 1991. Targeted disruption of the c-src proto-oncogene leads to osteopetrosis in mice. Cell 64, 693-702.

Sparks, A.B., Quilliam, L.A., Thorn, J.M., Der, C.J., Kay, B.K., 1994. Identification and characterization of Src SH3 ligands from phage-displayed random peptide libraries. J Biol Chem 269, 23853-23856.

Stangler, T., Tran, T., Hoffmann, S., Schmidt, H., Jonas, E., Willbold, D., 2007. Competitive displacement of full-length HIV-1 Nef from the Hck SH3 domain by a high-affinity artificial peptide. Biol Chem 388, 611-615.

Stautz, D., Leyme, A., Grandal, M.V., Albrechtsen, R., van Deurs, B., Wewer, U., Kveiborg, M., 2012a. Cell-surface metalloprotease ADAM12 is internalized by a clathrin- and Grb2-dependent mechanism. Traffic (Copenhagen, Denmark) 13, 1532-1546.

Stautz, D., Sanjay, A., Hansen, M.T., Albrechtsen, R., Wewer, U.M., Kveiborg, M., 2010. ADAM12 localizes with c-Src to actin-rich structures at the cell periphery and regulates Src kinase activity. Exp Cell Res 316, 55-67.

Stautz, D., Wewer, U.M., Kveiborg, M., 2012b. Functional analysis of a breast cancer-associated mutation in the intracellular domain of the metalloprotease ADAM12. PloS one 7, e37628.

Stoeck, A., Keller, S., Riedle, S., Sanderson, M.P., Runz, S., Le Naour, F., Gutwein, P., Ludwig, A., Rubinstein, E., Altevogt, P., 2006. A role for exosomes in the constitutive and stimulus-induced ectodomain cleavage of L1 and CD44. Biochem J 393, 609-618.
Stover, D.R., Furet, P., Lydon, N.B., 1996. Modulation of the SH2 binding specificity and kinase activity of Src by tyrosine phosphorylation within its SH2 domain. J Biol Chem 271, 12481-12487.

Sun, C., Beard, R.S., Jr., McLean, D.L., Rigor, R.R., Konia, T., Wu, M.H., Yuan, S.Y., 2013. ADAM15 deficiency attenuates pulmonary hyperpermeability and acute lung injury in lipopolysaccharide-treated mice. American journal of physiology. Lung cellular and molecular physiology 304, L135-142.

Sun, C., Wu, M.H., Guo, M., Day, M.L., Lee, E.S., Yuan, S.Y., 2010. ADAM15 regulates endothelial permeability and neutrophil migration via Src/ERK1/2 signalling. Cardiovasc Res 87, 348-355.

Sun, C., Wu, M.H., Lee, E.S., Yuan, S.Y., 2012. A disintegrin and metalloproteinase 15 contributes to atherosclerosis by mediating endothelial barrier dysfunction via Src family kinase activity. Arterioscler Thromb Vasc Biol 32, 2444-2451.

Sun, Z.Y., Frueh, D.P., Selenko, P., Hoch, J.C., Wagner, G., 2005. Fast assignment of 15N-HSQC peaks using high-resolution 3D HNcocaNH experiments with non-uniform sampling. J Biomol NMR 33, 43-50.

Sundberg, C., Thodeti, C.K., Kveiborg, M., Larsson, C., Parker, P., Albrechtsen, R., Wewer, U.M., 2004. Regulation of ADAM12 cell-surface expression by protein kinase C epsilon. J Biol Chem 279, 51601-51611.

Superti-Furga, G., Fumagalli, S., Koegl, M., Courtneidge, S.A., Draetta, G., 1993. Csk inhibition of c-Src activity requires both the SH2 and SH3 domains of Src. Embo j 12, 2625-2634.

Takahashi, H., Nakanishi, T., Kami, K., Arata, Y., Shimada, I., 2000. A novel NMR method for determining the interfaces of large protein-protein complexes. Nat Struct Mol Biol 7, 220-223.

Talamonti, M.S., Roh, M.S., Curley, S.A., Gallick, G.E., 1993. Increase in activity and level of pp60c-src in progressive stages of human colorectal cancer. J Clin Invest 91, 53-60.

Tari, A.M., Lopez-Berestein, G., 2001. GRB2: a pivotal protein in signal transduction. Semin Oncol 28, 142-147.

Teyra, J., Sidhu, S.S., Kim, P.M., 2012. Elucidation of the binding preferences of peptide recognition modules: SH3 and PDZ domains. FEBS Lett 586, 2631-2637.

Toquet, C., Colson, A., Jarry, A., Bezieau, S., Volteau, C., Boisseau, P., Merlin, D., Laboisse, C.L., Mosnier, J.-F., 2012. ADAM15 to α5β1 integrin switch in colon carcinoma cells: A late event in cancer progression associated with tumor dedifferentiation and poor prognosis. International Journal of Cancer 130, 278-287.

Ungerer, C., Doberstein, K., Bürger, C., Hardt, K., Boehncke, W.-H., Böhm, B., Pfeilschifter, J., Dummer, R., Mihic-Probst, D., Gutwein, P., 2010. ADAM15 expression is downregulated in melanoma metastasis compared to primary melanoma. Biochemical and Biophysical Research Communications 401, 363-369.

Uversky, V.N., 2011. Intrinsically disordered proteins from A to Z. Int J Biochem Cell Biol 43, 1090-1103.

Vasioukhin, V., Serfas, M.S., Siyanova, E.Y., Polonskaia, M., Costigan, V.J., Liu, B., Thomason, A., Tyner, A.L., 1995. A novel intracellular epithelial cell tyrosine kinase is expressed in the skin and gastrointestinal tract. Oncogene 10, 349-357.

Vasioukhin, V., Tyner, A.L., 1997. A role for the epithelial-cell-specific tyrosine kinase Sik during keratinocyte differentiation. Proceedings of the National Academy of Sciences of the United States of America 94, 14477-14482.

Verbeek, B.S., Vroom, T.M., Adriaansen-Slot, S.S., Ottenhoff-Kalff, A.E., Geertzema, J.G.N., Hennipman, A., Rijksen, G., 1996. c-Src PROTEIN EXPRESSION IS INCREASED IN HUMAN BREAST CANCER. AN IMMUNOHISTOCHEMICAL AND BIOCHEMICAL ANALYSIS. The Journal of Pathology 180, 383-388.

Vidal, M., Gigoux, V., Garbay, C., 2001. SH2 and SH3 domains as targets for anti-proliferative agents. Critical reviews in oncology/hematology 40, 175-186.

Vidarsson, G., Dekkers, G., Rispens, T., 2014. IgG subclasses and allotypes: from structure to effector functions. Frontiers in immunology 5, 520.

Vranken, W.F., Boucher, W., Stevens, T.J., Fogh, R.H., Pajon, A., Llinas, M., Ulrich, E.L., Markley, J.L., Ionides, J., Laue, E.D., 2005. The CCPN data model for NMR spectroscopy: Development of a software pipeline. Proteins: Structure, Function, and Bioinformatics 59, 687-696.

Wang, T.C., Jee, S.H., Tsai, T.F., Huang, Y.L., Tsai, W.L., Chen, R.H., 2005. Role of breast tumour kinase in the in vitro differentiation of HaCaT cells. The British journal of dermatology 153, 282-289.

Weaver, A.M., Karginov, A.V., Kinley, A.W., Weed, S.A., Li, Y., Parsons, J.T., Cooper, J.A., 2001. Cortactin promotes and stabilizes Arp2/3-induced actin filament network formation. Current biology : CB 11, 370-374.

Weaver, A.M., Silva, C.M., 2007. Signal transducer and activator of transcription 5b: a new target of breast tumor kinase/protein tyrosine kinase 6. Breast Cancer Res 9, R79.
Wheeler, D.L., Iida, M., Dunn, E.F., 2009. The Role of Src in Solid Tumors. The Oncologist 14, 667-678.

Wild-Bode, C., Fellerer, K., Kugler, J., Haass, C., Capell, A., 2006. A basolateral sorting signal directs ADAM10 to adherens junctions and is required for its function in cell migration. J Biol Chem 281, 23824-23829.

Williamson, M.P., 2013. Using chemical shift perturbation to characterise ligand binding. Progress in Nuclear Magnetic Resonance Spectroscopy 73, 1-16.

Wilson, L.K., Luttrell, D.K., Parsons, J.T., Parsons, S.J., 1989. pp60c-src tyrosine kinase, myristylation, and modulatory domains are required for enhanced mitogenic responsiveness to epidermal growth factor seen in cells overexpressing c-src. Mol Cell Biol 9, 1536-1544.

Wittekind, M., Mapelli, C., Lee, V., Goldfarb, V., Friedrichs, M.S., Meyers, C.A., Mueller, L., 1997. Solution structure of the Grb2 N-terminal SH3 domain complexed with a ten-residue peptide derived from SOS: direct refinement against NOEs, J-couplings and 1H and 13C chemical shifts. Journal of molecular biology 267, 933-952.

Witz, I.P., 2006. The involvement of selectins and their ligands in tumor-progression. Immunology letters 104, 89-93.

Xiang, B., Chatti, K., Qiu, H., Lakshmi, B., Krasnitz, A., Hicks, J., Yu, M., Miller, W.T., Muthuswamy, S.K., 2008. Brk is coamplified with ErbB2 to promote proliferation in breast cancer. Proceedings of the National Academy of Sciences of the United States of America 105, 12463-12468.

Xiaohui Duan, X.M.a.W.S., 2013. ADAM15 is involved in MICB shedding and mediates the effects of gemcitabine on MICB shedding in PANC-1 pancreatic cancer cells. Molecular medicine reports 7, 991-997.

Xu, G., Ye, Y., Liu, X., Cao, S., Wu, Q., Cheng, K., Liu, M., Pielak, G.J., Li, C., 2014a. Strategies for protein NMR in Escherichia coli. Biochemistry 53, 1971-1981.

Xu, Y., Zhang, H., Lit, L.C., Grothey, A., Athanasiadou, M., Kiritsi, M., Lombardo, Y., Frampton, A.E., Green, A.R., Ellis, I.O., Ali, S., Lenz, H.J., Thanou, M., Stebbing, J., Giamas, G., 2014b. The kinase LMTK3 promotes invasion in breast cancer through GRB2-mediated induction of integrin beta(1). Science signaling 7, ra58.

Yasui, A., Matsuura, K., Shimizu, E., Hijiya, N., Higuchi, Y., Yamamoto, S., 2004. Expression of splice variants of the human ADAM15 gene and strong interaction between the cytoplasmic domain of one variant and Src family proteins Lck and Hck. Pathobiology 71, 185-192.

Yin, J., Cai, Z., Zhang, L., Zhang, J., He, X., Du, X., Wang, Q., Lu, J., 2013. A recombined fusion protein PTD-Grb2-SH2 inhibits the proliferation of breast cancer cells in vitro. Int J Oncol 42, 1061-1069.

Yu, H., Rosen, M.K., Schreiber, S.L., 1993. 1H and 15N assignments and secondary structure of the Src SH3 domain. FEBS Lett 324, 87-92.

Zang, X.P., Siwak, D.R., Nguyen, T.X., Tari, A.M., Pento, J.T., 2004. KGF-induced motility of breast cancer cells is dependent on Grb2 and Erk1,2. Clin Exp Metastasis 21, 437-443.

Zhang, S., Yu, D., 2012. Targeting Src family kinases in anti-cancer therapies: turning promise into triumph. Trends in Pharmacological Sciences 33, 122-128.

Zhang, X.H., Wang, Q., Gerald, W., Hudis, C.A., Norton, L., Smid, M., Foekens, J.A., Massague, J., 2009. Latent bone metastasis in breast cancer tied to Src-dependent survival signals. Cancer Cell 16, 67-78.

Zhang, X.P., Kamata, T., Yokoyama, K., Puzon-McLaughlin, W., Takada, Y., 1998. Specific interaction of the recombinant disintegrin-like domain of MDC-15 (metargidin, ADAM-15) with integrin alphavbeta3. J Biol Chem 273, 7345-7350.

Zheng, Y., Peng, M., Wang, Z., Asara, J.M., Tyner, A.L., 2010. Protein tyrosine kinase 6 directly phosphorylates AKT and promotes AKT activation in response to epidermal growth factor. Mol Cell Biol 30, 4280-4292.

Zhong, J.L., Poghosyan, Z., Pennington, C.J., Scott, X., Handsley, M.M., Warn, A., Gavrilovic, J., Honert, K., Kruger, A., Span, P.N., Sweep, F.C.G.J., Edwards, D.R., 2008. Distinct Functions of Natural ADAM-15 Cytoplasmic Domain Variants in Human Mammary Carcinoma. Molecular Cancer Research 6, 383-394.

Zhou, P., Wagner, G., 2010. Overcoming the Solubility Limit with Solubility-Enhancement Tags: Successful Applications in Biomolecular NMR Studies. Journal of biomolecular NMR 46, 23-31.

Zibert, J.R., Wallbrecht, K., Schon, M., Mir, L.M., Jacobsen, G.K., Trochon-Joseph, V., Bouquet, C., Villadsen, L.S., Cadossi, R., Skov, L., Schon, M.P., 2011. Halting angiogenesis by non-viral somatic gene therapy alleviates psoriasis and murine psoriasiform skin lesions. J Clin Invest 121, 410-421.